DISSERTATION

KINETIC AND CATALYTIC STUDIES OF VANADIUM CATECHOL DIOXYGENASE MODEL SYSTEMS, PLUS RE-INVESTIGATION OF A CLAIMED ADAMANTANE DIOXYGENASE BASED ON A Ru-INCORPORATED POLYOXOMETALATE

Submitted by

Cindy-Xing Yin

Department of Chemistry

In partial fulfillment of the requirements

For the Degree of Doctor of Philosophy

Colorado State University

Fort Collins, Colorado

Summer 2005

COLORADO STATE UNIVERSITY

April 27, 2005

WE HEREBY RECOMMEND THAT THE DISSERTATION PREPARED UNDER OUR SUPERVISION BY XING YIN ENTITLED KINETIC AND CATALYTIC STUDIES OF VANADIUM CATECHOL DIOXYGENASE MODEL SYSTEMS, PLUS RE-INVESTIGATION OF A CLAIMED ADAMANTANE DIOXYGENASE BASED ON A Ru-INCORPORATED POLYOXOMETALATE BE ACCEPTED AS FULFILLING IN PART REQUIREMENTS FOR THE DEGREE OF DOCTOR OF PHILOSOPHY.

Committee on Graduate Work

Ellen R. Fisher/Chair

Louis S. Hegedus

Steven H. Strauss

Kenneth F. Reardon

Richard G. Finke/Advisor

Anthony K. Rappé/Department Head/Director

ABSTRACT OF DISSERTATION

KINETIC AND CATALYTIC STUDIES OF VANADIUM CATECHOL DIOXYGENASE MODEL SYSTEMS, PLUS RE-INVESTIGATION OF A CLAIMED ADAMANTANE DIOXYGENASE BASED ON A Ru-INCORPORATED POLYOXOMETALATE

Following a review of catechol dioxygenases and related biomimetic systems, a series of studies aimed at understanding vanadium catechol dioxygenase model systems were performed. Specific studies undertaken were: 1) spectroscopic and catalytic studies revealing a common catalyst in ten vanadium catechol dioxygenase systems; and 2) kinetic studies determining how the vanadium catechol dioxygenase precursors evolve into that common catalyst. In addition to polyoxometalate catechol dioxygenase systems, simple vanadium catecholate/semiquinone complexes were included in the study investigating the identity of the true catalyst. Selectivity, catalytic lifetime, EPR, negative ion ESI–MS and kinetic results on both polyoxometalate and simple vanadium catecholate systems all point to a common catalyst, Pierpont's crystallographically characterized complex, $[VO(DBSQ)(DTBC)]_2$ (where DBSQ stands for 3,5-di-*tert*-butylsemiquinone anion and DTBC stands for 3,5-di-*tert*-butylcatecholate dianion). Pierpont's complex as the common catalyst explains the remarkable similarity in

selectivity, catalytic lifetime and other properties for the ten vanadium catechol dioxygenase systems studied.

More detailed kinetic studies were performed in order to understand how the vanadium-containing precursors evolve into Pierpont's catalyst. H_2O_2, a product of the autoxidation of the catechol to its corresponding benzoquinone, was found to be the key to turning on the catechol oxygenation catalysis.

Finally, an important Ru_2-based sandwich-type polyoxometalate, $\{[WZnRu^{III}_2(OH)(H_2O)](ZnW_9O_{34})_2\}^{11-}$, was re-investigated. This literature compound is claimed to be a dioxygenase catalyst for adamantane hydroxylation and alkene epoxidation reactions in a *Nature* paper (Neumann, R.; Dahan, M. *Nature* **1997**, *388*, 353-355). However, in our hands, kinetic studies, byproduct detection, stoichiometry, and initiation / inhibition results show that the title sandwich Ru_2-polyoxometalate catalyzes adamantane hydroxylation reaction via a free-radical-chain mechanism and not the dioxygenase mechanism claimed in the literature.

Cindy-Xing Yin
Chemistry Department
Colorado State University
Fort Collins, CO 80523
Summer 2005

ACKNOWLEDGMENTS

I dedicate this dissertation to my mom and dad. Without them, I could not have possibly done all this. I also dedicate this to my husband, Peng Wu, who has always been by my side throughout this journey.

I want to thank my advisor, Professor Richard G. Finke, who sets higher standards for students, for helping me to reach my goals. I am also grateful for the critical thinking skills and ways to approach problems he taught me.

I also want to thank Lisa Starkey Ott for her patience and enormous effort proofreading this dissertation, and everyone who inspired me to do better in Chemistry.

TABLE OF CONTENTS

CHAPTER I

INTRODUCTION

This dissertation is written in the "journals-format" style (see Appendix A for a discussion of this type of dissertation). It is based on three separate publications, each written in a format set by the American Chemical Society (Chapters III–V). A brief overview of each chapter is presented below.

Chapter II is a review of the literature of catechol dioxygenases and related biomimetic oxidation systems. This chapter also introduces the scientific issues that will be addressed in the later chapters.

Chapter III presents the study discovering a common catalyst in ten vanadium catechol dioxygenase systems from the literature tested to date. This finding explains the similar catalytic selectivity shown by disparate vanadium precatalysts previously reported in the literature. This finding is also vital to the work described in Chapter IV.

Chapter IV describes more detailed kinetic studies on two vanadium-containing polyoxometalate precatalysts and one vanadium catecholate precatalyst. H_2O_2, a product from autoxidation of the reaction substrate, removes the induction periods of three

vanadium catechol dioxygenase precatalysts. Additionally, the mechanism of H_2O_2-mediated conversion of a polyoxometalate precatalyst to Pierpont's catalyst resting state, plus a catalytic cycle starting with the Pierpont's catalyst, is proposed. This study presents a prototype example of the interesting phenomenon of an autoxidation-product-initiated selective dioxygenase reaction.

Chapter V includes the re-investigation of an important Ru_2-based sandwich polyoxometalate that was claimed by others to be an inorganic dioxygenase for adamantane hydroxylation and alkene epoxidation. Compelling kinetic, initiation / inhibition, stoichiometry and other studies strongly suggest this sandwich polyoxometalate catalyzes the adamantane hydroxylation via a free-radical-chain mechanism, not the previously claimed dioxygenase mechanism.

The most important hypotheses tested in this dissertation are, then, that: (i) a common catalyst explains the similar selectivity observed for different vanadium catechol dioxygenase systems; (ii) sigmoidal, autocatalytic kinetics shown by vanadium-containing catechol dioxygenase precatalysts is diagnostic of an autoxidation product formed during the induction period and which triggers the desired dioxygenase catalysis; and that (iii) kinetic, product, and stoichiometry studies together with initiation / inhibition studies are the most important experiments for distinguishing a true dioxygenase reaction from a free-radical-chain reaction.

CHAPTER II

A REVIEW OF CATECHOL DIOXYGENASES AND RELATED BIOMIMETIC OXIDATION SYSTEMS

This chapter is an introduction to the later chapters and also a literature review of mostly Fe- and V-containing catechol dioxygenases as well as polyoxometalate-based biomimetic oxidation systems.

A Review of Catechol Dioxygenases and Related Biomimetic Oxidation Systems

Cindy-Xing Yin and Richard G. Finke

Contents

I. Introduction

a. Oxygen activation and oxygenases

Oxygen (O_2, also known as dioxygen) is one of the most desirable oxidants owing to its abundance and its clean side product after oxidation, water.[1,2,3,4] Molecular oxygen activation is difficult due to the spin state of molecular oxygen (two unpaired electrons, triplet state). Additionally, once oxygen is activated, it is notorious for its low selectivity—radical intermediates are formed, and oftentimes radical-chain reactions take place. The use of oxygen as an oxidant without the initiation of radical chain reactions is called selective oxidation. Selective oxidation can be initiated by a paramagnetic metal ion binding with oxygen, resulting in electron-delocalization onto the bound oxygen. Alternatively, a diamagnetic metal can activate an electron-rich substrate, which can subsequently be attacked by oxygen, Figure 2.1.[4,5,6,7]

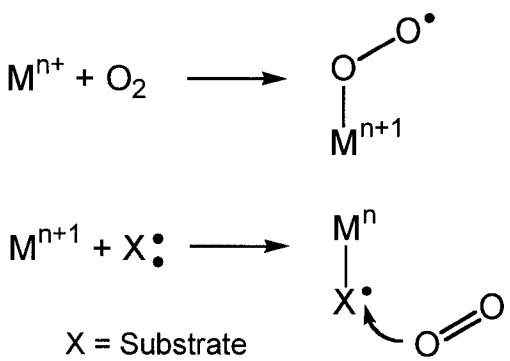

Figure 2.1 Oxygen activation via metal activation or substrate activation routes.

There are several significant oxygenation reactions that have not been realized with O_2 as the only oxidant, commonly called "Holy Grail" or "dream" reactions:[2] namely, the selective oxidation of methane to methanol, propylene to propylene oxide,

and benzene to phenol, Figure 2.2. The current state-of-the-art technology for these processes either needs a multi-step process (i.e., natural gas goes through steam reforming to generate CO and H_2 which are then used to make methanol) or gives less useful co-products (i.e., styrene or phenol productions generate by-products of propylene oxide or acetone, respectively). Realization of direct oxygenation reactions is significant both from an industrial perspective and as a scientific challenge.[1,4]

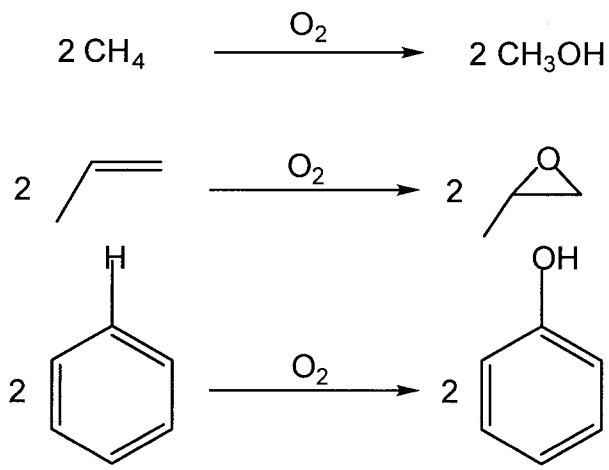

Figure 2.2 Important selective oxygenation reactions yet to be realized with O_2 as the sole oxidant.

In nature, enzymes capable of incorporating molecular oxygen into their substrates have been known since 1955.[8] These enzymes are oxygenases, fundamentally different from another class of enzymes which interact with O_2, oxidases. Oxygenase enzymes catalyze the incorporation of either one or both oxygen atoms from molecular oxygen into the substrate, while oxidase enzymes use oxygen simply as an electron acceptor, Figure 2.3.

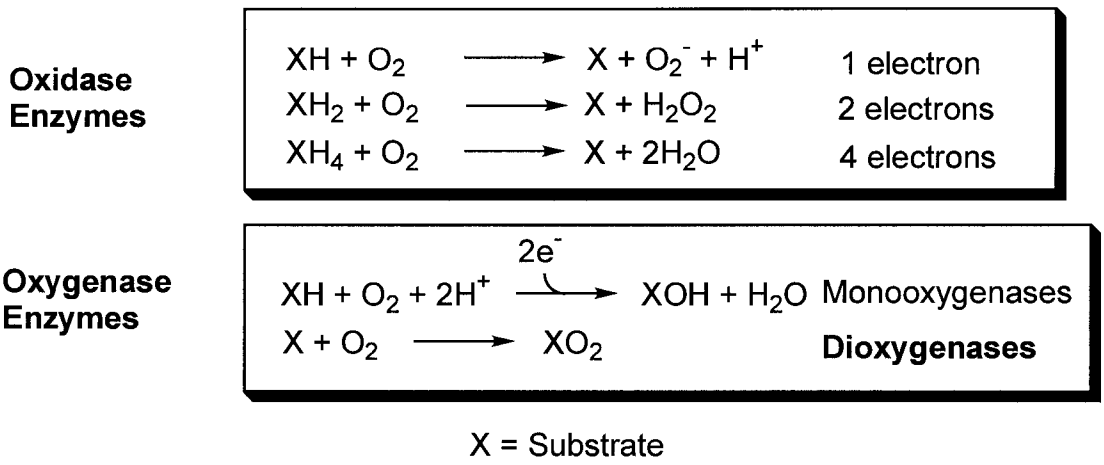

Figure 2.3 Oxidase and oxygenase enzyme catalyzed reactions.

b. Monooxygenases and dioxygenases

Monooxygenase enzymes and dioxygenase enzymes are two kinds of oxygenase enzymes. For monooxygenase enzymes, one oxygen atom of molecular oxygen is incorporated into the product and the other oxygen atom is reduced to produce water. In reactions catalyzed by dioxygenase enzymes, both oxygen atoms are incorporated, as illustrated in Figure 2.3. Reactions catalyzed by dioxygenase enzymes are more efficient and direct than those catalyzed by monooxygenase enzymes. However, some monooxygenases are capable of activating more stable, less reactive substrates than dioxygenases: for example, methane is activated and selectively converted to methanol by methane monooxygenase.

Both monooxygenase and dioxygenase enzymes are widely distributed in nature from plants and animals to microorganisms. Oxygenases play indispensable roles in the biosphere from amino acid metabolism to aromatic compound metabolism.[9] However, it is still not viable to utilize oxygenase enzymes for the manufacture of bulk chemicals yet. Nevertheless, oxygenase enzymes are important systems for many biomimetic studies

Table 2.1 Oxygenase Distributions in Nature and Representative Examples.

	Microbial Oxygenases	**Animal Oxygenases**	**Plant Oxygenases**
Amino Acid Metabolism	Lysine monooxygenases	Tryptophan 5-monooxygenase, homogentisate 3,4-dioxygenase	-
Lipid Metabolism	-	Sheep vesicular gland lipoxygenase	Soybean lipoxygenase
Carbonhydrate Metabolism	Fe-containing dioxygenase	-	-
Nucleic Acid Metabolism	D-thymidine α-KG dioxygenase	-	-
Aromatic Compounds Metabolism	Catechol dioxygenases	Cytochrome P-450	Cytochrome P-450

aimed at better understanding and, eventually, industrial applications, including the selective oxidation of hydrocarbons (alkanes, alkenes, and aromatics) with oxygen.[4]

II. Catechol Dioxygenases

a. Introduction

Catechol dioxygenases are Fe- or Mn- containing enzymes involved in aromatic compound metabolism.[6,7,10] These enzymes catalyze the addition of two oxygen atoms to catechol (1,2-dihydroxybenzene) or its derivatives, and simultaneously catalyze the cleavage of the benzene ring into acyclic compounds, Figure 2.4. Depending on which position of the benzene ring is cleaved, dioxygenases are classified as intradiol or extradiol. Intradiol dioxygenases cleave the carbon-carbon bond between the two *ortho*-hydroxy groups, while extradiol dioxygenases break the C–C bond adjacent to either of

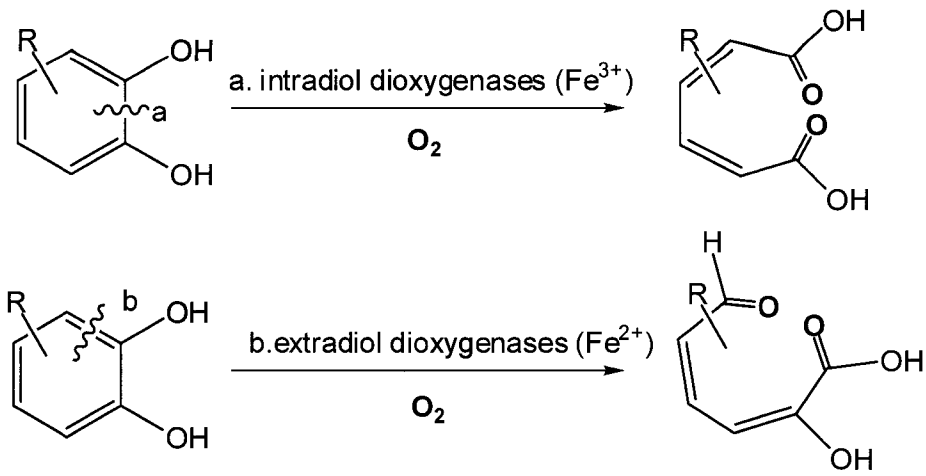

Figure 2.4 Catechol dioxygenases reactions catalyzed by intradiol and extradiol dioxygenases.

the two hydroxy groups. As shown in Figure 2.4, different oxidation states of the active metal center in these enzymes were found: Fe(III) in intradiol dioxygenases and Fe(II) in extradiol dioxygenases. Both the oxidation state of the Fe center and coordination geometry around the metal have been proposed as possible reasons for the observed ring cleavage sites.[11,12] However, it is still an unfinished puzzle as to how the enzyme controls the selection of these two reaction pathways.[13]

Catechol dioxygenases are also able to catalyze a step in the microbial degradation of benzoic acids (including chlorinated benzoic acids); Figure 2.5 illustrates the reactions in some detail.

b. Structural information for catechol dioxygenase enzymes

Although the first dioxygenase enzyme was discovered in 1950, it was 1988 before the first X-ray crystal structure of a catechol dioxygenase (the intradiol-cleavage

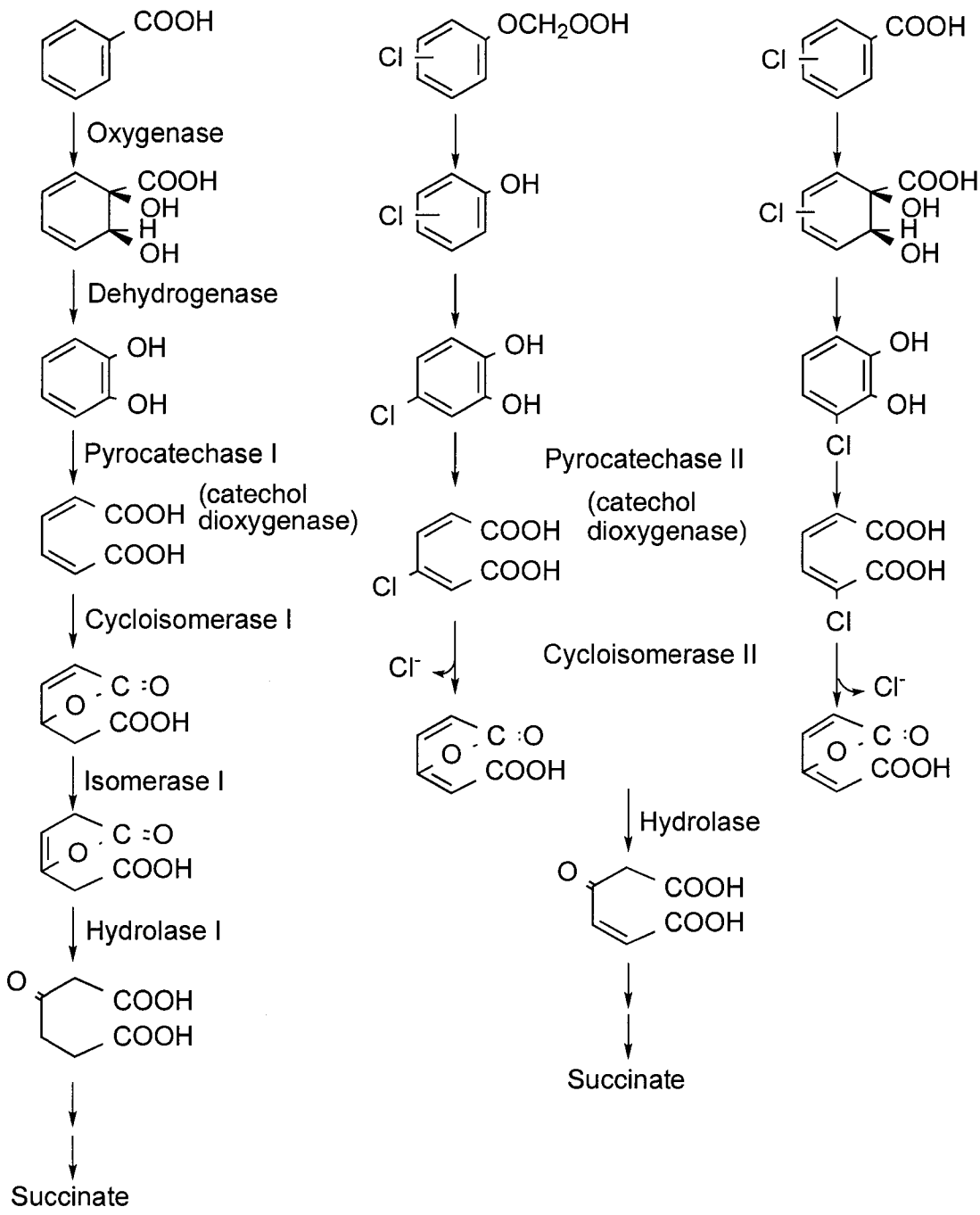

Figure 2.5 Catechol dioxygenases (pyrocatechase I and II) reactions in the degradation of benzoic acid, chlorophenoxyacetic acids and chlorobenzoic acids.[14,i] Reprinted from reference 15.

[i] Specificity matters in the degradation pathway; that is, not all chlorinated substrates are degraded at the same rate. For the substrates in Figure 2.5, 4- and 2,4-dichlorophenoxyacetic acids and 3-, 4- and 3,5-dichlorobenzoic acids degrade much easier than the other substrates shown.[14]

protocatechuate 3,4-dioxygenase from *Pseudomonas putida)* was solved by Ohlendorf and co-workers.[15] The non-heme Fe(III) cofactor is ligated by four amino groups and a solvent molecule (two histidine groups, two tyrosine groups, and a water molecule) in a trigonal bipyramidal geometry.[15] A similar active site was found for another intradiol-cleavage enzyme, catechol 1,2-dioxygenase from *Acinetobacter* sp. ADP1.[16] By X-ray crystallography, six catechol dioxygenases have been structurally characterized as summarized in Table 2.2.

Table 2.2 Summary of Crystallized Catechol Dioxygenases.

	Type of cleavage	Source material	Fe	Active site	Ref.
Catechol 1,2 dioxygenase (1,2-CTD)	Intradiol	*Acinetobacter* sp. ADP1	III	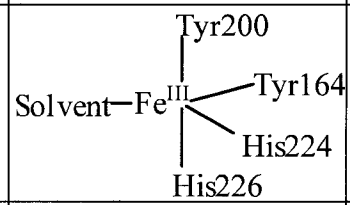	16
Protocatechuate 3,4-dioxygenase (3,4-PCD)	Intradiol	*Pseudomonas putida, Acinetobacter calcoaceticus* and *Acinetobacter* strain ADP1	III	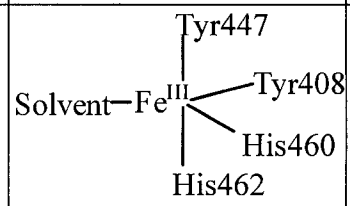 from *Pseudomonas putida*	15,17, 18,19
2,3-Dihydroxybi-phenl dioxygenase (BphC)	Extradiol	*Pseudomonas cepacia* LB400, *Pseudomonas* sp. strain KKS102	II	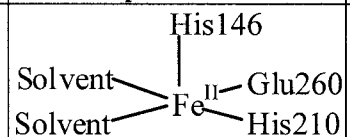 from *Pseudomonas cepacia* LB400	20,21, 22
Catechol 2,3-dioxygenase (2,3-CTD)	Extradiol	*Pseudomonas putida mt-2*	II	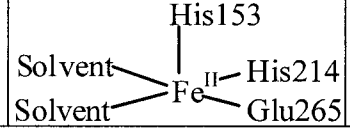	23

Protocatechuate 4,5-dioxygenase (4,5-PCD)	Extradiol	*Sphingomonas paucimobilis* SYK-6	II	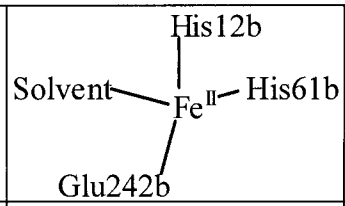	24
Human homogentisate dioxygenase	Extradiol	Selenomethionine substituted (SeMet) homogentisate dioxygenase	II	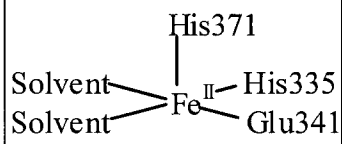	25

Commonly, extradiol dioxygenases have two histidine groups, one glutamic acid group and one or two molecules of solvent ligated to their Fe^{II} centers. For both intradiol and extradiol enzymes, two *cis*- sites on the metal are vacant for the coordination of the bidentate substrate, catechol. In the case of intradiol dioxygenases, the axial tyrosine group and equatorial solvent group dissociate upon substrate binding; extradiol dioxygenases bind the substrate with the loss of two coordinated solvent molecules.[26,27,28,29] Studies on the enzyme substrate binding mode were performed using different catecholate substrates and inhibitors (e.g., cyanide and nitric oxide as inhibitors).[28]

c. Catechol dioxygenase model systems

Along with the research on enzymatic catechol dioxygenases, biomimetic studies of catechol dioxygenases are also a topic of intensive investigations.[6,7,30] Fe-containing model compounds constitute the major fraction of all catechol dioxygenase model systems used to mimic the native enzymes (Table 2.2); non-Fe dioxygenase model systems are less well studied. Among the systems using other metals, V-containing systems are the focus of our research and will appear in the following chapters. 3,5-Di-

tert-butylcatechol (hereafter 3,5-DTBC) is chosen as the substrate in most of the model studies due to its comparatively high activity (two electron donating groups on the aromatic ring) and the ease of separating and identifying its oxygenated products.

i. Fe systems

Funabiki and co-workers first showed that a mixed solution of 3,5-DTBC with $Fe^{2+/3+}$, 2,2'-bipyridine and pyridine in THF gives both the intradiol and the extradiol oxygenation products besides the autoxidation product, 3,5-di-*tert*-butylbenzoquinone.[31,32,33] In 1982, Weller and Weser reported the first Fe complex which acts as an analog of the enzyme-substrate complex of pyrochatechase $[Fe^{III}(NTA)(DBC)]^{2-}$ (NTA is nitrilotriacetate, DBC is 3,5-di-*tert*-butylcatecholate anion).[34] Following up on this important model, Que and co-workers identified the structure of $[Fe^{III}(NTA)(DBC)]^{2-}$ by X-ray crystallography. Additionally, $^{18}O_2$-labeling study showed the clean incorporation of a single ^{18}O label into the product.[35,ii] Since then, many [Fe(L)(Cat)] complexes have been synthesized with a variety of tetradentate or tridentate ligands L and substituted catechols Cat (see a focused review[30] listing all the [Fe(L)(Cat)] complexes as of 2002 and a recent review[7] as of 2004).

Que and co-workers have made significant progress modeling Fe-systems and in related mechanistic studies.[35,36,37,38] The best Fe model system to date for intradiol cleavage is $[Fe^{III}(TPA)DBC]BPh_4$ (TPA is tris(2-pyridylmethyl)amine, a tetradentate ligand) synthesized by Que et al.[38] This complex reacts with oxygen within minutes,

[ii] The other ^{18}O label was in the water as an end product from the ring-closure step of 2,4-di-*tert*-butyl-2,4-hexadienedioic acid to product **2**, Figure 2.6.

producing intradiol cleavage products in 98% yield.[39,iii] The high activity is correlated with the semiquinone character in the TPA complex, resulting from an electron transfer from the ligand DBC to the Fe^{III} center.

Extradiol-cleavage biomimetic models make use of tridentate ligands. The best systems to date are formulated as $[Fe^{III}(L)(DBC)]Cl$ (L = TACN or Me_3TACN, where TACN stands for the tridentate ligand 1,4,7-triazacyclononane). These systems produce near-quantitative yields of extradiol cleavage products with or without addition of Lewis bases (the Lewis bases' role is not totally clear but is thought to coordinate to the metal center).[12,40,41] Unfortunately, although most extradiol catechol dioxygenase enzymes have Fe^{II} in the active site, these extradiol model systems are Fe^{III} complexes because the Fe^{II}-hydrogencatecholate is easily oxidized by O_2 to form an Fe^{III}-catecholate complex.[7]

ii. V systems

Vanadium-dependent catechol dioxygenases have not yet been discovered: however, reports of vanadium complexes used as models of catechol dioxygenase enzymes are common in the literature, Table 2.3. Tatsuno et al. first found that simple vanadium complexes, such as $VO(acac)_2$ (acac = acetylacetonate), could react with 3,5-DTBC and oxygen to generate a mixture of intradiol and extradiol cleavage products as well as the autoxidation product, **6**, Figure 2.6.[42]

All of the products in Figure 2.6 have been previously characterized.[43,44,45] Product **4** appeared in an earlier report with an incorrect structure,[46] but was crystallized and unequivocally characterized by Weiner and Finke in 1999.[47] Weiner and Finke also

[iii] 98% intradiol cleavage products are composed of 60% anhydride (product **2** in Figure 2.6) and 38% furanone acid (product **5** in Figure 2.6). Notably, the system of potassium or sodium 3,5-di-*tert*-butylcatecholate plus dioxygen without catalyst gives 20–60% furanone acid (product **5**).[39]

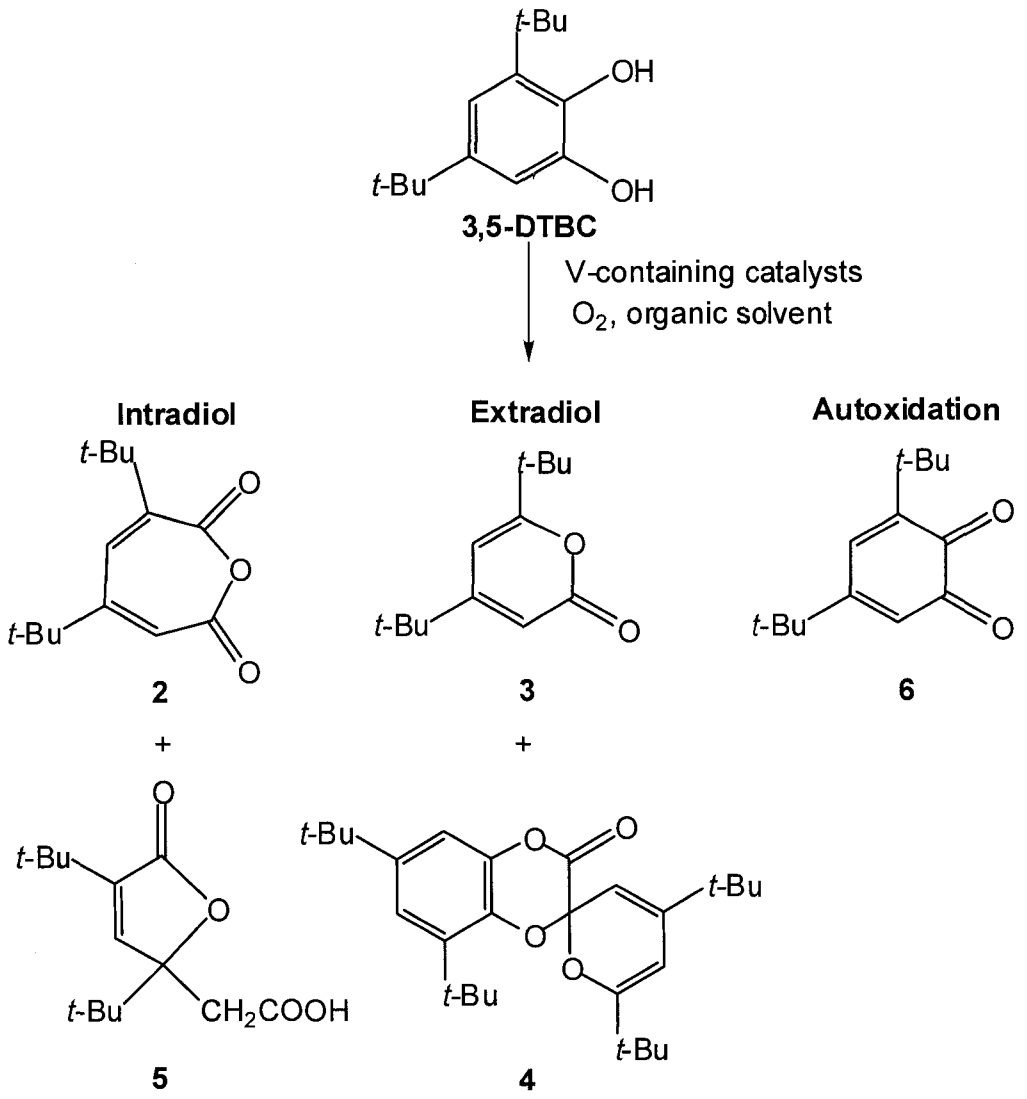

Figure 2.6 General reaction scheme of vanadium-containing dioxygenase analogs: **2**, 3,5-di-*tert*-butyl-1-oxacyclohepta-3,5-diene-2,7-dione; **3**, 4,6-di-*tert*-butyl-2-pyranone; **4**, spiro[1,4-benzodioxin-2,2'-pyran]-3-one, 4', 6, 6', 8-tetrakis(1,1-dimethylethyl); **5**, 3,5-di-*tert*-butyl-5-(carboxymethyl)-2-furanone; and **6**, 3,5-di-*tert*-butyl-1,2-benzoquinone.[47]

achieved excellent mass balance (94 ± 5 %) and improved the catalytic lifetime abilities of vanadium-containing dioxygenases by at least two orders of magnitude (total turnovers, TTOs, extended from ~500 to ~100,000). To date, there are eleven publications of vanadium-containing complexes showing dioxygenase-like activity, Table 2.3.

Table 2.3 Vanadium-Containing Systems With Dioxygenase Activity.

Entry	Precatalyst(s)[a]	Product Distributions	Mass Balance and TTO	Ref
1	$VO(acac)_2$, VO(salen), VCl(salen) and VCl(saldpt)	**2** = 39–43%; **3** = 6–15%; **6** = 22–28%	Mass balance ≤ 83% [b]TTO_{max} = 1000; [c]TTO_{conv} = 1000; [d]TTO_{yield} ≤ 750	42
2	$[V(salen)(DbcatH)_2]\cdot 1/2CH_2Cl_2$ and $[V(saldpt)(DBcatH)]\cdot CH_2Cl_2$[e]	**2** = 42%; **3** = 11%; **6** = 24%	Mass balance = 77% TTO_{max} = 100; TTO_{yield} = 77	48
3	$[VO(acac)(OCH_3)]_2$, $[VO(tmh)(OCH_3)]_2$, $(VOaap)_2$, $(VOdmba)_2$, $(VOdba)_2$ and $(VO(acac)OCH_3)_2$	**2** = 46–48%; **3** = 7–10%; **6** = 22–25%	Mass balance ≤ 82% TTO_{max} = 100; TTO_{conv} = 100; TTO_{yield} ≤ 82	49
4	[LVO(acac)], $[LVO(phen)]^+PF_6^-$ and $[LVO(bipy)]^+PF_6^-$	**2** < 10%; **6** = 70%	Mass balance < 80%	50
5	VO(acac)(TCCat)	**2** = 45%; **3** = 6%; **6** = 24%	Mass balance = 75% TTO_{max} = 100; TTO_{yield} = 75	51
6	$PV_{14}O_{42}^{9-}$, $MnV_{13}O_{38}^{7-}$, $NiV_{13}O_{38}^{7-}$ and $VO(acac)_2$	**2** = 34–36%; **3** = 11–20%; **4** = 3–13%; **6** = 15–21%	Mass balance ≤ 82% TTO_{max} = 100; TTO_{yield} ≤ 82	46
7	[VO(acac)(DTBCat)]	**2** = 45%; **3** = 6%; **6** = 24%	Mass balance = 75%	52
8	*cis*-$V_2W_4O_{19}^{4-}$, 1,4,9-$[PV_3W_9O_{40}]^{6-}$, $V_{10}O_{28}^{6-}$ and $VO(acac)_2$	**2** = 15–39%; **6** = 5–19%	Mass balance ≤ 58% TTO_{max} = 100; TTO_{yield} ≤ 58	53
9	$VO(HL)_2OH$, $(VO)_2L_2SO_4\cdot 4H_2O$	**2** = 45–48%; **3** = 5–10%; **6** = 23–25%	Mass balance ≤ 82% TTO_{max} = 100; TTO_{conv} = 100; TTO_{yield} ≤ 82	54
10	TEA[VO(TEA)]	**2** = 80% (should be the sum of **2** and **6** due to its "red" color) **5** = 3%	Mass balance ≤ 82% TTO_{max} = 10; TTO_{yield} = 8.2	55

11	$SiW_9V_3O_{40}^{7-}$, $Fe^{II}{\cdot}SiW_9V_3O_{40}^{5-}$, $P_2W_{15}V_3O_{62}^{9-}$, $Fe^{II}{\cdot}P_2W_{15}V_3O_{62}^{7-}$, $PV_{14}O_{42}^{9-}$, $VO(acac)_2$, etc. (28 catalysts total)	**2** = 40–57%; **3** = 6–15%; **4** = 10–18%; **6** = 9–25%	Mass balance ≤ 94% TTO_{max} = 4500; TTO_{conv} = 4500; $TTO_{yield} \leq 4230$ $TTO_{conv\ or\ yield} \geq$ 100,000 when TTO_{max} = 129,000	47

[a]The inactive vanadium-containing precatalysts that are not listed in the above table, but are listed here, as the following: $[V(salen)(cat)]{\cdot}0.1CH_2Cl_2$ and $[V(salen)(4\text{-}Bcat)]{\cdot}H_2O$;[48] $Na[VO(DBcat)_2]$ and $Na_2[VO(OCH_3)(DBcat)_2]$;[46] VO(acac)(cat) and VO(acac)(3-Bcat);[52] $VW_5O_{19}^{3-}$;[53] VO(NTA)[55] and $SiW_{11}VO_{40}^{5-}$.[47]

[b]TTO_{max} is the maximum TTO number possible, calculated using the equation $moles_{substrate}/moles_{precatalyst}$.

[c]TTO_{conv} is the experimentally observed TTO based on $moles_{substrate,\ consumed}/moles_{precatalyst}$.

[d]TTO_{yield} is the experimentally observed TTO based on $moles_{sum\ of\ products}/moles_{precatalyst}$.

[e]The product distribution was not reported for the denoted precatalyst.

[f]Abbreviations: salen ≡ ethylenebis(salicylideneaminato); saldpt ≡ *N,N'*-(3,3'-dipropylamine)bis(salicylideneaminato); tmh ≡ 2,2,6,6-tetramethylheptandione; H_2aap ≡ *o*-hydroxyacetophenone; H_2dmba ≡ 1,5-bis(*p*-methoxyphenyl)-1,3,5-pentanedione; H_2dba ≡ 1,5-diphenyl-1,3,5-pentanetrione; L (entry 4) ≡ $[\eta\text{-}CpCo\{P(O)(OC_2H_5)_2\}_3]^-$; bipy ≡ 2,2'-bipyridine; TCCat ≡ tetrachlorocatecholate; DBcat/DTBCat ≡ 3,5-di-*tert*-butylcatecholate; H_2L (entry 9) ≡ 2,2'-dihydroxy-3,3'-diacetyl-5,5'-dichlorodiphenylmethane; TEA ≡ triethanolamine; cat ≡ pyrocatecholate; Bcat ≡ *tert*-butylcatechol; and NTA ≡ nitrilotriacetic acid.

Similar product ratios of these V-containing systems are listed in Table 2.3: the intradiol-cleavage product is the major product (product **2** in Figure 2.6, 40–50%), followed by the autoxidation product (product **6**, 20–30%) and then extradiol-cleavageproducts (product **3** and **4**, 10–20% in sum). Pierpont mentioned this similarity in his 1994 review, but no further explanation was provided.[56] The only exception to this product ratio is observed when using vanadium complexes with a bulky ligand.[50] We suggest that the bulky ligand system, $[LVO(acac)]$, $[LVO(phen)]^+PF_6^-$ and $[LVO(bipy)]^+PF_6^-$ where L is $[\eta\text{-}CpCo\{P(O)(OC_2H_5)_2\}_3]^-$, gives a different product ratio because the vanadium coordination environment is not optimal for substrate and oxygen binding due to the bulky, tridentate ligand attached to vanadium. In the following

chapters, our research results and insights into the reasons for the similar selectivities in the various different vanadium model systems will be presented.

iii. Other systems

Researchers have also investigated the biomimetic abilities of other model systems with metal ions besides Fe and V, namely Cu, Rh, Ru, Co, Mn and Ir. The oxidative cleavage reaction of catechol with oxygen catalyzed by CuCl and pyridine was first discovered by Tsuji et al. in 1975.[57,58] Later, Rogic and co-workers found that the same reaction would also proceed with or without oxygen.[43,59] A (η^1-superoxo)(η^2-semiquinonato)Rh(III) complex has been reported for which less than 10% of its products originate from oxidative cleavage.[60] The complex $RuCl_2(PPh_3)_3$ was reported to produce a mixture of oxidative cleavage products (intradiol:extradiol = 26:64) in 90% yield.[61] Currently, Cu, Co, Mn and Ir are studied mostly for their roles in the autoxidation of 3,5-DTBC to 3,5-di-*tert*-butyl-1,2-benzoquinone.[39,62,63,64,65]

III. Mechanism of Catechol Dioxygenases

a. Intermediate isolation

Isolation of a reaction intermediate can dramatically assist in the elucidation of a reaction mechanism. Two metal-O_2-catecholate adducts have been isolated and characterized and serve as structural analogs of possible intermediates in the catechol dioxygenase catalytic cycle:[6] [(triphos)Rh(η^1-O_2)(η^2-3,5-DBSQ)]$^{(+)}$[60]and [(triphos)Ir-(O-O)-(3,5-DBSQ)]$BPh_4 \cdot 0.5CH_2Cl_2$[64,66] (triphos, $MeC(CH_2PPh_2)_3$; 3,5-DBSQ, 3,5-di-tert-butylsemiquinonate), Figure 2.7. The crystal structures of [(triphos)Ir-(O-O)-(phenSQ)]

$BPh_4 \cdot 0.5CH_2Cl_2$ (phenSQ = 9,10-phenanthrenesemiquionate) and $[Rh(PPh_3)_2(O_2$-phenSQ)Cl]$\cdot C_6H_6$ have been reported.[66,67]

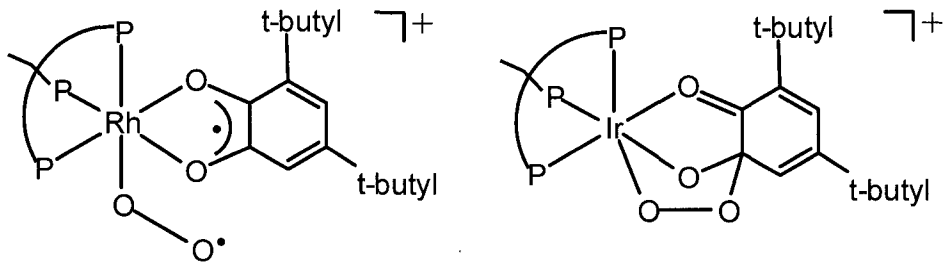

Figure 2.7 Structures of two metal catecholate-oxygen complexes which are thought to serve as models of possible intermediates.

As Halpern notes, detectable intermediates in a catalytic process are often not involved in the catalysis.[68] This is probably true for catechol dioxygenase catalytic systems as well. The two adducts in Figure 2.7 are not very reactive for catechol dioxygenase catalysis: the Rh adduct catalyzes the oxidative cleavage of 3,5-DTBC giving 92% of the autoxidation product and less than 10% of the other products;[60] the Ir intermediate catalyzes 3,5-DTBC oxidation mostly in an autoxidation manner.[66] Similarly, this helps to explain why no Fe (or V) catechol-oxygen intermediate has been reported yet—they are too unstable and thus reactive.

b. Intradiol mechanism

A novel substrate activation mechanism has been proposed based on the biomimetic studies by Que and co-workers.[38,69,70] It was hypothesized that intradiol catechol dioxygenases operate beginning with the activation of the catechol substrate by the Fe(III) metal center to form a Fe(II)-semiquinone complex (step 1 in Figure 2.8).

Oxygen is then bound to the activated substrate, and the bound peroxy radical binds with the Fe(II) center giving an Fe(III)-O_2-catecholate complex, step 2 in Figure 2.8. This Fe(III)-O_2-catecholate ternary compound is analogous to the Ir-O_2-catecholate adduct shown in Figure 2.7. A Criegee-type rearrangement affords muconic acid anhydride, as shown in step 4 below.

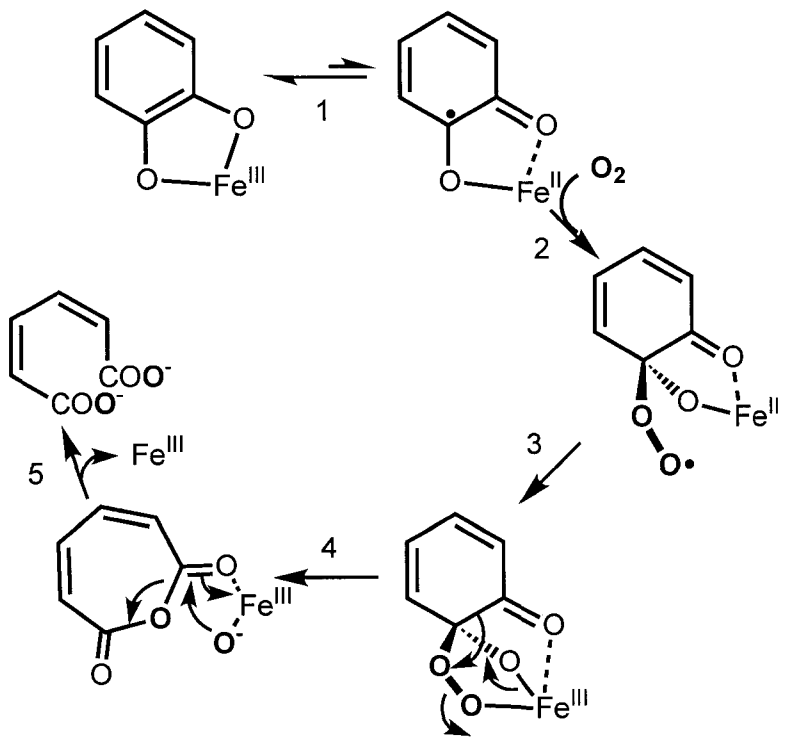

Figure 2.8 Substrate activation mechanism for intradiol catechol dioxygenases by Que et al.[6]

Bugg and co-workers have proposed a supplementary mechanism for the final step of the acyl group migration involving a benzene oxide-oxepin interconversion based on C–C cleavage reactions of catechol analogs, 6-acetoxycyclohexa-2,4-dienones.[71]

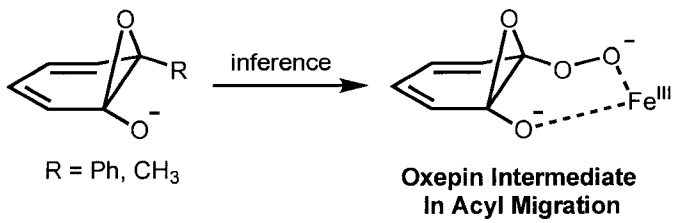

c. Extradiol mechanism

Extradiol catechol dioxygenases mechanistic studies are more difficult than those of intradiol catechol dioxygenases, in significant part due to fewer available spectroscopic tools for the Fe(II) center. Based on crystallographic and spectroscopic results[26,72] it had been hypothesized that catechol binds to Fe(II) in a bidentate, but *monoanionic,* manner as shown in Figure 2.9. O_2 then binds to the Fe(II) center, in

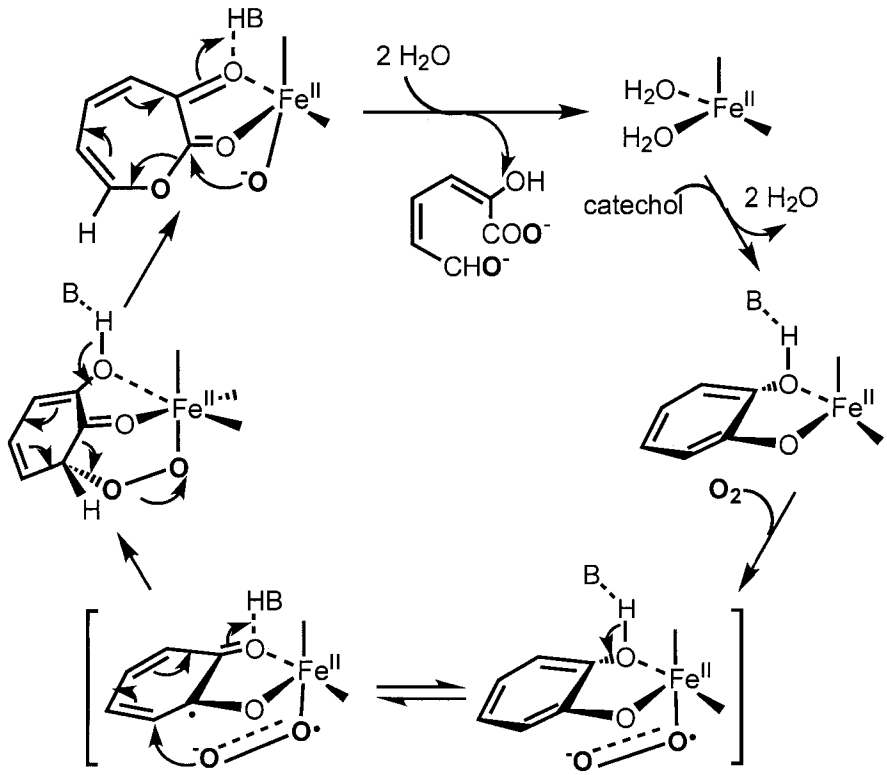

Figure 2.9 Proposed mechanism for extradiol catechol dioxygenases.[6]

contrast to its binding to the metal-activated-semiquinone in intradiol catechol dioxygenases. Electron transfer from Fe(II) to the bound oxygen is proposed to make oxygen more nucleophilic, facilitating the formation of a Fe(II)-O_2-catecholate ternary complex. Previously, this ternary complex was proposed to be distally bound (relative to either of the two oxo group bound to the metal center; for a proximally bound complex see the intermediate in the intradiol mechanism in Figure 2.8), going through a Criegee-type rearrangement to produce the observed product.[6]

In a follow-up study, Bugg and coworkers utilized synthetic analogs of both distally bound hydroperoxide and proximally bound hydroperoxide intermediates to clarify the peroxy radical binding position on the catechol ring. In their study, the –OOH functional group was replaced by a $-CH_2OH$ group and cyclohexadienone was simplified to cyclohexanone, as in Figure 2.10.

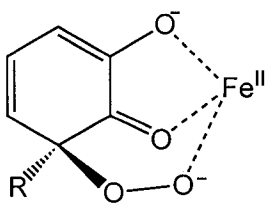

distally bound hydroperoxide

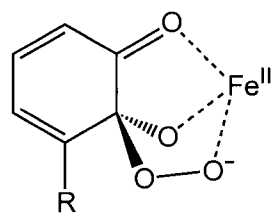

proximally bound hydroperoxide

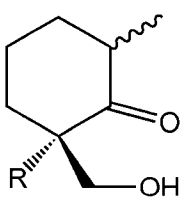

no inhibition

Axial $-CH_2OH$

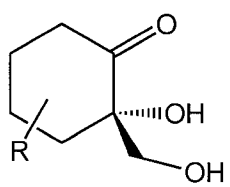

R = 3-t-butyl K_i 4.9 mM
R = 3-phenyl K_i 0.7 mM
R = 5-t-butyl K_i 7.6 mM

Equitorial $-CH_2OH$

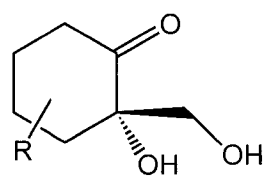

R = 3-methyl no inhibition
R = 5-t-butyl no inhibition

Figure 2.10 Synthesized carba-analogs and inhibition study results for 2,3-dihydroxyphenylpropionate 1,2-dioxygenase (MhpB) extradiol enzyme.[73]

Inhibition studies using these carba-analogs showed that proximally bound analogs with axial-CH_2OH could inhibit the MhpB enzyme (extradiol-cleavage), but distally bound analogs show no inhibition for the MhpB enzyme.[73] These inhibition studies disprove the presence of a distally bound hydroperoxide intermediate in the extradiol catechol dioxygenase mechanism. However, some inconsistencies exist in this study: proximally bound analogs with equatorial-CH_2OH inhibited an intradiol-cleavage enzyme (3,4-PCD) in one case and failed to inhibit cleavage in another case.[73] From these studies, a common proximal hydroperoxide intermediate is implicated. Consequently, the mechanisms of both intradiol and extradiol catechol dioxygenases converge to the same intermediate, as shown in Figure 2.11.

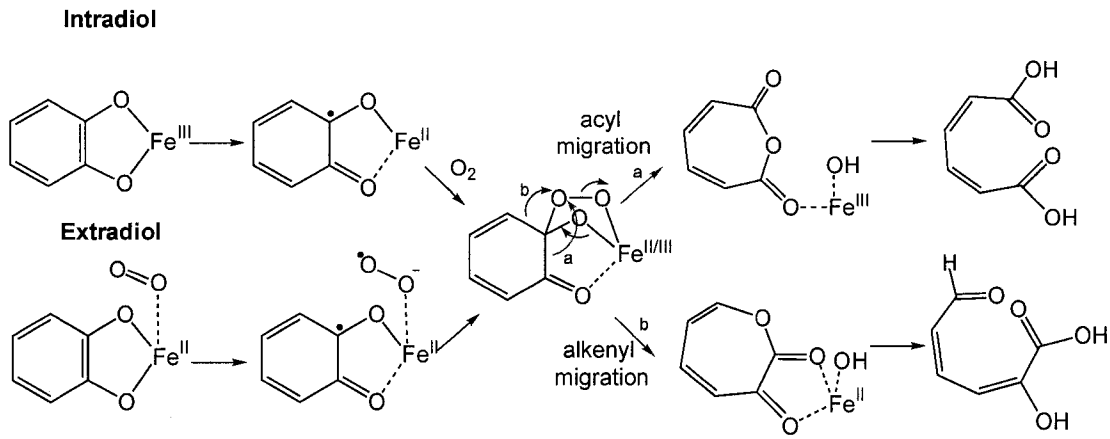

Figure 2.11 Mechanism of intradiol and extradiol catechol dioxygenases with a common proximal hydroperoxide intermediate.[13,73]

So, what controls whether catechol cleavage proceeds via the intradiol or extradiol pathway? Two hypotheses have been forwarded to answer this question. First, Lipscomb and co-workers proposed that the redox state of the active center Fe determined the ring cleavage site.[11,74] This is consistent with the observation of different oxidation states in the native catechol dioxygenases: Fe(III) in intradiol catechol

dioxygenases and Fe(II) in extradiol catechol dioxygenases. Later, the model studies by Jo and Que,[12] and the inhibition studies performed by Bugg and co-workers,[73] emphasized the importance of the coordination geometry of the metal center. Specifically, Jo and Que could tune the regiospecificity and selectivity of [(L)Fe^{III}(DBC)]Cl complexes by using different ligands having different geometries. Notably, an extradiol-cleavage model complex with an Fe(III) active site and with a tridentate ligand bound to the metal gives almost quantitatively extradiol products.[12] This emphasizes the observation that the influence of the coordination geometry of the metal center on selectivity is stronger than that of the oxidation state of the metal center. Bugg proposed that the coordination chemistry of the metal center, and specifically the configuration of the hydroperoxide O-O bond, leads to different reaction pathways. They found that an axial position of the superoxide O-O bond leads to extradiol cleavage, while an equatorial position favors intradiol cleavage.[73] A recent study of an extradiol dioxygenase homoprotocatechuate (HPCA) 2,3-dioxygenase showed the unprecedented ability to catalyze intradiol cleavage by mutating a second sphere residue (histidine) near the iron site.[75] This result illustrates the importance of the geometry of the ternary enzyme-substrate-O_2 complex over the oxidation state of the metal center. In summary, a definitive elucidation of the selectivity puzzle remains to be completed.

IV. Polyoxometalates in Selective Oxidations

a. Introduction to polyoxometalates

Polyoxometalates (or polyoxoanions, heteropolyanions, etc.) are a broad class of metal oxide compounds, $M_xO_y^{n-}$ or $M_xX_mO_y^{n-}$ where M is a heteroatom (Si and P are the

most common) and X is an addenda atom (oftentimes W or Mo). There are two basic structural types of polyoxometalates: Keggin type (struture analogous to $PW_{12}O_{40}^{3-}$) and Wells-Dawson type (structure analogous to $P_2W_{18}O_{62}^{6-}$), Figure 2.12.[76,77,78,79]

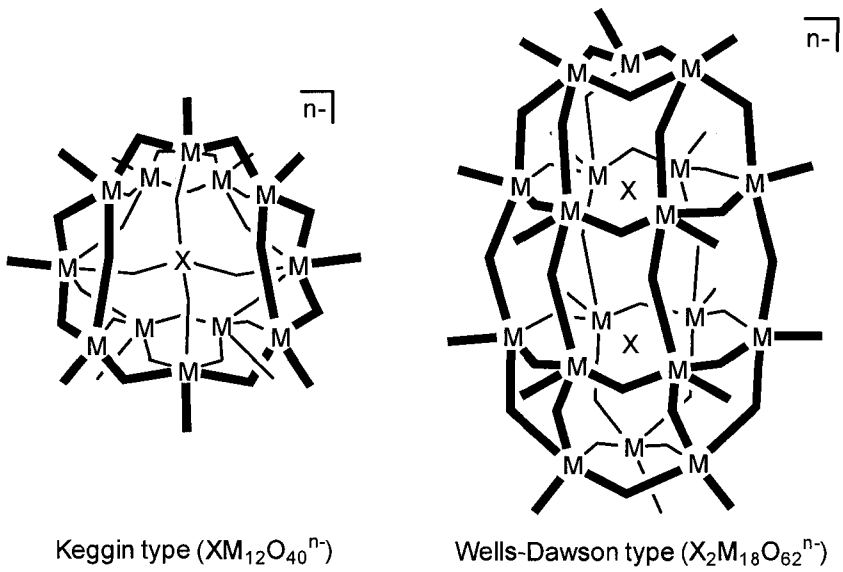

Keggin type ($XM_{12}O_{40}^{n-}$) Wells-Dawson type ($X_2M_{18}O_{62}^{n-}$)

Figure 2.12 Keggin type and Wells-Dawson type polyoxometalates.

Polyoxometalates have been studied extensively in catalysis, especially in oxidation catalysis. First, there are a great number of polyoxometalates with unique structures and properties. Structure variation and different addenda atoms can impart distinct catalytic abilities to specific polyoxometalate compounds. Polytungstovanadate or polymolybdovanadate mixed-addenda catalysts (e.g., $H_6PW_9V_3O_{40}$, $(NH_4)_5H_4PMo_6V_6O_{40}$) are good catalysts for the oxidation of alkanes by O_2.[80] $K_5ZnPW_{11}O_{39}$ and several other polyoxometalates are effective catalysts for H_2S oxidation by molecular oxygen to form high purity sulfur (S_8, >99.5%).[81] Polyoxometalates are discrete, modifiable and fully characterizable at the molecular level (for example, by X-ray crystallography, mass spectrometry and multinuclear NMR).[79]

Second, polyoxometalates have high thermal stabilities, generally up to 350 °C under oxygen. This characteristic is important for high-temperature gas-phase or liquid-phase oxidations of hydrocarbons with molecular oxygen. Compared to non-stoichiometric or amorphous transition-metal oxides, commonly used in industrially important petrochemical oxidations, polyoxometalates are better compositionally and structurally defined. Third, polyoxometalates are inherently resistant to oxidation due to their all-inorganic nature. This property has opened the possibility of replacing easily self-oxidized organometallic compounds with oxidation-resistant polyoxometalates. A well-known example is the Catalytica catalyst system for ethylene oxidation using ~0.1 mM Pd^{II}, ~5–25 mM Cl^-, and ~0.30 M phosphomolybdovanadic acid partial salt $\{Na_yH_{(3+x-y)}PMo_{(12-x)}V_xO_{40}\}$.[82] The V^V-containing polyoxometalate functions as an oxidant to couple with the Pd^{II}/Pd^0 redox cycle in which ethylene is oxidized by the $Pd^{II}Cl_n^{(2-n)+}$ active species. The reduced V^{IV}-polyoxometalate is regenerated by O_2 and oxidized at temperatures ≥100 °C as fast as O_2 can diffuse into the solution. Fourth, polyoxometalates are synthesized by self-assembly in acidic solutions from simple metal oxides such as WO_4^{2-} or MoO_4^{2-}. Fifth, the solubilities of polyoxometalates are tunable by changing their countercations. Specifically, heteropolyacids (protonated polyoxometalates) are soluble in water and most protic and aprotic polar solvents and their other cation salts can often be made simply by adding these cations (e.g., Na^+, K^+, Cs^{2+}, etc.). Organic solvent soluble polyoxometalates can be obtained by reacting heteropolyacids with an organic base (e.g., tetrabutylammonium hydroxide) followed by the removal of water. In summary, polyoxometalates are excellent candidates for the developments of new oxidation catalysts.

b. Polyoxometalates in dioxygenase model studies

Two publications concerning the applications of polyoxometalates in biomimetic dioxygenase catalysis have been published prior to our work. The first one utilizes $PV_{14}O_{42}^{9-}$, $MnV_{13}O_{38}^{7-}$ and $NiV_{13}O_{38}^{7-}$ to react with 3,5-DTBC in organic solvents.[46] This study, however, did not provide kinetic studies of the catalyst evolution, nor did it provide any clear idea of the true nature of the catalysts.

The other study is based on a ruthenium-substituted, sandwich-type polyoxometalate, $[WZnRu^{III}_2(OH)(OH_2)(ZnW_9O_{34})_2]^{11-}$, which is reported to be an inorganic "dioxygenase" in a 1997 *Nature* paper,[83] Figure 2.13.[83,84]

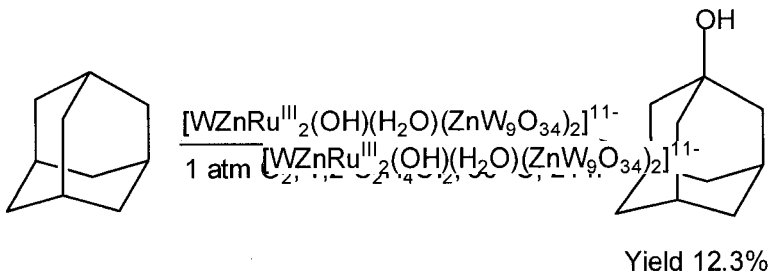

Figure 2.13 Reaction scheme showing the Ru-incorporated, sandwich-type POM catalyst of adamantane hydroxylation.[83,84]

This second system is interesting and intriguing when considering several experimental observations.[83,84] The sandwich polyoxometalate catalyst system reacts slowly with alkanes, yet not at all with olefins (surprising considering the lower C–H allylic BDE of olefins vs alkanes) except after a pre-incubation period with 1,2-dichloroethane solvent and O_2. This system exhibits a long induction period before oxidation occurs, which strongly suggests that the polyoxometalate is not the true

catalyst. A re-investigation of this claimed inorganic dioxygenase is included as Chapter V of this work.

In the history of the application of polyoxometalates in catalysis by our research group, polyoxometalate-supported organometallic compounds (i.e., (1,5-COD)Ir·$P_2W_{15}Nb_3O_{62}^{8-}$, where 1,5-COD stands for 1,5-cyclooctadiene) have been successfully used as transition metal nanocluster precursors, with the polyoxometalate ultimately serving as a superior anionic stabilizer of nanoclusters.[79] In oxidation catalysis, niobium-containing and vanadium-containing polyoxometalates were found to act as inorganic analogs of catechol dioxygenase enzymes.[47,85] The niobium counterpart reacts stoichiometrically, providing useful stoichiometric (1: 1: 1 for 3,5-DTBC: O_2: Fe^{II}·$P_2W_{15}Nb_3O_{62}^{7-}$). Kinetic results were also obtained.[85] The vanadium-containing systems, mentioned in the previous section where V model systems were discussed, gave an excellent 94 ± 5% mass balance with the definitive characterization of a previously misidentified product (**4**), Figure 2.14. Additionally, a record (over 100,000 TTOs)

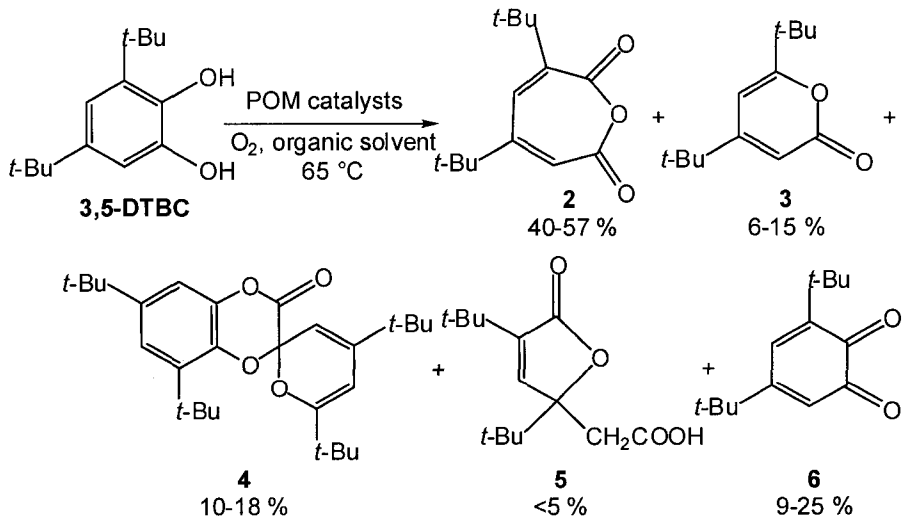

Figure 2.14 Reaction scheme and product distribution in the catalytic oxygenation of 3,5-DTBC.[47]

catalytic lifetime abilities was demonstrated by one of the vanadium-containing polyoxometalates, $(n\text{-}Bu_4N)_5[Fe^{II}\cdot SiW_9V_3O_{40}]$.[47] However, the true catalyst in these systems remained to be identified and is one goal of this thesis.

Mizuno and co-workers have studied the Keggin-type polyoxometalate $[\gamma\text{-}SiW_{10}\{Fe^{3+}(OH_2)\}_2O_{38}]^{6-}$ for the selective epoxidation of several alkenes with molecular oxygen, Figure 2.15.[86] Good to excellent selectivities and 10^3~10^4 turnover numbers were obtained. Interestingly, for the epoxidation of cyclooctene to cyclooctene oxide, the amount of epoxide produced is about twice the amount of oxygen consumed. This ~2:1 stoichiometry implies that the polyoxometalate $[\gamma\text{-}SiW_{10}\{Fe^{3+}(OH_2)\}_2O_{38}]^{6-}$ is an inorganic dioxygenase for the epoxidation of cyclooctene. There are some flaws in the inhibition experiments, however (the [inhibitor] used may be too low),[86] as well as in the interpretation of the adamantane selectivity results (a tertiary/secondary C–H bond selectivity of 11 actually falls within the range of free-radical reaction selectivities, 3–20).[87] The same polyoxometalate $[\gamma\text{-}SiW_{10}\{Fe^{3+}(OH_2)\}_2O_{38}]^{6-}$ was reported earlier to catalyze the oxidation of cyclohexane via a free-radical autoxidation mechanism.[88] History also shows that it is dangerous to make mechanistic conclusions on the basis of studying only one olefin (or one alkane, in the case of adamantane[83,84]).

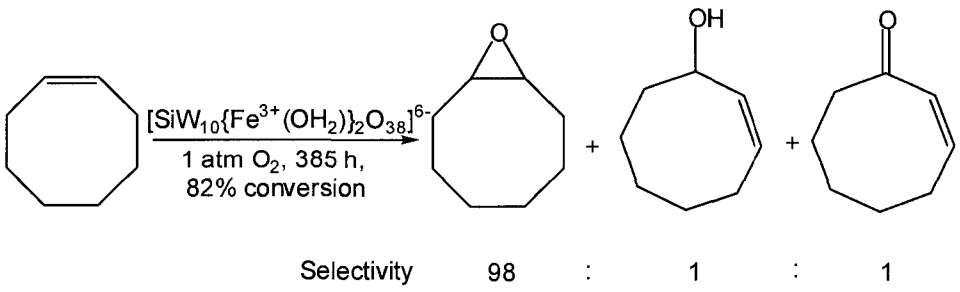

Figure 2.15 Reaction scheme of cyclooctene epoxidation using Mizuno's Fe-incorporated catalyst.[86]

In summary, catalysis using polyoxometalates has shown good selectivity and long catalytic lifetime in the above examples. As such, polyoxometalates are good model systems to be explored in oxidation catalysis. Unfortunately, some studies do not have enough evidence to rule out the presence of a free-radical-chain mechanism.[83,84] It is fulfilling this gap, namely the identification of the true catalysts and whether or not free-radical-chain or true dioxygenase mechanisms are operative, that is the focus of this thesis.

V. References

[1] Oyama, S. T.; Desikan, A. N.; Hightower, J. W. In *Catalytic Selective Oxidation*; Oyama, S. T., Hightower, J. W., Eds.; ACS Symposium Series 523; American Chemical Society: Washington, D. C., 1993, pp 1-14.

[2] Hill, C. L.; Weinstock, I. A. *Nature* **1997**, *388*, 332-333.

[3] Hill, C. L. *Nature* **1999**, *401*, 436-437.

[4] Sheldon, R. A. In *Biomimetic Oxidations Catalyzed by Transition Metal Complexes*; Meunier, B., Ed.; Imperial College Press: London, 2000, pp 613-662.

[5] Wallar, B. J.; Lipscomb, J. D. *Chem. Rev.* **1996**, *96*, 2625-2657.

[6] Que, L., Jr.; Ho, R. Y. N. *Chem. Rev.* **1996**, *96*, 2607-2624.

[7] Costas, M.; Mehn, M. P.; Jensen, M. P.; Que, L., Jr. *Chem. Rev.* **2004**, *104*, 939-986.

[8] Hayaishi, O.; Katagiri, M.; Rothberg, S. *J. Am. Chem. Soc.* **1955**, *77*, 5450-5451.

[9] Hayaishi, O.; Editor *Molecular Mechanisms of Oxygen Activation*; Academic Press: New York, 1974.

[10] Nozaki, M. In *Molecular Mechanisms of Oxygen Activation*; Hayaishi, O., Ed.; Academic Press: New York, 1974, pp 135-165.

[11] Lipscomb, J. D.; Orville, A. M.; Frazee, R. W.; Miller, M. A.; Ohlendorf, D. H. In *Keio University Symposia for Life Science and Medicine*, 1998; Vol. 1, pp 263-275.

[12] Jo, D.-H.; Que, L., Jr. *Angew. Chem., Int. Ed. Engl.* **2000**, *39*, 4284-4287.

[13] Bugg, T. D. H.; Lin, G. *Chem. Commun.* **2001**, 941-952.

[14] Ghosal, D.; You, I. S.; Chatterjee, D. K.; Chakrabarty, A. M. *Science* **1985**, *228*, 135-142.

[15] Ohlendorf, D. H.; Lipscomb, J. D.; Weber, P. C. *Nature* **1988**, *336*, 403-405.

[16] Vetting, M. W.; Ohlendorf, D. H. *Structure* **2000**, *8*, 429-440.

[17] Vetting, M. W.; D'Argenio, D. A.; Ornston, L. N.; Ohlendorf, D. H. *Biochemistry* **2000**, *39*, 7943-7955.

[18] Ohlendorf, D. H.; Orville, A. M.; Lipscomb, J. D. *J. Mol. Biol.* **1994**, *244*, 586-608.

[19] Vetting, M. W.; Earhart, C. A.; Ohlendorf, D. H. *J. Mol. Biol.* **1994**, *236*, 372-373.

[20] Han, S.; Eltis, L. D.; Timmis, K. N.; Muchmore, S. W.; Bolin, J. T. *Science* **1995**, *270*, 976-980.

[21] Sugiyama, K.; Narita, H.; Yamamoto, T.; Senda, T.; Kimbara, K.; Inokuchi, N.; Iwama, M.; Irie, M.; Fukuda, M.; et al. *Proteins: Struct., Funct., and Genet.* **1995**, *22*, 284-286.

[22] Sugiyama, K.; Senda, T.; Narita, H.; Yamamoto, T.; Kimbara, K.; Fukuda, M.; Yano, K.; Mitsui, Y. *Proc. Jpn. Acad., Ser. B: Phys. Biol. Sci.* **1995**, *71*, 32-35.

[23] Kita, A.; Kita, S.-I.; Fujisawa, I.; Inaka, K.; Ishida, T.; Horiike, K.; Nozaki, M.; Miki, K. *Structure* **1999**, *7*, 25-34.

[24] Sugimoto, K.; Senda, T.; Aoshima, H.; Masai, E.; Fukuda, M.; Mitsui, Y. *Structure* **1999**, *7*, 953-965.

[25] Titus, G. P.; Mueller, H. A.; Burgner, J.; De Córdoba, S. R.; Peñalva, M. A.; Timm, D. E. *Nat. Struct. Biol.* **2000**, *7*, 542-546.

[26] Senda, T.; Sugiyama, K.; Narita, H.; Yamamoto, T.; Kimbara, K.; Fukuda, M.; Sato, M.; Yano, K.; Mitsui, Y. *J. Mol. Biol.* **1996**, *255*, 735-752.

[27] Senda, T.; Fukuda, M. *International Congress Series* **2002**, *1233*, 221-228.

[28] Orville, A. M.; Lipscomb, J. D. *Biochemistry* **1997**, *36*, 14044-14055.

[29] Orville, A. M.; Lipscomb, J. D.; Ohlendorf, D. H. *Biochemistry* **1997**, *36*, 10052-10066.

[30] Yamahara, R.; Ogo, S.; Masuda, H.; Watanabe, Y. *J. Inorg. Biochem.* **2002**, *88*, 284-294.

[31] Funabiki, T.; Sakamoto, H.; Yoshida, S.; Tarama, K. *J. Chem. Soc., Chem. Commun.* **1979**, 754-755.

[32] Funabiki, T.; Mizoguchi, A.; Sugimoto, T.; Yoshida, S. *Chem. Lett.* **1983**, 917-920.

[33] Funabiki, T.; Mizoguchi, A.; Sugimoto, T.; Tada, S.; Mitsuji, T.; Sakamoto, H.; Yoshida, S. *J. Am. Chem. Soc.* **1986**, *108*, 2921-2932.

[34] Weller, M. G.; Weser, U. *J. Am. Chem. Soc.* **1982**, *104*, 3752-3754.

[35] White, L. S.; Nilsson, P. V.; Pignolet, L. H.; Que, L., Jr. *J. Am. Chem. Soc.* **1984**, *106*, 8312-8313.

[36] Que, L., Jr.; Kolanczyk, R. C.; White, L. S. *J. Am. Chem. Soc.* **1987**, *109*, 5373-5380.

[37] Cox, D. D.; Que, L., Jr. *J. Am. Chem. Soc.* **1988**, *110*, 8085-8092.

[38] Jang, H. G.; Cox, D. D.; Que, L., Jr. *J. Am. Chem. Soc.* **1991**, *113*, 9200-9204.

[39] Speier, G.; Tyeklár, Z. *J. Mol. Catal.* **1990**, *57*, L17-L19.

[40] Dei, A.; Gatteschi, D.; Pardi, L. *Inorg. Chem.* **1993**, *32*, 1389-1395.

[41] Ito, M.; Que, L., Jr. *Angew. Chem., Int. Ed. Engl.* **1997**, *36*, 1342-1344.

[42] Tatsuno, Y.; Tatsuda, M.; Otsuka, S. *J. Chem. Soc., Chem. Commun.* **1982**, 1100-1101.

[43] Demmin, T. R.; Rogic, M. M. *J. Org. Chem.* **1980**, *45*, 4210-4214.

[44] Funabiki, T.; Mizoguchi, A.; Sugimoto, T.; Yoshida, S. *Chem. Lett.* **1983**, 917-920.

[45] Funabiki, T.; Mizoguchi, A.; Sugimoto, T.; Tada, S.; Mitsuji, T.; Sakamoto, H.; Yoshida, S. *J. Am. Chem. Soc.* **1986**, *108*, 2921-2932.

[46] Tatsuno, Y.; Nakamura, C.; Saito, T. *J. Mol. Catal.* **1987**, *42*, 57-66.

[47] Weiner, H.; Finke, R. G. *J. Am. Chem. Soc.* **1999**, *121*, 9831-9842.

[48] Tatsuno, Y.; Tatsuda, M.; Otsuka, S.; Tani, K. *Chem. Lett.* **1984**, 1209-1212.

[49] Casellato, U.; Tamburini, S.; Vigato, P. A.; Vidali, M.; Fenton, D. E. *Inorg. Chim. Acta* **1984**, *84*, 101-104.

[50] Roman, E.; Tapia, F.; Barrera, M.; Garland, M. T.; Le Marouille, J. Y.; Giannotti, C. *J. Organomet. Chem.* **1985**, *297*, C8-C12.

[51] Galeffi, B.; Postel, M.; Grand, A.; Rey, P. *Inorg. Chim. Acta* **1987**, *129*, 1-5.

[52] Galeffi, B.; Postel, M.; Grand, A.; Rey, P. *Inorg. Chim. Acta* **1989**, *160*, 87-91.

[53] Nishida, Y.; Kikuchi, H. *Z. Naturforsch., B: Chem. Sci.* **1989**, *44*, 245-247.

[54] Russo, U.; Zarli, B.; Zanonato, P.; Vidali, M. *Polyhedron* **1991**, *10*, 1353-1361.

[55] Zhang, B. Y.; Zhang, Y.; Chen, B. W.; Wang, K. *Chin. Chem. Lett.* **1997**, *8*, 547-550.

[56] Pierpont, C. G.; Lange, C. W. In *Prog. Inorg. Chem.*; John Wiley & Sons, Inc.: New York, 1994; Vol. 41, pp 331-442.

[57] Tsuji, J.; Takayanagi, H.; Sakai, I. *Tetrahedron Lett.* **1975**, 1245-1246.

[58] Tsuji, J. a. T., H. *Polyhedron* **1978**, *34*, 641-644.

[59] Rogic, M. M.; Demmin, T. R. *J. Am. Chem. Soc.* **1978**, *100*, 5472-5487.

[60] Bianchini, C.; Frediani, P.; Laschi, F.; Meli, A.; Vizza, F.; Zanello, P. *Inorg. Chem.* **1990**, *29*, 3402-3409.

[61] Matsumoto, M.; Kuroda, K. *J. Am. Chem. Soc.* **1982**, *104*, 1433-1434.

[62] Simándi, L. I.; Simándi, T. L. *J. Chem. Soc., Dalton Trans.* **1998**, 3275-3279.

[63] Bock, H.; Jaculi, D. *Angew. Chem.* **1984**, *96*, 298-299.

[64] Barbaro, P.; Bianchini, C.; Frediani, P.; Meli, A.; Vizza, F. *Inorg. Chem.* **1992**, *31*, 1523-1529.

[65] Nishinaga, A. In *Catal. Met. Complexes*; Kluwer Academic Publishers: Dordrecht, The Netherlands, 1997; Vol. 19, pp 157-194.

[66] Barbaro, P.; Bianchini, C.; Mealli, C.; Meli, A. *J. Am. Chem. Soc.* **1991**, *113*, 3181-3183.

[67] Dutta, S.; Peng, S.-M.; Bhattacharya, S. *Inorg. Chem.* **2000**, *39*, 2231-2234.

[68] Halpern, J. *Science* **1982**, *217*, 401-407.

[69] Que, L., Jr.; Kolanczyk, R. C.; White, L. S. *J. Am. Chem. Soc.* **1987**, *109*, 5373-5380.

[70] Cox, D. D.; Que, L., Jr. *J. Am. Chem. Soc.* **1988**, *110*, 8085-8092.

[71] Eley, K. L.; Crowley, P. J.; Bugg, T. D. H. *J. Org. Chem.* **2001**, *66*, 2091-2097.

[72] Shu, L.; Chiou, Y.-M.; Orville, A. M.; Miller, M. A.; Lipscomb, J. D.; Que, L., Jr. *Biochemistry* **1995**, *34*, 6649-6659.

[73] Winfield, C. J.; Al-Mahrizy, Z.; Gravestock, M.; Bugg, T. D. H. *Perkin 1* **2000**, 3277-3289.

[74] Broderick, J. B. *Essays in Biochemistry* **1999**, *34*, 173-189.

[75] Groce, S. L.; Lipscomb, J. D. *J. Am. Chem. Soc.* **2003**, *125*, 11780-11781.

[76] Pope, M. T.; Müller, A.; Editors *Polyoxometalates: From Platonic Solids to Anti-Retroviral Activity. [In: Top. Mol. Organ. Eng., 1994; 10]*; Kluwer Academic Publishers: Dordrecht, The Netherlands, 1994.

[77] Hill, C. L.; Editor *Chem. Rev.* **1998**, *98*, 1-390.

[78] Pope, M. T.; Müller, A.; Editors *Polyoxometalate Chemistry From Topology via Self-Assembly to Applications*; Kluwer Academic Publishers: Dordrecht, The Netherlands, 2001.

[79] Finke, R. G. In *Polyoxometalate Chemistry From Topology via Self-Assembly to Applications*; Pope, M. T., Müller, A., Eds.; Kluwer Academic Publishers: Dordrecht, The Netherlands, 2001, pp 363-390.

[80] Hill, C. L.; Prosser-McCartha, C. M. *Coord. Chem. Rev.* **1995**, *143*, 407-455.

[81] Harrup, M. K.; Hill, C. L. *Inorg. Chem.* **1994**, *33,* 5448.

[82] Grate, J. H.; Hamm, D. R.; Mahajan, S. In *Polyoxometalates: From Platonic Solids to Anti-Retroviral Activity. [In: Top. Mol. Organ. Eng., 1994; 10]*; Pope, M. T., Müller, A., Eds.; Kluwer Academic Publishers: Dordrecht, The Netherlands, 1994; Vol. 10, pp 281-305.

[83] Neumann, R.; Dahan, M. *Nature* **1997**, *388*, 353-355.

[84] Neumann, R.; Dahan, M. *J. Am. Chem. Soc.* **1998**, *120*, 11969-11976.

[85] Weiner, H.; Hayashi, Y.; Finke, R. G. *Inorg. Chim. Acta* **1999**, *291*, 426-437.

[86] Nishiyama, Y.; Nakagawa, Y.; Mizuno, N. *Angew. Chem., Int. Ed. Engl.* **2001**, *40*, 3639-3641.

[87] Goldstein, A. S.; Beer, R. H.; Drago, R. S. *J. Am. Chem. Soc.* **1994**, *116*, 2424-2429.

[88] Nozaki, C.; Misono, M.; Mizuno, N. *Chem. Lett.* **1998**, 1263-1264.

CHAPTER III

VANADIUM-BASED, RECORD CATALYTIC LIFETIME CATECHOL DIOXYGENASES: EVIDENCE FOR A COMMON CATALYST

This dissertation chapter contains the manuscript of a full paper accepted by *Journal of the American Chemical Society*. The finding of a common catalyst in ten catechol dioxygenase systems greatly simplifies and unifies the disparate literature of vanadium catechol dioxygenases.

Vanadium-Based, Record Catalytic Lifetime Catechol Dioxygenases: Evidence For a Common Catalyst

Cindy-Xing Yin and Richard G. Finke

Abstract

In 1999 a catechol dioxygenase derived from a V-polyoxometalate was reported which was able to perform a record >100,000 total turnovers of 3,5-di-tert-butylcatechol oxygenation using O_2 as the oxidant (H. Weiner, R. G. Finke, *J. Am. Chem. Soc.* **1999**, *121*, 9831). An important goal is to better understand this and *other* vanadium-based catechol dioxygenases. A scrutiny of 11 literature reports of vanadium-based catechol dioxygenases yielded the insight that they all proceed with *closely similar selectivities.* This in turn led to a "common catalyst hypothesis" for the broad range of vanadium V-based catechol dioxygenases precatalysts presently known. The following three classes of V-based compounds, 10 complexes total, have been explored to test the "common catalyst" hypothesis: (i) six vanadium-based polyoxometalate precatalysts, (n-$Bu_4N)_4H_5PV_{14}O_{42}$, (n-$Bu_4N)_7SiW_9V_3O_{40}$, (n-$Bu_4N)_5[(CH_3CN)_xFe^{II}{\cdot}SiW_9V_3O_{40}]$, ($n$-$Bu_4N)_9P_2W_{15}V_3O_{62}$, ($n$-$Bu_4N)_5Na_2[(CH_3CN)_xFe^{II}{\cdot}P_2W_{15}V_3O_{62}]$ and (n-$Bu_4N)_4H_2$-γ-

$SiW_{10}V_2O_{40}$; (ii) three vanadium catecholate complexes, $[V^{V}O(DBSQ)(DTBC)]_2$, $[Et_3NH]_2[V^{IV}O(DBTC)_2]\cdot 2CH_3OH$ and $[Na(CH_3OH)_2]_2[V^{V}(DTBC)_3]_2\cdot 4CH_3OH$ (where DBSQ = 3,5-di-*tert*-butylsemiquinone anion and DTBC = 3,5-di-*tert*-butylcatecholate dianion), plus (iii) simple $VO(acac)_2$. Product selectivity studies, catalytic lifetime tests, electron paramagnetic resonance spectroscopy (EPR), negative-ion-mode electrospray ionization-mass spectrometry (negative ion ESI–MS) and kinetic studies provided compelling evidence for a common catalyst or catalyst resting state, namely Pierpont's structurally characterized vanadyl semiquinone catecholate dimer complex, $[VO(DBSQ)(DTBC)]_2$, formed from *V-leaching* from the precatalysts. The results provide a considerable simplification and unification of a previously disparate literature of V-based catechol dioxygenases.

Introduction

Oxygen activation for selective oxidation reactions continues to be a central and challenging subject in catalysis.[1,2,3,4] In nature, the discovery of dioxygenase enzymes—that is, enzymes catalyzing the incorporation of both oxygen atoms of O_2 into substrates with no added protons or electrons—dates back to the 1950s with the discovery of oxygen incorporation into catechol by pyrocatechase of *Pseudomonas* sp.[5] Since that time, mild, selective and facile man-made dioxygenases have been the Holy Grail of biomimetic studies of oxidation catalysis.[3]

One important class of dioxygenase enzymes, catechol dioxygenases, catalyze the degradation of aromatic compounds.[6] Catechol dioxygenases have been classified into two groups, intradiol and extradiol dioxygenases, Figure 3.1. Catechol dioxygenase

enzymes containing non-heme $Fe^{II/III}$ or Mn^{II} have been discovered in nature.[7,8,9,10] Biomimetic model systems containing Fe(II/III),[8,10,11,12,13,14,15,16,17,18,iv] V(IV/V) (Table 3.1), Ru(II)[19], Rh(III)[20,21] as well as several other metals[22] are known to catalyze catechol dioxygenation reactions.

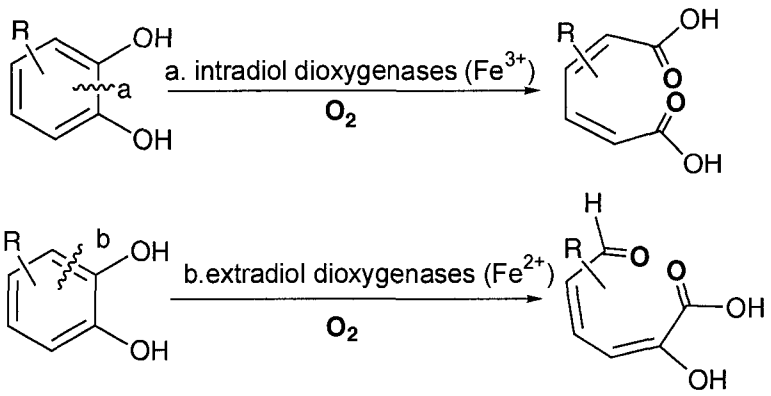

Figure 3.1 Definitions, and Fe^{3+} vs Fe^{2+} intradiol catechol dioxygenases (cleavage of the C–C bond between the two hydroxyl groups) vs extradiol catechol dioxygenases (cleavage of one of the C–C bonds adjacent to the two hydroxyl groups).

Vanadium-based non-enzymatic dioxygenase catalysts react with 3,5-di-*tert*-butylcatechol (hereafter 3,5-DTBC) to produce mixtures of three classes of products, Figure 3.2:[23] intradiol cleavage products, **2**, 3,5-di-*tert*-butyl-1-oxacyclohepta-3,5-diene-2,7-dione and **5**, 3,5-di-*tert*-butyl-5-(carboxymethyl)-2-furanone; extradiol cleavage products, **3**, 4,6-di-*tert*-butyl-2*H*-pyran-2-one and **4**, spiro[1,4-benzodioxin-2(3*H*),2'(2*H*)-pyran]-3-one, 4', 6, 6', 8-tetrakis(1,1-dimethylethyl); and the autoxidation

[iv] Fe-based catechol dioxygenase model systems have been intensively studied during the last decade.[13] In most of the studies, 3,5-di-*tert*-butylcatechol is employed as the substrate. The best intradiol and extradiol models reported provide almost exclusively intradiol or extradiol products, respectively. Premier Fe model systems to date are: the catechol intradiol dioxygenase $[Fe^{III}(TPA)DTBC]BPh_4$ (TPA ≡ tris(2-pyridylmethyl)amine, tetradentate ligand) which adds oxygen to bound DTBC to yield the intradiol-cleavage products (product **2** (60%) and **5** (38%), Figure 3.2) in an overall 98% yield[14] and the catechol extradiol dioxygenase $[Fe^{III}(L)DBC]Cl$ (L ≡ TACN or Me_3TACN, TACN ≡ 1,4,7-triazacyclononane, tridentate ligand) which yields a near-quantitative yield of the extradiol-cleavage product **3** (Figure 3.2, plus an isomer of product **3**, 3,5-di-*tert*-butyl-2-*H*-pyran-2-one) with or without added Lewis bases.[15,16,17]

product **6**, 3,5-di-*tert*-butyl-1,2-benzoquinone. The product numbers in Figure 3.2 will be used subsequently throughout this paper.

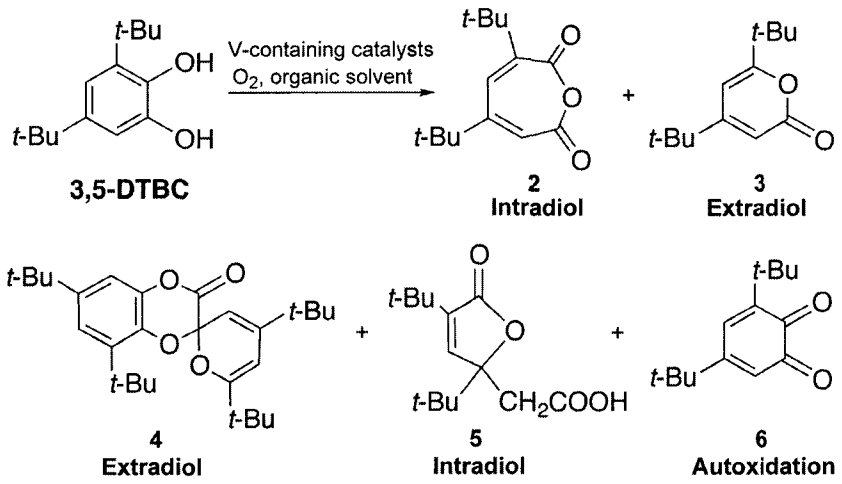

Figure 3.2 Oxidative cleavage of 3,5-DTBC by vanadium-based, non-enzymatic catechol dioxygenase catalysts.

Previously, a survey of 28 vanadium-containing precatalysts revealed that the vanadium polyoxometalate plus Fe^{II} precatalyst, $(n\text{-}Bu_4N)_5[(CH_3CN)_xFe^{II}\cdot SiW_9V_3O_{40}]$, was able to accomplish 125,000 Total Turnovers (hereafter, TTOs) of DTBC dioxygenation in ~300 hrs.[23] (For leading reviews on polyoxometalates, see elsewhere.[24,25,26]) This level of combined catalytic activity and lifetime is an improvement of *two orders of magnitude* over the previous record of ~500 TTOs.[27] Practically, it means that a *few mg*s of V-based precatalyst are able to convert *10 g* of DTBC into grams of isolable, pure products in ≤312 hrs.[23] Our prior work also shows that the O_2-uptake kinetics, beginning with V-based polyoxometalates such as $SiW_9V_3O_{40}^{7-}$ or $P_2W_{15}V_3O_{62}^{9-}$, could be curve-fit with the two-step mechanism, A → B, then A + B → 2B, where the latter step is the kinetic definition of autocatalysis in which

a product (B) is also a reactant.[28] Kinetics studies of four of the 28 precatalysts examined revealed that the true catalysts were *not* the starting vanadium complexes; rather, the V-based precatalysts reacted with a DTBC-derived product, B, to generate the true catalyst. This precatalyst conversion demands that understanding the nature of the true catalyst, and eventually improving the broad selectivity seen with such V-based dioxygenase catalysts (Figure 3.2), are important goals within the broader context of dioxygenase chemistry.

Tatsuno and co-workers reported catechol oxygenation catalysis using the heteropolyvanadates, $PV_{14}O_{42}^{9-}$, $MnV_{13}O_{38}^{7-}$ and $NiV_{13}O_{38}^{7-}$.[29] Isolation of the reaction intermediate afforded a blue compound, tentatively assigned as the dimer complex "$[V(DBSQ)(DBCatH)]_2$" by elemental analysis, IR, EPR results and a cryoscopic measurement of the approximate molecular weight (DBCatH ≡ mono-protonated di-*tert*-butylcatecholate anion).[29]

The present contribution also builds off an important, earlier observation by Professor C. G. Pierpont at the University of Colorado who, in his review of metal compounds containing catecholate and semiquinone ligands, noted that the "product distribution is rather similar" for catechol oxidations beginning with different sources of vanadium (see p. 347 elsewhere).[30] Significantly, he also proposed that a mixed-catecholate and semiquinone vanadium oxo compound, $[VO(DBSQ)(DTBC)]_2$, could be a soluble component of catechol oxidation by vanadium-based catalysts. Hence, the questions raised and addressed herein are: "is there a common catalyst for the broad range of vanadium precursors employed for V-based catechol dioxygenases?"

Alternatively, "do vanadium-based dioxygenases inherently lack selectivity for some as of yet unexplained reason(s)?"

Herein, we test the specific hypothesis that there is in fact a common catalyst for the rather different vanadium-based catechol dioxygenase systems described in the literature. We report reaction selectivity, catalytic lifetime, EPR, MS, and kinetic evidence which support this "common vanadium catechol dioxygenases catalyst" hypothesis. Our evidence supports Pierpont's suggestion that $[VO(DBSQ)(DTBC)]_2$ is that common catalyst. A subsequent paper in this series presents kinetic studies which reveal how virtually any V-based precursors can yield the same V-based DTBC dioxygenase catalyst, via the novel concept of autoxidation-product-initiated dioxygenase catalysis.[31]

Experimental Section

Reagents. 3,5-DTBC (purchased from Aldrich, 99%, m.p. 96–99 °C) was recrystallized three times using *n*-pentane under argon (m.p. 99–100 °C) and stored in a Vacuum Atmosphere drybox (O_2 level ≤ 5 ppm). (NB: it is important to recrystallize the 3,5-DTBC substrate ≥3 times to remove impurities such as 3,5-di-*tert*-butylbenzoquinone.) The polyoxometalate precursors, $(n\text{-}Bu_4N)_4H_5PV_{14}O_{42}$,[32] $(n\text{-}Bu_4N)_7SiW_9V_3O_{40}$,[33] $(n\text{-}Bu_4N)_9P_2W_{15}V_3O_{62}$,[33,34] $(n\text{-}Bu_4N)_5Fe^{II}\cdot SiW_9V_3O_{40}$[23] and $(n\text{-}Bu_4N)_5Na_2Fe^{II}\cdot P_2W_{15}V_3O_{62}$[23] were synthesized according to the most recent literature procedures. $(n\text{-}Bu_4N)_4H_2\text{-}\gamma\text{-}SiW_{10}V_2O_{40}$, a gift from Prof. N. Mizuno, was prepared as described[35] and characterized by ^{183}W-NMR. $VO(acac)_2$ (Aldrich, 95%) and VCl_3 (Aldrich) were stored in the drybox and used as received. $NaOCH_3$ (Fisher Scientific)

were stored under N_2 and used as received. $[Co^{III}(3,5\text{-DBSQ})(CN)_4]^{2-}$ crystals[36] were a gift from Prof. M. Wicholas. HPLC grade solvents (1,2-dichloroethane, acetonitrile, diethyl ether and ethyl acetate) and anhydrous grade methanol were purchased from Aldrich and stored in the drybox; each of the above solvents was dried by standing for at least 48 h over ~5 vol % 3-Å or 4-Å molecular sieves that had been preactivated by heating at >170 °C under vacuum (≤1 Torr) for at least 12 h, then cooled under dry N_2 in the drybox. Anhydrous grade toluene was purchased from Aldrich, stored in the drybox, and used without further drying. Et_3N (Mallinckrodt) was distilled over BaO under Ar and stored in the drybox. Anhydrous certified ACS grade diethyl ether was purchased from Fisher Scientific and used as received. Argon gas was purchased from General Air (99.985%) and used as received.

Instrumentation. Air-sensitive samples were prepared in a drybox prior to analyses. GC analyses were performed on an HP (Hewlett-Packard) 5890 Series II gas chromatograph equipped with a FID detector and a SPB-1 capillary column (30 m, 0.25 mm I. D.) with the following temperature program: initial temperature, 200 °C (initial time, 2 min); heating rate, 2 °C/min; final temperature, 240 °C (final time, 3 min); injector temperature, 250 °C; FID detector temperature, 250 °C. GC-MS analyses were performed under the same temperature program on an Agilent 5973N/GC 6890 instrument equipped with a mass selective detector (70 eV) and an Agilent HP-5MS column (30 m). Negative-ion electrospray ionization mass spectrometry (negative ion ESI–MS) analyses were performed on a Thermo Finnigan LCQ Advantage Duo MS directly coupled with a syringe pump (5 μL/min feeding speed and 15 μL/min at purging; spray voltage –4.5 kV, capillary voltage –(38–42) V, capillary temperature 180 °C) or on

a Fisons VG Quattro-SQ spectrometer by directly injecting an acetonitrile solution (spray voltage –2.9 kV, sample cone voltage –25 V, source temperature 80 °C). NMR spectra were obtained in $CDCl_3$ or CD_3CN (Cambridge Isotope Lab). ^1H-, ^{31}P- and ^{51}V-NMR were recorded in 5-mm o.d. tubes on a Varian Inova (JS-300) NMR spectrometer. ^1H-NMR was referenced to the residual impurity in the deuterated solvent, ^{31}P-NMR was referenced to 85% H_3PO_4 in H_2O using the external substitution method, and ^{51}V-NMR was referenced to neat $VOCl_3$ (Aldrich) using the external substitution method. Spectral parameters for ^{31}P-NMR include: tip angle = 60° (pulse width 10 μs); acquisition time, 1.6 s; sweep width, 10000 Hz. Spectral parameters for ^{51}V-NMR include: ^{51}V tip angle = 90° (pulse width 3.1 μs); acquisition time, 0.096 s; sweep width, 83682.0 Hz. Infrared spectra were obtained on a Nicolet 5DX spectrometer as KBr pellets (Aldrich, spectrophotometric grade) or in a CaF_2 cell (A = 0.1mm). UV-visible spectra were obtained on an HP 8452A diode spectrophotometer in glass UV cells sealed by ground-glass stopcocks. Electron paramagnetic resonance (EPR) spectra were recorded on a Bruker EMX 200U EPR spectrometer. Quartz EPR tubes of 4-mm o.d. were used, and DPPH (2,2-diphenyl-1-picrylhydrazyl) was used as the reference compound (g = 2.0037). Single crystal X-ray diffraction crystallography was performed on a Bruker SMART 1K CCD X-ray diffractometer. CHN elemental analyses were performed by Atlantic Microlab, Inc. (Norcross, Georgia) or Galbraith Laboratories (Knoxville, Tennessee).

Preparation of Polyoxometalate Precursors. The polyoxometalate precursors, $(n\text{-}Bu_4N)_4H_5PV_{14}O_{42}$,[32] $(n\text{-}Bu_4N)_7SiW_9V_3O_{40}$,[33] $(n\text{-}Bu_4N)_9P_2W_{15}V_3O_{62}$,[33,34] $(n\text{-}Bu_4N)_5Fe^{II}{\cdot}SiW_9V_3O_{40}$[23] and $(n\text{-}Bu_4N)_5Na_2Fe^{II}{\cdot}P_2W_{15}V_3O_{62}$[23] were prepared according to

the most recent literature procedures. Further details about the syntheses and characterizations are provided in the Supporting Information.

Preparation and Characterization of Vanadium-Catecholate Complexes. Three vanadium catecholate complexes, $[VO(DBSQ)(DTBC)]_2$,[37] $[Et_3NH]_2[VO(DTBC)_2]\cdot 2CH_3OH$,[38] and $[Na(CH_3OH)_2]_2[V(DTBC)_3]_2\cdot 4CH_3OH$,[39,v] were chosen from the literature as the best available examples of relatively simple, well-characterized vanadium-catecholate complexes that provide three alternative hypotheses as to common components in V-based catechol dioxygenase reactions. The details of their synthesis and characterization are provided in the Supporting Information.

Synthesis and Characterization of Deprotonated Di-*tert*-butylcatecholate Salt Na_2(3,5-DTBC). The details of these experiments are recorded in the Supporting Information, including Figures S3.8 and S3.9.

Selectivity Experiments. The DTBC dioxygenase selectivities of the ten vanadium model compounds which follow were examined with the same substrate-to-vanadium ratio to test whether or not they produce a similar product distribution: $(n\text{-}Bu_4N)_4H_5PV_{14}O_{42}$, $(n\text{-}Bu_4N)_7SiW_9V_3O_{40}$, $(n\text{-}Bu_4N)_5[Fe^{II}\cdot SiW_9V_3O_{40}]$, $(n\text{-}Bu_4N)_9P_2W_{15}V_3O_{62}$, $(n\text{-}Bu_4N)_5Na_2[Fe^{II}\cdot P_2W_{15}V_3O_{62}]$, $(n\text{-}Bu_4N)_4H_2\text{-}\gamma\text{-}SiW_{10}V_2O_{40}$, $[V^{V}O(DBSQ)(DTBC)]_2$, $[Et_3NH]_2[V^{IV}O(DBTC)_2]\cdot 2CH_3OH$,

---

[v] (a) Cass, M. E.; Gordon, N. R.; Pierpont, C. G. *Inorg. Chem.* **1986**, *25*, 3962-3967. (b) Cass, M. E.; Ph.D. Thesis, University of Colorado, Boulder, CO., 1984, p 67. (c) Private communication with Professor Cort G. Pierpont. In our preparation of $Na[V(DTBC)_3]\cdot 4CH_3OH$ using a V(II) solution (prepared by **Zn**/Hg amalgam reduction of a NH_4VO_3 solution), crystals identified by UV-visible, EPR and X-ray crystallography as $\mathbf{Zn^{II}}$(Cat-N-SQ)(BQ-N-SQ) were obtained instead. (Chaudhuri, P.; Hess, M.; Hildenbrand, K.; Bill, E.; Weyhermüller, T.; Wieghardt, K. *Inorg. Chem.* **1999,** *38,* 2781-2790; $(Cat\text{-}N\text{-}SQ)^{2-}$ and $(BQ\text{-}N\text{-}SQ)^{0}$ are two redox isomers of $(Cat\text{-}N\text{-}BQ)^{-}$, which is bis(3,5-di-*tert*-butyl-1-hydroxy-2-phenyl)amine anion.) That this known, dark green crystalline compound was not the intended vanadium complex $Na[V(DTBC)_3]\cdot 4CH_3OH$ was determined by its room-temperature EPR (a multi-line spectrum shown as Figure S3.4 of the Supporting Information, and its UV-visible maximum in $CHCl_3$ is at 736 nm instead of the reported[va)] 650 nm of $Na[V(DTBC)_3]\cdot 4CH_3OH$).

$[Na(CH_3OH)_2]_2[V^V(DTBC)_3]_2 \cdot 4CH_3OH$ and $VO(acac)_2$. Oxygenation experiments were carried out on a volume-calibrated oxygen-uptake line as detailed in the Supporting Information elsewhere.[23] The standard procedure used for these experiments is as follows: 400 ± 5 mg (ca. 1.8 mmol) of three-times-recrystallized 3,5-DTBC were weighed in the drybox into a 50 mL round-bottom reaction flask equipped with a septum, side-arm and an egg-shaped 3/4" × 3/8'' Teflon-coated magnetic stir bar. Using a 10-mL glass syringe, approximately 8 mL pre-dried HPLC grade 1,2-dichloroethane were transferred into the flask. Then, the flask was sealed with a Teflon stopcock and taken out of the drybox. The flask was connected to the oxygen-uptake line through an O-ring joint, and the reaction solution was frozen in a dry ice/ethanol bath (-76 °C). Two pump-and-fill cycles with O_2 as the refill gas were performed. Next, the dry ice bath was replaced with a temperature-controlled oil bath. The temperature of the flask was raised to 40 ± 0.7 °C and allowed to equilibrate with stirring for 25 min. In the drybox, 0.5–2.0 mg of a predetermined vanadium precatalyst (mole ratio of substrate to the vanadium in the precatalysts of ca. 1000:1) were weighed into a glass vial and dissolved in ca. 0.2 mL of 1,2-dichloroethane (0.2 mL toluene was used for $[Na(CH_3OH)_2]_2[V(DTBC)_3]_2 \cdot 4CH_3OH$ because of its greater solubility in toluene). The resultant precatalyst solution was drawn into a 1-mL gas-tight syringe and brought out of the drybox with its needle protected from air via its insertion into a septum-capped vial. This precatalyst solution was then injected through the sidearm of the reaction flask and t = 0 was set. Pressure readings from the manometer were used to follow the reaction (±1 Torr or ca. ±1% precision over a pressure loss of ca. 80–100 Torr). The reaction was

stopped at 23.5 h unless noted otherwise, and the reacted mixture was diluted 21 fold using 1,2-$C_2H_4Cl_2$ prior to GC analysis.

Catalytic Lifetime Experiments. These experiments were performed to determine if the V complexes: $(n\text{-}Bu_4N)_4H_5PV_{14}O_{42}$, $(n\text{-}Bu_4N)_7SiW_9V_3O_{40}$, $(n\text{-}Bu_4N)_5[Fe^{II}\cdot SiW_9V_3O_{40}]$, $(n\text{-}Bu_4N)_9P_2W_{15}V_3O_{62}$, $(n\text{-}Bu_4N)_5Na_2[Fe^{II}\cdot P_2W_{15}V_3O_{62}]$, $[V^{V}O(DBSQ)(DTBC)]_2$, $[Et_3NH]_2[V^{IV}O(DBTC)_2]\cdot 2CH_3OH$, $[Na(CH_3OH)_2]_2[V^{V}(DTBC)_3]_2\cdot 4CH_3OH$ and $VO(acac)_2$ differ in their catalytic lifetimes. Experiments were performed with the apparatus described in the literature;[23] a catalytic lifetime experiment is briefly described below in which, about half the amount of substrate (~29 mmol), yielding ≤50,000 TTOs, is employed in comparison to the largest scale previously employed (~63 mmol substrate which yielded 100,000–150,000 TTOs[23]). The precatalyst amounts were in the range of 0.4–0.7 μmol for all the catalytic lifetime experiments.

The ≤50,000 TTO catalytic lifetime experiment proceeded as follows: ca. 6.50 g (29.2 mmol) of three-times-recrystallized 3,5-DTBC were weighed into a 250 mL round-bottom flask with a sidearm and an egg-shaped 1" × 1/2" Teflon-coated magnetic stir bar. About 125 mL 1,2-$C_2H_4Cl_2$, measured in a graduated cylinder, were added to the reaction flask. Then, 1.1–4.0 mg of a chosen precatalyst were weighed into a vial (the mole ratio of substrate to the catalyst is ca. 45000:1), dissolved in ca. 0.2 mL 1,2-$C_2H_4Cl_2$, and quantitatively transferred into the reaction flask via a pipet. The flask was sealed, brought out of the drybox, and frozen in a dry ice/ethanol bath (-76 °C) for 1 h. Next, the flask was connected to a condenser under an argon flow. Two pump-and-fill cycles with O_2 as the refill gas were performed, followed by heating the solution to 65 ± 1 °C via a

temperature-controlled oil bath (this took ca. 30 min). Once a constant temperature was achieved, t = 0 was noted. The flask was connected to an oxygen tank through a bubbler, keeping a slow positive flow of O_2 (ca. 0–5 psig) atop the solution. An aliquot of ca. 0.15 mL was drawn from the solution every 24–48 h with a disposable polyethylene 1-mL syringe equipped with a pre-dried stainless steel needle. The aliquot was diluted 21-fold using 1,2-$C_2H_4Cl_2$, and then subjected to GC analysis.

The 100,000–150,000 TTO catalytic lifetime experiments were performed via the same procedures as above, except ca. 14 g of 3,5-DTBC was employed (substrate to precursor mole ratio within 100,000–150,000).

$VO(acac)_2$ Aging Studies. The effects of aging the $VO(acac)_2$ were tested due to our inability to reproduce the low TTOs observed (<6,000) in the TTO catalytic lifetime experiment reported in our previous studies.[23] A putatively fresh sample was purchased from Aldrich (95%) and stored in the drybox upon receiving. One aged sample of $VO(acac)_2$ was prepared by placing the fresh $VO(acac)_2$ in a vial, taking the vial out of the drybox, and then exposing the sample to atmospheric oxygen for two months. The other sample was prepared by heating ground $VO(acac)_2$ (from a bottle which had been stored outside the drybox for over two years) in a 60 °C thermostatic oven in air for 6 days. During this time, the color darkened from green to green-black. The above two aged samples together with a fresh sample were examined by EPR in CH_2Cl_2 (the two aged samples did not totally dissolve, presumably due to the presence of insoluble decomposition products). Double-integrated EPR peak areas of the 3 compounds were compared, but no difference was found within experimental error. The first aged sample was also tested in a 100,000–150,000 TTO catalytic lifetime experiment and yields the

same catalytic lifetime within experimental error as the fresh sample, Table S3.3 of the Supporting Information.

^{31}P-NMR Following Oxygen-uptake Using Precatalyst (n-$Bu_4N)_9P_2W_{15}V_3O_{62}$. Results are shown in Figure S3.10; and the experimental details are included in the Supporting Information.

EPR Following Oxygen-uptake Experiments. The procedure employed here is exactly as reported above in the "Selectivity Experiments," except that: (i) the precatalyst amount was chosen so that the amount of vanadium from the precatalyst was ca. 6–8 μmol; (ii) toluene was employed as the solvent in place of 1,2-dichloroethane, with the toluene being frozen using liquid nitrogen instead of dry ice/acetone; and (iii) the precatalyst was premixed with DTBC in the drybox instead of being injected into a stirred DTBC/O_2 solution. The oxygen pressure loss was monitored with a manometer. An aliquot of the reaction solution was drawn under an oxygen flow at ca. 0.5–2 h after the oxygen pressure started to decrease. The reaction solution was sampled again after no further pressure change was observed for >2 h.

Quantitative EPR Analysis. The standard solutions were prepared by dissolving an air-stable, semiquinone-containing crystal $[Co^{III}(3,5\text{-DBSQ})(CN)_4]^{2-}$,[36] into toluene (1.0 M) and serial diluting to concentrations of 0.10 M and 0.010 M. The reaction solution (catalyzed by the precatalyst $VO(acac)_2$) was harvested ca. 2 h after oxygen-uptake ceased, as described above (in the section titled "EPR Following Oxygen-uptake Experiments"). The double integrated area of $[VO(DBSQ)(DTBC)]_2$ was compared to that of $[Co^{III}(3,5\text{-DBSQ})(CN)_4]^{2-}$ to estimate the concentration of $[VO(DBSQ)(DTBC)]_2$.

Negative Ion ESI–MS Analysis. These experiments were performed on a mass spectrometer (Thermo Finnigan LCQ) directly coupled to a syringe pump. The solvent in the syringe serves as the matrix for the negative ion ESI–MS. Solid samples were diluted in the drybox using predried acetonitrile to ca. 10 μM, (ca. 0.01–0.1 mg in 1 mL) and placed in a 2-mL septum screw-capped vial. The sample was then transferred into a rinsed 500-μL syringe outside the drybox, the syringe needle was inserted into the MS sampler hose as fast as possible to avoid oxygen contamination. The injection rate was controlled by a syringe pump. The MS peaks were observed ca. <1 min after the injection. The influence of water in the ESI–MS matrix was examined with a set of control experiments using $[VO(DBSQ)(DTBC)]_2$ as the sample and varying the ratio of CH_3CN:H_2O from 1:0, 9:1, 1:1, 1:9 to 0:1 in the solvent. Although this instrument is not optimal for pure water samples (as shown by the lower signal level as the water ratio goes up), the same peaks were observed as in neat acetonitrile.

Kinetic Competence Experiments. The kinetic competence experiments were set up the same way as the "Selectivity Experiments" described above, except that a higher concentration (0.46–0.48 mM) of the precursor was used to increase the O_2-uptake rate.

Attempted Catalyst Isolations. Isolation and characterization of the actual catalyst, if possible, would of course provide direct evidence of the identity of the true catalyst—although the obvious caveat here is that good catalysts are often metastable transients that are not readily isolable (see "Halpern's Rules" as detailed elsewhere[40]). Nevertheless, it was important to attempt to isolate an active catalyst (or even a deactivated form of the active catalyst) from the vanadium-containing polyoxometalate

precatalysts, especially in light of earlier indications that this *might* be possible.[23,29] However, in the end, we were not able to isolate analytically pure catalysts from these particular studies, so that we turned to the use of in-situ spectroscopic studies (vide infra). Details of the attempted isolation studies are in the Supporting Information, along with figures showing IR, negative ion ESI–MS, or EPR, of the resultant materials (Figures S3.11-S3.14).

Results and Discussion

A Literature Survey of V-Based 3,5-Di-tert-butylcatechol Oxygenations. The published selectivity and lifetime data for the eleven reports of vanadium-based DTBC oxygenations are shown in Table 3.1. The tabulated data yield the following insights: muconic acid anhydride (**2**) is the major product (40–50%), followed in decreasing order by 3,5-di-*tert*-butylquinone (**6**, 20–30%), pyranone (**3**), the spiro product (**4**) and the furanone product (**5**); the last three products have a combined yield of 10–20%. *Clearly, the product selectivities are rather similar for all the V-based DTBC precatalysts examined in the literature to date and which are active,* as Professor Pierpont had hinted.[30] A second, relevant insight comes from the literature Fe catechol dioxygenase models:[13] the product distributions therein are often quite different compared to those in Table 3.1. For example, Fe(III) model complexes with tripodal N_4-donor ligands and catecholate ligands catalyze the intradiol cleavage of 10–100 equivalents 3,5-DTBC to product **2** in 30–84% yield (the yield of the autoxidation product **6** is less than 6%);[18] $[Fe^{III}(tacn)Cl(DTBC)]$ (where tacn = 1,4,7-triazacyclononane) reacts with O_2 to produce extradiol cleavage product **3** in up to 78% yield with the addition of 1 equivalent $AgBF_4$

Table 3.1 A Compilation of the Product Distributions and Mass Balance of Eleven Literature Reports of V-Based Oxidative Cleavage of 3,5-DTBC.

Entry	Precatalyst(s)[a]	Product Distributions	Mass Balance and TTOs	
1	$VO(acac)_2$, VO(salen), VCl(salen) and VCl(saldpt)	**2** = 39–43%; **3** = 6–15%; **6** = 22–28%	Mass balance ≤ 83% [b]TTO_{max} = 1000; [c]TTO_{conv} = 1000; [d]$TTO_{yield} \leq 750$	27
2	$[V(salen)(DbcatH)_2]\cdot 1/2CH_2Cl_2$ and $[V(saldpt)(DBcatH)]\cdot CH_2Cl_2$ [e]	**2** = 42%; **3** = 11%; **6** = 24%	Mass balance = 77% TTO_{max} = 100; TTO_{yield} = 77	41
3	$[VO(acac)(OCH_3)]_2$, $[VO(tmh)(OCH_3)]_2$, $(VOaap)_2$, $(VOdmba)_2$, $(VOdba)_2$ and $(VO(acac)OCH_3)_2$	**2** = 46–48%; **3** = 7–10%; **6** = 22–25%	Mass balance ≤ 82% TTO_{max} = 100; TTO_{conv} = 100; $TTO_{yield} \leq 82$	42
4	[LVO(acac)], $[LVO(phen)]^+PF_6^-$ and $[LVO(bipy)]^+PF_6^-$	**2** < 10%; **6** = 70%[f]	Mass balance < 80%	43
5	VO(acac)(TCCat)	**2** = 45%; **3** = 6%; **6** = 24%	Mass balance = 75% TTO_{max} = 100; TTO_{yield} = 75	44
6	$PV_{14}O_{42}^{9-}$, $MnV_{13}O_{38}^{7-}$, $NiV_{13}O_{38}^{7-}$ and $VO(acac)_2$	**2** = 34–36%; **3** = 11–20%; **4** = 3–13%; **6** = 15–21%	Mass balance ≤ 82% TTO_{max} = 100; $TTO_{yield} \leq 82$	29
7	[VO(acac)(DTBCat)]	**2** = 45%; **3** = 6%; **6** = 24%	Mass balance = 75%	45
8	*cis*-$V_2W_4O_{19}^{4-}$, 1,4,9-$[PV_3W_9O_{40}]^{6-}$, $V_{10}O_{28}^{6-}$ and $VO(acac)_2$	**2** = 15–39%; **6** = 5–19%	Mass balance ≤ 58% TTO_{max} = 100; $TTO_{yield} \leq 58$	46
9	$VO(HL)_2OH$, $(VO)_2L_2SO_4\cdot 4H_2O$	**2** = 45–48%; **3** = 5–10%; **6** = 23–25%	Mass balance ≤ 82% TTO_{max} = 100; TTO_{conv} = 100; $TTO_{yield} \leq 82$	47
10	TEA[VO(TEA)]	**2** = 80%[g] **5** = 3%	Mass balance ≤ 82% TTO_{max} = 10; TTO_{yield} = 8.2	48

11	$SiW_9V_3O_{40}^{7-}$, $Fe^{II}{\cdot}SiW_9V_3O_{40}^{5-}$, $P_2W_{15}V_3O_{62}^{9-}$, $Fe^{II}{\cdot}P_2W_{15}V_3O_{62}^{7-}$, $PV_{14}O_{42}^{9-}$, $VO(acac)_2$, etc. (28 catalysts total)	**2** = 40–57%; **3** = 6–15%; **4** = 10–18%; **6** = 9–25%	Mass balance ≤ 94% TTO_{max} = 4500; TTO_{conv} = 4500; $TTO_{yield} \leq 4230$ $TTO_{conv\ or\ yield} \geq$ 100,000 when TTO_{max} = 129,000	23

[a]Inactive vanadium-containing precatalysts omitted from the above table, but listed here for the sake of completeness, are: [V(salen)(cat)]·0.1CH_2Cl_2 and [V(salen)(4-Bcat)]·H_2O;[41] $Na[VO(DBcat)_2]$ and $Na_2[VO(OCH_3)(DBcat)_2]$;[29] VO(acac)(cat) and VO(acac)(3-Bcat);[45] $[VW_5O_{19}^{3-}]$;[46] VO(NTA)[48] and $[SiW_{11}VO_{40}^{5-}]$.[23]
[b]TTO_{max} = $moles_{substrate}/moles_{precatalyst}$.
[c]TTO_{conv} = $moles_{substrate,\ consumed}/moles_{precatalyst}$.
[d]TTO_{yield} = $moles_{sum\ of\ products}/moles_{precatalyst}$.
[e]The product distribution was not reported for the denoted precatalyst.
[f]We speculate the reason for this different selectivities is that the bulky ligand L blocks the oxygen binding to the vanadium-catecholate compound.
[g]This yield should be the sum of **2** and **6** due to its "red" color, the yield of **5** is 3%.
Abbreviations: salen ≡ ethylenebis(salicylideneaminato); saldpt ≡ *N,N'*-(3,3'-dipropylamine)bis(salicylideneaminato); tmh ≡ 2,2,6,6-tetramethylheptandione; H_2aap ≡ *o*-hydroxyacetophenone; H_2dmba ≡ 1,5-bis(*p*-methoxyphenyl)-1,3,5-pentanedione; H_2dba ≡ 1,5-diphenyl-1,3,5-pentanetrione; L (entry 4) ≡ $[\eta\text{-CpCo}\{P(O)(OC_2H_5)_2\}_3]^-$; bipy ≡ 2,2'-bipyridine; TCCat ≡ tetrachlorocatecholate; DBcat/DTBCat ≡ 3,5-di-*tert*-butylcatecholate; H_2L (entry 9) ≡ 2,2'-dihydroxy-3,3'-diacetyl-5,5'-dichlorodiphenylmethane; TEA ≡ triethanolamine; cat ≡ pyrocatecholate; Bcat ≡ *tert*-butylcatechol; and NTA ≡ nitrilotriacetic acid.

and 20 equivalent 4-methylpyridine (the yield of an isomer of product **3**, 3,5-di-*tert*-butyl-2*H*-pyran-2-one, is 20%; the yield of product **6** is less than 1%).[17] These results show that, as one would expect, there is not an inherent insensitivity in the DTBC oxygenation product selectivities, at least when considering different metals.

The hypothesis for the remainder of this work then became the "common catalyst hypothesis," namely that there is a common catalyst for the rather different vanadium-based catechol dioxygenase systems described in the literature, Table 3.1. The results in Table 3.1 are, of course, themselves consistent with and supportive of this hypothesis.

Choice of Three Simple, Well-Characterized Vanadium-Containing DTBC Complexes for Further Investigation. Given the data in Table 3.1 and the resultant "common catalyst hypothesis," the next task was to identify vanadium-DTBC and/or -DBSQ complexes known in the literature that were logical starting points as either: (i) precatalysts closer in composition and structure to the hypothesized true catalyst(s); or conceivably (ii) actual catalysts themselves. Three vanadium-DTBC or DTBC/DBSQ complexes quickly rose to the top of the list from a scrutiny of the literature: Pierpont and co-worker's[37] $[V^{V}O(DBSQ)(DTBC)]_2$, Raymond and co-worker's[38] $[Et_3NH]_2[V^{IV}O(DTBC)_2]\cdot 2CH_3OH$ and Luvena and co-worker's[39] $[Na(CH_3OH)_2]_2[V^{V}(DTBC)_3]_2\cdot 4CH_3OH$, Figure 3.3. In addition, it proved productive to examine the simple $VO(acac)_2$ as an example of a well-known V-precatalyst without DTBC or DBSQ ligands. The $VO(acac)_2$ was purchased commercially (Aldrich, 95%), whereas the other three complexes were prepared according to the literature as detailed in the Supporting Information.

All three vanadium catecholate complexes were characterized by UV-visible spectroscopy, negative ion electrospray ionization mass spectrometry (ESI–MS), and elemental analysis (plus single crystal X-ray crystallography in the case of $[Na(CH_3OH)_2]_2[V^{V}(DTBC)_3]_2\cdot 4CH_3OH$). The elemental analysis results of different batches of $[VO(DBSQ)(DTBC)]_2$ show that a variable amount of methanol solvates are present in the compounds; hence, the difficulty in obtaining single crystals is ascribed to crystal deterioration due to solvate loss at room temperature.[37] In summary, analytically pure samples of each of the three literature vanadium DTBC/DBSQ complexes were

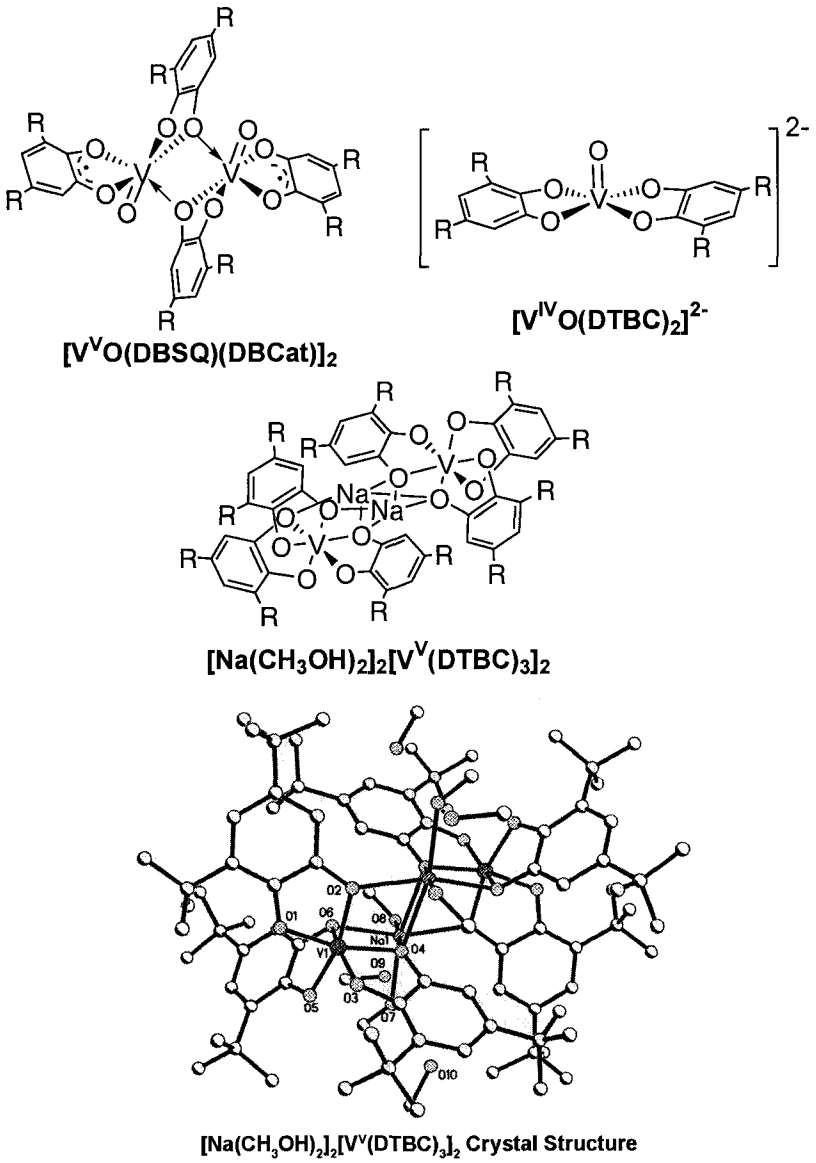

Figure 3.3 Structures of the three vanadium catecholate complexes studied herein (*tert*-butyl groups are shown as R, only one isomer of $[V^{IV}O(DTBC)_2]^{2-}$ is shown, and coordinated methanol is not shown in the middle structure for the sake of clarity). Also shown is the structure of $[Na(CH_3OH)_2]_2[V(DTBC)_3]_2 \cdot 4CH_3OH$ obtained through X-ray single crystal diffraction.

prepared so that their DTBC oxygenation selectivities, kinetics and catalytic lifetimes could be studied.

Confirmation of the Similar Selectivities For the Three Vanadium DTBC/DBSQ Complexes, $VO(acac)_2$, As Well As for Six V-Polyoxometalate

Precatalysts. Selectivity experiments were carried out in 1,2-$C_2H_4Cl_2$ for the 10 complexes; studies of isolated, active components and control studies were also performed, entries 11–15, Table 3.2, for a total of 15 studies. The key results include the following: (i) The selectivities are the same for the three V-precatalysts, as well as $VO(acac)_2$, entries 1–4, Table 3.2. The O_2-uptake values are also the same and, interestingly, no induction periods are observed for $[VO(DBSQ)(DTBC)]_2$ or $VO(acac)_2$ (the absence of an induction period for $VO(acac)_2$ is as reported in the literature[23]). Note that the lack of an induction period is kinetic evidence that we are closer to the catalyst in these cases—if not at a true catalyst in the $[VO(DBSQ)(DTBC)]_2$ case, *vide infra*;

(ii) The vanadium-containing polyoxometalates are all the same within experimental error in their selectivities and O_2-uptake values.[vi] Interestingly, there are no discernable induction periods for two of the polyoxometalates, $(n\text{-}Bu_4N)_4H_5PV_{14}O_{42}$ and $(n\text{-}Bu_4N)_4H_2\text{-}\gamma\text{-}SiW_{10}V_2O_{40}$. This, plus knowledge of the properties of these particular polyoxometalates,[32,35] suggests the release of $V^VO_2^+$ or possibly $V^{IV}O^{2+}$ from the polyoxometalate structure,[49] as supported by the thermogravimetric studies on $H_2(V^VO_2)PW_{12}O_{40}$ and by the structure of $Na_2(V^{IV}O)[SiW_{12}O_{40}]\cdot 13H_2O$;[49a)]

(iii) Note that Fe is not needed for the oxygenation catalysis activity—*only V is required for facile dioxygenase catalysis* from the 15 entries in Table 3.2. A control using $(n\text{-}Bu_4N)_4SiW_{12}O_{40}$ confirms that polyoxometalates lacking V are *inactive* toward catechol oxygenation;[23]

[vi] Ca. 14–18% less of product **4** in the cases of the vanadium-base polyoxometalate precatalysts and $VO(acac)_2$ compared to our literature[23] are seen due, presumably, to the instability of product **4** in the reaction solution (higher yields of product **4** can be obtained if sampled immediately after the O_2-uptake ceases).

Table 3.2 Catalytic Selectivity Experiments, as Well as O_2-Uptake and Induction-Period Observations, for the Three Classes of Vanadium-Based Compounds.[a]

		Products Yield (%)				Induction Period?	ΔMol_{O2}/ Mol_{DTBC}
		2	**3**	**4**	**6**		
	Four Simple V-Complexes						
1	$[VO(DBSQ)(DTBC)]_2$	40 ± 2	12 ± 1	-	18 ± 1	No	0.64
2	$[Et_3NH]_2[VO(DTBC)_2]$ $\cdot 2CH_3OH$	38 ± 1	12 ± 1	-	18 ± 1	Yes	0.63
3	$[Na(CH_3OH)_2]_2$ $[V(DTBC)_3]_2 \cdot 4CH_3OH$	38 ± 1	14 ± 1	1 ± 1	18 ± 1	Yes	0.62
4	$VO(acac)_2$	42 ± 1	11 ± 1	-	16 ± 1	No	0.63
	V-Based Polyoxometalate Precatalysts						
5	$(n\text{-}Bu_4N)_4H_5PV_{14}O_{42}$	46 ± 2	13 ± 1	-	16 ± 1	No	0.64
6	$(n\text{-}Bu_4N)_7[SiW_9V_3O_{40}]$	49 ± 1	17 ± 1	2 ± 1	11 ± 1	Yes	0.61
7	$(n\text{-}Bu_4N)_5[Fe^{II} \cdot$ $SiW_9V_3O_{40}]$	40 ± 1	13 ± 1	3 ± 1	12 ± 1	Yes	0.59
8	$(n\text{-}$ $Bu_4N)_9[P_2W_{15}V_3O_{62}]^b$	40 ± 2	14 ± 1	3 ± 1	18 ± 1	Yes	0.49
9	$(n\text{-}Bu_4N)_7[Fe^{II} \cdot$ $P_2W_{15}V_3O_{62}]^b$	42 ± 2	13 ± 1	4 ± 1	22 ± 1	Yes	0.55
10	$(n\text{-}Bu_4N)_4H_2\text{-}\gamma\text{-}$ $SiW_{10}V_2O_{40}$	43 ± 1	13 ± 1	-	18 ± 1	No	0.66
11	$(n\text{-}Bu_4N)_5SiW_{11}VO_{40}$ (control; data from literature[23])	~1	-	-	-	-	-
	Isolated Active Components						
12	Isolated active species from $(n\text{-}$ $Bu_4N)_4H_5PV_{14}O_{42}$	39 ± 2	13 ± 1	-	19 ± 1	No	0.61
13	Isolated active species from $(n\text{-}Bu_4N)_5[Fe^{II} \cdot$ $SiW_9V_3O_{40}]^c$	40 ± 2	7 ± 1	-	13 ± 1	No	0.45
	Controls						
14	$Na_2(DTBC)^d$	-	-	-	30 ± 3	-	-
15	$[Co^{II}(CH_3CN)_6](BF_4)_2^e$	-	-	-	2 ± 1	-	-

[a]Experimental conditions: ca. 400 mg 3,5-di-*tert*-butylcatechol, ca. 1000:1 mole ratio of substrate to vanadium in the precatalysts, 40.0 ± 0.7 °C, 9 mL 1,2-$C_2H_4Cl_2$ solvent; reaction stopped at 23.5 h; product yields obtained by GC.
[b]These two reactions were stopped at ca. 42 and 24 h, respectively.

[c]This reaction was stopped at ca. 94 h; the exact number of moles of the precatalyst are not known for this incompletely characterized compound.
[d]This experiment was run with ca. 410 mg Na_2DTBC (1.55 mmol), 2 equivalent (n-Bu_4N)Br (1 g, 3.1 mmol, to facilitate the phase-transfer of Na_2DTBC into the organic phase), 8 mL 1,2-$C_2H_4Cl_2$ solvent; reaction stopped at 161 h; product mixture was concentrated, acidified with 5% HCl, and then extracted into 1,2-$C_2H_4Cl_2$ and analyzed by GC.
[e]Substrate to precatalyst mole ratio is ca. 700:1.

(iv) The control using (n-$Bu_4N)_5SiW_{11}VO_{40}$, Table 3.2, entry 11 (data from our previous study[23]), reveals *the inactivity of this single-vanadium-containing polyoxometalate*. This inactivity is consistent with either its stability and/or the possibility that more than one vanadium is needed for oxygenation catalysis;

(v) The two active species isolated from (n-$Bu_4N)_5[Fe^{II}{\cdot}SiW_9V_3O_{40}]$[23] (grayish black, in the presence of DTBC under O_2) and (n-$Bu_4N)_4H_5PV_{14}O_{42}$[29] (blue, in the presence of DTBC under N_2) give the same selectivities within experimental error as the other species in Table 3.2. The blue species, was tentatively assigned by Tatsuno and co-workers as "$[V(DBSQ)(DBCatH)]_2$" (DBCatH, mono-protonated di-*tert*-butylcatecholate anion);[29]

(vi) The (no vanadium) control of Na_2(DTBC) alone was also examined under our conditions. Previously, deprotonated 3,5-DTBC was reported to react with dissolved oxygen in ether.[50] Depending on the amount of H_2O present, 3,5-di-*tert*-butyl-5-(carboxymethyl)-2-furanone (product **5**) can be obtained in 20–60% yield.[50] In our hands, the light blue disodium salt of 3,5-DTBC in diethyl ether plus O_2 yields furanone (**5**) in 13–21% yield (following acidifying the product mixture with 5% HCl and then extracting with 1,2-$C_2H_4Cl_2$). The major product in the vanadium-catalyzed reactions, muconic acid anhydride (product **2**), is barely detectable by GC (<0.01%). If the above

reaction is carried out in 1,2-$C_2H_4Cl_2$ (i.e., in the solvent used for most of our selectivity experiments,) instead of in Et_2O, then the major products are 3,5-di-*tert*-butyl-1,2-benzoquinone (30% yield) and an unknown compound (m/z = 248, yield ~57% estimated from the area ratio to 3,5-di-*tert*-butyl-1,2-benzoquinone). All other products (i.e., **2–5**) are less than 1%. A control experiment showed that the GC product yields are identical for the original product solution compared to the extracted solution acidified with 5% HCl. In short, the major intradiol cleavage dioxygenase reaction product **2** is obtained *only* upon interaction with a metal, in our case vanadium;

(vii) The control experiment using $[Co^{II}(CH_3CN)_6](BF_6)_2$ produces only 2% of benzoquinone product **6**, showing that the vanadium-based systems do give very different products and selectivities than such slow autoxidation systems.

In summary, the twelve vanadium precursors in Table 3.2 all give same selectivities within experimental error in DTBC oxygenation catalysis.

Catalytic Lifetimes of the Four Simple V-Complexes and Five V-Polyoxometalate Precatalysts.

A) ≤50,000 Total Turnover (TTO) Experiments.[vii] A series of catalytic lifetime experiments (≤50,000 TTOs) were carried out with ca. 29 mmol 3,5-DTBC and ca. 0.7 μmol precatalyst to determine if the catalyst lifetimes vary or are similar. The four simple vanadium complexes and five vanadium polyoxometalate complexes show the same catalytic lifetimes within experimental error, Figure 3.4. The product selectivities are also the same within experimental error for these nine precatalysts examined in the catalytic lifetime experiments. (Full details are provided in Table S3.2 of the Supporting

[vii] The catalytic lifetime experiments at ≤50,000 TTOs (with 29 mmol 3,5-DTBC) are ca. half the largest scale used in the previous work[23] (with ca. 63 mmol 3,5-DTBC). All other conditions are the same: 0.5–0.7 μmol precatalyst, ca. 125 mL 1,2-$C_2H_4Cl_2$, 65 °C, and 1 atm O_2.

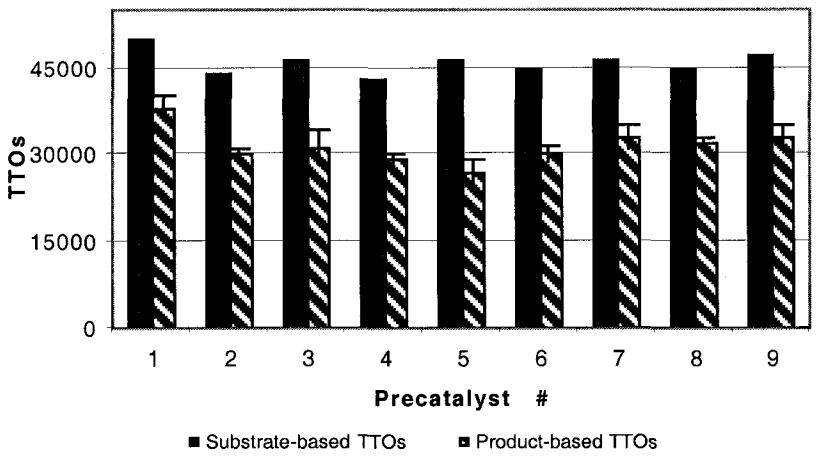

Figure 3.4 Catalytic lifetime study using nine different vanadium-based precatalysts. 1 = $[VO(DBSQ)(DTBC)]_2$; 2 = $[Et_3NH]_2[VO(DTBC)_2]\cdot 2CH_3OH$; 3 = $[Na(CH_3OH)_2]_2[V^V(DTBC)_3]_2\cdot 4CH_3OH$; 4 = $VO(acac)_2$; 5 = $(n\text{-}Bu_4N)_4H_5PV_{14}O_{42}$; 6 = $(n\text{-}Bu_4N)_7SiW_9V_3O_{40}$; 7 = $(n\text{-}Bu_4N)_5[Fe\cdot SiW_9V_3O_{40}]$; 8 = $(n\text{-}Bu_4N)_9P_2W_{15}V_3O_{62}$; 9 = $(n\text{-}Bu_4N)_5Na_2[Fe\cdot P_2W_{15}V_3O_{62}]$. Error bars for the substrate-based TTOs are not available due to the complete conversion (>99%) of the substrate at the end of each reaction.

Information.) Rather clearly, the true catalyst can not be polyoxometalate-based. In short, the results offer further support for the hypothesis that a common catalyst is generated regardless of the V-based precursor employed.

B) 100,000–150,000 TTO Experiments. Several larger-scale catalytic lifetime experiments were carried out with mole ratios of substrate to catalyst (3,5-DTBC to $(n\text{-}Bu_4N)_7SiW_9V_3O_{40}$ or $(n\text{-}Bu_4N)_5Fe^{II}\cdot SiW_9V_3O_{40}$) from 100,000:1 to 150,000:1 to verify the prior record TTOs of ca. 100,000. The results show the product-based TTO catalytic lifetimes of the above two precursors of 60,000–80,000 (±5,000) are comparable with the previous results employing $(n\text{-}Bu_4N)_5Fe^{II}\cdot SiW_9V_3O_{40}$ of 90,000–100,000 (±10,000) product-based TTOs.[23] Details of the results are provided in Table S3.3 of the Supporting Information.

Before our previous studies,[23] the highest reported catalytic lifetime of $VO(acac)_2$ was only ~500 TTOs.[27] Our previous result of the modest TTOs (<6,000) exhibited by $VO(acac)_2$[23] was >10-fold better than the literature[27] so that the <6,000 TTOs seemed reliable at the time. However, given that our current experimental data show that all the vanadium-based precatalysts exhibit the same, high catalytic lifetimes within experimental error, a re-examination of the maximum TTOs exhibited by $VO(acac)_2$ seemed in order. Those experiments reveal that $VO(acac)_2$ exhibits the same 29,000 (±1,000) TTOs of DTBC oxygenation as do all the other V-precatalysts within experimental error. Even after deliberately exposing the somewhat O_2 sensitive $VO(acac)_2$ to atmospheric oxygen, neither the double-integrated EPR area, nor the catalytic lifetime result of aged $VO(acac)_2$ differ from those obtained from a fresh sample (details of the aging procedure are in the Experimental Section, lifetime results are provided in Table S3.3, Supporting Information). Hence, and despite the fact that the underlying cause of the lower TTO performance of $VO(acac)_2$ in previous studies including ours is not clear,[23] the present reproducible result (three experiments) is that $VO(acac)_2$ behaves as a prototypical V DTBC dioxygenase catalyst. In addition and although $VO(acac)_2$ oxidation is slow (by EPR), we suggest that this precatalyst be treated as oxygen sensitive.

^{31}P-NMR Control Confirming the Expected (n-$Bu_4N)_9P_2W_{15}V_3O_{62}$ Precatalyst's Degradation Under Catalytic Conditions. Because a clear prediction of our results so far is that polyoxometalate structures are at least partially degraded under DTBC / O_2 dioxygenase catalysis, an important control was to confirm this prediction by a direct method such as ^{31}P NMR. As the further information and Figure S3.10 of the

Supporting Information detail, a paramagnetic species is formed in the "V_3 cap" of (n-$Bu_4N)_9P_2W_{15}V_3O_{62}$ upon the addition of just 3,5-DTBC (i.e., no O_2). Following the addition of O_2 and catalysis, the ^{31}P NMR peak shifts and loss of intensity confirm that the polyoxoanion structure has been at least somewhat degraded as predicted, Figure S3.10.

EPR Detection of A Common Active Species, $[VO(DBSQ)(DTBC)]_2$. EPR of reaction solutions employing three representative precursors, $(n\text{-}Bu_4N)_4H_5PV_{14}O_{42}$, $[Et_3NH]_2[VO(DTBC)_2]\cdot 2CH_3OH$ and $VO(acac)_2$, all show an EPR signal at center field (g = 2.003–2.004) and a weak broad signal at g = 2.036–2.038. A clear, resolved view at the center signal (g = 2.003–2.004) was obtained by scanning at a magnetic field of 50 G instead of the whole field, 1000 G. The reaction solution employing $VO(acac)_2$ shows a 10 line signal (g = 2.006–2.007, A_{51V} = 2.1 G, Table 3.3) as reported in the literature.[37] We speculate that the EPR detected during the O_2-uptake reactions is a binary or ternary complex between the catalyst, the substrate, and O_2.[viii]

The post-reaction, center-field-scan results show that the *same* EPR spectrum is observed for the three disparate vanadium precatalysts shown in Table 3.3 following 3,5-DTBC oxygenation in toluene. A nine-line spectrum centered at g = 2.004–2.006 (±0.002) with an average hyperfine coupling value (A_{51V}) of 3.04–3.08 (±0.1) G is observed in the EPR spectra of all three post-reaction solutions. Significantly, the literature[37] reports a nine-line EPR spectrum for $[VO(DBSQ)(DTBC)]_2$ centered at g = 2.004 with A_{51V} = 2.85 G (this coupling constant was obtained by simulation[37]), *a*

[viii] The compound exhibiting the 10-line EPR spectrum is tentatively assigned to $V(DBSQ)_3$ in the literature[37] via a parent ion at m/z = 712. In our experience, many different compounds can give this 712 peak (see Table 3.5 in the main text), so that the identity of the compound responsible for the 10-line EPR spectrum remains unclear, a point confirmed by Prof. Pierpont.

spectrum within experimental error of the EPR we observed, Table 3.3 and Figure 3.5. This small coupling constant signifies the weak coordination of the semiquinone ligand DBSQ to the single diamagnetic vanadium(V). *This EPR spectrum serves as a signature of [VO(DBSQ)(DTBC)]$_2$,[37] since most V^{IV} compounds show an eight-line spectrum with hyperfine coupling A_{51V} ~100 G.* Given that we know that [VO(DBSQ)(DTBC)]$_2$: is as active as any complex tested, reacts without an induction period (*vide infra*), displays the maximum O_2-uptake rate of –0.5 mmol O_2/h (*vide infra*), and also gives a high TTO value, it follows from this EPR and other evidence that [VO(DBSQ)(DTBC)]$_2$ is at least a resting state of the true catalyst.

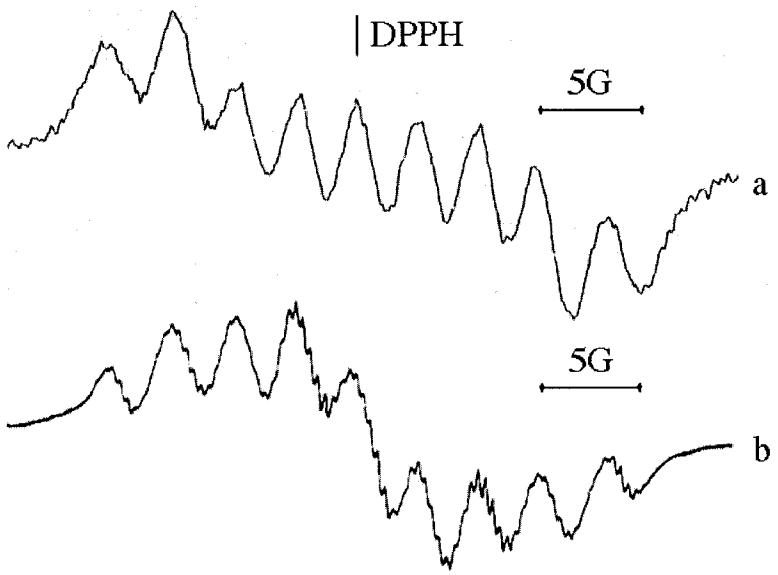

Figure 3.5 Center-field EPR specturm of the post-reaction solution of 3,5-DTBC and $VO(acac)_2$ in toluene (**a**). This resonance is identical within experimental error to those of post-reaction solutions using precatalysts $(n\text{-}Bu_4N)_4H_5PV_{14}O_{42}$ and $[Et_3NH]_2[VO(DTBC)_2]\cdot nCH_3OH$, as shown in Table 3.3, as well as the authentic [VO(DBSQ)(DTBC)]$_2$ in Toluene (**b**).[37]

Importantly, if additional substrate was added to the post-reaction solution of 3,5-DTBC and $VO(acac)_2$ under O_2, the oxygen-uptake continued and the EPR changed back to the EPR observed during reaction. Additionally, the identical EPR diagnostic of $[VO(DBSQ)(DTBC)]_2$ was observed again once all the substrate was consumed, Figure S3.15 of the Supporting Information. *These additional EPR experiments show that the vanadium species we observe in the three post-reaction solutions (Table 3.3) with its characteristic 9-line EPR spectrum is intimately connected to the catalytic cycle of DTBC oxygenation.* Since that 9-line spectrum is seen for authentic $[VO(DBSQ)(DTBC)]_2$, it follows that $[VO(DBSQ)(DTBC)]_2$ is an intimate part of the catalytic cycle.

Table 3.3 EPR Spectra of O_2-uptake Solutions of Three Disparate Kinds of Precatalysts During and After the Reaction.[a]

Pre-catalyst	(n-$Bu_4N)_4H_5PV_{14}O_{42}$	$[Et_3NH]_2[VO(DTBC)_2]\cdot nCH_3OH$	$VO(acac)_2$[b]
Post-induction period / During reaction (Full Spectrum)	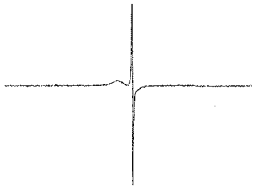	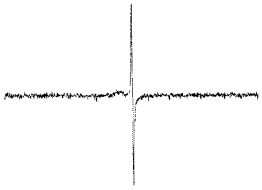	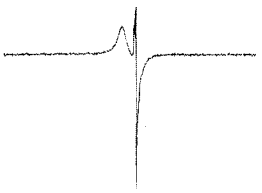
(Center-field-scan)	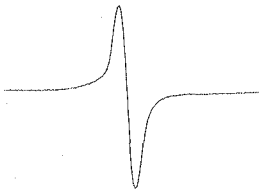	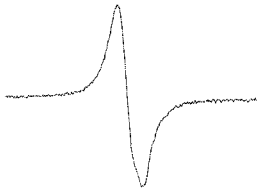	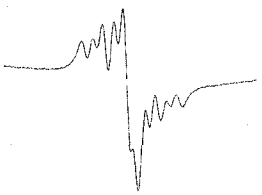
Post reaction (center-field-scan)	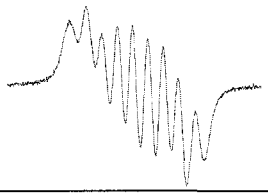	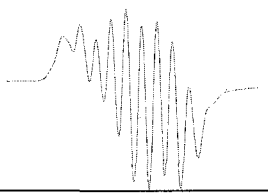	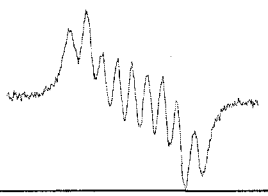

[a]The full spectra were scanned at a magnetic field width of 1000 G while the center-field-scans were obtained at 50 G.

[b]The spectra of the oxygenation reaction solution using $VO(acac)_2$ are different from those of (n-$Bu_4N)_4H_5PV_{14}O_{42}$ or $[Et_3NH]_2[VO(DTBC)_2]\cdot nCH_3OH$. The reason for the lack of hyperfine coupling in the center-field-scan spectra is not known, but may result from interference from the additional ligands present in those two cases.

Quantitation of the $[VO(DBSQ)(DTBC)]_2$ EPR Signal. Given the high sensitivity of EPR, it was important to determine whether or not $[VO(DBSQ)(DTBC)]_2$ is present more than at a trace level. Hence, the amount of the vanadyl semiquinone dimer complex in the post-reaction solution was compared by double integration to the air-stable free-radical in crystalline $[Co^{III}(3,5\text{-}DBSQ)(CN)_4]^{2-}$,[36] a sample generously provided by Professor M. Wicholas. This comparison indicates that the $[VO(DBSQ)(DTBC)]_2$ semiquinone complex is present at ca. 5 mol% of the precatalyst ($VO(acac)_2$) concentration (ca. 0.035 mM), an estimate that is necessarily an approximation since $[VO(DBSQ)(DTBC)]_2$ is oxygen sensitive and slowly degrades under aerobic conditions. The results, again, support $[VO(DBSQ)(DTBC)]_2$ as a key species intimately connected to the catalytic cycle.

Negative Ion ESI–MS Evidence of a Common Catalyst, $[VO(DBSQ)(DTBC)]_2$. When crystalline $[VO(DBSQ)(DTBC)]_2$ is dissolved in acetonitrile, the molecular ion peak at m/z = 1015 is observable, together with two main fragment peaks at (m/z =) 507, assigned to $[VO(DTBC)_2]^-$, and at (m/z =) 711.4, assigned to $[V(DTBC)_3]^-$, Figure 3.6. When MS-MS was applied to the molecular ion peak, a peak attributable to $[VO(DTBC)_2]^-$ (m/z = 507) was observed.

The m/z = 507, 711 and 1015 peaks were simulated using the software Isotope Viewer (version 1.0; in the Qual Browser of the Thermo Finnigan MS). The corresponding formulae reproducing the observed molecular weights and isotopic abundances are $VO(C_{14}H_{20}O_2)_2$ corresponding to $[VO(DTBC)_2]^-$, $V(C_{14}H_{20}O_2)_3$ corresponding to $[V(DTBC)_3]^-$, and $[V_2O_2(C_{14}H_{20}O_2)_3(C_{14}H_{21}O_2)]$ corresponding to$[V_2O_2(DBSQ)(DBSQ–H)(DTBC)_2]^-$ (where $C_{14}H_{20}O_2$ corresponds to 3,5-di-*tert*-

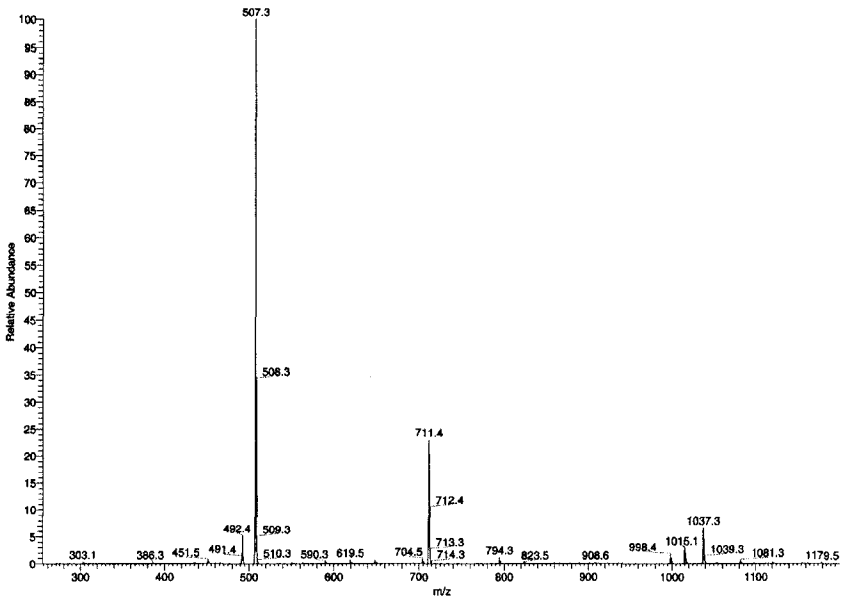

Figure 3.6 Negative Ion ESI–MS spectrum of crystalline $[VO(DBSQ)(DTBC)]_2$. The parent ion peak is at m/z = 1015; the additional peak at m/z = 1037 is due to an exchange of two H^+ with Mg^{2+} of $MgSO_4$ from the distillation step. The base peak, at m/z = 507, is due to $[VO(DTBC)_2]^-$.

Table 3.4 Observed vs Computer Simulated Parent Peaks and Isotopic Abundance Patterns For $[VO(DTBC)_2]^-$, $[V(DTBC)_3]^-$ and $[V_2O_2(DBSQ)(DBSQ–H)(DTBC)_2]^-$.

	$[VO(DTBC)_2]^-$ (i.e., $VC_{28}H_{40}O_5$, m/z 507)[a]	$[V(DTBC)_3]^-$ (i.e., $VC_{42}H_{60}O_6$, m/z 711)[b]	$[V_2O_2(DBSQ)(DBSQ–H)(DTBC)_2]^-$ (i.e., $V_2C_{56}H_{81}O_{10}$, m/z 1015)[c]
Observed	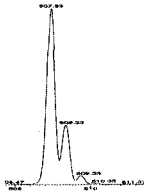	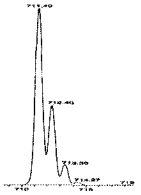	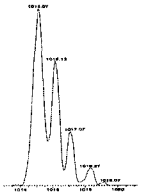
Simulated	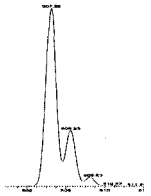	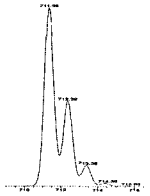	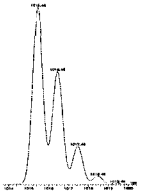

[a]Observed peaks: 507.3, 508.3 and 509.3, simulated peaks: 507.2, 508.2 and 509.2;
[b]Observed peaks: 711.4, 712.4 and 713.3, simulated peaks: 711.4, 712.4 and 713.4;
[c]Observed peaks: 1015.1, 1016.1, 1017.1 and 1018.3, simulated peaks: 1015.5, 1016.5, 1017.5 and 1018.3.

butylcatecholate dianion or 3,5-di-*tert*-butylsemiquinone anion and $C_{14}H_{21}O_2$ corresponds to protonated 3,5-di-*tert*-butylsemiquinone (3,5-DBSQ–H) radical). The observed MS spectra and simulations are shown in Table 3.4. The match between the observed and simulated spectra is excellent.

As a semi-quantitative method, ESI–MS is capable of identifying the main species in solution.[51,52,53] Significantly, two common major peaks ($VO(DTBC)_2^-$ of m/z 507, and $V(DTBC)_3^-$ of m/z 711.5) are detected in the mass spectra for two of the three vanadium catecholate compounds and the two isolated active components from the vanadium polyoxometalates, Table 3.5.

Table 3.5 Negative Ion Electrospray-Ionization Mass Spectrometry Identified Peaks of Various Precursors.

ESI–MS Peaks, m/z	451.4	491.4	**507.3**	**711.4**	998.4	1015.1
	Relative Abundance					
Simple V-Catecholate Complexes						
$[VO(DBSQ)(DTBC)]_2$	<5	<5	**100**	**25**	<5	<5
$[Et_3NH]_2[VO(DTBC)_2]\cdot 2CH_3OH$			**86**	**100**	30	<10
$[Na(CH_3OH)_2]_2[V(DTBC)_3]_2\cdot 4CH_3OH$		<10	**<5**[a]	**100**		
Isolated Active Components						
Isolated active species from $(n\text{-}Bu_4N)_5[Fe^{II}\cdot SiW_9V_3O_{40}]$	93		**100**	**17**		
Isolated active species from $(n\text{-}Bu_4N)_4H_5PV_{14}O_{42}$	25	<5	**30**	**100**		

[a] $[Na(CH_3OH)_2]_2[V(DTBC)_3]_2\cdot 4CH_3OH$ only shows a trace amount of $[VO(DTBC)_2]^-$ in its negative ion ESI–MS as expected since it lacks an oxo ligand.

The possibility of either hydrolysis or oxygenation during the process of electrospray ionization needs to be considered. Oxygenation was minimized by sealing

the sample in the drybox and exposing it to air only briefly just before injection. The effect of water was tested with several controls detailed in the Experimental Section; these experiments show the two common peaks ($VO(DTBC)_2^-$ and $V(DTBC)_3^-$) are *not* generated through a reaction with water. Overall, the mass spectral data further support the hypothesis that the active species in the reaction solution is $[VO(DBSQ)(DTBC)]_2$, since its diagnostic fragment peak $VO(DTBC)_2^-$ at m/z = 507 as seen from authentic material $[VO(DBSQ)(DTBC)]_2$ is observed in the post-reaction solution from disparate vanadium precatalysts including active components isolated from two different V-containing polyoxometalate precatalysts.

Kinetic Competence of $[VO(DBSQ)(DTBC)]_2$, But Not of $[Na(CH_3OH)_2]_2[V(DTBC)_3]_2 \cdot 4CH_3OH$. In oxygen-uptake experiments, Figure 3.7, $[VO(DBSQ)(DTBC)]_2$ was shown to be an active oxygenation catalyst with no induction period. Moreover, its rate is as fast as any catechol oxygenation catalysis we have observed for our conditions herein,[ix] $d[O_2]/dt_{max} \sim -0.5$ mmol/h. This establishes $[VO(DBSQ)(DTBC)]_2$ as a kinetically competent catalyst or catalyst resting state.

The remaining question is whether the other common MS peak (m/z = 711.5, $V(DTBC)_3^-$) is one of the catalytic species. In kinetic trials, an induction period of about 10 min is observed when $[Na(CH_3OH)_2]_2[V(DTBC)_3]_2 \cdot 4CH_3OH$ is used as the precatalyst. Therefore, $V(DTBC)_3^-$ can be ruled out as a dominant catalyst.

[ix] The maximum rate, measured from the post-induction period (or initial rate in the case of $[VO(DBSQ)(DTBC)]_2$), is approaching the O_2 gas-to-solution mass transfer limit under our experimental conditions of: 400 mg (1.8 mmol) DTBC, 0.46–0.48 mM precatalyst/catalyst, ca. 9 mL 1,2-$C_2H_4Cl_2$, 40 (± 0.7) °C, 1 atm O_2, and stirring rate of ca. 700–800 rpm.

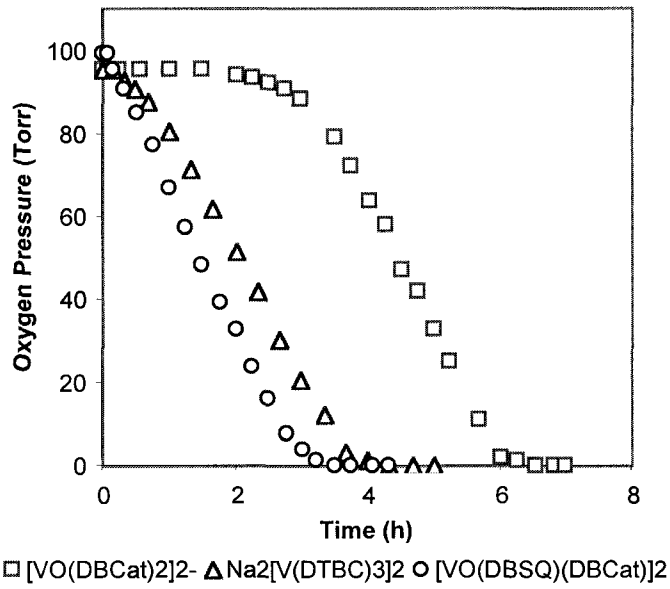

Figure 3.7 Kinetic competence or incompetence of the three vanadium catecholate complexes. Experimental conditions: 400 mg (1.8 mmol) DTBC, 0.46–0.48 mM precatalyst/catalyst, ca. 9 mL 1,2-$C_2H_4Cl_2$, 40 (± 0.7) °C, and 1 atm O_2.

In summary, $[VO(DBSQ)(DTBC)]_2$ is a kinetically competent catalyst or catalyst resting state. It is proposed as an active catalyst component in (at least) the eleven tabulated vanadium catechol dioxygenases, based on the observation of its signature EPR spectrum in the post-reaction solution of three different classes of precatalysts, and the observation of its diagnostic half fragment ($VO(DTBC)_2^-$) in the negative ion ESI–MS spectra of post-reaction solutions beginning with disparate precatalysts including vanadium catecholate complexes and polyoxometalates. The EPR and negative ion ESI–MS signatures reported herein can now be used to expand or refute the "common catalyst" finding herein with any other vanadium-based DTBC dioxygenase system.

Conclusions

In conclusion, we have: i) shown that a survey of eleven literature reports of vanadium-based catechol dioxygenases reveals that they all give very similar product ratios, an insight which in turn implies that a common catalyst is present; ii) shown that ten vanadium compounds that we have tested to date behave remarkably similar in their DTBC oxygenation catalysis selectivities and TTOs, again implying the existence of a common active catalyst; and iii) provided EPR, negative ion ESI–MS and kinetic data which all point to a common resting form of the catalyst, namely Pierpont's novel $[VO(DBSQ)(DTBC)]_2$ complex.

This study also provides an excellent example of the phenomenon of "leaching" of a soluble form of the true catalyst from both heterogeneous[54] and homogeneous precatalysts. Combined with previous work,[54] our results indicate, for example, that the task of preparing single-site, supported V_x catalysts[55,56] (e.g., x = 1,2) which stay firmly supported and do not leach, is an important but probably very difficult challenge. Put in different terms, facile ligand substitution, and leaching, especially in the presence of H_2O_2[31] and powerfully chelating ligands such as DTBC dianion, is hereby established as the dominant hypothesis to be disproved for future V-based oxygenation catalysis.

In a subsequent paper we provide further evidence that $[VO(DBSQ)(DTBC)]_2$ is a catalyst resting state that reversibly fragments to its reactive monomer, [VO(DBSQ)(DTBC)], as well as evidence for a novel autoxidation-product-initiated mechanism for the release of V from V-based precatalysts to form $[VO(DBSQ)(DTBC)]_2$, that is, for a novel autoxidation-initiated dioxygenase.[31]

Acknowledgement. We thank Professor Cort G. Pierpont for multiple insightful discussions relevant to this work and Professor Mark Wicholas for his generous gift of air-stable cobalt semiquinone crystals employed in the quantitative EPR analysis. We thank Mr. Don Dick for his expert assistance with the GC-MS and negative ion ESI–MS experiments, Mr. Don Heyse for his expert assistance with the EPR experiments, and Dr. Susie Miller for her expert assistance with the single crystal X-ray crystallography. This research is supported by NSF fund 9531110.

Supporting Information Available: 35 pages, including: preparation of polyoxometalate precursors; preparation and characterization of $[VO(DBSQ)(DTBC)]_2$, $[Et_3NH]_2[VO(DTBC)_2]\cdot nCH_3OH$, and $[Na(CH_3OH)_2]_2[V(DTBC)_3]_2\cdot 4CH_3OH$; preparation and characterization of deprotonated 3,5-di-*tert*-butylcatecholate salt Na_2(3,5-DTBC) and $[Et_3NH][V(DTBC)_3]\cdot 1.5CH_3OH$; ^{31}P-NMR following oxygen-uptake using $(n\text{-}Bu_4N)_9P_2W_{15}V_3O_{62}$; catalyst isolation attempts; spectroscopic information (UV-visible, negative ion ESI–MS, or ^{1}H-NMR) of $[VO(DBSQ)(DTBC)]_2$, $[Et_3NH]_2[VO(DTBC)_2]\cdot nCH_3OH$ and $[Na(CH_3OH)_2]_2[V(DTBC)_3]_2\cdot 4CH_3OH$; EPR spectrum of Zn(Cat-N-SQ)(BQ-N-SQ); crystal data for $[Na(CH_3OH)_2]_2[V(DTBC)_3]_2\cdot 4CH_3OH$; IR spectrum of Na_2(3,5-DTBC) and 3,5-DTBC; ^{31}P-NMR following the O_2-uptake of $(n\text{-}Bu_4N)_9P_2W_{15}V_3O_{62}$ with DTBC; IR spectrum of $(n\text{-}Bu_4N)_5Fe^{II}\cdot SiW_9V_3O_{40}$ and the isolated active species from $(n\text{-}Bu_4N)_5Fe^{II}\cdot SiW_9V_3O_{40}$; negative ion ESI–MS spectrum of isolated catalyst from $(n\text{-}Bu_4N)_5Fe^{II}\cdot SiW_9V_3O_{40}$; solid EPR of the material isolated from $(n\text{-}Bu_4N)_4H_5PV_{14}O_{42}$; center-field, 9-line EPR spectrum of a post-reaction solution of 3,5-DTBC and $VO(acac)_2$ in toluene which had additional fresh DTBC and O_2 added; tabulated literature overview of vanadium catecholate

organometallic complexes relevant to dioxygenase catalysis; details for ≤50,000 TTO catalytic lifetime experiments (data for Figure 3.4 in the Main Text) and 100,000–150,000 TTO catalytic lifetime experiments.

References

[1] Hayaishi, O.; Editor *Molecular Mechanisms of Oxygen Activation*; Academic Press: New York, 1974.

[2] Oyama, S. T.; Desikan, A. N.; Hightower, J. W. In *Catalytic Selective Oxidation*; Oyama, S. T., Hightower, J. W., Eds.; ACS Symposium Series 523; American Chemical Society: Washington, D. C., 1993, pp 1-14.

[3] Hill, C. L.; Weinstock, I. A. *Nature* **1997**, *388*, 332-333.

[4] Sheldon, R. A. In *Biomimetic Oxidations Catalyzed by Transition Metal Complexes*; Meunier, B., Ed.; Imperial College Press: London, 2000, pp 613-662.

[5] (a) Hayaishi, O.; Hashimoto, K. *J. Biochem. (Tokyo)* **1950**, *37*, 371-374. (b) Hayaishi, O.; Katagiri, M.; Rothberg, S. *J. Am. Chem. Soc.* **1955**, *77*, 5450-5451.

[6] Nozaki, M. In *Molecular Mechanisms of Oxygen Activation*; Academic Press: New York, 1974, pp 135-165.

[7] Nozaki, M. *Top. Curr. Chem.* **1979**, *78*, 145-186.

[8] Que, L., Jr.; Ho, R. Y. N. *Chem. Rev.* **1996**, *96*, 2607-2624.

[9] Que, L., Jr.; Reynolds, M. F. *Met. Ions Biol. Syst.* **2000**, *37*, 505-525.

[10] Costas, M.; Mehn, M. P.; Jensen, M. P.; Que, L., Jr. *Chem. Rev.* **2004**, *104*, 939-986.

[11] Funabiki, T. In *Catalysis by Metal Complexes*; Funabiki, T., Ed.; Kluwer Academic Publishers: Dordrecht, The Netherlands, 1997; Vol. 19, pp 105-155.

[12] Krüger, H.-J. In *Biomimetic Oxidations Catalyzed by Transition Metal Complexes*; Meunier, B., Ed.; Imperial College Press: London, 2000, pp 363-413.

[13] Yamahara, R.; Ogo, S.; Masuda, H.; Watanabe, Y. *J. Inorg. Biochem.* **2002**, *88*, 284-294 and references therein.

[14] Jang, H. G.; Cox, D. D.; Que, L., Jr. *J. Am. Chem. Soc.* **1991**, *113*, 9200-9204.

[15] Dei, A.; Gatteschi, D.; Pardi, L. *Inorg. Chem.* **1993**, *32*, 1389-1395.

[16] Ito, M.; Que, L., Jr. *Angew. Chem., Int. Ed. Engl.* **1997**, *36*, 1342-1344.

[17] Jo, D.-H.; Que, L., Jr. *Angew. Chem., Int. Ed. Engl.* **2000**, *39*, 4284-4287.

[18] Pascaly, M.; Duda, M.; Schweppe, F.; Zurlinden, K.; Müller, F. K.; Krebs, B. *J. Chem. Soc., Dalton Trans.* **2001**, 828-837.

[19] Matsumoto, M.; Kuroda, K. *J. Am. Chem. Soc.* **1982**, *104*, 1433-1434.

[20] Bianchini, C.; Frediani, P.; Laschi, F.; Meli, A.; Vizza, F.; Zanello, P. *Inorg. Chem.* **1990**, *29*, 3402-3409.

[21] Vlcek, A., Jr. *Chemtracts: Inorganic Chemistry* **1991**, *3*, 275-280.

[22] Nishinaga, A. In *Catal. Met. Complexes*; Kluwer Academic Publishers: Dordrecht, The Netherlands, 1997; Vol. 19, pp 157-194.

[23] Weiner, H.; Finke, R. G. *J. Am. Chem. Soc.* **1999**, *121*, 9831-9842.

[24] Pope, M. T.; Müller, A.; Editors *Polyoxometalates: From Platonic Solids to Anti-Retroviral Activity. [In: Top. Mol. Organ. Eng., 1994; 10]*; Kluwer Academic Publishers: Dordrecht, The Netherlands, 1994.

[25] Hill, C. L.; Editor *Chem. Rev.* **1998**, *98*, 1-390.

[26] Pope, M. T.; Müller, A.; Editors *Polyoxometalate Chemistry From Topology via Self-Assembly to Applications*; Kluwer Academic Publishers: Dordrecht, The Netherlands, 2001.

[27] Tatsuno, Y.; Tatsuda, M.; Otsuka, S. *J. Chem. Soc., Chem. Commun.* **1982**, 1100-1101.

[28] Watzky, M. A.; Finke, R. G. *J. Am. Chem. Soc.* **1997**, *119*, 10382-10400 and ref 34 therein.

[29] Tatsuno, Y.; Nakamura, C.; Saito, T. *J. Mol. Catal.* **1987**, *42*, 57-66.

[30] Pierpont, C. G.; Lange, C. W. *Prog. Inorg. Chem.* **1994**, *41*, 331-442.

[31] Yin, C.-X.; Sasaki, Y.; Finke, R. G. "Autoxidation-Product-Initiated Dioxygenases: Vanadium-Based, Record Catalytic Lifetime Catechol Dioxygenase Catalysis and Its Mechanism of Action," manuscript in preparation.

[32] (a) Preuss, F.; Schug, H. *Z. Naturforsch., B: Anorg. Chem., Org. Chem.* **1976**, *31B*, 1585-1591. (b) Kato, R.; Kobayashi, A.; Sasaki, Y. *J. Am. Chem. Soc.* **1980**, *102*, 6571-6572. (c) Kato, R.; Kobayashi, A.; Sasaki, Y. *Inorg. Chem.* **1982**, *21*, 240-246.

[33] Finke, R. G.; Rapko, B.; Saxton, R. J.; Domaille, P. J. *J. Am. Chem. Soc.* **1986**, *108*, 2947-2960.

[34] Hornstein, B. J.; Finke, R. G. *Inorg. Chem.* **2002**, *41*, 2720-2730.

[35] Nakagawa, Y.; Uehara, K.; Mizuno, N. *Inorg. Chem.* **2005**, *44*, 14-16.

[36] Arzberger, S.; Soper, J.; Anderson, O. P.; La Cour, A.; Wicholas, M. *Inorg. Chem.* **1999**, *38*, 757-761.

[37] Cass, M. E.; Green, D. L.; Buchanan, R. M.; Pierpont, C. G. *J. Am. Chem. Soc.* **1983**, *105*, 2680-2686.

[38] Cooper, S. R.; Koh, Y. B.; Raymond, K. N. *J. Am. Chem. Soc.* **1982**, *104*, 5092-5102.

[39] Luneva, N. P.; Mironova, S. A.; Lysenko, K. A.; Antipin, M. Y. *Russ. J. Coord. Chem. (Transl. of Koord. Khim.)* **1997**, *23*, 844-849.

[40] Hagen, C. M.; Vieille-Petit, L.; Laurenczy, G.; Süss-Fink, G.; Finke, R. G. *Organometallics,* **2005**, *24*, 1819-1831; see footnote 45 therein.

[41] Tatsuno, Y.; Tatsuda, M.; Otsuka, S.; Tani, K. *Chem. Lett.* **1984**, 1209-1212.

[42] Casellato, U.; Tamburini, S.; Vigato, P. A.; Vidali, M.; Fenton, D. E. *Inorg. Chim. Acta* **1984**, *84*, 101-104.

[43] Roman, E.; Tapia, F.; Barrera, M.; Garland, M. T.; Le Marouille, J. Y.; Giannotti, C. *J. Organomet. Chem.* **1985**, *297*, C8-C12.

[44] Galeffi, B.; Postel, M.; Grand, A.; Rey, P. *Inorg. Chim. Acta* **1987**, *129*, 1-5.

[45] Galeffi, B.; Postel, M.; Grand, A.; Rey, P. *Inorg. Chim. Acta* **1989**, *160*, 87-91.

[46] Nishida, Y.; Kikuchi, H. *Z. Naturforsch., B: Chem. Sci.* **1989**, *44*, 245-247.

[47] Russo, U.; Zarli, B.; Zanonato, P.; Vidali, M. *Polyhedron* **1991**, *10*, 1353-1361.

[48] Zhang, B. Y.; Zhang, Y.; Chen, B. W.; Wang, K. *Chin. Chem. Lett.* **1997**, *8*, 547-550.

[49] (a) Cadot, E.; Marchal, C.; Fournier, M.; Tézé, A.; Hervé, G. In *Polyoxometalates: From Platonic Solids to Anti-Retroviral Activity.* [In: *Top. Mol. Organ. Eng.*, 1994; 10]; Pope, M. T., Müller, A., Eds.; Kluwer Academic Publishers: Dordrecht, The Netherlands, 1994; Vol. 10, pp 315-326. (b) Kozhevnikov, I. V. *Chem. Rev.* **1998**, *98*, 171-198 (see pp 189-191 and references therein). (c) A detailed speciation study on H^+–H_2VO_4–H_2O_2 systems: Andersson, I.; Angus-Dunne, S.; Howarth, O.; Pettersson, L. *J. Inorg. Biochem.* **2000**, *80*, 51-58.

[50] Speier, G.; Tyeklár, Z. *J. Mol. Catal.* **1990**, *57*, L17-L19.

[51] Ralph, S. F.; Iannitti, P.; Kanitz, R.; Sheil, M. M. *Eur. Mass Spectrom.* **1996**, *2*, 173-179. This key, early paper provides an example showing that ESI–MS peak intensities correlate well with known compositions in solution, at least for the particular system examined.

[52] Raymond, C. C.; Dick, D. L.; Dorhout, P. K. *Inorg. Chem.* **1997**, *36*, 2678-2681.

[53] (a) Deery, M. J.; Fernandez, T.; Howarth, O. W.; Jennings, K. R. *J. Chem. Soc., Dalton Trans.* **1998**, 2177-2183. (b) Fyles, T. M.; Zeng, B. *Supramol. Chem.* **1998**, *10*, 143-153. (c) Pasilis, S. P.; Pemberton, J. E. *Inorg. Chem.* **2003**, *42*, 6793-6800.

[54] Arends, I. W. C. E.; Sheldon, R. A. *Appl. Catal., A* **2001**, *212*, 175-187.

[55] Rulkens, R.; Tilley, D. T. *J. Am. Chem. Soc.* **1998**, *120*, 9959-9960.

[56] Khodakov, A.; Olthof, B.; Bell, A. T.; Iglesia, E. *J. Catal.* **1999**, *181*, 205-216.

Supporting Information For

Vanadium-Based, Record Catalytic Lifetime Catechol Dioxygenases: Evidence For a Common Catalyst

Cindy-Xing Yin and Richard G. Finke

Preparation of Polyoxometalate Precursors

(n-$Bu_4N)_4H_5PV_{14}O_{42}$ was prepared by metathesis of the potassium salt $K_4H_5PV_{14}O_{42}$, which was prepared according to the literature procedures.[1] (n-$Bu_4N)_4H_5PV_{14}O_{42}$ was characterized by IR spectroscopy and CHN analysis, calculated for (n-$Bu_4N)_4H_5PV_{14}O_{42}$ (found): C 32.15% (32.30%), H 6.28% (6.22%), N 2.34% (2.30%). (n-$Bu_4N)_7SiW_9V_3O_{40}$ and (n-$Bu_4N)_9P_2W_{15}V_3O_{62}$ were prepared via the preparation method described previously.[2,3] The yield of (n-$Bu_4N)_7SiW_9V_3O_{40}$ was 4.3 g (1.0 mmol) (89% yield based on its precursor (n-$Bu_4N)_4H_3SiW_9V_3O_{40}$ and of ca. 84% purity by ^{51}V-NMR in comparison to ~85% in the literature, also by ^{51}V-NMR).[2] The IR (as a KBr pellet) matched the literature fingerprint.[2] The yield of (n-$Bu_4N)_9P_2W_{15}V_3O_{62}$ was 0.93 g (0.15 mmol) (80% based on its precursor (n-$Bu_4N)_5H_4P_2W_{15}V_3O_{62}$ and of ca. 80% purity by ^{31}P-NMR; some $P_2W_{16}V_2O_{62}^{8-}$ is the most probably contaminant based on our recent work).[3] The IR (as a KBr pellet) matched the literature.[4] Note that these literature as well as our present polyoxoanion purities are more than sufficient for the present studies which show that active catalysts need only contain V which, in the end, is extracted from the polyoxometalate structures to yield the true active catalyst. (n-$Bu_4N)_5Fe^{II}{\cdot}SiW_9V_3O_{40}$ and (n-$Bu_4N)_5Na_2Fe^{II}{\cdot}P_2W_{15}V_3O_{62}$ were synthesized according to the literature;[4] the yield of (n-$Bu_4N)_5Fe^{II}{\cdot}SiW_9V_3O_{40}$ was 631 mg (0.169 mmol; 60% based on (n-$Bu_4N)_7SiW_9V_3O_{40}$; lit. yield 48–52%); the yield of (n-$Bu_4N)_5Na_2Fe^{II}{\cdot}P_2W_{15}V_3O_{62}$ was 39 mg (0.0074 mmol; 37% based on (n-$Bu_4N)_9P_2W_{15}V_3O_{62}$; lit. yield 82–88%). The low yield in the latter case

---

[1] (a) Preuss, F.; Schug, H. *Z. Naturforsch., B: Anorg. Chem., Org. Chem.* **1976**, *31B*, 1585-1591; (b) Kato, R.; Kobayashi, A.; Sasaki, Y. *J. Am. Chem. Soc.* **1980**, *102*, 6571-6572; (c) Kato, R.; Kobayashi, A.; Sasaki, Y. *Inorg. Chem.* **1982**, *21*, 240-246.
[2] Finke, R. G.; Rapko, B.; Saxton, R. J.; Domaille, P. J. *J. Am. Chem. Soc.* **1986**, *108*, 2947-2960.
[3] Hornstein, B. J.; Finke, R. G. *Inorg. Chem.* **2002**, *41*, 2720-2730.
[4] Weiner, H.; Finke, R. G. *J. Am. Chem. Soc.* **1999**, *121*, 9831-9842.

is due to the smaller, ca. 1/10 scale employed in comparison to the original literature,[4] but provided sufficient amounts for the present studies. Both Fe^{II}-supported polyoxometalates were identified through their IR (fingerprint) spectra.[4]

Preparation and Characterization of Vanadium-Catecholate Complexes

$[VO(DBSQ)(DTBC)]_2$. Following the literature,[5] 0.26–0.27 g $VO(acac)_2$ (ca. 1.0 mmol) and 1.1–1.2 g of *crude*, non-recrystallized 3,5-DTBC (ca. 4.9 mmol) were both weighed and combined in a 50 mL round-bottomed Schlenk flask in the drybox. (The use of as-received 3,5-DTBC is as reported in the literature.[5]) Next, 30 mL methanol were added to a separate flask containing ca. 2–4 g of anhydrous $MgSO_4$. Both flasks were sealed and brought out of the drybox. The flask containing methanol and $MgSO_4$ was attached to a distillation apparatus consisting of a Y-shaped adapter with a Vigreux condenser plus the pre-prepared receiving flask contained $VO(acac)_2$ and 3,5-DTBC all under a flow of argon. Next, the flask containing methanol was frozen with liquid N_2 and the whole system was subjected to two pump-and-fill cycles with Ar as the refill gas. Then, the 30 mL of methanol was distilled over 3–4 h into the flask containing $VO(acac)_2$ and 3,5-DTBC under an argon flow. The reaction solution turned dark blue upon addition of the methanol. After the distillation, the sidearm of the flask with the reaction solution was opened to air for several seconds (ca. 10 s) and then re-sealed, *all as reported in the literature.*[5] The stirring was stopped and the whole apparatus was then left to stand for 2–3 h. An aliquot of the dark-blue solution was examined under a microscope for a crystal suitable for X-ray crystallography, but none were found. (In a repeat synthesis *in anisole*, no suitable single crystals were obtained, although the

[5] Cass, M. E.; Green, D. L.; Buchanan, R. M.; Pierpont, C. G. *J. Am. Chem. Soc.* **1983**, *105*, 2680-2686.

literature teaches that single crystals can sometimes be obtained from anisole.[5,6]) Next, the blue solution was filtered through a glass frit and the solid was collected (yield 0.14 g, 0.13 mmol, 26%, lit. yield not reported). The solid was then washed twice with ca. 5 mL methanol in air (an additional step vs the literature procedure[5]). The black-blue crystalline powder was collected from the filter and transferred into the drybox for storage. The final yield was ca. 0.1–0.2 g, ~18–36%.

Characterization of $[VO(DBSQ)(DTBC)]_2$

UV-visible spectroscopy. As shown in Figure S3.1 in the Supporting Information, the spectrum in toluene solution under N_2 has absorbance peaks at 294 nm (~30,000 $M^{-1}\cdot cm^{-1}$) and 668 nm (~27,000 $M^{-1}\cdot cm^{-1}$). Depending on the precise level of O_2-inclusion employed during the synthesis, sometimes a precursor with UV-visible absorbances at 294 nm (~19,000 $M^{-1}\cdot cm^{-1}$) and 476 nm (~12,000 $M^{-1}\cdot cm^{-1}$) can be observed prior to the appearance of the absorbances reported above (by exposing the solution to air shortly). This observation, however, does not change the conclusions in the main text drawn from the kinetic, EPR and ESI–MS results. The appearance of a peak at 388 nm was observed after the sample in the UV cell was bubbled with pure oxygen for 5 min and then kept under O_2 for 1 h (the 668 nm peak absorbance intensity was lower at this point). The literature reports that $[VO(DBSQ)(DTBC)]_2$ has an absorbance at 640 nm in toluene.[5,7]

Negative Ion ESI–MS. The mass spectrum is shown in Figure 3.6 of the main text with a parent ion peak at m/z 1015, corresponding to the formula of

---

[6] Cass, M. E.; Ph.D. Thesis, University of Colorado, Boulder, CO., 1984, p 53.

[7] The electronic spectrum of $[VO(DBSQ)(DTBC)]_2$ in solution was not provided in the literature (although a solid electronic spectrum of $[VO(DBSQ)(DTBC)]_2$ was provided).[5] The authors noted the disappearance of a band from the solid state spectrum at 300 nm when dissolving $[VO(DBSQ)(DTBC)]_2$ in toluene. They also observed a peak at 390 nm in the solid state, which we have observed in solution only in a sample that had been bubbled with O_2.

$[V^{IV}_2O_2(DBSQ)(DBSQ–H)(DTBC)_2]^-$, (i.e., $V_2C_{56}H_{81}O_{10}$), together with two main fragments at m/z 507 ($VO(DTBC)_2^-$) and 711.4 ($V(DTBC)_3^-$). The peak at m/z 1037 is possibly due to the parent ion peak with two H^+ exchanged by Mg^{2+} (apparently from the distillation step with $MgSO_4$, *vide supra*).

Elemental analysis. No microanalysis data were reported in the literature.[5] Different batches made from methanol vary in their elemental compositions due to varying amounts of methanol solvate present. Calculated (as $[VO(DBSQ)(DTBC)]_2\cdot(CH_3OH)_n$, i.e., $V_2C_{56}H_{82}O_{10}(CH_4O)_n$ with n = 3): C (63.65%), H (8.51%), N (0.0%); observed: batch #1: C (64.08%), H (8.02%), N (0.0%), batch #2: C (63.97%), H (7.84%), N (0.0%); calculated (with n = 5): C (62.23%), H (8.73%), N (0.0%); observed: batch #3: C (62.3%), H (7.9%), N (<0.5%).

$[Et_3NH]_2[VO(DTBC)_2]\cdot nCH_3OH$ (n = 2 reported in the literature[8]). Following the literature,[8] 1.1 g $VO(acac)_2$ (4.1 mmol) with 3.1 g *once recrystallized* 3,5-DTBC (13.95 mmol) in 50 mL anhydrous methanol and 10 mL Et_3N were refluxed for one hour under Ar. The solution was concentrated to ca. 25 mL under vacuum. The product, a green powder, was obtained by filtering the solution through a glass frit and washed with ca. 30 mL diethyl ether in air and then air dried (for ca. 0.5 h) as reported in the literature.[8] The yield is 0.52 g, 18%. A repeat using only 5 mL diethyl ether for the last washing step resulted in an improved yield of 2.3 g, 79% (lit. yield is 72%[8]).

Characterization of $[Et_3NH]_2[VO(DTBC)_2]\cdot nCH_3OH$

[8] Cooper, S. R.; Koh, Y. B.; Raymond, K. N. *J. Am. Chem. Soc.* **1982**, *104*, 5092-5102.

UV-visible spectroscopy. A spectrum, Figure S3.2, taken in 0.1 M $NaOH/CH_3OH$ solution as the literature[8,9] exhibits a broad absorbance at 656 nm (literature, 654 nm). The extinction coefficient at 656 nm is ~250 $M^{-1}\cdot cm^{-1}$ vs the literature value of 150 $M^{-1}\cdot cm^{-1}$.[8]

Negative Ion ESI–MS. The spectrum is shown in Figure S3.3, with an ion peak at m/z = 507.4 (due to the oxidized vanadium(V) $V^{V}O(DTBC)_2^-$) together with a peak at m/z of 711.5 (due to $V(DTBC)_3^-$ or $[Et_3NH]_2[VO(DTBC)_2]^-$). These peaks match with simulated spectra based on the calculated formula and isotopic abundances. Two minor peaks at m/z = 998.5 and 1202.5 are assigned to $V_2O(DTBC)_4^-$ and $V_2(DTBC)_5^-$, respectively.

Elemental analysis. Calculated (based on $[Et_3NH]_2[VO(DTBC)_2]\cdot CH_3OH$): C (66.19%), H (10.30%), N (3.77%); observed: batch #1: C (66.45%), H (9.83%), N (3.60%); batch #2: C (66.41%), H (9.87%), N (3.74%).

$[Na(CH_3OH)_2]_2[V(DTBC)_3]_2\cdot 4CH_3OH$. According to the literature[10,11], 1.7 g three-time-recrystallized DTBC (7.6 mmol) and 0.32 g $NaOCH_3$ (6.0 mmol) were weighed out and combined in a 100 mL round-bottom flask in the drybox. Under

---

[9] An apparent typographical error in the literature is:[8] 0.2 M NaOH/EtOH in Table VI should be 0.1 M $NaOH/CH_3OH$ as stated in the main text on p 5096. The UV-visible spectrum of $[Et_3NH]_2[VO(DTBC)_2]\cdot nCH_3OH$ in 0.2 M NaOH/EtOH gave a shifted absorbance maximum at 605 nm (880 $M^{-1}\cdot cm^{-1}$) rather than the reported peak at 654 nm (150 $M^{-1}\cdot cm^{-1}$) in 0.1 M $NaOH/CH_3OH$.

[10] Luneva, N. P.; Mironova, S. A.; Lysenko, K. A.; Antipin, M. Y. *Russ. J. Coord. Chem. (Transl. of Koord. Khim.)* **1997**, *23*, 844-849.

[11] a) Cass, M. E.; Gordon, N. R.; Pierpont, C. G. *Inorg. Chem.* **1986**, *25*, 3962-3967; b) Cass, M. E.; Ph.D. Thesis, University of Colorado, Boulder, CO., 1984, p 67; c) Private communication with Professor Cort G. Pierpont. In our preparation of $Na[V(DTBC)_3]\cdot 4CH_3OH$ using a V(II) solution (prepared by Zn/Hg amalgam reduction of a NH_4VO_3 solution), crystals identified by UV-visible, EPR and X-ray crystallography as Zn^{II}(Cat-N-SQ)(BQ-N-SQ) were obtained instead (Chaudhuri, P.; Hess, M.; Hildenbrand, K.; Bill, E.; Weyhermüller, T.; Wieghardt, K. *Inorg. Chem.* **1999,** *38,* 2781-2790; $(Cat\text{-}N\text{-}SQ)^{2-}$ and $(BQ\text{-}N\text{-}SQ)^0$ are two redox isomers of $(Cat\text{-}N\text{-}BQ)^-$, which is bis(3,5-di-*tert*-butyl-1-hydroxy-2-phenyl)amine anion). That this known, pale blue crystalline compound was not the intended vanadium complex $Na[V(DTBC)_3]\cdot 4CH_3OH$ was determined by its room-temperature EPR (a multi-line spectrum shown as Figure S3.4 of the Supporting Information, and its UV-visible maximum in $CHCl_3$ is at 736 nm instead of the reported[11a] 650 nm of $Na[V(DTBC)_3]\cdot 4CH_3OH$).

dimmed lights (to protect the light-sensitive VCl_3), 0.24 g VCl_3 (1.5 mmol) was dissolved in 50 mL methanol and added to the flask with DTBC and $NaOCH_3$. The solution turned dark reddish brown upon mixing. The flask containing the above reaction solution was sealed and taken out of the drybox. Next, the solution was stirred in the air for 20 min while the color changed from reddish brown to dark blue, after which the stirring was stopped and the solution was left to stand overnight in air. Dark blue crystals were collected in the air by filtration through a glass frit, then dried under vacuum for 1 h and stored in the drybox. The yield was 0.7–0.8 g, 27–29% based on VCl_3; no yield was reported in the literature.[10,11a,11b]

The synthesis of the related tris(di-*tert*-butylcatecholate) vanadium(V) compound, $[Et_3NH][V^V(DTBC)_3]\cdot 1.5CH_3OH$ according to the literature[8] proved inconsistent in our hands over 6 trials. Depending on the oxygen-exclusion technique employed (3 trials with careful solvent degassing plus syringe and cannula techniques; 3 other trials with less rigorous oxygen-exclusion techniques), a low yield to no dark blue (to sometimes greenish-blue) powder was obtained. Further details are provided in the section titled "Preparation of $[Et_3NH][V^V(DTBC)_3]\cdot 1.5CH_3OH$" below. The resulting compound contains the impurity $[Et_3NH]_2[V^{IV}(DTBC)_3]\cdot nCH_3OH$ as shown by its EPR (8 line, g = 1.966, A_{51V} ~80 G).

Characterization of $[Na(CH_3OH)_2]_2[V(DTBC)_3]_2\cdot 4CH_3OH$.

Single crystal X-ray diffraction. Crystal data and details of the structure determination for $[Na(CH_3OH)_2]_2[V(DTBC)_3]_2\cdot 4CH_3OH$ are included in a separate section of this Supporting Information. The results confirm the structure reported in the

literature, except that four methanol solvates were found instead of the reported one methanol solvate.[10]

UV-visible spectroscopy. As shown in Figure S3.5, the spectrum taken in CH_3CN solution exhibits absorbance at 625 nm (literature for $Na[V(DTBC)_3]\cdot 4CH_3OH$,[11a] 650 nm). The extinction coefficient at 625 nm is 19,000 $M^{-1}\cdot cm^{-1}$, comparable to the literature value of 15,000 $M^{-1}\cdot cm^{-1}$.[11a]

Negative Ion ESI-MS. The spectrum is shown in Figure S3.6, with a molecular ion peak at m/z = 1445.5 (due to $Na[V(DTBC)_3]_2^-$) together with a peak at m/z of 711.5 (due to $V(DTBC)_3^-$). These peaks match with the simulated spectra based on the calculated formula and isotopic abundance.

^{1}H-NMR. As shown in Figure S3.7: ($CDCl_3$) δ 6.72 (d, 1H, Ph-H), 6.49 (d, 1H, Ph-H), 3.38 (d, 4.22H, CH_3OH), [s, 1.41 (1H); s, 1.30 (~6H); d, 1.26 (~2H)] (~9H total, t-Bu-H), [d, 1.20 (1H); s, 1.15 (~6H), d, 0.94 (~2H)] (~9H total, t-Bu-H).

Preparation of Deprotonated 3,5-di-*tert*-butylcatecholate Salt Na_2(3,5-DTBC). This compound was prepared in order to perform a control experiment testing the report[12] that deprotonated catecholate can react directly with O_2 (i.e., without any deliberately added catalyst) to form the intradiol cleavage product, **5**. Following the literature,[12] 0.424 g (0.010 mol) NaOH (ACS grade, 98%) was dissolved in ca. 10 mL de-ionized water. The NaOH solution was purged with Ar and then transferred using a double-tipped needle into a flask under Ar which contained 1.156 g (5.199 mmol) 3,5-DTBC and a stir bar. The solution turned dark greenish blue instantly, and was immediately placed under vacuum. After all of the water had been removed, the light-

[12] Speier, G.; Tyeklár, Z. *J. Mol. Catal.* **1990**, *57*, L17-L19.

blue powder was dried at 100 °C for 20 h in a temperature-controlled oil bath. The yield of Na_2(3,5-DTBC) is 1.286 g (4.829 mmol, 93%).

Characterization of Na_2(3,5-DTBC)

IR Spectroscopy. A ca. 0.1 M CH_2Cl_2 solution of Na_2(3,5-DTBC) was placed into a CaF_2 cell in a drybox, the septa-capped cell was removed from the drybox, and its IR obtained, Figure S3.8. The IR of 3,5-DTBC was also obtained in CH_2Cl_2 for comparison, Figure S3.9. The peaks in the range of 3541–3582 cm^{-1}, assigned to ν(O-H) stretching peaks,[13] had been totally removed by the addition of two equivalents of NaOH.

Preparation of $[Et_3NH][V(DTBC)_3]\cdot 1.5CH_3OH$. According to the literature,[8] 3.0 g of one-time-recrystallized 3,5-DTBC (ca. 13.5 mmol) were dissolved in 40 mL anhydrous methanol (Aldrich, dried over mol. sieves), sealed and brought out of the drybox. Then, 0.5 g NH_4VO_3 (Aldrich, 99.99%, 4.3 mmol) in 10 mL methanol and 10 mL Et_3N (distilled over BaO) was also sealed and taken out. The above two solutions containing 3,5-DTBC and NH_4VO_3 plus Et_3N were separately degassed by two freeze-pump-thaw cycles. The NH_4VO_3 plus Et_3N solution was added to the 3,5-DTBC solution via cannula technique under pre-purified Ar (passed through O_2-scavenging and mol. sieve drying columns). Then, the reaction solution was refluxed for 5 h under an argon flow and then concentrated to ca. 20 mL. Next, this solution was taken back into the drybox and then filtered through a glass frit. The greenish blue powder on the frit was washed twice with 5 mL methanol. The yield was 0.12 g, ca. 3% (lit. value[8] 0.6 g, 16%). In two other repeat trials, none to very low yield (ca. 20 mg) of a dark-blue powder was obtained after washing with methanol (the blue powder has the same UV-visible

[13] Drago, R. S. *Physical Methods for Chemists*; 2 ed.; Surfside Scientific Publishing: Gainesville, FL, 1992, p187.

absorption maximum as the greenish blue powder obtained above). In three earlier attempts using less rigorous oxygen exclusion techniques, none of the desired product was obtained.

Characterization of $[Et_3NH][V(DTBC)_3]\cdot 1.5CH_3OH$

UV-visible spectroscopy. The spectrum was taken in CH_3CN. The peak maximum was red-shifted (622 nm vs the literature value of 645nm in CH_3CN or CH_3OH), extinction coefficient of ca. 9,000 $M^{-1}\cdot cm^{-1}$ (literature value 13,000 $M^{-1}\cdot cm^{-1}$ in CH_3CN or CH_3OH).

Negative Ion ESI–MS. The spectrum has the molecular ion peak at m/z = 711.4 $[V(DTBC)_3]^-$ together with the 507.4 $[VO(DTBC)_2]^-$ peak and a peak at m/z = 998.5 assigned as $[V_2(O)(DTBC)_4]^-$.

EPR. An 8-line spectrum characteristic of a V^{IV} compound was observed in toluene at room temperature: g = 1.966, A_{51V} = 79.5 G.

Elemental Analysis. Calculated as $[Et_3NH]_2[V^{IV}(DTBC)_3]\cdot nCH_3OH$: (n = 4) C (66.70%), H (10.42%), N (2.68%); observed: C (66.7%), H (9.7%), N (3.5%). The results suggest that the product contains ≤0.25 equiv. of excess Et_3N.

^{31}P-NMR Following Oxygen-uptake Using $(n\text{-}Bu_4N)_9P_2W_{15}V_3O_{62}$. ^{31}P-NMR was used to probe whether or not the polyoxometalate precatalyst is destroyed during the catechol oxygenation catalytic reaction (^{51}V-NMR is not applicable here due to the direct evolution of vanadium in the polyoxometalate into a catalyst with a paramagnetic semiquinone ligand). Due to the low sensitivity of NMR spectroscopy, a ~ 6-fold higher concentration of the precatalyst than that under the actual reaction conditions (ca. 4.0 mM

vs 0.7 mM) was used. An internal standard, $Ph_3P=O$, was chosen because of its inertness to further oxidation.

First, precatalyst $(n\text{-}Bu_4N)_9P_2W_{15}V_3O_{62}$ (81 mg, 0.013 mmol) and $Ph_3P=O$ (1.8 mg, 0.0065 mmol) were weighed and then dissolved in 0.4 mL 1:1 CD_3CN:CH_3CN solvent in the drybox. The solution was placed in an NMR tube, removed from the drybox, and subjected to ^{31}P-NMR analysis (Figure S3.10, a). A $Ph_3P=O$ standard solution (16 mM) in 1:1 CD_3CN:CH_3CN was prepared and stored in the drybox. Next, 98 mg $(n\text{-}Bu_4N)_9P_2W_{15}V_3O_{62}$ (0.016 mmol) and 202 mg 3,5-DTBC (0.91 mmol) were dissolved in 0.5 mL of the standard $Ph_3P=O$ plus deuterated solvent solution under N_2; this solution was transferred into an NMR tube, sealed, taken out of the drybox and analyzed by ^{31}P-NMR (Figure S3.10, b). A standard O_2-uptake experiment was set up exactly as the procedures described under the subtitle of "Selectivity Experiments" in the main text, except 196.7 mg precatalyst $(n\text{-}Bu_4N)_9P_2W_{15}V_3O_{62}$ (0.032 mmol) was used. Half the reaction solution (ca. 4 mL) was removed from the reaction flask during the post-induction period, and that 4 mL solution was concentrated under vacuum. The concentrated residue was dissolved in 0.5 mL of the standard $Ph_3P=O$ plus deuterated solvent solution under N_2 and analyzed by ^{31}P-NMR (Figure S3.10, c). The post-reaction NMR sample (t = 161 h) was prepared exactly as above for the post-induction period sample (Figure S3.10, d). All ^{31}P-NMR chemical shifts are referenced to 85% H_3PO_4 in H_2O using the external substitution method.

As shown in Figure S3.10, a reference ^{31}P-NMR of $(n\text{-}Bu_4N)_9P_2W_{15}V_3O_{62}$ was first obtained with half an equivalent of $Ph_3P=O$ present, (a); upon mixing with substrate, but before being exposed to oxygen, the upfield line at about –13.5 ppm is broadened while

the downfield line at about –5.8 ppm disappeared, (b). This means that the PO_4^{3-} in the polyoxometalate connected to the V_3 cap is experiencing a paramagnetic species. After the induction period (i.e., during the O_2-uptake process (c) and after the O_2-uptake (d)), the reaction solution was evaporated to dryness, and deuterated solvent and the $Ph_3P{=}O$ internal standard were added prior to NMR analysis. The peaks observed are shifted from their original positions and have been split into multiple peaks with the reappearance of the downfield peak now around –6.0 to –7.5 ppm rather than its initial –5.8 ppm position.

Overall, these ^{31}P-NMR results make it clear that a paramagnetic catalyst is formed upon the addition of DTBC to $P_2W_{15}V_3O_{62}^{9-}$. With the consumption of the substrate DTBC, the polyoxometalate phosphorous peaks are somewhat, but not completely restored, indicating some deterioration of the polyoxometalate structure. These results are consistent with vanadium being "leached" out of the polyoxometalate to form the true active catalyst.

Catalyst Isolation Attempts. Several different methods were used in attempts to isolate active catalyst from the vanadium-based precursors.[4,14,15,16,17] Unfortunately, none of the literature methods gives an analytically pure compound nor a single crystal. Three prior isolation attempts by Dr. H. Weiner[4] and Dr. Y. Sasaki[14] in our laboratory using the precursors $(n\text{-}Bu_4N)_5Fe^{II}{\cdot}SiW_9V_3O_{40}$ and $(n\text{-}Bu_4N)_4H_5PV_{14}O_{42}$ were repeated as part of this work. However, each of the isolated compounds proved impure by mass spectrometry. Column chromatography (silica gel, 1 × 1 × 12'' column, CH_2Cl_2 then

[14] Tatsuno, Y.; Nakamura, C.; Saito, T. *J. Mol. Catal.* **1987**, *42*, 57-66.
[15] Galeffi, B.; Postel, M.; Grand, A.; Rey, P. *Inorg. Chim. Acta* **1987**, *129*, 1-5.
[16] Galeffi, B.; Postel, M.; Grand, A.; Rey, P. *Inorg. Chim. Acta* **1989**, *160*, 87-91.
[17] Zhang, B. Y.; Zhang, Y.; Chen, B. W.; Wang, K. *Chin. Chem. Lett.* **1997**, *8*, 547-550.

CH_3CN) was performed in the drybox, but the chromatographed material was still not analytically pure. Additionally, it is quite possible that the silica gel column promotes oxidation/degradation of the oxygen-sensitive compounds during separation.[18]

The failure to isolate the catalyst from complex polyoxometalate precursors is not a surprise, however, considering the remainder of the polyoxometalate structure and components present in the (thereby impure) solution. These failed isolation attempts illustrate the value of the in-situ spectroscopic (EPR) and spectrometric (ESI–MS) tools successfully employed in the main text.

In a previous paper by Pierpont,[5] a single crystal of $[VO(DBSQ)(DTBC)]_2$ (albeit not a high yield of isolable, pure compound) was obtained from the reaction of $VO(acac)_2$ with 3,5-DTBC in methanol or anisole carried out under an inert atmosphere followed by opening to air for a few seconds. An isolation trial was performed herein using a similar method, except using the polyoxometalate precatalyst, $(n\text{-}Bu_4N)_7SiW_9V_3O_{40}$, in place of $VO(acac)_2$. No crystal, nor even a powder, was obtained at the end of the reaction.

Attempted Catalyst Isolation Beginning with $(n\text{-}Bu_4N)_5Fe^{II}\cdot SiW_9V_3O_{40}$. The isolation procedures were carried out exactly as the literature.[4] The final yield of the isolated species is 184 mg (lit. ~80 mg[4]). Infrared spectrum of the active isolated species is identical to the precursor, $(n\text{-}Bu_4N)_5Fe^{II}\cdot SiW_9V_3O_{40}$ (as shown in Figure S3.11). The isolation procedure did not completely destroy the polyoxometalate structure, as shown in the IR fingerprint region (1200–400 cm^{-1}), and also seen by ^{31}P-NMR for $P_2W_{15}V_3O_{62}^{9-}$, *vide supra*. Negative ion ESI–MS spectrum of the isolated species from

[18] Now that we have shown $[VO(DBSQ)(DTBC)]_2$ is a common, active catalyst, others interested in isolation this from their V-based precatalyst product mixtures can do the control of seeing how authentic $[VO(DBSQ)(DTBC)]_2$ behaves under various chromatographic and other isolation conditions.

(n-$Bu_4N)_5Fe^{II}{\cdot}SiW_9V_3O_{40}$ is shown in Figure S3.12 and implies a complicated composition that includes m/z 507 and 711 peaks, however.

Attempted Isolation of "$[V(DBSQ)(DBCatH)_2]_2$" Beginning with (n-$Bu_4N)_4H_5PV_{14}O_{42}$ *under* N_2. Two isolation attempts were made beginning with (n-$Bu_4N)_4H_5PV_{14}O_{42}$, both being done with a slight modification of the literature procedure.[14] Note that these isolations are under N_2 and, therefore, can not produce Pierpont's oxo complex, $[VO(DBSQ)(DTBC)]_2$. One batch was prepared without the final extraction step, and the other was extracted with room-temperature n-hexane in a N_2 drybox. The first batch yielded 401 mg (0.28 mmol calculated, based on the tentatively assigned formula from the literature[14]: "$[V(DBSQ)(DBCatH)_2]_2$," 84% yield based on the moles of vanadium initially present) while the second batch yielded 305 mg (0.21 mmol, 57%). The decomposition point for the latter batch was 123 °C (heating rate of ca. 1–2 °C/min) vs the previously reported[14] decomposition temperature of 160 °C.

Characterization of the Material Isolated from (n-$Bu_4N)_4H_5PV_{14}O_{42}$

EPR spectroscopy. A room temperature EPR spectrum was obtained on a solid sample under N_2, Figure S3.13. The resultant spectrum is identical to that in the literature[14] obtained in CH_2Cl_2 under nitrogen (g = 2.006 and 2.029; lit, g = 2.004 and 2.035[14]).

Negative Ion ESI–MS. The major fragment peaks are at m/z of 711.5 and 507.3, Figure S3.14. No higher, parent ion peak could be assigned.

Attempted Isolation of the Catalyst From (n-$Bu_4N)_7SiW_9V_3O_{40}$. A smaller-scale isolation was carried out similar to the method used by Cass et al[5]: 212 mg (n-$Bu_4N)_7SiW_9V^V{}_3O_{40}$ (0.0508 mmol vs the 1.0 mmol of $V^{IV}O(acac)_2$ used in the literature)

and 59 mg *crude* 3,5-DTBC (ca. 0.27 mmol) were both weighed into a 25 mL round-bottomed Schlenk flask in the drybox. Approximately 2 mL of anhydrous methanol were transferred into the reaction flask dropwise, resulting in a blue reaction solution. After the methanol was added, the solution was left unstirred in the drybox for 2 hours. The flask was brought out of the drybox, the sidearm was opened to air for several seconds (to simulate the literature procedures for exposure to O_2),[5] and then re-sealed. The reaction flask was left on the bench for an additional 2–3 h and then the solution was filtered through a glass frit. However, no solid could be collected on the frit. This experiment was repeated once with identical, negative results.

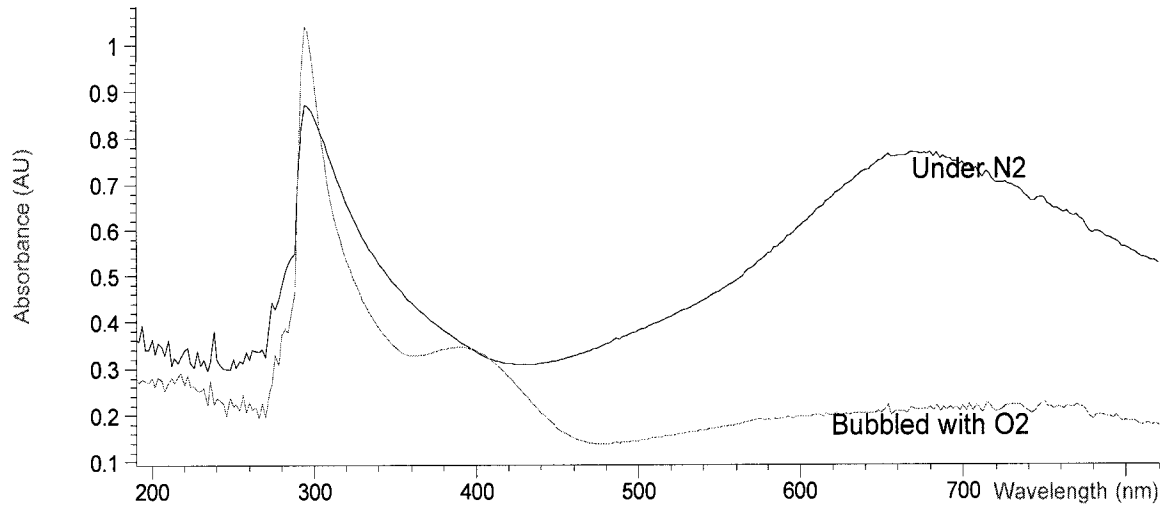

Figure S3.1 UV-visible spectrum of $[VO(DBSQ)(DTBC)]_2$ (0.028 mM under N_2 in toluene; the sample was prepared and sealed in the drybox) and the same sample after bubbling with O_2.

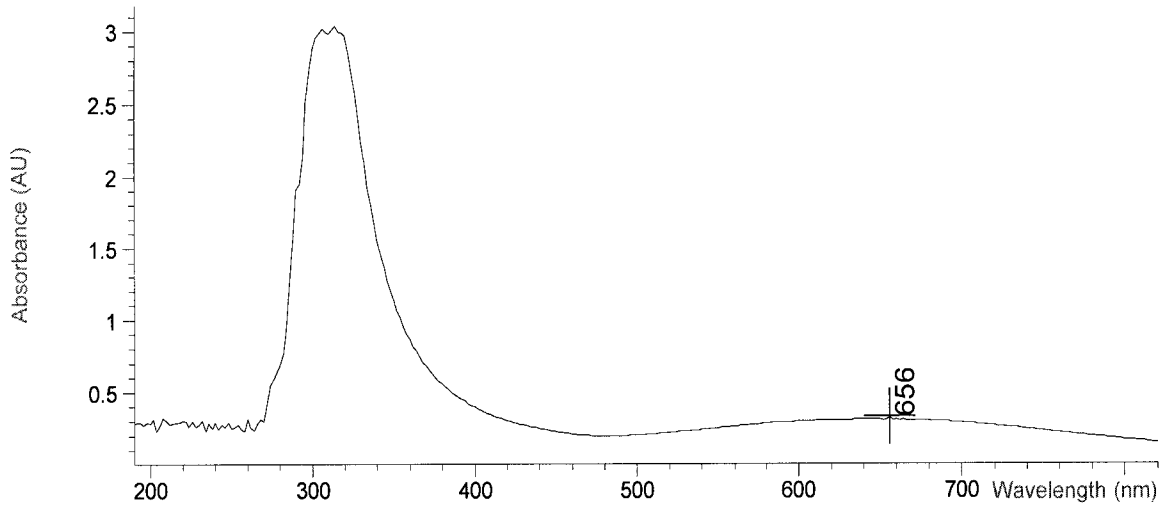

Figure S3.2 UV-visible spectrum of $[Et_3NH]_2[VO(DTBC)_2]\cdot nCH_3OH$ (1.3 mM in 0.1 M $NaOH/CH_3OH$ under N_2; the sample was prepared and sealed in the drybox).

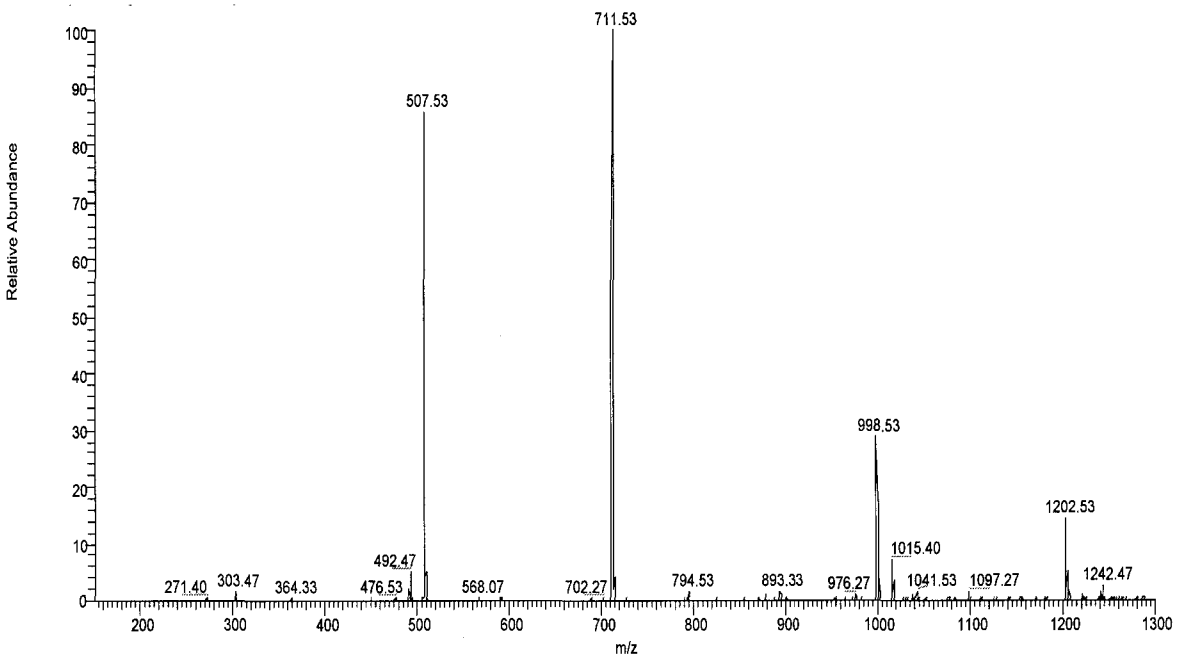

Figure S3.3 Negative ion ESI–MS spectrum of $[Et_3NH]_2[VO(DTBC)_2]\cdot nCH_3OH$ in CH_3CN. Key parts of the spectrum are the m/z = 507.5 ($VO(DTBC)_2^-$), m/z = 711.5 ($V(DTBC)_3^-$ or $[Et_3NH]_2[VO(DTBC)_2]^-$), m/z = 998.5 ($V_2O(DTBC)_4^-$) and m/z = 1202.5 ($V_2(DTBC)_5^-$).

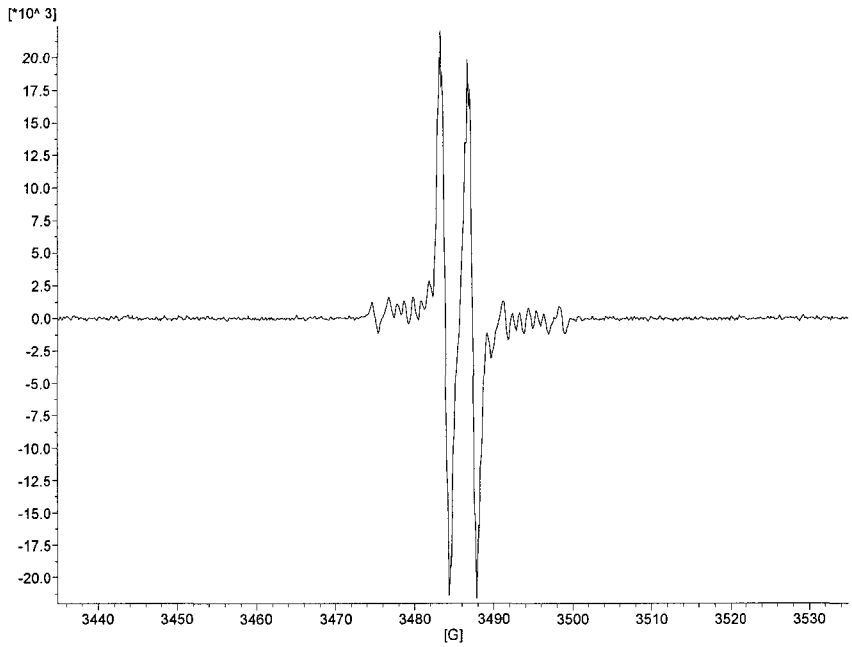

Figure S3.4 EPR spectrum of crystalline, dark green Zn^{II}(Cat-N-SQ)(BQ-N-SQ) dissolved in toluene, g = 2.002, A ~ 1.26–1.27 G. [$(Cat\text{-}N\text{-}SQ)^{2-}$ and $(BQ\text{-}N\text{-}SQ)^0$ are two redox isomers of $(Cat\text{-}N\text{-}BQ)^-$, which is bis(3,5-di-*tert*-butyl-1-hydroxy-2-phenyl)amine anion. See Chaudhuri, P.; Hess, M.; Hildenbrand, K.; Bill, E.; Weyhermüller, T.; Wieghardt, K. *Inorg. Chem.* **1999,** *38,* 2781-2790 for more detail.]

Crystal data for $[Na(CH_3OH)_2]_2[V(DTBC)_3]_2 \cdot 4CH_3OH$

Empirical formula	$C_{92}\ H_{148}\ Na_2\ O_{20}\ V_2$	
Formula weight	1721.96	
Temperature	273(2) K	
Wavelength	0.71073 Å	
Crystal system	Triclinic	
Space group	*P*-1	
Unit cell dimensions	a = 11.7291(11) Å	a= 106.088(2)°.
	b = 15.5341(14) Å	b= 109.458(2)°.
	c = 15.7892(14) Å	g = 104.263(2)°.
Volume	2417.3(4) $Å^3$	
Z	1	
Density (calculated)	1.183 Mg/m^3	
Absorption coefficient	0.266 mm^{-1}	
F(000)	928	
Crystal size	0.31 x 0.17 x 0.09 mm^3	
Theta range for data collection	1.47 to 28.51°.	
Index ranges	-15<=h<=15, -20<=k<=20, -20<=l<=21	
Reflections collected	22888	
Independent reflections	11457 [R(int) = 0.0440]	
Completeness to theta = 28.51°	93.4 %	
Absorption correction	Multi_scan	
Max. and min. transmission	0.9777 and 0.9228	
Refinement method	Full-matrix least-squares on F^2	
Data / restraints / parameters	11457 / 0 / 524	
Goodness-of-fit on F^2	1.036	
Final R indices [I>2sigma(I)]	R1 = 0.0627, wR2 = 0.1650	
R indices (all data)	R1 = 0.1047, wR2 = 0.1897	
Largest diff. peak and hole	1.121 and -1.022 $e.Å^{-3}$	

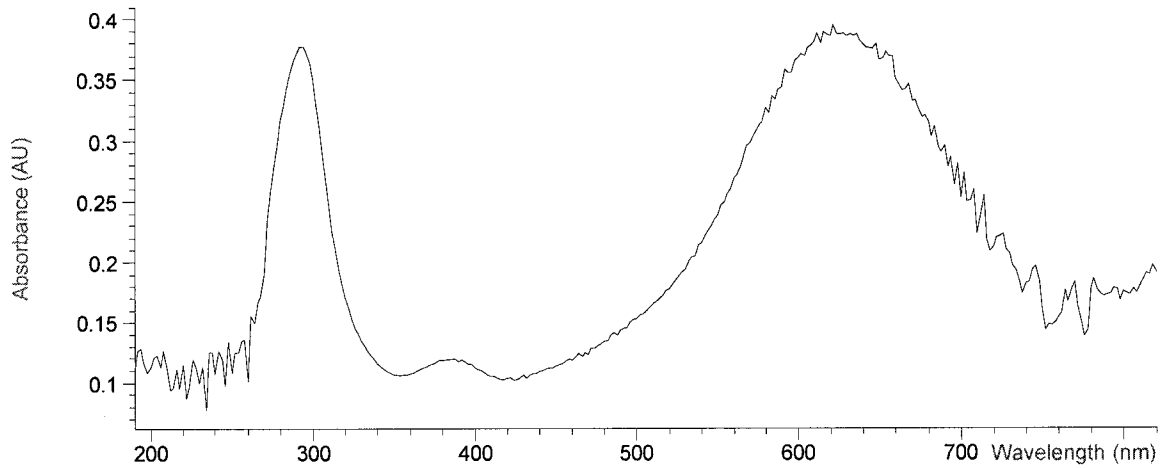

Figure S3.5 UV-visible spectrum of $[Na(CH_3OH)_2]_2[V(DTBC)_3]_2 \cdot 4CH_3OH$ (0.020 mM in CH_3CN, prepared and sealed in the drybox).

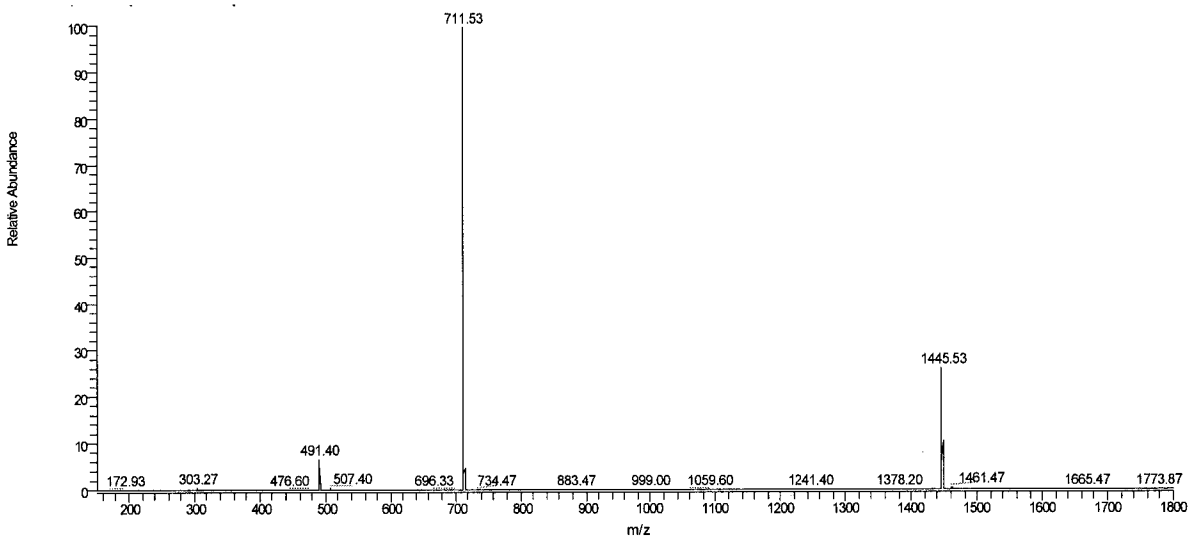

Figure S3.6 Negative ion ESI–MS spectrum of $[Na(CH_3OH)_2]_2[V(DTBC)_3]_2 \cdot 4CH_3OH$ in CH_3CN. Key features of the spectrum are the molecular ion peak at m/z = 1445.5 (due to $Na[V(DTBC)_3]_2^-$) together with a peak at m/z of 711.5 (due to $V(DTBC)_3^-$).

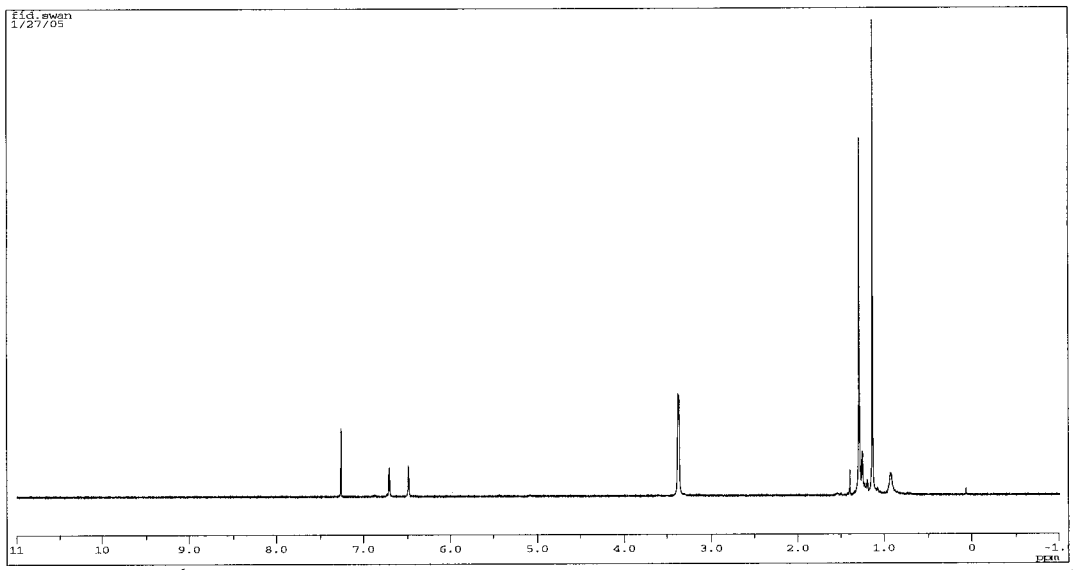

Figure S3.7 ^{1}H-NMR spectrum of $[Na(CH_3OH)_2]_2[V(DTBC)_3]_2 \cdot 4CH_3OH$ in $CDCl_3$. Peak assignments: [d, 0.94 (~2H); s, 1.15 (~6H); d, 1.20 (1H)] (~9H total, t-Bu-H), [d, 1.26 (~2H); s, 1.30 (~6H); s, 1.41 (1H)] (~9H total, t-Bu-H), 3.38 (d, 4.22H, CH_3OH), 6.49 (d, 1H, Ph-H), 6.72 (d, 1H, Ph-H).

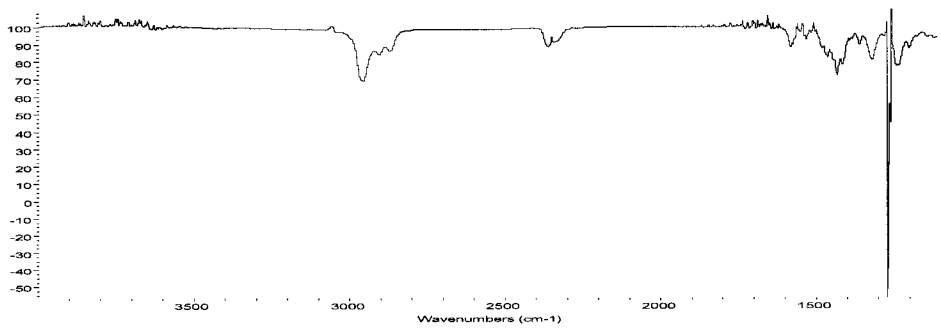

Figure S3.8 IR spectrum of Na_2(3,5-DTBC) (ca. 0.1 M in CH_2Cl_2, CaF_2 cell, under N_2).

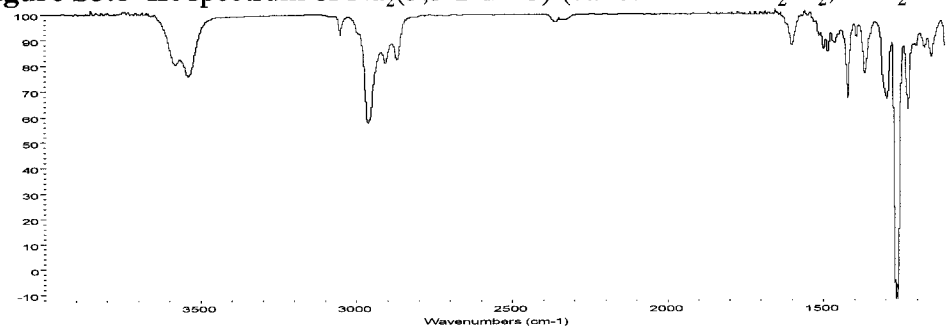

Figure S3.9 IR spectrum of 3,5-DTBC (ca. 0.1 M in CH_2Cl_2, CaF_2 cell, under N_2).

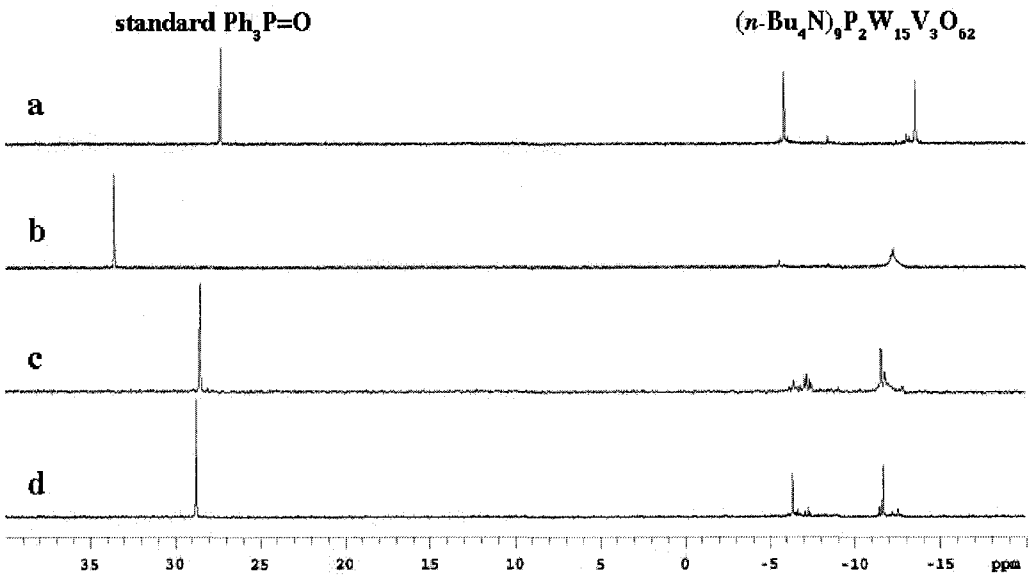

Figure S3.10 ^{31}P-NMR following the reaction of $(n\text{-}Bu_4N)_9P_2W_{15}V_3O_{62}$ with DTBC, and then O_2. (a) The precatalyst $(n\text{-}Bu_4N)_9P_2W_{15}V_3O_{62}$ plus internal standard under N_2; (b) the unreacted mixture of precatalyst and substrate (3,5-DTBC) plus internal standard under N_2; (c) the reaction solution post the induction period plus internal standard; (d) the after-reaction solution taken to dryness plus internal standard. All samples are 0.032 mM in 1:1 CH_3CN:CD_3CN with 0.016 mM internal standard added just prior to NMR analysis (i.e., and not in the reaction flask). The changed chemical shift of the internal standard in (b) arises from the presence of an excess amount of substrate.

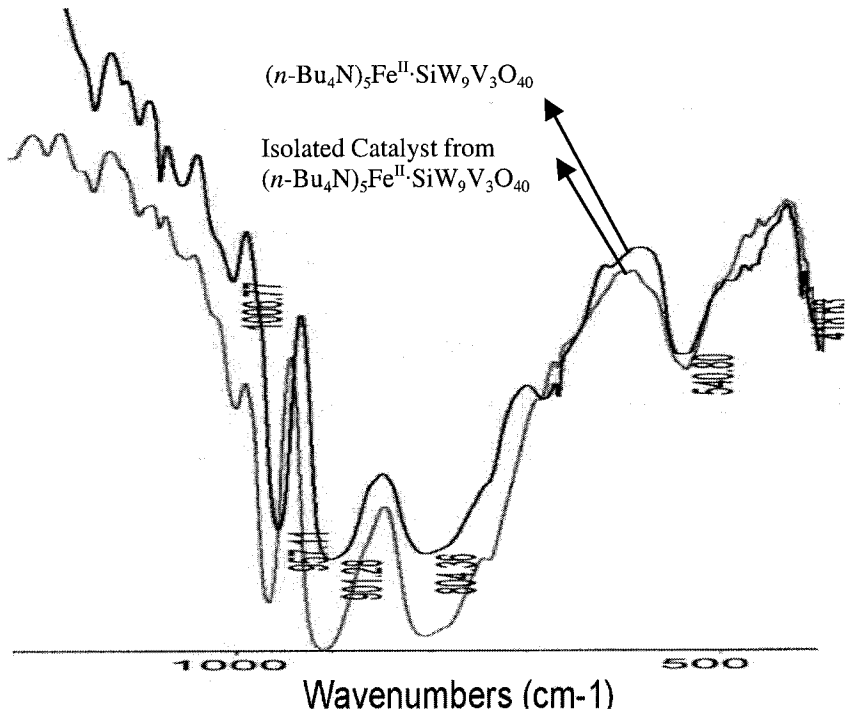

Figure S3.11 IR spectrum (KBr pellets) of $(n\text{-}Bu_4N)_5Fe^{II}\cdot SiW_9V_3O_{40}$ and the isolated, catalytically active species showing that most of the polyoxometalate structure remains intact post ~100 TTOs of DTBC/O_2 oxygenation.

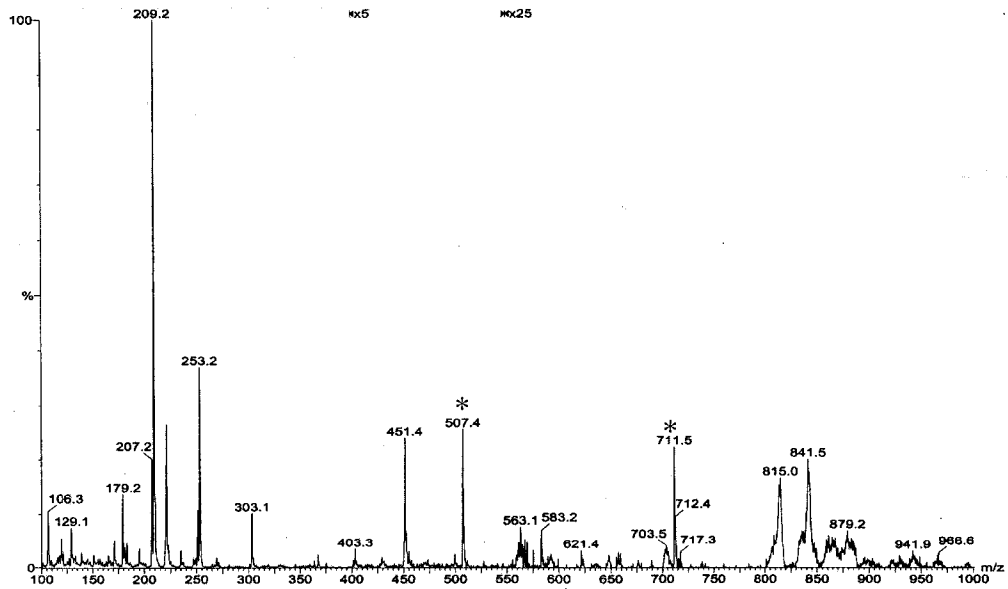

Figure S3.12 Negative ion ESI–MS spectrum of isolated catalyst from $(n\text{-}Bu_4N)_5Fe^{II}\cdot SiW_9V_3O_{40}$. Notable peaks (*) are the 507.4 and 711.5 peaks assigned in the main text. Parts of the above spectrum were magnified 5 times (i.e., above m/z ~ 400; see the top of the spectrum) or 25 times (above m/z ~ 530).

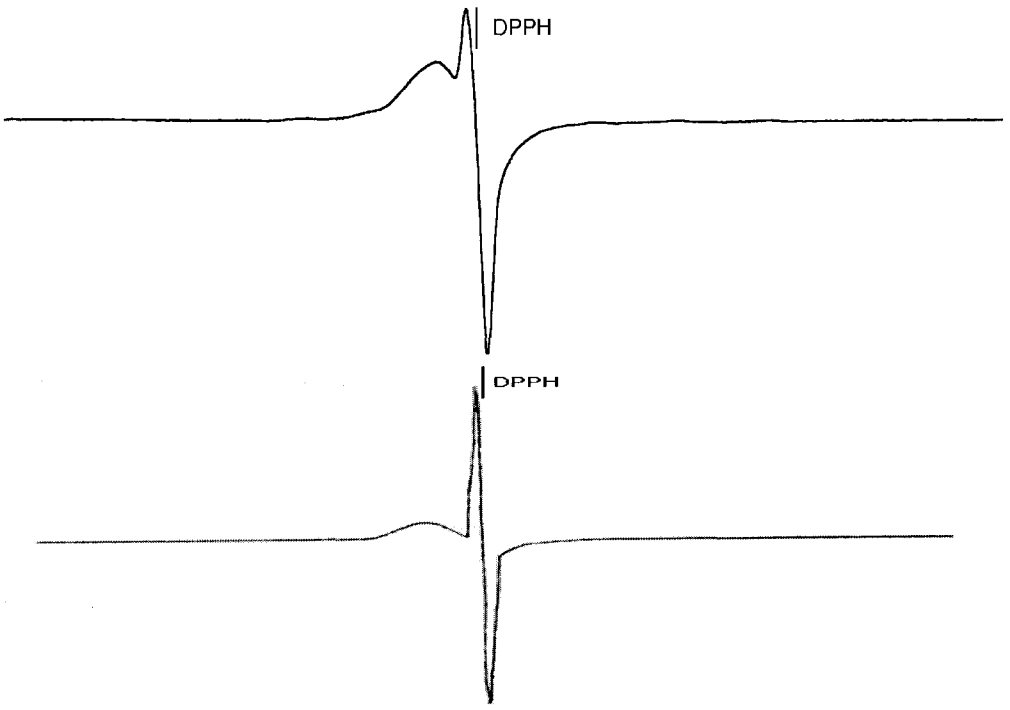

Figure S3.13 Observed (solid, top) and literature EPR[14] (in CH_2Cl_2, bottom) spectra of the material isolated from $(n\text{-}Bu_4N)_4H_5PV_{14}O_{42}$ and DTBC under N_2. DPPH (2,2-diphenyl-1-picrylhydrazyl radical) was used as a g = 2.0037 external standard.

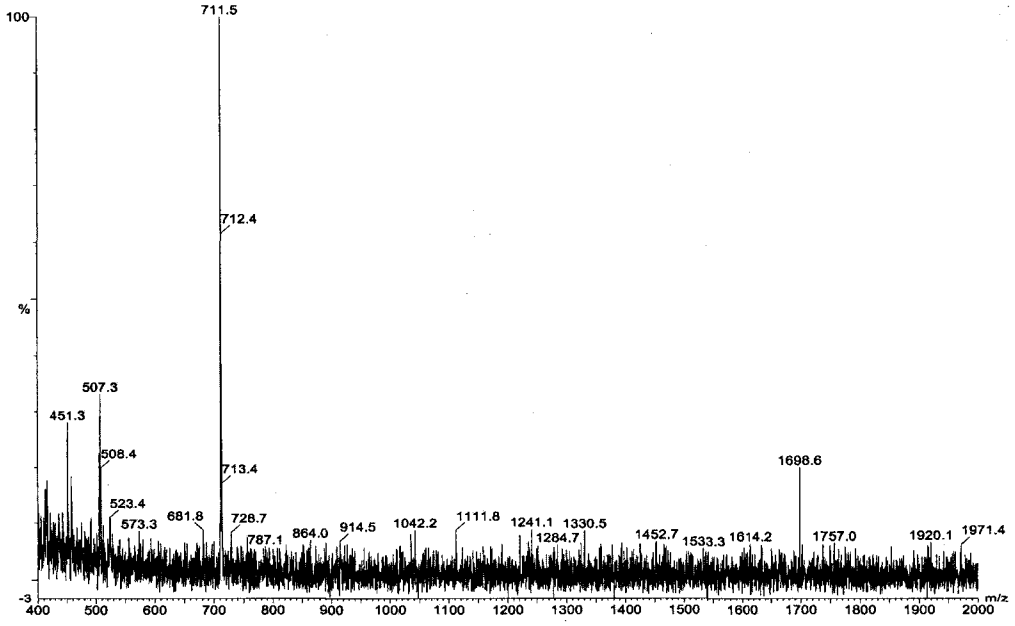

Figure S3.14 Negative ion ESI–MS spectrum of the blue material isolated from $(n\text{-}Bu_4N)_4H_5PV_{14}O_{42}$ and DTBC under N_2. The main assignable peaks are m/z = 451.3, 507.3 ($VO(DTBC)_2^-$) and 711.5 ($V(DTBC)_3^-$). The peak at m/z = 451.3 is a fragment peak of 507.3 peak ($VO(DTBC)_2^-$ minus C_4H_8, or *t*-Bu-H).

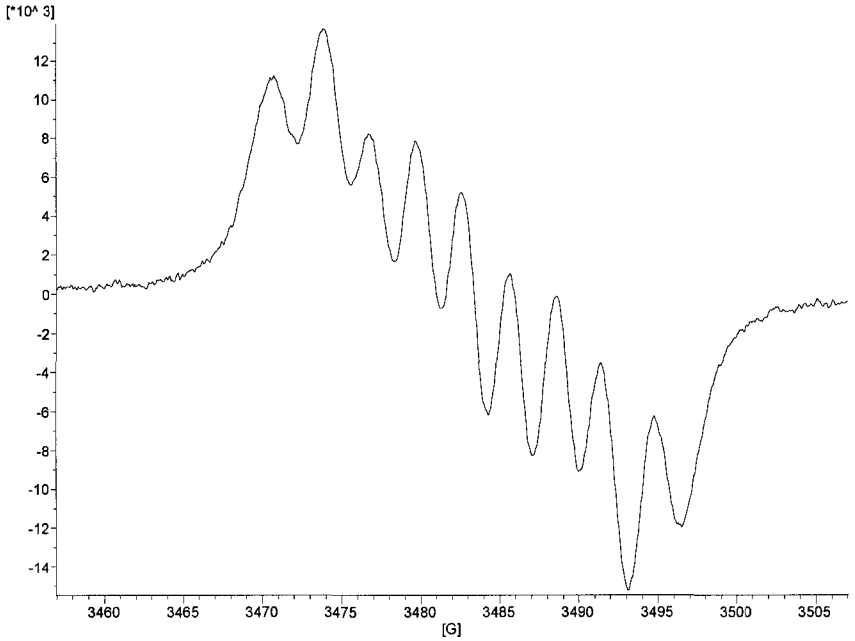

Figure S3.15 Center-field, 9-line EPR spectrum of a post-reaction solution of 3,5-DTBC and $VO(acac)_2$ in toluene which had additional (83 equivalents vs. the precatalyst $VO(acac)_2$) fresh 3,5-DTBC and O_2 added. This EPR spectrum shows that the 9-line spectrum diagnostic of $[VO(DBSQ)(DTBC)]_2$ is retained upon further DTBC oxygenation catalysis.

Table S3.1 Literature overview of *vanadium* catecholate organometallic complexes relevant to dioxygenase catalysis.

	Year	Topic	Summary of contents
1	**2004**	Visible absorption spectra of metal-catecholate and metal-tironate complexes Sever, M. J.; Wilker, J. J. *J. Chem. Soc., Dalton Trans.* **2004**, 1061-1072.	**UV-visible spectra for catecholate and tironate complexes** of the first row transition metals were reported. The UV-visible spectra, obtained by titration of the metal catecholate solution with NaOH, were compared to the literature.
2	**2004**	A novel pentacoordinated dioxovanadium(V) salicylaldiminate: Solvent specific crystallization of dimorphs with contrasting coordination geometries, ligand conformations and supramolecular architectures Baruah, B.; Rath, S. P.; Chakravorty, A. *Eur. J. Inorg. Chem.* **2004**, 1873-1878.	**A dioxovandium(V) salicylaldiminate complex** was crystallized using methanol or acetonitrile resulting **in two geometries**: distorted trigonal bipyramidal or distorted square pyramidal. The two crystals form the same species in solution as judged by IR, UV-visible, and ^{51}V-NMR. The polarity of the solvent was proposed to cause different supramolecular architectures (π-π stacking vs C–H···O hydrogen bonding).
3	**2002**	Vanadium(IV/V) complexes containing $[VO]^{2+}$, $[VO]^{3+}$, $[VO_2]^+$ and $[VO(O_2)]^+$ cores with ligands derived from 2-acetylpyridine and *S*-benzyl- or *S*-methyldithiocarbazate Maurya, M. R.; Khurana, S.; Zhang, W.; Rehder, D. *Eur. J. Inorg. Chem.* **2002**, 1749-1760.	Eleven **vanadium mono/di-oxo/peroxo complexes** were synthesized; two of those complexes were structurally characterized by X-ray single crystal diffraction analysis. Characterizations were performed via TGA, IR, NMR, EPR and UV-visible spectroscopy. The peroxo complexes transfer one oxygen atom in the peroxo ligand to PPh_3 generating the corresponding dioxo complexes.
4	**2002**	A Family of Vanadate Esters of Monoionized and Diionized Aromatic 1,2-Diols: Synthesis, Structure, and Redox Activity Baruah, B.; Das, S.; Chakravorty, A. *Inorg. Chem.* **2002**, *41*, 4502-4508.	Eight vanadate esters were synthesized and three molecular structures were determined by X-ray diffraction. Six of those esters have one proton attaching to the catechol oxygen. One type of the vanadate ester (**VO(xsal)(H-Catecholate)**) is able to **catalyze the autoxidation of 3,5-DTBC to benzoquinone only**. The hydrogen on the bound catecholate oxygen was proposed to play a crucial role in the oxygen-uptake.

5	**2001**	Molecular and Electronic Structure of Octahedral *o*-Aminophenolato and *o*-Iminobenzosemiquinonato Complexes of V(V), Cr(III), Fe(III), and Co(III). Experimental Determination of Oxidation Levels of Ligands and Metal Ions Chun, H.; Chaudhuri, P.; Wieghardt, K. et al *Inorg. Chem.* **2001**, *40*, 4157-4166.	A series of complexes, including $[M^{III}(L^{ISQ})_3]$ (M=Cr, Fe and Co), **$[V^{V}(L^{ISQ})(L^{AP}\text{-}H)_2]$, $[V^{V}(L^{AP}\text{-}H)_2(L^{AP})]$, and $[V^{V}O\{(L^{AP})N(L^{AP}\text{-}H)\}]$** ($H[L^{AP}]$ represents 2-anilino-4,6-di-*tert*-butylphenol), were synthesized and characterized. Oxidation states of the metal were determined by high-quality X-ray crystallography; the molecular and electronic structure were compared with the *o*-semiquinonato analogues; some arguments were made with the structure assignment of the vanadium complex analogues, $[V^{III}(SQ)_3]$.
6	**2001**	Unexpected reduction of vanadium(IV) to vanadium(III) in the presence of the chelate ligands 2,2'-bipyridine (bpy) and 1,8-hydroxyquinoline (Hquin) Manos, M. J.; Kabanos, T. A. et al *J. Chem. Soc., Dalton Trans.* **2001**, 1556-1558.	Two V(III) compounds, ***cis*-$[V^{III}Cl_2(acac)(bpy)]$ and $[V^{III}(quin)_3]\cdot 2CH_3OH$**, were synthesized from a V^{IV} precursor and bpy or Hquin ligands; these compounds together with $[Et_3NH][V^{V}O_2(\mu\text{-}dtbc)]_2$ were characterized.
7	**2001**	Polyoxoanions in Catalysis: From Record Catalytic Lifetime Nanocluster Catalysis to Record Catalytic Lifetime Catechol Dioxygenase Catalysis Finke, R. G. In *Polyoxometalate Chemistry From Topology via Self-Assembly to Applications*; Pope, M. T., Mueller, A., Eds.; Kluwer Academic Publishers: Dordrecht, The Netherlands, 2001, pp 363-390.	A review with 51 references; polyoxoanion-based compounds were used to stabilize transition metal nanoclusters, and then **polyoxoanion-based precatalysts are active in catalyzing catechol dioxygenase oxidations**; both give high catalytic lifetimes. References relevant to polyoxometalates and oxygenation catalysis are included.
8	**1999**	An All-Inorganic, Polyoxometalate-Based Catechol Dioxygenase That Exhibits >100 000 Catalytic Turnovers Weiner, H.; Finke, R. G. *J. Am. Chem. Soc.* **1999,** *121,* 9831-9842.	**Four V-containing polyoxoanion dioxygenases** were synthesized and characterized; these catalysts show high activities toward oxidative cleavage of 3,5-DTBC; excellent mass balance (95%) was reported for the reaction along with the identification by X-ray crystallography of a previously mis-identified oxidation product; several other polyoxoanion catalysts were also tested; O_2-uptake studies showed that an autocatalytic mechanism is involved; a record catalytic lifetime catalyst was discovered (>100,000 total turnovers).

9	**1999**	Synthesis, Structure, and Catecholase Reaction of a Vanadate Ester System Incorporating Monoionized Catechol Chelation Rath, S. P.; Rajak, K. K.; Chakravorty, A. *Inorg. Chem.* **1999**, *38*, 4376-4377.	Several **vanadate esters** show different reactivities towards **3,5-DTBC**; the most reactive one is **oxidized to** form only the corresponding **quinone**; the reaction is reversible for catechol addition. Electrochemical studies suggest that the phenolic hydrogen seems to be crucial for the reactivity; a hypothesis of hydrogen bonding to facilitate O_2-uptake was proposed.
10	**1997**	Nonheme oxovanadium(V,IV) complexes catalyze the oxidative cleavage of catechols Zhang, B. Y.; Zhang, Y.; Chen, B. W.; Wang, K. *Chin. Chem. Lett.* **1997**, *8*, 547-550.	Two oxo-vanadium(V) complexes were synthesized according to the previous lit.; their abilities of catalyzing the **oxidative cleavage of 3,5-DTBC** were probed; one of the two catalysts ((**TEA**)[V^V**O**(**TEA**)]) gives product mixtures (not fully separated and characterized, however); the other (VO(NTA)) gives a ternary complex stable enough to be isolated; a mechanism of oxidative cleavage was proposed.
11	**1997**	On the structure of the vanadium(V) complex with 3,5-di-*tert*-butylpyrocatechol: redox properties of vanadium(II-V) complexes with 3,5-di-*tert*-butylpyrocatechol in methanol solutions Luneva, N. P.; Mironova, S. A. Lysenko, K. A.; Antipin, M. Y. *Russ. J. Coord. Chem. (Transl. of Koord. Khim.)* **1997**, *23*, 844-849.	The synthesis and the crystal structure of **[V^V(Dbcat)$_3$]$_2$[Na(MeOH)$_2$]·2MeOH** were reported; the sequence of the **redox transitions in the V(II-V) complexes** coupled with 3,5-DTBC in alkaline media was proposed; the factors necessary for the catalytic capability of reducing *nitrogenase* substrates were listed.
12	**1996**	Monooxovanadium(V) mixed ligand complexes of schiff bases and catecholates: synthesis, spectral and electrochemical characterization Asgedom, G.; Sreedhara, A.; Rao, C. P.; Kolehmainen, E. *Polyhedron* **1996**, *15*, 3731-3729.	**Twelve monooxovanadium(V) complexes of four different Schiff bases and three substituted catechols** were synthesized and characterized; all of the complexes (VOL(R-cat)) formed LVO_2 in DMSO (rapid decomposition with the addition of H_2O). A correlation was found between the $E_{1/2}$ and ^{51}V NMR chemical shifts.
13	**1994**	The Chemistry of Transition Metal Complexes Containing Catechol and Semiquinone Ligands Pierpont, C. G.; Lange, C. W. *Prog. Inorg. Chem.* **1994**, *41*, 331-442.	A key review with 308 references; **catecholate and semiquinone complexes** were reviewed in nine groups of the periodic table; their relevances to charge distribution, metal-quinone electron transfer, catechol oxidation reactions and metal-semiquinone magnetic exchange interactions are included.

14	**1993**	Ligands for Oxovanadium(IV): Bis(catecholamide) Coordination and Intermolecular Hydrogen Bonding to the Oxo Atom Dewey, T. M.; Du Bois, J.; Raymond, K. N. *Inorganic Chemistry* **1993**, *32*, 1729-1738.	As a step in molecular design, two macrocyclic ligands (phenCam, **1** and bencam, **2**) were synthesized to bind VO^{2+} ion while the phenol-hydrogen of **1** is expected to be hydrogen-bonded with vanadyl oxygen; **[VO(1)] and [VO(2)]** were characterized; it was found out that the hydrogen bond occurs intermolecularly instead of intramolecularly; V=O bond length change due to the hydrogen bonding was observed in the solid state.
15	**1993**	Formation of Tris-chelated Vanadium(IV) Complexes by Interaction of Oxovanadium(IV) with Catecholamines, 3-(3,4-Dihydroxyphenyl)alanine and Related Ligands in Aqueous Solution Buglyó, P.; Dessì, A.; Kiss, T.; Micera, G.; Sanna, D. *J. Chem. Soc., Dalton Trans.* **1993,** 2057-2063.	A series of ***o*-catecholic ligands reacted with V(IV) compounds** were studied in aqueous solution by EPR, absorption spectroscopy and pH-potentiometry; V(IV) with no, mono-, di- and tri-catecholate complexes were observed; the tri-catecholate chelated complexes were formed by increasing the ligand/metal ratio (>25:1); a sequence of the stability of $[VA_3]$ was given and two factors account for the differences in the stability.
16	**1992**	Complexes of Vanadium(III) and Vanadium(IV) Containing Bipyridine and Tetrachlorocatecholate Ligands. Insights into the Tunicate Vanadium(III) Coordination Environment Simpson, C. L.; Pierpont, C. G. *Inorg. Chem.* **1992,** *31,* 4308-4313.	Syntheses **of V(bpy)(Cl_4Cat)$_2^n$**, (n = -1, 0, 1) complexes as well as **V(bpy)(acac)(Cl_4Cat)** were reported; X-ray diffraction, electrochemisty and UV-vis spectroscopy were used to characterize those complexes; the relevance to tunicate coordination environment was discussed.
17	**1992**	Reaction Mechanism of Protocatechuate 3,4-Dioxygenase Nishida, Y.; Yoshizawa, K.; Takahashi, S.; Watanabe, I. *Z. Naturforsch., C: Biosci.* **1992**, *47*, 209-214.	**Protocatechuate 3,4-dioxygenase reaction mechanism** was proposed; some coordinated iron complexes and vanadium complexes display SOD-like function; molecular orbital theory was used to explain the difference in the SOD-like function; catalytic cleavage of 3,5-DTBC was correlated with the SOD-like function; an Fe^{III}(edta)/ascorbic acid system supports the existence of an Fe^{III}-peroxide intermediate.

18	**1992**	Synthesis and X-Ray Structures of Bis(3,5-di-*tert*-butylcatecholato)(phenanthroline)vanadium(IV) and its Vanadium(V) Analogue [V(dtbc)$_2$(phen)][SbF$_6$] Kabanos, T. A.; White, A. J. P.; Williams, D. J.; Woollins, J. D. *J. Chem. Soc., Chem. Commun.* **1992**, 17-18.	Two non-oxo vanadium complexes were synthesized and crystallized: **[V^{IV}(DBCat)$_2$(phen)] and [V^{V}(DBCat)$_2$(phen)](SbF$_6$)**; their structures were compared. It was found that only the coordination angles, not the bond lengths, change with different oxidation states.
19	**1992**	New Non-oxo Vanadium-(IV) and -(V) Complexes Kabanos, T. A.; Slawin, A. M. Z.; Williams, D. J.; Woollins, J. D. *J. Chem. Soc., Dalton Trans.* **1992**, 1423-1427.	**[V^{IV}(DBCat)$_2$L] and [V^{V}(DBCat)$_2$L]X** (L = phen, bipy and X = SbF_6^-, BF_4^-) were synthesized and crystallized; these complexes were characterized by microanalysis, electrochemistry, etc. By comparing the crystallographic data of the V^{IV} and V^{V} complexes, only different bond angle was found, confirming the previous conclusion in ref. 18.
20	**1992**	Vanadium(V) Complexes of 1,5,10-Tris(2,3-dihydroxybenzoyl)-1,5,10-triazadecane and Its Analogs Butler, A.; De la Rosa, R.; Zhou, Q.; Jhanji, A.; Carrano, C. J. *Inorg. Chem.* **1992**, *31*, 5072-5077.	**V(V) catecholate compounds** were synthesized using linear polycatecholates and cyclic tricatecholate ligands; the compounds were studies with optical and ^{51}V-NMR spectroscopies as well as solution thermodynamic measurements; most stable complexes synthesized were chelated with 1,5,10-tris(2,3-dihydroxybenzoyl)-1,5,10-triazadecane and its sulfonated analog (3,4-LICAM and LICAMS); protonation scheme for V^{V}(3,4-LICAMS) was established; Fe^{III} was found to bind tighter with polycatecholates than V^{V}.
21	**1991**	Preparation of Mono- and Binuclear Complexes of Copper(II), Nickel(II), Cobalt(II), Iron(II) and Vanadyl(V) with 2,2'-dihydroxy-3,3'-diacetyl-5,5'-dichlorodiphenylmethane Russo, U.; Zarli, B.; Zanonato, P.; Vidali, M. *Polyhedron* **1991**, *10*, 1353-1361.	2,2'-dihydroxy-3,3'-diacetyl-5,5'-dichlorodiphenylmethane (**V**) were synthesized and used as the ligand to form mono- and binuclear complexes with Cu(II), Ni(II), Co(II), Fe(III) and V(V); all the complexes were characterized; **Fe(III) and V(V) complexes react with 3,5-DTBC through an oxidative cleavage pathway**; the products were characterized and product selectivities were tabulated; attempts were made to make macrocyclic complexes using ligand **V** and either amine or ethyl acetate.

22	**1991**	Synthesis and Characterization of Neutral Tris(bidentate) Vanadium(V) Complexes containing $N_3S_2^{3-}$ and Catecholate Ligands Kabanos, T. A.; Woollins, J. D. *J. Chem. Soc., Dalton Trans.* **1991**, 1347-1350.	Details are provided on the syntheses of **$V(N_3S_2)LL'$ (L = cat, 3,5-DBCat; L' = phen, bipy)**; microanalysis, IR, electronic absorption, ^{51}V-NMR spectroscopies, electrochemisty and FAB-MS were used to characterize a total of six new complexes.
23	**1990**	The Preparation and X-Ray Structure of $V(N_3S_2)$(dtbc)(phen)·$CHCl_3$ (dtbc = di-t-butylcatecholate, phen = phenanthroline) Kabanos, T. A.; Slawin, A. M. Z.; Williams, D. J.; Woollins, J. D. *J. Chem. Soc., Chem. Commun.* **1990**, 193-194.	Among a series of **$V(N_3S_2)LL'$ (L = cat, 3,5-DBCat; L' = phen, bipy)** complexes synthesized, $V(N_3S_2)$(dtbc)(phen)·$CHCl_3$ were crystallized; all complexes were characterized by IR, ^{51}V-NMR and cyclic voltammetry. (Details on characterization see the full paper listed as ref. 22).
24	**1990**	Potentiometric and spectroscopic studies on oxovanadium(IV) complexes of salicylic acid and catechol and some derivatives Jezowska-Bojczuk, M.; Kozlowski, H; Zubor, A.; Kiss, T.; Branca, M.; Micera, G. Dessì, A. *J. Chem. Soc., Dalton Trans.* **1990**, 2903-2907.	**Oxovanadium(IV) with ligands** (such as salicylic acid, catechol) was studies in aqueous solution by **UV-visible, ESR, ENDOR** spectroscopies. Speciation was also studies in different PH solutions.
25	**1990**	The Reaction of Alkali Metal Catecholates with Dioxygen in Aprotic Solvents Speier, G. and Tyeklár, Z. *J. Mol. Catal.* **1990,** *57,* L17-L19.	**Sodium or potassium salts of 3,5-DTBC** take up O_2 in ether or DMSO to **generate oxidative ring cleavage products**; the reaction was proposed to proceed through dioxetane intermediate (chemiluminescent); water-exclusion is proposed to effect product yields due to semiquinone and superoxide disproportionations.
26	**1990**	Formation and Structure of the Tris(catecholato)vanadate(IV) Complex in Aqueous Solution Branca, M.; Micera, G; Dessì, A.; Sanna, D.; Raymond, K. N. *Inorg. Chem.* **1990,** *29,* 1586-89.	**EPR** in aqueous solution or acetonitrile were recorded **on different mixtures with the ratio of VO^{2+} to catechol varying from 1:1 to 1:100**; a tri-chelated complex could be identified by EPR that is identical to the known complex $[V(Cat)_3]^{2-}$; the molecular geometry and electronic energy levels were deduced from the EPR parameters.

27	**1989**	High Catalytic Activity of Vanadium(V) Oxo-polymers for Oxidative Cleavage of Catechol Nishida, Y.; Kikuchi, H. *Z. Naturforsch., B: Chem. Sci.* **1989**, *44*, 245.	Several **vanadium-containing oxopolymers** were prepared and those with more than two vanadium per molecule acted **as dioxygenase catalysts** toward 3,5-DTBC; product yields of quinone and muconic acid anhydride were given; it was proposed that a binuclear complex may be the true catalyst; several polynuclear complexes containing Cu^{II}, Fe^{III} and Mn^{II} were found to be inactive.
28	**1989**	Proton electron nuclear double resonance study of oxovanadium(IV) complexes of o-diphenolic ligands Branca, M.; Micera, G.; Dessì, A. *J. Chem. Soc., Dalton Trans.* **1989**, 1289-1291.	Proton electron nuclear double resonance **(ENDOR) spectroscopy** at 110 K was used to study several oxovanadium(IV) complexes. A ^{1}H ENDOR pattern is diagnostic of vanadium(IV)-phenolate coordination.
29	**1989**	Synthesis and Characterization of (Catecholato)bis(β-diketonato)vanadium(IV) Complexes Hawkins, C. J.; Kabanos, T. A. *Inorg. Chem.* **1989,** *28,* 1084-1087.	Syntheses of **three non-vanadyl vanadium(IV) complexes, $[V(Cat)(acac)_2]$, $[V(Cat)(bzac)_2]$ and $[V(DBCat)(bzac)_2]$** were reported; characterization was performed using IR, UV-vis, elemental analysis, etc.; the stability of $[V^{IV}(Cat)(acac)_2]$ was confimed by electrochemisty and the most stable oxidation state varies in different non-mixed-ligand complexes like $[V(Cat)_3]^{n-}$ and $[V(acac)_3]^{n-}$.
30	**1989**	Easy Access to Molecular Vanadium Catecholates: Reactivity Towards Oxygen Galeffi, B.; Postel, M.; Grand, A; Rey, P. *Inorg. Chim. Acta* **1989,** *160*, 87-91.	Three different catechols with different pK_as were used to synthesize **VO(acac)L (L=Cat for 2, TBCat for 3 and DTBCat for 4)**; these complexes were characterized by microanalysis, IR etc.; only **complex 4 was found to react with catechol under O_2, forming oxidative cleavage products**; several possible catalytic intermediate structures were proposed to account for the observed activity.
31	**1988** **1987**	Oxidation of Catechols Catalyzed by Heteropolyvanadates Tatsuno, Y.; Nakamura, C.; Saito, T. *Stud. Org. Chem. (Amsterdam)* **1988**, *33*, 321. Heteropolyvanadates as Catalysts for Oxygenation of 3,5-Di-t-butylcatechol Tatsuno, Y.; Nakamura, C.; Saito, T. *J. Mol. Catal.* **1987**, *42*, 57.	Several **vanadium-containing polyoxometalates and V^{V}(DBCat)L** complexes were investigated for their **oxidative activity toward 3,5-DTBC**; vanadium was found to be essential for the activity, though mononuclear V^{V}-catecholate complexes were inactive; ^{18}O-labeling study shows oxygen gas, not the oxygen from the polyoxometalate catalyst, was included into the products; an isolated complex $[V(DBSQ)(DBCatH)_2]_2$ was tentatively formulated as an active species based on the available data.

32	**1987**	Catalytic Oxygenation of Pyrocatechols by O_2 in the Presence of Vanadium. Synthesis, Characterization, Electronic Structure and Reactivity of the Vanadium(IV)/Tetrachloro-*o*-quinone System Galeffi, B.; Postel, M.; Grand, A.; Rey, P. *Inorg. Chim. Acta* **1987**, *129*, 1.	**VO(acac)(TCCat) (1)** was synthesized and characterized; EHT calculations confirmed the electronic structure deduced from the experimental data; complex **1** was shown to be **an active catalyst for ring cleavage of 3,5-DTBC**; a dark blue complex was isolated with addition of excess 3,5-DTBC though the complex was not purified successfully.
33	**1986**	Catecholate and Semiquinone Complexes of Vanadium. Factors That Direct Charge Distribution in Metal-Quinone Complexes Cass, M. E.; Gordon, N. R.; Pierpont, C. G. *Inorg. Chem.* **1986,** *25,* 3962-7.	**$V^{III}(SQ)_3$ and $V(Cat)_3^-$** together with **$V^{III}(Cl_4SQ)_3$ and $V(Cl_4Cat)_3^-$** were prepared and their spectroscopic properties were studied; $V(Cl_4SQ)_3$ and $Na[V(DBCat)_3]\cdot 4CH_3OH$ were characterized by crystallography; electrochemistry carried out on $V(Cl_4SQ)_3$ and $V(Cl_4Cat)_3^-$ showed that their charge distribution were different from the way they were in the solid state; factors influencing the charge distribution were discussed.
34	**1985**	New Oxovanadium Complexes Coordinated To a *fac*-Tridentate Organometallic Ligand and X-ray Crystal Structure of [η-$CpCo\{P(O)(OC_2H_5)_2\}_3VO(acac)$]: Their Role in Oxidative Catalysis Roman, E.; Tapia, F.; Barrera, M.; Garland, M. T.; Le Marouille, J. Y.; Giannotti, C. *J. Organomet. Chem.* **1985**, *297*, C8.	Three binuclear organometallic compounds were synthesized either by reacting $VO(acac)_2$ with a facial-tridentate ligand [η-$CpCo\{P(O)(OEt)_2\}_3]^-$ **(L)** or by ligand exchange, namely, **[LVO(acac)] (I), $[LVO(phen)]^+PF_6^-$ (II) and $[LVO(bipy)]^+PF_6^-$ (III)**; X-ray diffraction crystal structure was obtained on **I**; all three of the compounds were characterized by elemental analysis, IR, etc.; **oxidative cleavage of 3,5-DTBC with compound I-III** was reported with a high ratio of quinone product.
35	**1984**	Vanadium-catecholato Complexes as Reaction Intermediates In the Vanadium Catalyzed Oxygenation of Catechols Tatsuno, Y.; Tatsuda, M.; Otsuka, S.; Tani, K. *Chem. Lett.* **1984**, 1209.	Several new vanadium-catecholate complexes with Schiff base ligands were synthesized such as **$[V(salen)(DBCatH)_2]\cdot 1/2CH_2Cl_2$, $[V(salen)(DbpyrH_2)_2]\cdot 1/2H_2O$**, etc.; they were characterized by elemental analysis and IR.; it was found that the **monodentate catecholato complexes show catalytic activity either as the catalyst or as the reactant with oxygen to give ring cleavage products**; product distribution was reported.

36	**1984**	Binuclear Oxovanadium(IV) Complexes as Catalyst for the Oxygenation of the Catechols Casellato, U.; Tamburini, S.; Vigato, P. A.; Vidali, M.; Fenton, D. E. *Inorg. Chim. Acta* **1984**, *84*, 101.	A series of **binuclear vanadyl(IV) complexes** were made via reported methods and found to be **active catalysts for oxidative cleavage of 3,5-DTBC**; product yields were given for all of the V(IV) complexes, control experiments showed that the oxygenation did not go through quinone as an intermediate; therefore, the vanadyl complexes behave similar to pyrocatecase enzymes.
37	**1984**	Syntheses and Characterization of Some Neutral and Ionic (Catecholato) Complexes of Vanadium (IV) in the Presence of Bidentate N~N Counterligand Galeffi, B.; Postel, M. *Nouv. J. Chim.* **1984,** *8,* 481.	Syntheses **of catechol-oxo-V^{IV} complex chelating with N~N bipyridine and phenanthroline ligands** were performed; these complexes were characterized by IR, EPR, etc.; the study is the first report of vanadium catecholate complexes containing N-donor ligands.
38	**1983**	Orthoquinone Complexes of Vanadium and Their Reactions with Molecular Oxygen Cass, M. E.; Greene, D. L.; Buchanan, R. M.; Pierpont, C. G. *J. Am. Chem. Soc.* **1983,** *105,* 2680-2686.	The reaction between $V(CO)_6$ and 3,5-di-*tert*-butylquinone (**1**) was studied by EPR, which provided evidence for several intermediates; the **crystal structure of [VO(DBSQ)(DBCat)]$_2$ (2)** was determined; the same reaction process occurred starting with $VO(acac)_2$ and 3,5-DTBC; the reaction scheme of vanadium is similar to that of Mo; relevance to the Shilov N_2-reduction system was briefly discussed. (The authors reported that different products could be obtained in catalytic reactions with excess 3,5-DTBC substrate in Ref. 13 in comparison to the stoichiometric reaction reported herein.)
39	**1982**	Synthetic, Structural, and Physical Studies of Bis(triethylammonium) Tris(catecholato)vanadate(IV), Potassium Bis(catecholato)oxovanadate(IV), and Potassium Tris(catecholato)vanadate(III) Cooper, S. R.; Koh, Y. B.; Raymond, K. N. *J. Am. Chem. Soc.* **1982,** *104,* 5092-5102.	In an attempt to reproduce the data from previous literature (ref 21 therein); definitive syntheses and characterization of **$V^{IV}O(cat)_2^{2-}$, (1), $V^{IV}O(DBCat)_2^{2-}$, (2), $V^{IV}(cat)_3^{2-}$, (3), $V^{V}(DBCat)_3^{-}$, (4) and $V^{III}(cat)_3^{3-}$, (5)** were reported; $V(catecholate)_3^{n-}$ was synthesized by replacing the vanadyl oxygen; the crystal structures of **1**, **3** and **5** were reported; a clarification of the data in the ref 21 was provided. (A previously invisible EPR spectrum of **3** in aqueous solution is reported in ref 26)

40	**1982**	Redox Chemistry of Metal-Catechol Complexes in Aprotic Media. 4. Synthesis and Characterization of 3,5-di-*tert*-butylcatecholato Complexes of Vanadium(V), -(IV), and -(III) Bosserman, P. J.; Sawyer, D. T. *Inorg. Chem.* **1982,** *21,* 1545-1551.	**Syntheses of Na salts of $[V^{V}O(OMe)(DBCat)_2]^{2-}$, (1), $[V^{IV}O(DBCat)_2]^{2-}$, (2), $[V^{IV}Cl_2(DBCat)_2]^{2-}$, (3) and $[V^{III}(DBCat)_3]^{3-}$, (4)** were performed; these species were studied with UV-vis, EPR and electrochemistry; a conclusion was drawn that vanadium in lower oxidation states (IV, III) is not stable in protic media; a comparison of the properties of vanadyl complex and non-vanadyl complex was made.
41	**1982**	Effective Oxygenation of 3,5-Di-*tert*-butylpyrocatechol Catalysed by Vanadium(III or IV) Complexes Tatsuno, Y.; Tatsuda, M.; Otsuka, S. *J. Chem. Soc., Chem. Commun.* **1982**, 1100.	Several **vanadyl and non-vanadyl complexes** were reported to catalyze **the oxidative cleavage of 3,5-DTBC**; product yields and distribution were reported; several other inactive vanadium complexes and Fe, Co or Ni analogs were listed; solvent effect was observed; a similarity of this catalytic reaction to the pyrocatechase-catalyzed oxygenation reaction was proposed.
42	**1982**	Theoretical study of *o*-quinone complexes of chromium and vanadium Gordon, D. J.; Fenske, R. F. *Inorg. Chem.* **1982**, *21*, 2907-2915.	**Molecular orbital calculations on a number of *o*-quinone complexes of chromium and vanadium** are presented (Fenske-Hall method). The relative energies of the frontier orbitals could be used to explain the hyperfine coupling constants in the EPR spectra of isoelectronic structures.
43	**1973**	Hydrolysis of the oxovanadium(IV) ion and the stability of its complexes with the 1,2-dihydroxybenzenato(2-) ion Henry, R. P.; Mitchell, P. C. H.; Prue, J. E. *J. Chem. Soc., Dalton Trans.* **1973**, *11*, 1156-1159.	An early study of **pH titrations of $V(IV)O^{2+}$ with/without the addition of catechol in aqueous solutions** was reported. Long equilibrium time is needed during the titrations. When the ratio of catechol:V^{IV} varies from 1:1 to >2:1, the species derived from the titration curves are VO(catecholate)$(OH)^{-}$ and VO(catecholate)$_2^{2-}$, respectively. No evidence for the existence of V(catechoat)$_3^{2-}$ was obtained.

Table S3.2 ≤ 50,000 TTO catalytic lifetime experiments (data for Figure 3.4 in the Main Text).

Catalyst	Experimental Conditions	Amt. DTBC (mmol)	Amt. Catalyst (mmol)	DTBC Conv. (%)	Σ(Prod. **2–6**) (mmol) Selectivity% Prod. **2, 3, 4, 6**	DTBC-TTO (Product yield TTO)
$(n\text{-}Bu_4N)_4H_5PV_{14}O_{42}$	130 mL 1,2-$C_2H_4Cl_2$ < 72 h reaction time	29.4	6.3×10^{-4}	>99	16.9 ± 0.5 31 (1), 9 (1), 5 (1), 13 (1)	46000 (27000 ± 2000)
$(n\text{-}Bu_4N)_7SiW_9V_3O_{40}$	130 mL 1,2-$C_2H_4Cl_2$ 96 h reaction time	29.2	6.7×10^{-4}	ND	17.4 ± 0.6 34 (1), 3 (1), 5(1), 17 (1)	ND (26000 ± 1000)
	130 mL 1,2-$C_2H_4Cl_2$ 101 h reaction time	29.4	6.5×10^{-4}	>99	19.3 ± 0.5 36 (1), 3(1), 6 (1), 20 (1)	45000 (30000 ± 1500)
$(n\text{-}Bu_4N)_5$ $[Fe{\cdot}SiW_9V_3O_{40}]$	119 mL 1,2-$C_2H_4Cl_2$ 141 h reaction time	29.4	6.4×10^{-4}	>99	20.8 ± 0.6 40 (2), 4 (1), 5 (1), 21 (1)	46000 (33000 ± 2000)
$(n\text{-}Bu_4N)_9P_2W_{15}V_3O_{62}$	129 mL 1,2-$C_2H_4Cl_2$ 120 h reaction time	29.5	6.5×10^{-4}	>99	21.1 ± 0.6 45 (2), 6 (1), 4 (1), 17 (1)	45000 (32000 ± 1000)
	124.5 mL 1,2-$_2H_4Cl_2$ 95 h reaction time	29.5	6.2×10^{-4}	>99	17.8 ± 0.4 34 (1), 3 (1), 6 (1), 18 (1)	48000 (29000 ± 1000)
$(n\text{-}Bu_4N)_5Na_2$ $[Fe{\cdot}P_2W_{15}V_3O_{62}]$	129mL 1,2-$C_2H_4Cl_2$ 169 h reaction time	29.6	6.3×10^{-4}	>99	20.7 ± 0.7 39 (2), 5 (1), 4 (1), 22 (1)	47000 (33000 ± 2000)
	126mL 1,2-$C_2H_4Cl_2$ 142 h reaction time	*29.6	6.6×10^{-4}	>99	18.3 ± 0.3 36 (1), 4 (1), 4 (1), 18 (1)	45000 (28000 ± 1000)
$[VO(DBSQ)(DTBC)]_2$	125.5 mL1,2-$C_2H_4Cl_2$ 118 h reaction time	29.1	5.8×10^{-4}	>99	22.2 ± 0.4 43 (1), 9 (1), 6 (1), 18 (1)	50000 (38000 ± 2000)
$[Et_3NH]_2[VO(DTBC)_2]{\cdot}$ CH_3OH	126 mL1,2-$C_2H_4Cl_2$ 144 h reaction time	28.8	6.6×10^{-4}	>99	19.8 ± 0.4 39 (1), 7 (1), 4 (1), 19 (1)	44000 (30000 ± 1000)
$[Na(CH_3OH)]_2{\cdot}$ $[V(DTBC)_3]_2{\cdot}4CH_3OH$	129 mL1,2-$C_2H_4Cl_2$ 92 h reaction time	*29.4	6.4×10^{-4}	>99	20.1 ± 0.2 35 (1), 11 (1), 4 (1), 19(1)	46000 (31000 ± 3000)
$VO(acac)_2$	126 mL1,2-$C_2H_4Cl_2$ 163 h reaction time	*29.4	6.8×10^{-4}	>99	19.9 ± 0.8 35 (2), 6 (1), 4 (1), 22 (1)	43000 (29000 ± 1000)
No catalyst added	122 mL1,2-$C_2H_4Cl_2$ 144 h reaction time	*29.7	0	16	1.7 ± 0.1 < 1, < 1, < 1, 6 (1)	-

Experimental conditions: 65 ± 1 °C, 1 atm O_2; product yields established by GC calibrated with authentic compounds or effective carbon number rules;[19] the asterisk (*) indicates that the substrate is with a melting point of 1 or 2 °C lower than the standard value (99 °C-100 °C); numbers in the parentheses in the selectivity column are the error bars for the selectivties; ND, not determined.

Table S3.3 100,000–150,000 TTO catalytic lifetime experiments.

Catalyst	Experimental Conditions	Amt. DTBC (mmol)	Amt. Catalyst (mmol)	DTBC Conv. (%)	Σ(Prod. **2–6**) (mmol) Selectivity% Prod. **2, 3, 4, 5, 6**	DTBC-TTO (Product yield TTO)
TTO optimization by varying substrate-to-precursor mole ratios						
$(n\text{-}Bu_4N)_5[Fe{\cdot}SiW_9V_3O_{40}]$	139 mL 1,2-$C_2H_4Cl_2$ 311 h reaction time	69.7	6.1×10^{-4}	97 ± 9	42.0 ± 1.5 37 (2), 4 (1), 1 (1), 2 (1), 16 (1)	110000 ± 10000 (69000 ± 4000)
	131 mL 1,2-$C_2H_4Cl_2$ 413 h reaction time	56.0	4.3×10^{-4}	> 99	31.2 ± 0.5 29 (1), 3 (1), 2 (1), 1 (1), 20 (1)	129000 (73000 ± 4000)
	125 mL 1,2-$C_2H_4Cl_2$ 425 h reaction time	63.0	4.8×10^{-4}	99 ± 9	38.1 ± 0.6 34 (1), 5 (1), 1 (1), 3 (1), 17 (1)	130000 ± 8000 (79000 ± 5000)
$(n\text{-}Bu_4N)_7SiW_9V_3O_{40}$	131 mL 1,2-$C_2H_4Cl_2$ 337 h reaction time	63.1	6.2×10^{-4}	99 ± 9	37.6 ± 2.1 34 (3), 4 (1), 1 (1), 2 (1), 18 (1)	100000 ± 11000 (61000 ± 4000)
	132 mL 1,2-$C_2H_4Cl_2$ 336 h reaction time	61.6	4.8×10^{-4}	> 99	36.0 ± 0.9 34 (1), 4 (1), 2 (1), 1 (1), 18 (1)	130000 (75000 ± 4000)
Fresh and aged $VO(acac)_2$ TTO results						
Fresh $VO(acac)_2$	128 mL 1,2-$C_2H_4Cl_2$ 546 h reaction time	63.1	4.9×10^{-4}	97 ± 4	29.1 ± 1.0 23 (1), 1 (1), -, 5 (1), 17 (1)	129000 ± 5500 (59000 ± 3000)
Aged $VO(acac)_2$ (2 month at RT)	135 mL 1,2-$C_2H_4Cl_2$ 549 h reaction time	63.0	4.9×10^{-4}	99 ± 5	34.5 ± 0.8 29 (1), 1 (1), -, 5 (1), 20 (1)	127000 ± 4000 (70000 ± 2000)

Experimental conditions: 65 ± 1 °C, 1 atm O_2; product yields established by GC calibrated with authentic compounds or effective carbon number rules;[19] numbers in the parentheses in the selectivity column are the error bars for the selectivties.

[19] Grob, R. L.; Editor *Modern Practice of Gas Chromatography*; 3rd ed.; John Wiley & Sons, Inc.: New York, 1995, pp 279-80.

CHAPTER IV

AUTOXIDATION-PRODUCT-INITIATED DIOXYGENASES: VANADIUM-BASED, RECORD CATALYTIC LIFETIME CATECHOL DIOXYGENASE CATALYSIS AND ITS MECHANISM OF ACTION

This dissertation chapter contains the manuscript of a full paper to be submitted to an ACS journal. This chapter presents kinetic studies of how polyoxometalate catechol dioxygenase precatalysts evolve into the Pierpont's catalyst resting state during the observed induction period. An interesting autoxidation-product-initiated catechol dioxygenase phenomenon is elucidated.

The initial kinetic (polyoxometalates with H_2O_2, DBQuinone, HBF_4) and H_2O_2 detection experiments were performed by Dr. Yoh Sasaki. The manuscript was prepared by Cindy-Xing Yin with assistance and editing by R. G. F.

Autoxidation-Product-Initiated Dioxygenases: Vanadium-Based, Record Catalytic Lifetime Catechol Dioxygenase Catalysis and Its Mechanism of Action

Cindy-Xing Yin, Yoh Sasaki and Richard G. Finke

Abstract

In recent work it was shown that V-containing polyoxometalates such as (n-$Bu_4N)_7SiW_9V_3O_{40}$ or (n-$Bu_4N)_9P_2W_{15}V_3O_{62}$, as well as 8 other V-containing precatalysts tested, evolve to a high activity, long catalytic lifetime (≥30,000-100,000 total turnovers) 3,5-di-*tert*-butylcatechol dioxygenase in which Pierpont's complex $[VO(DBSQ)(DTBC)]_2$ could be identified as a common catalyst or catalyst resting state (Yin, C.-X.; Finke, R. G. "Vanadium-Based, Record Catalytic Lifetime Catechol Dioxygenases: Evidence For a Common Catalyst," *J. Am. Chem. Soc.* **2005**, in press). Herein, those findings are followed up by studies aimed at answering the following questions about this record catalytic lifetime, 3,5-di-*tert*-butylcatechol dioxygenase catalyst: (i) what is the key to how V leaches from, for example, seemingly robust V-containing polyoxometalate precatalysts?; (ii) what is the key to the sigmoidal, apparently

autocatalytic kinetics observed?; (iii) what is the rate law for 3,5-di-*tert*-butylcatechol dioxygenation when one begins with Pierpont's $[VO(DBSQ)(DTBC)]_2$, and does it support the hypothesis that this complex is at least a catalyst resting state?; and if so (iv) can a mechanism be written from that information and the knowledge in the literature which accounts for the dioxygenase reaction? Key findings from the present work include that the reaction involves a novel, autoxidation-product induced dioxygenase, that is, one in which the *undesired* autoxidation of the 3,5-di-*tert*-butylcatechol substrate to the corresponding benzoquinone *and* H_2O_2 turns on the *desired* dioxygenase catalysis via a V-leaching process which eventually yields Pierpont's complex, $[VO(DBSQ)(DTBC)]_2$. Kinetics studies beginning with Pierpont's complex are consistent with it being a catalyst resting state; a minimum (Ockham's razor) mechanism is presented that is consistent with all our findings as well as the relevant dioxygenase literature. The results provide: a prototype example of the seemingly unlikely concept of an autoxidation-product-initiated dioxygenase; an unprecedented level of simplification of, and insight into, the previously disparate literature of V-based 3,5-di-*tert*-butylcatechol dioxygenase catalysis; as well as kinetically supported, postulated mechanism of action for the observed record catalytic lifetime, vanadium-based, DTBC dioxygenase catalysis.

Introduction

In 1999 we reported that a polyoxometalate vanadium-containing complex serves as an effective precatalyst for the dioxygenase-type oxidative cleavage of 3,5-di-*tert*-butylcatechol (hereafter 3,5-DTBC) with record, ≥100,000 total turnover (TTO) catalytic

lifetimes to produce the oxidative ring-cleavage products, **2–5**, plus the autoxidation product, **6**, Figure 4.1.[1] The new product **4** was also isolated and identified by X-ray crystallography as a part of that study. The above results are of considerable interest since man-made, highly catalytic, long-lived dioxygenase catalysts are the Holy Grail of oxidation catalysis.[2]

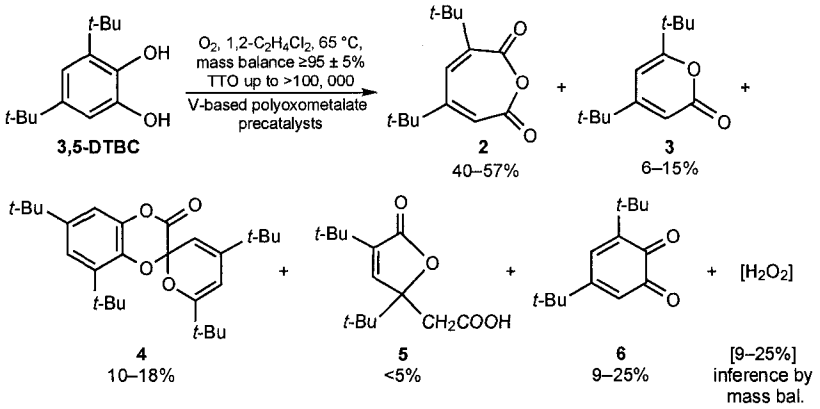

Figure 4.1 Oxidative cleavage of 3,5-DTBC by vanadium-containing polyoxometalate precatalysts. The products are: **2**, 3,5-di-*tert*-butyl-1-oxacyclohepta-3,5-diene-2,7-dione; **3**, 4,6-di-*tert*-butyl-*2H*-pyran-2-one; **4**, spiro[1,4-benzodioxin-2(*3H*),2'(*2H*)-pyran]-3-one, 4', 6, 6', 8-tetrakis(1,1-dimethylethyl); **5**, 3,5-di-*tert*-butyl-5-(carboxymethyl)-2-furanone, and **6**, 3,5-di-*tert*-butyl-1,2-benzoquinone.

As part of the 1999 study, initial O_2-uptake kinetic studies[1] revealed a novel product and catalyst evolution mechanism consisting of an A $\rightarrow$ B induction period (rate constant k_1) followed by an A + B $\rightarrow$ 2B, autocatalytic step (rate constant k_2), Figure 4.2. Note that A + B $\rightarrow$ 2B is the kinetic definition of autocatalysis, where the reaction product, B, is also a reactant. In this manner, the 2B-product-stoichiometry autocatalytically "turns on" the reaction (and, concomitantly we will see, the catalyst formation reaction, *vide infra*) resulting in sigmoidal-shaped kinetic curves as seen in Figure 4.2.

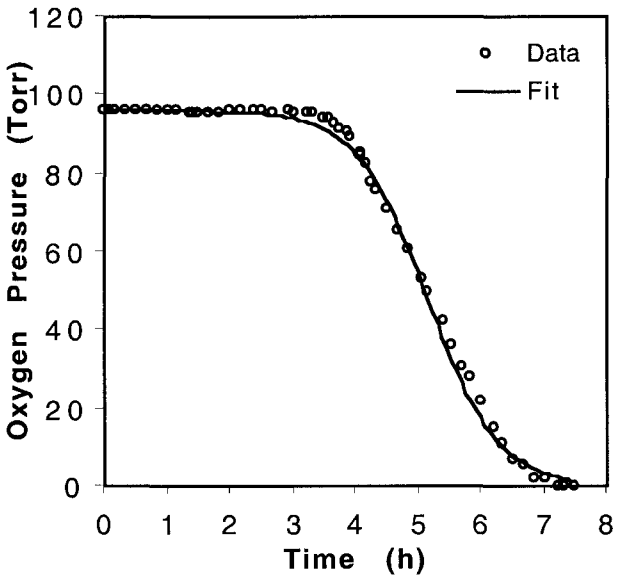

Figure 4.2 Autocatalytic O_2-uptake kinetic curve and curve fit of a 3,5-DTBC plus precatalyst (n-$Bu_4N)_7SiW_9V_3O_{40}$ and O_2 reaction. Conditions: 1.8 mmol 3,5-DTBC, 5.6 μmol precatalyst, 8.4 mL 1,2-$C_2H_4Cl_2$, 40 °C, and 0.8 atm O_2; note that the final pressure has been subtracted from the initial pressure to "zero" the y axis so that the *net pressure change* is shown above and in analogous curves hereafter. The curve fit is to the analytic kinetic equations for the two-step mechanism A → B (k_1) and A + B → 2B (k_2) as detailed elsewhere.[3,4] The rate constants obtained from the fit are: $k_1 = (1.8 \pm 0.3) \times 10^{-4}$ h^{-1} and $k_2 = (1.9 \pm 0.1) \times 10^{-2}$ $Torr^{-1} \cdot h^{-1}$; these rate constants are the same within experimental error as those obtained previously by an independent researcher in our labs,[1,x] $k_1 = (2.8 \pm 0.9) \times 10^{-4}$ h^{-1} and $k_2 = (1.6 \pm 0.1) \times 10^{-2}$ $Torr^{-1} \cdot h^{-1}$. Note that it is the sigmoidal form of the curve and its A → B and A + B → 2B curve fit, but not precise rate constants, that is the key result here for reasons discussed in the section which follows titled "The Pseudoelementary Step Treatment of the Autocatalytic Kinetics and Active Catalyst Formation Steps".

In more recent work, evidence from EPR (electron paramagnetic resonance) spectroscopy, negative ion ESI–MS (electrospray ionization mass spectrometry), kinetics, catalytic activity, selectivity and lifetime studies revealed that Pierpont's vanadium semiquinone catecholate dimer complex, $[VO(DBSQ)(DTBC)]_2$ (where DBSQ is 3,5-di-*tert*-butylsemiquinone and DTBC is the 3,5-di-*tert*-butylcatecholate dianion) is a

[x] The units of k_1 and k_2 in the Figure 4 and 5 captions in our previous studies[1] should have been h^{-1} and $Torr^{-1}h^{-1}$, the numbers are not changed.

common component—and apparently either the catalyst resting state or the true catalyst—produced from a wide variety of V-containing precatalysts.[5] This statement proved true regardless if one starts with the above V-containing polyoxometalate or nine other vanadium-containing precatalysts including simple $VO(acac)_2$.[5] Those studies show that virtually any V-based precatalyst appears to leach vanadium under the dioxygenase reaction conditions to produce $[VO(DBSQ)(DTBC)]_2$.

However, several important questions remained unanswered, including: (i) what is the reaction product, B, which turns on the V-leaching and sigmoidal, $A + B \rightarrow 2B$ autocatalytic evolution of the true catalyst? The most likely candidates are: H_2O_2 derived from the initial DTBC autoxidation[6] (H_2O_2 being a precedented[7]) product required by mass balance when the benzoquinone autoxidation product **6**, is produced, Figure 4.1); possibly the semiquinone anion; benzoquinone, **6**; or perhaps H_2O_2 in combination with the benzoquinone, product **6**. If H_2O_2 is B, then we have discovered an example of the seemingly improbable situation of where *undesired autoxidation* turns on the *desired dioxygenase chemistry*, a novel "*autoxidation-initiated dioxygenase*".[xi] Another important question is (ii) can H_2O_2 be detected among the reaction products or is it as rapidly consumed as it is made? Additionally, (iii) a rate law for DTBC plus O_2 dioxygenase catalysis beginning with the isolated catalyst-resting state $[VO(DBSQ)(DTBC)]_2$ remained to be obtained; is the intact dimer active or must this dimer fragment to an active monomer prior to reaction with O_2? In addition, (iv) can that rate law and the extensive literature of catechol dioxygenase catalysis be used to construct a minimal, "Ockham's razor", mechanism for V-based DTBC dioxygenase

[xi] We define an "autoxidation-product-initiated reaction" as one where a ROOH or other product of a (typically unintended) autoxidation initiates and facilitates an otherwise slow reaction.

catalysis, and lastly (v) from that mechanism or the literature, is it possible to add chelating ligands, for example, to change and improve the selectivity of the dioxygenase reaction in Figure 4.1 more towards a single product? Such enhanced selectivity, man-made dioxygenase catalysts that are also highly catalytically active remain an unsolved problem. It is just the above questions and issues that are the focus of the present paper.

Experimental Section

Reagents. 3,5-DTBC (Aldrich, 99%) was recrystallized three times using *n*-pentane (Fisher Scientific, 98%, pesticide grade) under argon (melting point 99–100 °C, lit. mp 96–99 °C) and stored in a Vacuum Atmosphere drybox (O_2 level ≤ 5 ppm). (NB: it is important to recrystallize the 3,5-DTBC substrate ≥3 times to remove impurities like 3,5-di-*tert*-butylsemiquinone, due to effects such as shown in Figure 4.3 in the main text.) 3,5-di-*tert*-butylbenzoquinone (Aldrich, 98%) was re-crystallized twice from *n*-pentane and stored in the drybox (melting point 114–115 °C, lit. mp 113–115 °C). All the polyoxometalate precursors were synthesized according to the most recent literature procedures.[8,9] Na/Hg amalgam (Strem, 20% Na of 99.9+% purity), 1,4,7-triazacyclononane (Strem, 97%) and 1,4,7-trimethyl-1,4,7-triazacyclononane (Strem, 97% min.) were stored in the drybox and used as received. HPLC grade solvents (1,2-dichloroethane, acetonitrile) were purchased from Aldrich and stored in the drybox; each of the above solvents was dried by standing for at least 48 h over ~5 vol.% 3-Å or 4-Å molecular sieves which were preactivated by heating at 170 °C under vacuum for at least 12 h, then cooling under dry N_2 in the drybox. THF (Fisher Scientific) was distilled over $LiAlH_4$ under Ar and stored under Ar. HBF_4 (Aldrich) was purchased as a 54 wt.%

diethyl ether solution and stored in the drybox. Sodium salt of 3,5-di-*tert*-butylsemiquinone (Na^+DBSQ^-) was prepared via the literature[10] by reacting an equivalent of Na amalgam with 3,5-di-*tert*-butylbenzoquinone. Its UV-visible absorbance in *t*-BuOH is at 728 nm (580 ± 20 $M^{-1}\cdot cm^{-1}$; measured under N_2), literature [11], 730 nm (680 $M^{-1}\cdot cm^{-1}$; no error bar were reported). A $Na_2S_2O_3$ aqueous solution (0.05 M) was prepared from $Na_2S_2O_3\cdot 5H_2O$ (Fisher Chemicals, certified ACS grade) and a pellet of KOH (Fisher Chemicals, certified ACS grade) was added for stabilization. KIO_3 (Mallinckrodt Powder, analytical grade), H_2SO_4 (Mallinckrodt analytical reagent), KI, starch (Fisher chemicals, certified ACS grade), and H_2O_2 (ca. 30 wt.% in H_2O, Fisher Scientific) were used as received.

Instrumentation. ^1H-, ^{31}P- and ^{51}V-NMR were recorded in 5-mm o.d. tubes on a Varian Inova (JS-300) NMR spectrometer. ^1H-NMR was referenced to the residual proton impurity in the deuterated solvent, ^{31}P-NMR was referenced to 85% H_3PO_4 in H_2O using the external substitution method, and ^{51}V-NMR was referenced to neat $VOCl_3$ using the external substitution method. Spectral parameters for ^{31}P-NMR include: tip angle = 60° (pulse width 10 μs); acquisition time, 1.6 s; sweep width, 10000 Hz. Spectral parameters for ^{51}V-NMR include: ^{51}V tip angle = 90° (pulse width 3.1 μs); acquisition time, 0.096 s; sweep width, 83682.0 Hz. GC analyses were performed on an HP (Hewlett-Packard) 5890 Series II gas chromatograph equipped with a FID detector and a SPB-1 capillary column (30 m, 0.25 mm i.d.) with the following temperature program: initial temperature, 200 °C (initial time, 2 min); heating rate, 2 °C/min; final temperature, 240 °C (final time, 3 min); FID detector temperature, 250 °C; injector temperature, 250 °C. An injection volume of 1 μL was used. Negative ion ESI–MS experiments were

performed on a Thermo Finnigan LCQ Advantage Duo MS directly coupled with a syringe pump (5 μL/min feeding speed; spray voltage –4.5 kV, capillary voltage –(38–42) V, capillary temperature 180 °C), CH_3CN as solvent.

Impurities in crude DTBC. GC accomplished under the above-noted conditions detected ~4% 3,5-DBQuinone impurity in crude DTBC while Liquid Secondary Ion–MS (LSI–MS), performed on a Fisons VG AutoSpec mass spectrometer at 27 KV with Cs^+ ion, *m*-nitrobenzyl alcohol as matrix, failed to detect any impurities (a 3,5-DBQuinone parent ion peak was not detected by LSI–MS, perhaps due to its ready fragmentation).

Preparation of Precatalysts. $(n\text{-}Bu_4N)_7SiW_9V_3O_{40}$ and $(n\text{-}Bu_4N)_9P_2W_{15}V_3O_{62}$ were prepared and characterized as described in the Supporting Information elsewhere.[5] $[Et_3NH]_2[VO(DTBC)_2]\cdot nCH_3OH$ (n ~ 1–2) and $[VO(DBSQ)(DTBC)]_2$ were prepared and characterized by UV-visible, elemental analysis, and negative ion ESI–MS as previously detailed.[5]

Oxygen-uptake Experiments Procedure. All the experiments except those for the rate law derivation (*vide infra*) were carried out on a volume-calibrated oxygen-uptake line as detailed in the Supporting Information elsewhere[1] (the total, calibrated volume, determined using three different-volume reaction flasks, is in the range of 246–257 mL). Our standard procedure is as follows: 400 ± 5 mg (ca. 1.8 mmol) of three-times-recrystallized 3,5-DTBC was weighed in the drybox into a 50 mL round-bottom reaction flask equipped with a septum, side-arm and an egg-shaped 3/8" × 3/16" Teflon-coated magnetic stir bar. Approximately 8 mL pre-dried HPLC grade 1,2-dichloroethane were transferred into the flask using a 10-mL glass syringe, the flask was sealed with a Teflon stopcock and taken out of the drybox. The flask was then connected

to the oxygen-uptake line through an O-ring joint, and the reaction solution was frozen in a dry ice/ethanol bath (-76 °C) for 10 min. Two pump-and-fill (with O_2) cycles were performed. Next, the dry ice bath was replaced with a temperature-controlled oil bath. The flask was brought up to 40 ± 0.7 °C and allowed to equilibrate with stirring for 25 min under O_2. In the drybox, 5.7 (±0.4) × 10^{-6} mol of a precatalyst was weighed into a 5 mL glass vial and dissolved in ca. 0.2 mL 1,2-dichloroethane. The catalyst solution was drawn into a 1 mL gas-tight syringe and brought out of the drybox with protection from air by insertion of the syringe needle into a septum-capped-vial. The catalyst was injected through the sidearm of the reaction flask and t = 0 was set. Pressure readings from the manometer were used to follow the reaction (±1 Torr or ca. ±1% precision over a pressure loss of ca. 80–100 Torr). The reaction was stopped when no oxygen loss was observed for 1–2 h.

Oxygen-uptake Experiments with Preselected Additives. The following substances were tested as candidates for the product, B, which is able to remove the induction period and speed up the reactions (Table 4.1 provides the specific amounts added): a 30% H_2O_2 water solution; H_2O; product **6** (3,5-di-*tert*-butyl-1,2-benzoquinone, abbreviated as 3,5-DBQuinone); product **5** (3,5-di-*tert*-butyl-5-(carboxymethyl)-2-furanone); 54% HBF_4 in diethyl ether; a free radical initiator, AIBN (2,2'-azobisisobutyronitrile); a mixture of 30% H_2O_2 plus product **6**; and the sodium salt of 3,5-di-*tert*-butylsemiquinone (NaDBSQ). *o*-Dichlorobenzene and H_2O saturated 1,2-dichloroethane were also examined as tests of the effects of solvent and trace water. The effect of each additive was monitored by comparing the induction period with the additive to the induction period under standard conditions without the additive. These

experiments were set up exactly as described in the previous section titled "Oxygen-uptake Experiments Procedure" except that the additive was injected at t = 2 min after the injection of the precatalyst.

H_2O_2 Detection Experiment Procedure. Because H_2O_2 was shown to eliminate the induction period for two vanadium-containing polyoxometalates and a vanadium catecholate precursor, and since the known stoichiometry is 1 H_2O_2 formed for every 1 equiv. of the 18–25% benzoquinone formed,[7] attempts were made to detect H_2O_2 in the product mixture at various times. Specifically: 0.05 M $Na_2S_2O_3$ solution was first standardized by titration with primary standard 0.01 M KIO_3 solution (10 mL) plus 5 mL of 10 w/v% KI solution and 4 mL of 9 M H_2SO_4. This results in a color change from dark brown to pale yellow. Next, an indicator starch solution was added to detect the presence of I_3^-; the titration reached the end point with a color change from violet to colorless. A blank titration was also performed to account for the effects of any possible oxidizing reagents in the background. Our H_2O_2 detection limit (set as 3σ of the signal seen as the background) is ~7.5×10^{-6} mol (0.4 mol.% of the reaction substrate).

Attempts to detect H_2O_2 were carried out at three different reaction times during an oxygen-uptake experiment: at 2h (i.e., during the induction period), at 5h (post the induction period, during the main active period of the reaction) and at 8h (after the reaction). The H_2O_2 test was accomplished as follows: the product solution was transferred into a separation funnel and the reaction flask was washed three times with fresh 1,2-dichloroethane and four times with distilled water. All of the washes were added to the separation funnel and shaken vigorously to extract any possible H_2O_2 into the aqueous layer. Next, 5 mL of 10 w/v% KI solution and 4 mL of 9 M H_2SO_4 were

added to the water layer and the I_3^- was titrated by the previously standardized 0.05 M $Na_2S_2O_3$ solution. The results are described in the main text and Figure 4.6.

Catalyst Evolution Stoichiometry Experiments. The experiments which follow were done to test the catalyst evolution steps postulated in Figure S4.12. The experiments immediately below were performed using a high vacuum line equipped with a high precision Baratron pressure transducer (±0.1 Torr up to 1000 Torr), which resides in Professor S. H. Strauss' labs at Colorado State University. The volume of the line was calibrated to be 96–97 mL via a calibration flask of known volume. Due to the necessity of using a larger amount of the precatalyst and a smaller amount of the substrate (i.e., so as to see a measurable amount of O_2 uptake), the reaction procedure was changed to the following: 210 ± 10 mg (ca. 0.05 mmol) of $(n\text{-}Bu_4N)_7SiW_9V_3O_{40}$ was weighed in the drybox into a 50 mL round-bottom reaction flask equipped with a septum, side-arm and an egg-shaped 3/8" × 3/16" Teflon-coated magnetic stir bar. Approximately 7.6 mL pre-dried HPLC grade 1,2-dichloroethane were transferred into the flask using a 10-mL glass syringe, the flask was sealed with a Teflon stopcock and taken out of the drybox. The flask was then connected to the oxygen-uptake line through an O-ring joint, and the reaction solution was frozen in a dry ice/ethanol bath (-76 °C) for 10 min. Two pump-and-fill (with ca. 500 Torr O_2) cycles were performed. Next, the dry ice bath was replaced with a temperature-controlled oil bath. The flask was brought up to 40 ± 0.5 °C and allowed to equilibrate with stirring for 2 h under O_2. In the drybox, 44–70 mg (ca. 0.2–0.3 mmol) of three-times-recrystallized 3,5-DTBC was weighed into a 5 mL glass vial and dissolved in ca. 0.4 mL 1,2-dichloroethane. The substrate solution was drawn into a 1 mL gas-tight syringe and brought out of the drybox with protection from air by

insertion of the syringe needle into a septum-capped-vial. The substrate was injected through the sidearm of the reaction flask and t = 0 was set (H_2O_2 was injected immediately after the addition of the substrate in one, separate run). Pressure readings from the transducer were used to follow the reaction. The reaction was stopped when no oxygen loss was observed for 10–15 min. The results are described in the section in the Supporting Information titled "Plausible Stoichiometries for Conversion of $SiW_9V_3O_{40}^{7-}$ to the Active Catalyst, $[V^V(O)(DBSQ)(DTBC)]_2$ Plus Initial Experimental Tests of Those Stoichiometries".

Confirmed Formation of $[VO(DBSQ)(DTBC)]_2$ from $[V(DTBC)_3]^-$ Under Catalytic Conditions By EPR. The predicted conversion of $V(DTBC)_3^-$ to $[VO(DBSQ)(DTBC)]_2$ under catalytic conditions was also tested in experiments in toluene that are described in the Supporting Information.

O_2-Uptake Kinetic Experiments and Rate Law Determination. These experiments were carried out as detailed elsewhere [12] on a computer-interfaced O_2-pressure transducer apparatus which permits the collection of high precision (≤±0.01 psig) pressure data at ≥1 data points per second. The reaction flask is a pressurized Fischer–Porter bottle attached via Swagelock quick-connects and flexible stainless steel tubing to both an oxygen tank and to a pressure transducer (total volume 148 mL).[12] In the drybox, 400 ± 5 mg (ca. 1.8 mmol) 3,5-DTBC was weighed into a 22 mm × 175 mm Pyrex culture tube along with a 5/8 × 5/16" Teflon stir bar. Pierpont's catalyst $[VO(DBSQ)(DTBC)]_2$ (typically 2–8 mg, 1.8–7.2 μmol) was weighed into a 5 mL glass vial and dissolved in a measured volume of 1,2-$C_2H_4Cl_2$ (1–3 mL). A pre-determined fraction (ca. 1/10–1/3; 0.4–0.8 μmol) of this stock solution was transferred into the

culture tube via a 1-mL syringe. The culture tube was then placed inside the Fischer–Porter bottle, sealed, brought out of the drybox, placed in a temperature-controlled oil bath, and attached to the oxygen uptake apparatus via the quick-connects. Stirring was initiated and the solution was equilibrated in the oil bath (40 °C) under N_2 (from the drybox gas) for 25 min. The Fischer-Porter bottle was then purged 15 times with ~13 psig of O_2 (or ~1.7 atm), 15 sec per purge, followed by equilibration for 1 min 15 s; 5 min total time elapsed before the pressure recordings were started. Note that the atmosphere pressure at the ca. 1 mile-high altitude of Fort Collins, Colorado is around 632 Torr, or 0.83 atm. The reaction vessel was then pressurized to 13 ± 1 psig and t = 0 was set. The results are shown in Figures 4.7 and S4.10-S4.11.

The O_2 rate vs catalyst concentration, gas-to-solution mass-transfer limitation plot is included in the Supporting Information as Figure S4.8. That data, obtained at a stirring rate of 1200 rpm, indicates a clean first-order catalyst dependence up to ca. 0.1 mM so that O_2 mass-transfer limitations should not be a concern for the kinetic experiments leading to the reaction orders in substrate and O_2 which were performed at ca. 0.05 mM and a 1200 rpm stirring rate. In all cases, the raw kinetic data from the O_2-uptake kinetics obtained with the pressure transducer were corrected for the contribution of the solvent vapor pressure in the early part of the curves prior (i.e., after flushing with O_2 to start the reaction and prior to those curves coming to equilibrium). This correction was done exactly as detailed earlier via the measurement of solvent-vapor pressure curve in an independent experiment[4] (an exemplary curve is provided in the Supporting Information as Figure S4.9 along with additional details of how the correction was accomplished). The corrected, typically initially linear, O_2 pressure time plots (e.g., Figures 4.7, S4.10,

S4.11) were analyzed by linear regression of their initial linear part to obtain initial rate data (see Figures S4.10 and S4.11 of the Supporting Information as examples and for additional details).

Reaction Rate of $[VO(DBSQ)(DTBC)]_2$ with O_2 as Estimated By UV-visible Spectroscopy. The rate of reaction of $[VO(DBSQ)(DTBC)]_2$ plus O_2 was estimated by following the decay of the absorbance peak at 684 nm of $[VO(DBSQ)(DTBC)]_2$ (0.15 μmol in 3 mL 1,2-$C_2H_4Cl_2$, 0.05 mM) after O_2 was bubbled into the UV-cell which had been prewarmed to ca. 40 °C. The initial rate of reaction, obtained from the first three data points over 20 min of reaction, is 1.9 h^{-1} (pesudo-first-order rate constant when assuming O_2 is in excess, $[O_2]_{solution}$ ~5 mM at[14] 293.2 K, 0.8 atm O_2; the initial second-order rate constant is ca. 380 $M^{-1}h^{-1}$ assuming a second-order rate law and using the $[O_2]_{solution}$ ~ 5 mM).

Kinetic Curve-Fitting. (I) Using Origin. OriginLab's non-linear least-squares curve-fitting program, Origin, plus the analytic equation shown below corresponding to the steps of A $\rightarrow$ B plus A + B $\rightarrow$ 2B, was used to fit the kinetic data in Figure 4.2 analogous to our prior work.

$$[A]_t = \frac{\frac{k_1}{k_2} + [A]_0}{1 + \frac{k_1}{k_2[A]_0}\exp^{(k_1 + k_2[A]_0)t}}$$

(II) Using MacKinetics. For the related equations in Figure 4.11 of A $\rightarrow$ 2B, B + O_2 $\rightarrow$ C + Products, 2C + 2DTBC $\rightarrow$ A; plus C + DTBC $\rightarrow$ B, numerical integration curve fitting via MacKinetics was employed. The oxygen pressure in psig was converted to soluble O_2 in M by setting up an "oxygen reservoir" to mimic the oxygen

concentration in the solution following the calculation method first used by D. K. Lyon[13] along with literature O_2 solubility data (a Henry's constant of 15340 Pa m^3/mol at 293.2 K in 1,2-dichloroethane);[14] the resultant ($[O_2]_t - [O_2]_{final}$)[xii] experimental data were then used in the fitting. To start, the chemical equations to be tested were written into Mackinetics along with the experimental data set. Next, a grid search was performed to fit the kinetic parameters to the experimental data. Specifically, the kinetic parameter search was performed first over a broad range of the parameters (10^{-10}–10^{10}) using the grid search command in Mackinetics. Then, the grid search was narrowed down to about half the previous range (e.g., if the first search gave $k_1 = 0.01$ and $k_2 = 0.1$ as the best fit in the range of 10^{-10}–10^{10}, then the second search was performed in the range of 10^{-7}–10^{3} for k_1 and 10^{-6}–10^{4} for k_2); the center of the new range was always set to equal the result from the last grid search as in the above examples. The search was deemed finished once a grid search was performed in a range no larger than two orders of magnitude. The curve-fit shown in Figure 4.7 (as well as Figures S4.10 and S4.11) is that obtained by performing a final integration, using the best set of kinetic parameters, and then co-plotting that data with the observed, experimental data. All other fits started with the parameters obtained from Figures 4.7, S4.10–4.11 and then performed a grid search over a range of $10^{\pm 2}$ from those parameters.

Effect of the Addition of an O-substituted Ligand to $[VO(DBSQ)(DTBC)]_2$ as Monitored by EPR. A drop of DMSO (Mallinckrodt, spectrometric grade) was added to a ca. 0.2 mM $[VO(DBSQ)(DTBC)]_2$ in toluene. The 9-line EPR characteristic[5] of

[xii] A result of using the zeroed, net $[O_2]$ concentration change which is necessary for the curve-fitting is that the different initial pressure is ignored; that is, $\Delta[O_2]$ is proportional only to the [DTBC](total). Hence, the averaged rate constants reported in Figure 4.11 are the result from curve-fitting just those eight sets of data obtained under the identical initial pressure (ca. 1.7 atm O_2).

$[VO(DBSQ)(DTBC)]_2$ (g = 2.006, A_{51V} = 3.01 G) changed to an asymmetric spectrum (a g = 2.02, broad peak and a g = 2.002 for 5 other sharp peaks, A_{51V} = 6.35 G) as shown in Figure S4.17 in the Supporting Information. A color change from blue to violet was also observed upon the addition of DMSO.

Results and Discussion

Oxygen-uptake Kinetics of Triply Recrystallized vs Crude DTBC. We began with a control experiment testing whether our normal precaution of triply recrystallizing the DTBC substrate under argon, and storing it under N_2, was necessary. The red 3,5-DBQuinone, **6**, is present in crude, brown-ish DTBC at a ~4% level by GC.

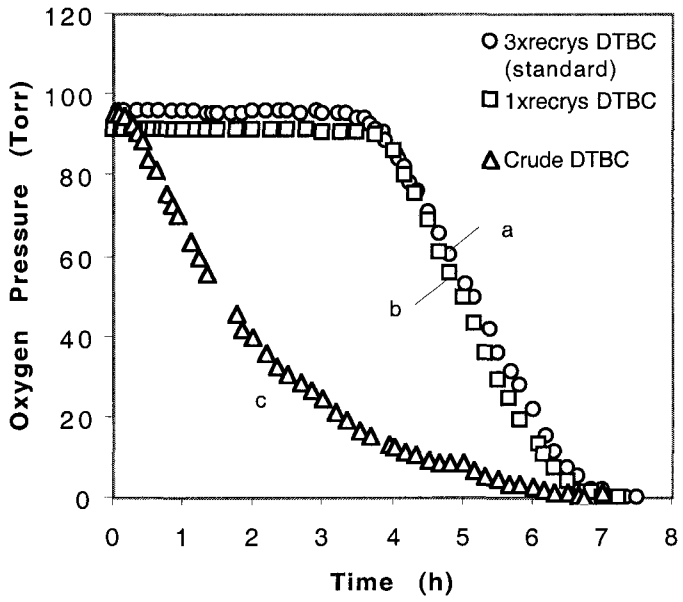

Figure 4.3 Kinetic O_2-uptake experiments for DTBC plus precatalyst (n-$Bu_4N)_7SiW_9V_3O_{40}$ and O_2 with (a) three-times-recrystallized DTBC; (b) once-recrystallized DTBC and (c) crude DTBC. Conditions: 1.8 mmol 3,5-DTBC, 5.6–5.7 μmol precatalyst, 8.2–8.4 mL 1,2-$C_2H_4Cl_2$, 40 °C, and 0.8 atm O_2; note that the y axis has been "zeroed" to show the net pressure change as described in the caption to Figure 4.2.

Figure 4.3a shows a normal DTBC oxygenation run using precatalyst (n-$Bu_4N)_7SiW_9V_3O_{40}$, triply recrystallized DTBC (mp 99–100 °C) under our standard reaction conditions as detailed in the Experimental Section. Note the typical, ca. 4 hour induction period, Figure 4.3a. Once recrystallized DTBC (mp 98–99 °C) behaves similarly, Figure 4.3b. However, *crude, as received DTBC (Aldrich, labeled mp as 96–99 °C; mp 92–95 °C in our hands) behaves much differently* exhibiting a 10–15 min induction period, Figure 4.3c, a repeatable result throughout different batches of crude DTBC and by two different experimentalists. GLC analysis shows that the product selectivity for the crude DTBC is the same within experimental error as the selectivity for triply recrystallized DTBC. These results: (i) emphasize that the continued use of triply recrystallized DTBC is crucial for the kinetic studies herein; and (ii) show that the crude DTBC contains a contaminant that, along with molecular O_2, is able to remove most of the induction period.

Oxygen-uptake Experiments with Selected Additives: Which Reaction Products Remove the Observed Induction Period? Our previous kinetic studies,[1] and our more recent studies,[5] both reveal that vanadium-containing polyoxometalates act as only precatalysts, displaying a significant, ca. 4 hr induction period in case of $SiW_9V_3O_{40}^{7-}$ before the oxygen uptake starts, for example, Figures 4.2 and 4.3. Hence, in 12 independent experiments we added each of the following key products or other additives at the beginning of the reaction to determine which additive(s) can turn on the reaction and eliminate the long induction period: H_2O_2, 3,5-DBQuinone (both these are DTBC autoxidation products), a mixed solution of H_2O_2 and 3,5-DBQuinone, H_2O, the carboxylic acid product, **5**, the strong acid HBF_4, a free radical initiator (AIBN; 2,2'-

azobisisobutyronitrile), or the semiquinone, NaDBSQ. The results from the 12 experiments are summarized in Table 4.1.

The most informative results came when examining 30% H_2O_2 in H_2O. The amount of H_2O_2 added all at once (18% relative to DTBC) corresponds to the maximum, ~18% amount produced in the reaction (i.e., 1 equiv. H_2O_2 produced for each equiv. of the 18% benzoquinone yield). This level of H_2O_2 reduced the induction periods of two different polyoxometalate precatalysts by a factor of 7–14, a complete removal of the induction period when the effects of the co-added H_2O are taken into account, *videinfra*. H_2O_2 also reduced the induction period of the precatalyst $[VO(DTBC)_2]^{2-}$ by a factor of 4. A control of adding the same amount of H_2O as present in the 70% H_2O / 30% H_2O_2 solution has the *opposite effect*, lengthening the induction period[xiii] as shown in Figure 4.4. Hence, it follows that the 18% H_2O_2 effectively eliminates the induction period when the masking effect of the added H_2O is removed. The added H_2O_2 (plus H_2O) did not change the catalyst performance as shown by the number of moles of oxygen consumed; the product yields are the same except that of benzoquinone increases ~10% (from ~18% to ~27% with the added H_2O_2). Adding H_2O_2 and the benzoquinone, **6**, together has no increased effect over adding the H_2O_2 alone, Table 4.1.

Other products or additives have smaller to no effects on the induction period: the autoxidation product 3,5-DBQuinone, **6**, alone shortens the induction period slightly from 3.5 h to 2.5 h, so that the 0.25 h induction period seen for crude DTBC (Figure 4.3, part c,

[xiii] H. Weiner's preliminary results indicating that added H_2O decreased the induction period[1] did not prove repeatable and is updated by the repeatable results reported herein showing that H_2O in fact increases the induction period. Two other findings different from the initial experimental results provided earlier[1] are that the pressure drop in the early part of Figure 5A elsewhere[1] is an artifact (of no consequence then or now) and that higher TTOs than previously obtained in Figure 6 (line (c)) elsewhere[1] using $VO(acac)_2$ have now been achieved as described elsewhere.[5]

vide supra) cannot be accounted for solely by the ~4% 3,5-DBQuinone impurity in unrecrystallized DTBC. Noteworthy here is that it is known from the literature,[15] as well as from our earlier work,[16] that the benzoquinone generally is *not* an intermediate (i.e., does not lead to the observed dioxygenase products). In the present, V-based system the almost linear GLC curve for the 3,5-DBQuinone product vs time in Figure 1 elsewhere[1] confirms that it is a stable product and does not go on to yield dioxygenase products.

The product **5** (3,5-di-*tert*-butyl-5-(carboxymethyl)-2-furanone, i.e., an RCOOH) has almost no effect on the induction period, Table 4.1. The strong acid HBF_4 does reduce the induction period some, but a significant, 1 h-induction period is still present, Figure 4.5 and Table 4.1.

The radical initiator AIBN had no effect on the oxygen-uptake kinetics under the reaction conditions, which argues against initiation of the dioxygenase reaction by adventitious free radicals. We also did controls to ensure that the solvent 1,2-$C_2H_4Cl_2$

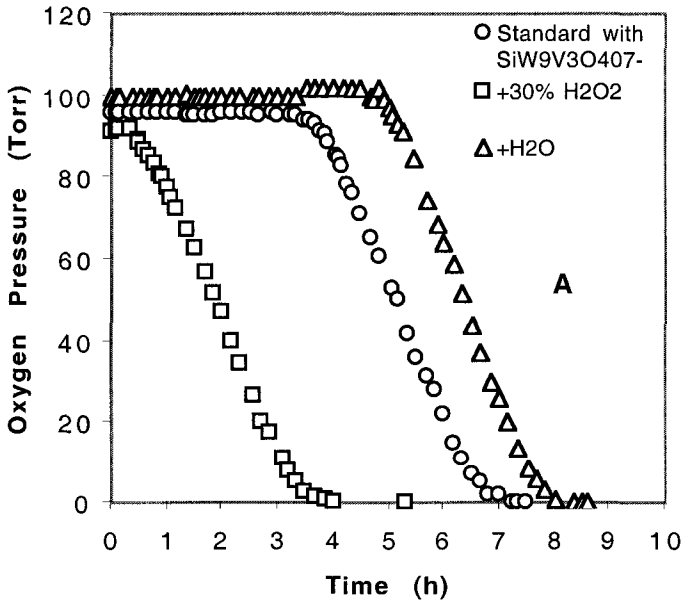

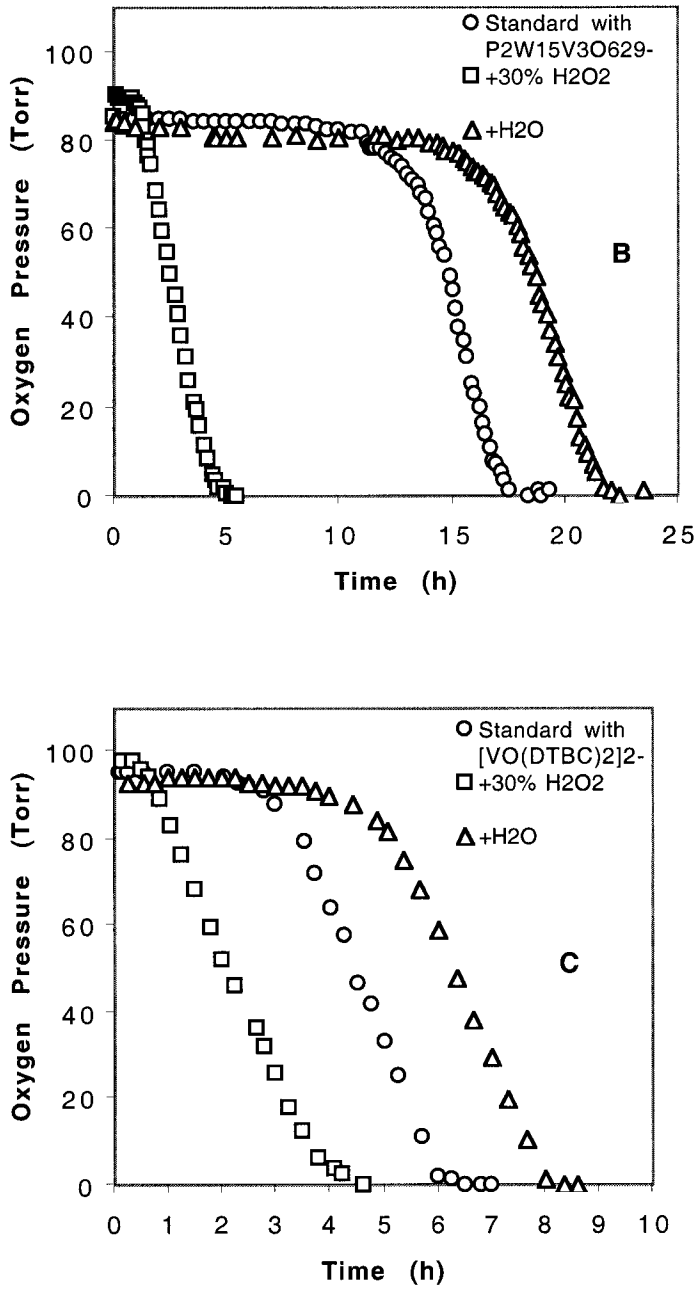

Figure 4.4 Kinetic O_2-uptake experiments for DTBC plus precatalyst alone or precatalyst with 30% H_2O_2 (0.33 mmol) or just H_2O (1.3 mmol) as a control: (**A**) precatalyst $(n\text{-}Bu_4N)_7SiW_9V_3O_{40}$; (**B**) precatalyst $(n\text{-}Bu_4N)_9P_2W_{15}V_3O_{62}$, or (**C**) precatalyst $[Et_3NH]_2[VO(DTBC)_2]\cdot nCH_3OH$. Other conditions: 1.8 mmol 3,5-DTBC, 4.4–5.7 μmol precatalyst, ca. 8 mL 1,2-$C_2H_4Cl_2$, 40 °C, and 0.8 atm O_2; note that the y axis has been "zeroed" to show the net pressure change.

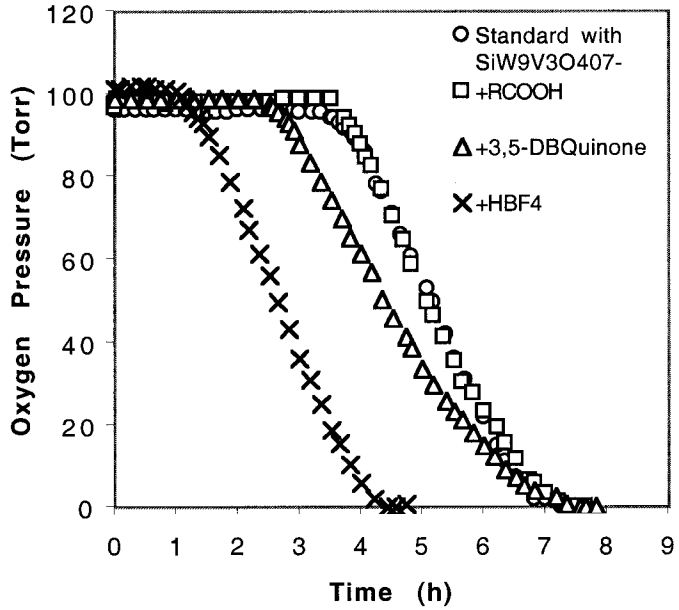

Figure 4.5 Kinetic O_2-uptake experiments forDTBC plus precatalyst (n-$Bu_4N)_7SiW_9V_3O_{40}$ with the addition of product **5** (0.090 mmol), 3,5-DBQuinone (0.32 mmol) or HBF_4 (7.2 μmol). Other conditions: 1.8 mmol 3,5-DTBC, 4.4–5.7 μmol precatalyst, ca. 8 mL 1,2-$C_2H_4Cl_2$, 40 °C, and 0.8 atm O_2; note that the y axis has been "zeroed" to show the net pressure change.

Table 4.1 The Effects of Products or Other Additives on the Induction Period of DTBC Oxygenation Beginning with Three Different Vanadium-Containing Precatalysts.

Additive(s)	Induction Period (h)	$\Delta n_{O2}/n_{DTBC}$ [a]	Figure
With Precatalyst (n-$Bu_4N)_7SiW_9V_3O_{40}$ (5.3–5.7 μmol)			
None (Standard Conditions[b])	3.5	0.75	4.3a
H_2O_2 (0.33 mmol)	0.3–0.5[c]	0.71	4.4
H_2O (1.3 mmol)	4.8	0.79	4.4
H_2O_2 (0.31 mmol) plus 3,5-DBQuinone (0.32 mmol)	0.3	0.70	S4.1
3,5-DBQuinone (0.32 mmol)	2.5	0.77	4.5
Product **5** (RCOOH, 0.090 mmol)	3.8	0.76	4.5
HBF_4 (7.2 μmol)	1.0	0.79	4.5
AIBN (0.018 mmol and 0.054 mmol)	3.8–3.9	0.73	S4.2
NaDBSQ (0.33 mmol)[d]	~0	*0.53*[d]	S4.3

In H_2O saturated 1,2-$C_2H_4Cl_2$	4.6	0.76	S4.4
In *o*-dichlorobenzene	3.3	0.75	S4.5
With Precatalyst (n-$Bu_4N)_9P_2W_{15}V_3O_{62}$ (5.7 μmol)			
None (Standard Conditions[b])	11.0	0.65	4.4
H_2O_2 (0.31 mmol)	1.0	0.69	4.4
H_2O (1.3 mmol)	14.6	0.66	4.4
With Precatalyst $[Et_3NH]_2[VO(DTBC)_2]\cdot nCH_3OH$ (4.4–4.7 μmol)			
None (Standard Conditions[b])	2.0	0.73	4.4
H_2O_2 (0.33 mmol)	0.5	0.74	4.4
H_2O (1.3 mmol)	2.5	0.70	4.4

[a]This ratio includes the autoxidation product, 3,5-di-*tert*-butylbenzoquinone (i.e., is not the dioxygenase only stoichiometry which would not include this product as discussed elsewhere[1]).
[b]Standard reaction conditions: 8 mL 1,2-$C_2H_4Cl_2$ solvent, 400 mg three-times-recrystallized DTBC, 40 °C, and 0.8 atm O_2.
[c]Two runs were carried out using one-time-recystallized DTBC.
[d]The stoichiometry and the final product, 100 ± 6% 3,5-DBQuinone (<0.5% yield of products **2-5**), show that this is an autoxidation reaction (i.e., and not an autoxidation-initiated catechol oxygenation reaction).

(with its C–H BDE of ca. 101 kcal/mol[17]) is not involved in the DTBC oxidation chemistry by showing that the same kinetics and O_2 uptake within experimental error are obtained in more oxidation resistant solvent, *o*-dichlorobenzene (C–H BDE of ca. 111 kcal/mol[17]), Table 4.1.

Autoxidation of 3,5-DTBC is initiated by the addition of $Na^+DBSQ^{-\bullet}$, but the resultant sole product is the benzoquinone, 3,5-DBQ with <0.5% of products **2-5** being detected, Table 4.1, results confirmed by our recent study on Na_2(DTBC) (which found benzoquinone, 6, as the sole product (30%), but <1% of product 2–5[5]).[xiv] This result is

[xiv] The products do show a solvent dependence: Na_2(DTBC) plus O_2 in diethylether yields 20–60% **5.** Speier, G.; Tyeklár, Z. *J. Mol. Catal.* **1990**, *57*, L17-L19.

consistent with our mechanistic finding (vide infra) of vanadium-bound semiquinone, but not free $DBSQ^{-\bullet}$, being important in DTBC dioxygenase catalysis.

The key finding is that H_2O_2 is effective at removing the induction periods of three different vanadium-containing catechol oxygenation precatalysts, Figures 4.4A, 4.4B and 4.4C. These kinetic results, the fact that H_2O_2 is an 18% product along with the benzoquinone, **6**, plus the fact that an A $\rightarrow$ B plus A + B $\rightarrow$ 2B kinetic scheme fits the parent kinetic curves (e.g., Figure 4.2) all require that a reaction product, B, is formed which then turns on the catalyst formation. The data strongly implicate H_2O_2 as that key reaction product, B.

We also know from our recent work that Pierpont's complex, $[VO(DBSQ)(DTBC)]_2$,[5] is detectable in solution from a range of different V-precatalysts and appears to be the catalyst-resting state. It is both precedented and makes chemical sense that H_2O_2 is the autoxidation-product that initiates the dioxygenase chemistry by forming [VO(DBSQ)(DTBC)], since O_2^{2-} is a powerful σ- and π-donor, one well-established to tightly bind and leach V and other transition-metals out of even polyoxometalate structures.[18,19,20,21,22] Precedent for this statement includes literature showing that $V_{10}O_{28}^{6-}$ plus H_2O_2 give[19] $V(O)O_2^+$ and the peroxy-complexes of vanadium $V(O)O_2^+$, $V(O)(O_2)^{2-}$, $V(O)(O_2)_4^{3-}$, $V(O_2)^{3-}$ that are all known.[20] Overall, the results provide excellent evidence for a previously little precedented H_2O_2 autoxidation-product-initiated dioxygenase catalysis.

Attempted Detection of H_2O_2 During Oxygen-uptake Experiments. The finding that H_2O_2 is highly effective at turning on the catalysis raises the question of

whether or not free H_2O_2 might be detectable at any time during the reaction. Alternatively, is H_2O_2 consumed as rapidly as it is formed?

Details of the experiments performed, plus several important controls, are provided in the Experimental Section. Not surprisingly, H_2O_2 could *not* be detected at any stage of catechol oxygenation: not during the induction period (t = 2 h), not in the middle of the oxygen-uptake reaction (5 h) and not after the reaction (8 h), even given our sensitive, detection limit of H_2O_2 (0.4 mol.% relative to the DTBC substrate). To confirm that H_2O_2 generated in the reaction is fairly rapidly consumed, four independent experiments were performed in which authentic, exogenous H_2O_2 (18–26% vs 3,5-DTBC, i.e., ca. 1–1.5-fold vs that are generated in the reaction) was added: (i) to pure solvent (1,2-$C_2H_4Cl_2$), (ii) to a substrate solution (3,5-DTBC in 1,2-$C_2H_4Cl_2$); (iii) to a precatalyst solution ((*n*-$Bu_4N)_7SiW_9V_3O_{40}$ in 1,2-$C_2H_4Cl_2$), or (iv) to a mixed solution of substrate and precatalyst. Figure 4.6 presents the results of the iodometric titration of the remaining, detectable H_2O_2 in these four experiments. As Figure 4.6 reveals, H_2O_2 added to the reaction mixture is consumed fairly rapidly when just the (*n*-$Bu_4N)_7SiW_9V_3O_{40}$ precatalyst is present, and even more rapidly when DTBC and the V-polyoxoanion precatalyst are both present—after 90 minutes, only 2% of the added H_2O_2 remains in this latter case.

The implied conclusion from the reaction stoichiometry which requires that 18% H_2O_2 is formed (concomitant with the 18% benzoquinone product, **6**), from the fact that, however, H_2O_2 is not detectable during the reaction (≤0.4%) (*vide supra*), as well from the above kinetic experiments in which added, authentic H_2O_2 is consumed fairly quickly is that H_2O_2 is the key product and *kinetically competent intermediate*, B, that turns on

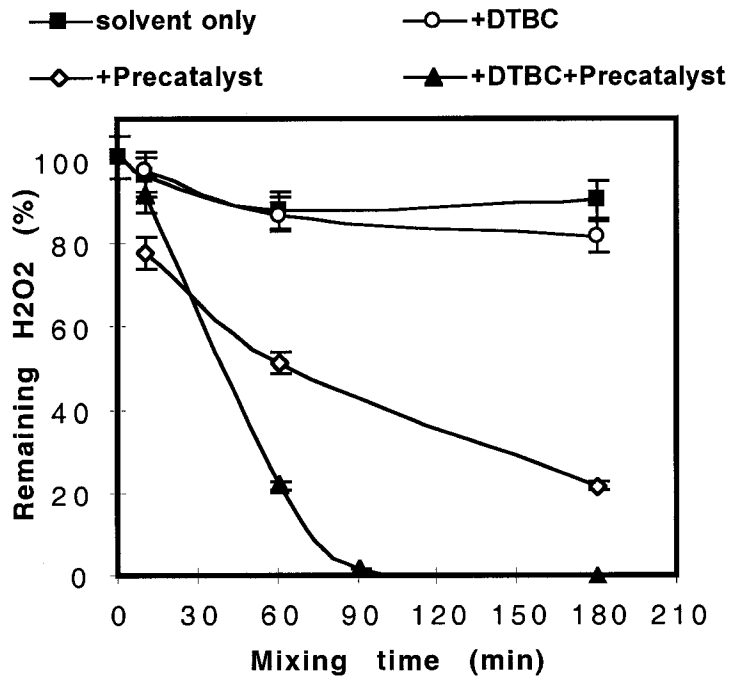

Figure 4.6 Percentages of exogenous H_2O_2 (0.3–0.5 mmol) remaining: in the 1,2-$C_2H_4Cl_2$ (8 mL) solvent alone; in a DTBC substrate solution (1.8 mmol DTBC in 8 mL 1,2-$C_2H_4Cl_2$); in a $(n\text{-}Bu_4N)_7SiW_9V_3O_{40}$ precatalyst solution (5.6 μmol precatalyst in 8 mL 1,2-$C_2H_4Cl_2$); and in a mixed substrate plus $(n\text{-}Bu_4N)_7SiW_9V_3O_{40}$ precatalyst solution (1.8 mmol DTBC and 5.6 μmol precatalyst in 8 mL 1,2-$C_2H_4Cl_2$).

the catalyst formation process. The novel part here is, again, that the usually to-be-avoided, but often facile, autoxidation is what initiates the desired catechol dioxygenase reaction: an example of the *undesired autoxidation-product initiating the desired dioxygenase catalysis!*

The Pseudoelementary Step Treatment of the Autocatalytic Kinetics and Active Catalyst Formation Steps. The reader may well be wondering exactly how one measures the kinetics of $-d[O_2]/dt$, as we have done, yet uses this information to learn about the conversion of the polyoxometalate precatalyst to the catalyst? The answer is the desired connection can be made through the use of a concept very useful for studying

more complicated reactions, the *pseudoelementary step* concept.[3,23] As discussed more elsewhere, the pseudoelementary concept was first used by Noyes as a kinetic tool in understanding oscillatory reactions. We have further developed this concept in our mechanistic work on a >>300 step self-assembly reaction forming $Ir(0)_{\sim 300}$ nanoclusters that, as it turns out, also displays an A $\rightarrow$ B, then A + B $\rightarrow$ 2B sequence of (of course quite different) pseudo-elementary reactions.[3]

As shown below, the pseudoelementary step concept applied to the present case allows us to use the overall reaction and precatalyst-to-catalyst conversion stoichiometry to connect the readily measurable $-d[O_2]/dt$ to the desired, but more difficult to obtain directly, -d[precatalyst]/dt and +d[catalyst]/dt. The pseudoelementary step treatment of the kinetics for the present catechol dioxygenase is summarized in the equations below in which A is the precatalyst (e.g., $(n\text{-}Bu_4N)_7SiW_9V_3O_{40}$) and B is H_2O_2; note that a key is that reactions (1) and (2) also must form the catalyst (i.e. or catalyst resting state), Pierpont's dimer, $[VO(DBSQ)(DTBC)]_2$. The third step, (3) below, is a fast "reporter" reaction which catalytically amplifies how much catalyst has been made at a given moment: the more catalyst, the faster the O_2-uptake reaction with, again, its overall sigmoidal shape due in large part to the A + B $\rightarrow$ 2B autocatalytic step. The sum reaction is a pseudoelementary reaction in that it is composed of other elementary (or even pseudoelementary) steps as detailed in the Supporting Information. Note also that DTBC and O_2 are involved in equations (1) and (2), but have been deliberately omitted to simplify eqs. (1)-(3) to their most essential features. In practice, if the DTBC and O_2 are in excess and if they remain relatively constant over the time course of the curve fitting (e.g., if one fits only the first-half of the kinetics), then these [DTBC] and $[O_2]$

concentrations can be treated as rough constants for the purposes of the semi-quantitative work herein *designed to determine the basic reactions* rather than to measure accurate rate constants.

A → B

$$x[\underline{SiW_9V_3O_{40}^{7-}} \rightarrow \underline{H_2O_2} + 1/2[VO(DBSQ)(DTBC)]_2] \quad (1)$$
$$\mathbf{A} \rightarrow \mathbf{B}$$

A + B → 2B

$$(1-x)[\underline{SiW_9V_3O_{40}^{7-}} + \underline{H_2O_2} \rightarrow \underline{2H_2O_2} + 1/2[VO(DBSQ)(DTBC)]_2] \quad (2)$$
$$\mathbf{A} + \mathbf{B} \rightarrow \mathbf{2B}$$

O_2 – uptake Reporter Reaction

$$\sim 300[DTBC + O_2 \xrightarrow{fast} \text{Dioxygenase Products}] \quad (3)$$

Sum: $SiW_9V_3O_{40}^{7-} + \sim 300\ DTBC + \sim 300\ O_2 \rightarrow H_2O_2 + 1/2[VO(DBSQ)(DTBC)]_2 + \sim 300$ [Dioxygenase Products]

The summed, pseudoelementary step allows the following, desired differentials to be written in the usual fashion: $-d[O_2]/300 \cdot dt = -d[A = \text{Precatalyst}]/dt = +d\{[VO(DBSQ)(DTBC)]_2\}/0.5 \cdot dt$, where the value of 300 results form our stoichiometry of 1.8 mmol DTBC vs ca. 6 μmol precatalyst, A. Hence, we can follow the kinetics of the dioxygenation of DTBC, but learn about the desired formation of catalyst, $-d[A = \text{Precatalyst}]/dt = +d[B = H_2O_2]/dt = +d[\text{Catalyst}]/0.5 \cdot dt$ *so long as equation (3) is faster than (1) and (2).* Steps (1) and (2) are co-rate-determining in this treatment.

Rate Law of $[VO(DBSQ)(DTBC)]_2$ Catalyzed DTBC Di-oxygenation: Support for This Dimer Being the Catalyst Resting State. Our previous paper[5] established Pierpont's complex $[VO(DBSQ)(DTBC)]_2$ as either a catalyst resting state or possibly an actual species within the main catalytic cycle. The application of one of the well-tested postulates of Halpern's "Rules" (really guidelines) as detailed elsewhere,[24]

that if you can isolate it (as one can with Pierpont's complex), it typically is not the catalyst (i.e., is too stable to be a top catalytic intermediate, and is likely ≥ 1 step away from the true catalytic cycle), predicts that $[VO(DBSQ)(DTBC)]_2$ is mostly likely a catalyst resting state.

The kinetics when beginning with pre-made, isolated $[VO(DBSQ)(DTBC)]_2$ were determined by following the oxygen pressure loss in order to confirm or refute this catalyst resting state hypothesis, that is, the hypothesis that this complex is directly connected to the catalytic cycle. In addition, we were interested in question of does the intact dimer complex can react directly with O_2 or if it must first fragment to a monomer before entering the catalytic cycle? Note that as before the measured O_2 uptake is due to the *catalytic* DTBC plus O_2 (i.e., and not the much smaller scale $[VO(DBSQ)(DTBC)]_2$ plus O_2 reaction) since we are using a 750-fold (to 9000-fold) excess of DTBC relative to the $[VO(DBSQ)(DTBC)]_2$ along with an excess of O_2 along with monitoring by our computer-interfaced O_2-pressure transducer apparatus. The details of how these experiments are done are also relevant to their correct interpretation: the mixture of $[VO(DBSQ)(DTBC)]_2$ and DTBC was brought out of the drybox and flushed with O_2, followed by its necessary equilibration under that O_2 atmosphere, for 5 minutes before pressure reading were started, as described in the Experimental Section.

A representative O_2-uptake curve obtained for the reaction of $[VO(DBSQ)(DTBC)]_2$, DTBC and O_2, is presented in Figure 4.7. Documentation that the linear plot in Figure 4.7 is representative is provided by the other representative kinetic curves under different DTBC or other conditions, Figures S4.10 and S4.11 of the Supporting Information, since the linear nature of these curves is a highly diagnostic and

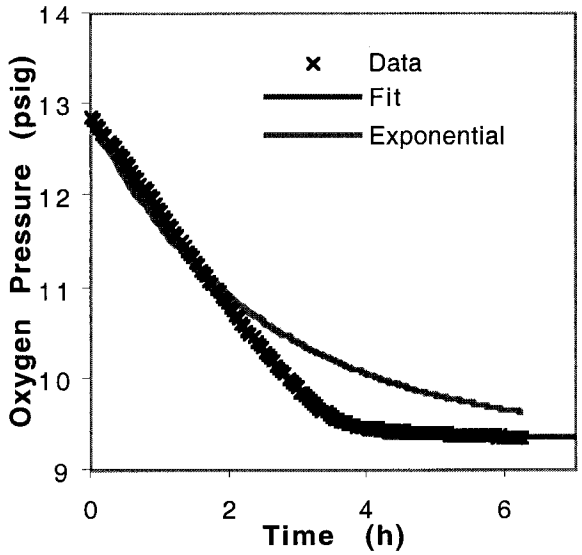

Figure 4.7 O_2-uptake curve of a representative kinetic run of DTBC plus $[VO(DBSQ)(DTBC)]_2$ and its curve-fit ala Figure 4.11. Reaction conditions: 1.8 mmol 3,5-DTBC, 0.4 μmol catalyst, 8 mL 1,2-$C_2H_4Cl_2$, 40 °C and 1.7 atm O_2. The initial rate obtained via a linear regression of the first 1 hour data is –1.0 psig/h (or –0.86 Torr/min). The fit (the solid line that fits the data so well it cannot be easily seen until at the bottom, right-hand end of the curve) is from numerical integration of the kinetic steps and mechanism in Figure 4.11 accomplished via MacKinetics. The individual rate constants defined from the curve-fitting (and as defined in Figure 4.11) are: k_3 ~600 h^{-1}; k_4 ~ 10^8 $M^{-1}h^{-1}$; k_5 ~ 3 x 10^7 $M^{-1}h^{-1}$; and k_6 ~ 7 x 10^9 $M^{-3}h^{-1}$. The data and fit above are also compared to a first-order, exponential kinetic curve ($pO_2(t) = pO_{2,t=0}\exp\{-k_{initial}(t)\}$).

telling, albeit initially unexpected, aspect of the kinetics. Note that at first glance (i) the initially linear concentration vs time plot would appear to imply a zero-order dependence upon $[O_2]$, so that (ii) we checked to be sure that O_2 mass-transfer is not limiting the observed reaction rate. The O_2 gas-to-solution mass-transfer rate for our apparatus, conditions and stirring rate is ca. 24 torr O_2/min•mM (the initial slope of the $-d[O_2]/dt$ vs $[[VO(DBSQ)(DTBC)]_2]$ plot shown in Figure S4.8 of the Supporting Information), so that even at our highest concentration of $[VO(DBSQ)(DTBC)]_2$ studied in this work, any MTL effects should cancel within a ≤5% error (note also the linear slope in Figure 4.7 is ~0.86 torr/min, below the 1.2 torr O_2/min mass-transfer limit). In short, there must be

some other explanation for the observed predominantly linear kinetic curves rather than the exponential curves initially expected due to the consumption of DTBC and/or O_2.

A successful solution to this kinetic puzzle came from the determination of the rate law by the initial rate method, some reflective thinking after being stumped by this for a bit, plus the use of MacKinetics numerical integration kinetic modeling. The initial rates were determined from the initial slope of the linear portion of the O_2-uptake curves. A logarithmic plot of the initial $-d[O_2]/dt$ vs the $[[VO(DBSQ)(DTBC)]_2]_{initial}$ is shown in Figure 4.8 and indicates a clean first-order dependence on $[VO(DBSQ)(DTBC)]_2$. A plot showing a zero-order dependence on the substrate $[DTBC]_{initial}$, as one might have predicted for the DTBC-saturated complex, $[VO(DBSQ)(DTBC)]_2$, is shown in Figure 4.9. Importantly, a *first-order rather than a zero-order dependence on* $pO_{2,initial}$ is demonstrated in Figure 4.10. The experimentally determined rate law for catalyst, DTBC and O_2 is, then, the following (where it is understood that initial rates and concentration subscripts apply to each term):

$$-\frac{d[O_2]}{dt} = k_{obs}[3,5\text{-}DTBC]^0([VO(DBSQ)(DTBC)]_2)^1[O_2]^1$$

Things began to make sense, and the most probable mechanism of action, began to unfold at this point. The first insight is that this rate law *is just that expected for intact Pierpont's catalyst,* $[VO(DBSQ)(DTBC)]_2$, *reacting with* O_2. The lack of a DTBC dependence is exactly as predicted if DTBC-saturated $[VO(DBSQ)(DTBC)]_2$ is directly connected to the catalytic cycle: this complex does not need more DTBC, but does need O_2, as confirmed by the zero- and first-order dependencies, respectively, on these components of the observed stoichiometry, Figure 4.1 (vide supra). The crucial and novel identification, in our prior paper,[5] of $[V^V(O)(DBSQ)(DTBC)]_2$ as directly

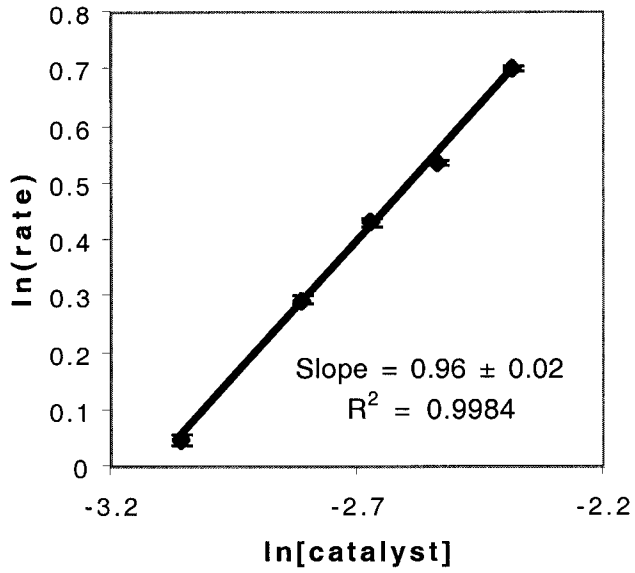

Figure 4.8 The logarithmic plot of the initial $-d[O_2]dt$ rate vs the concentration of $[VO(DBSQ)(DTBC)_2]_2$. Reaction conditions: 1.8 mmol 3,5-DTBC, 0.4–0.8 μmol catalyst, 8 mL 1,2-$C_2H_4Cl_2$, 40 °C and 1.7 atm O_2. A clean first-order dependence of the initial rate on the initial concentration of $[VO(DBSQ)(DTBC)_2]_2$ is apparent.

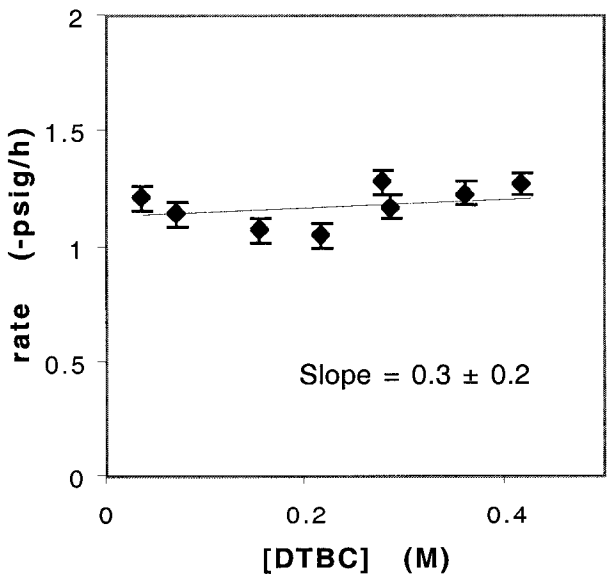

Figure 4.9 The plot of the initial rate vs substrate concentration. Reaction conditions: 0.3–3.6 mmol 3,5-DTBC, 0.4 μmol catalyst, 8 mL 1,2-$C_2H_4Cl_2$, 40 °C, and 1.7 atm O_2.

The ±0.2 error bar in the figure is at 1σ, so that a zero-order dependence on DTBC is apparent even at 2σ error bars (0.3 ± 0.4).

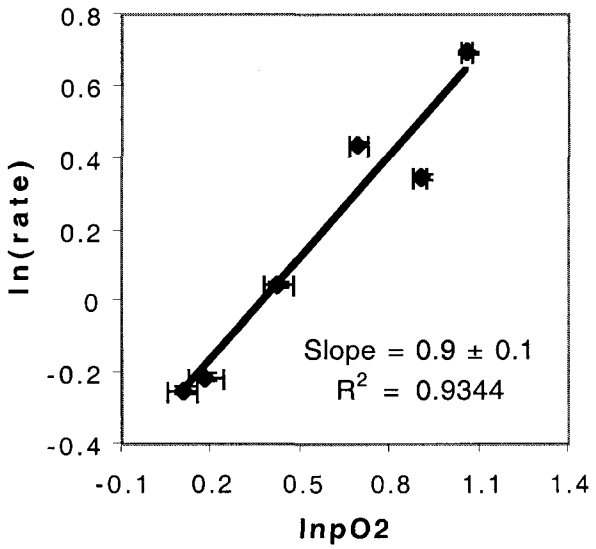

Figure 4.10 The logarithmic plot of the initial rate vs substrate pO_2 (in atm). Reaction conditions: 1.8 mmol 3,5-DTBC, 0.4 μmol catalyst, 8 mL 1,2-$C_2H_4Cl_2$, 40 °C, and 1.1–2.9 atm O_2. A first-order dependence on O_2 is apparent.

connected to the catalytic cycle is, therefore, fully supported and further fortified by the kinetic studies and observed rate law obtained as part of this study.

Given the observed first-order pO_2 dependence (plus the zero-order DTBC dependence), then the kinetic curve in Figure 4.7 should be exponential—if one also assumes a constant catalyst concentration. However, the exponential co-plotted in Figure 4.7 shows that the observed curve is clearly not exponential; instead it is linear over a substantial, typically ca. 40 to 70% of the catalytic reaction as shown in Figure 4.7 (and as also documented in Figures S4.10 and S4.11 of the Supporting Information). After some reflection we reasoned that an exponentially decreasing rate due to the consumption of pO_2 (i.e., its first-order dependence) is being compensated by an

effectively increasing (and thus rate-increasing) concentration of another component in the catalytic cycle. Given the rate law observed, the only option for that other component is the vanadium catalyst. We further reasoned that, therefore, it is highly probable that $[VO(DBSQ)(DTBC)]_2$ is acting as a catalyst resting state that is supplying another V-species that is more active species which reacts with O_2 directly within the main catalytic cycle.

A hypothesis for this hidden V-species quickly became apparent: the dimer, $[VO(DBSQ)(DTBC)]_2$, is very likely (i) fragmenting to two monomers, 2 VO(DBSQ)(DTBC), and (ii) that fragmentation is very likely reversible (to allow for a subsequent rate-determining reaction with O_2, as needed to account for the first-order pO_2 dependence). It also seems necessary that (iii) the overall rate of formation of the active monomer and the rate of the DTBC oxygenation in the catalytic cycle need to be occurring at comparable rates (i.e., when one begins with $[VO(DBSQ)(DTBC)]_2$) so that an increasing catalyst concentration is occurring on the same timescale as the O_2 consumption, Figures 4.7 (and S4.10 and S4.11).

The particular kinetic scheme we then wrote and tested via MacKinetics numerical integration is shown Figure 4.11. Key components of the "kinetic mechanism" shown in Figure 4.11 are: (i) a fast, reversible non-MTL O_2 gas to O_2 solution pre-equilibrium (as our MTL studies support), one in which the rate constants are artificially set as very high (i.e., to mimic a fast prior equilibrium), but where the ratio of rate constants correctly reflects the O_2 solubility in dichloroethane at 20 °C all as done previously[13] (i.e., an "O_2 reservoir"[13]); (ii) a reversible fragmentation of the dimer $[VO(DBSQ)(DTBC)]_2$ to two monomers, VO(DBSQ)(DTBC); (iii) the reaction of each

monomer with O_2 and conversion into VO(DBSQ) plus organic product, and then importantly (iv) a fast step regenerating the dimer, $[VO(DBSQ)(DTBC)]_2$.

(1) $O_{2(gas)} \xrightarrow{10^8\ h^{-1}} O_{2(solution)}$

(2) $O_{2(solution)} \xrightarrow{1.05\cdot10^{10}\ h^{-1}} O_{2(gas)}$

(3) $[VO(DBSQ)(DTBC)]_2 \xrightarrow{640\ h^{-1}} 2[VO(DBSQ)(DTBC)]$

(4) $2[VO(DBSQ)(DTBC)] \xrightarrow{10^8\ M^{-1}h^{-1}} [VO(DBSQ)(DTBC)]_2$

(5) $[VO(DBSQ)(DTBC)] + O_{2(solution)} \xrightarrow{5\cdot10^7\ M^{-1}h^{-1}} [VO(DBSQ)] + Products$

(6) $2[VO(DBSQ)] + 2DTBC \xrightarrow{4\cdot10^9\ M^{-3}h^{-1}} [VO(DBSQ)(DTBC)]_2$

Figure 4.11 A minimum-step, "kinetic mechanism" which fits the observed, linear kinetic data in Figure 4.7 and in S4.10 and S4.11 (plus five additional sets of data, 8 data sets tofal). Individual steps are shown as they must be entered into MacKinetics (i.e., steps (1) and (2) are just the O_2 gas-to-solution equilibrium, while steps (3) and (4) are the separate steps of the dimer to monomer equlibrium). The rate constants for steps (1) and (2) are meaningless as they were set at high, artificial values so as to provide a fast prior equilibrium; however, the important point is that their ratio does faithfully reflect the known solubility of O_2 in 1.2-$C_2H_4Cl_2$ at 20 °C and 1.7 atm O_2.[14]

Controls were done on the curve-fitting en route to arriving at the steps shown in Figure 4.11: if step (6) is replaced with a the monomer-forming step, [VO(DBSQ)] + DTBC → [VO(DBSQ)(DTBC)], then a poor fit is obtained as shown in Figure S4.14 in the Supporting Information. In addition, a mechanism in which intact $[VO(DBSQ)(DTBC)]_2$ is directly part of the catalytic cycle as illustrated in Figure S4.13 of the Supporting Material also cannot fit the observed data, Figure S4.15. The coefficients of *2* [VO(DBSQ)] plus *2* DTBC in step (6) Figure 4.11 merit some comment: since their sum is greater than three, this reaction cannot be an elementary step (i.e., must be pesudoelementary). Hence, controls on the curve-fitting were preformed by varying the coefficients: to 1 [VO(DBSQ)] and 1 DTBC to form $0.5[VO(DBSQ)(DTBC)]_2$ (an

excellent fit resulted with an essentially unchanged, $k_6 = 1.1 \cdot 10^{10}\ M^{-1}h^{-1}$) and 2 [VO(DBSQ)] and 1 DTBC (again an excellent fit, with the same rate constant within experimental error, $k_6 = 10^9\ M^{-2}h^{-1}$). An attempted fit with 1 [VO(DBSQ)] and 2 DTBC in step 6 did not converge, however. The end result of these curve-fitting controls is that they support the formulation of step 6 in Figure 4.11 as shown with *2* [VO(DBSQ)] reacting with 2 DTBC.

The accuracy of the resultant rate constants in Figure 4.11 is not obvious; our experience is that factors of 2 to 10 fold (or more) can result from such fitting of kinetic data to 4 unknowns, depending on the particulars of the kinetic scheme, the amount and quality of the data (which are high for the present pressure-transducer-obtained data), and other factors. Consistent with this, the rate constants for the data in Figures S4.10 and S4.11 in comparison to that for Figure 4.7 do show values that differ by factors of 2-7 fold. Hence, the rate constants reported in Figure 4.11 are the averages of Figures 4.7, S4.10, S4.11 and 5 other (8 total) data sets. In addition and as discussed next, an experiment was designed to independently test the reliability of the equilibrium and rate constants listed for the first 5 steps in Figure 4.11.

UV-Visible Monitoring of the Reaction of the Initial Rate of $[VO(DBSQ)(DTBC)]_2$ Plus O_2. Since step (5) is the rate-determining step following two, fast prior equilibria, Figure 4.11 and its rate constants predict that the observed rate constant for the summation of the first 5 steps will look like the following (obtained using the rate constant definitions and values contained in Figure 4.11 as well as the steady-state assumption on the dissolved O_2 and monomer intermediates): $k_{obs} = K_{1,2} \cdot K_{3,4} \cdot k_5$, where the equilibrium constants for steps 1 and 2, $K_{1,2}$, is $\sim 10^{-2}$, that for steps 3 and 4 is

$K_{3,4}$ ~7 x 10^{-6} M, and k_5 ~ 5 x 10^7 $M^{-1}h^{-1}$. Hence, the prediction from Figure 4.11 is *that* k_{obs} *~3.5* h^{-1}.

Experimentally, it was found that the reaction of $[VO(DBSQ)(DTBC)]_2$ with O_2, under the same conditions as the standard kinetic data was obtained by following the UV-absorbance decay of $[VO(DBSQ)(DTBC)]_2$ at 40 °C and 0.8 atm O_2, yields a *pleasingly similar, initial-rate determined* k_{obs} = *1.9* h^{-1} *that is within a factor of ~2 of that predicted.* This independent result provides both an idea of the precision of the rate constants in Figure 4.11 as well as a general confirmation of: the first 5 steps in Figure 4.11, the data fitting procedure, and the resultant rate constants, that steps 1-2 and 3-4 represent two fast, prior equilibria (and of the steady-state assumption on the dissolved O_2 and monomer intermediates).

Use of MacKinetics to Understand Better the Linear Kinetic Curves. Next, we used that numerical kinetic model in Figure 4.11 plus MacKinetics in their powerful, predictive way. First, we generated the calculated monomer concentration vs time curve shown in Figure 4.12. Note that it does indeed show the expected (vide infra) increasing concentration vs time needed to rationalize why the kinetic curves are linear: the rate-increasing effect of increasing monomer concentration is convoluted with the exponential rate-decrease due to the first-order loss of O_2 to provide an apparently linear kinetic curve (Figures 4.7, S4.10 and S4.11). Second, we generated the predicted kinetic curves as the initial $[VO(DBSQ)(DTBC)]_2$ concentration was changed (i.e., as in Figures 4.8), determined the initial rates from those data, and then plotted those initial rates vs the initial concentrations to be sure that the rate law determined from the initial rates is consistent with the kinetic model and rate constants in Figure 4.11. The result, Figure

S4.16 of the Supporting Information, again shows that the kinetic model in Figure 4.11 is fully consistent with the measure rate law obtained using initial rate methods.

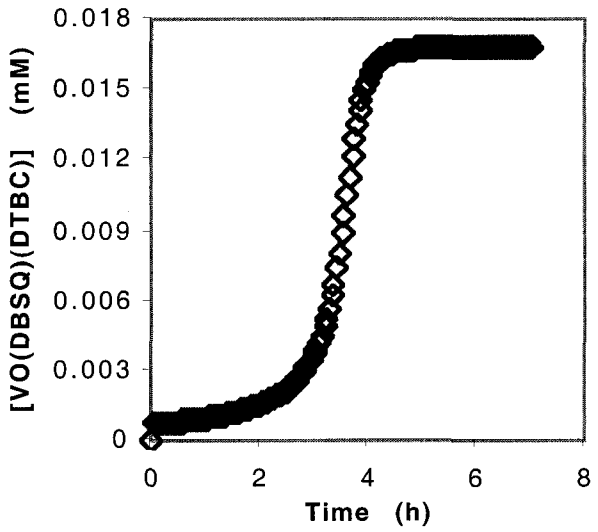

Figure 4.12 Calculated [VO(DBSQ)(DTBC]-monomer concentration vs time curve using the chemical equations and rate constants shown in Figure 4.11.

Of note here is that the mechanism in Figure 4.11 is the first example as near as we can tell of the generalized kinetic Scheme A $\leftrightarrow$ 2B, B + C $\rightarrow$ D + Product, then 2D + 2E $\rightarrow$ A. As such, it is of interest to study its general properties further by numerical integration simulations as a function of the concentrations of each variable and the 4 rate constants involved, so that such simulations are under separate study.[25]

A Proposed Mechanism Consistent with the Kinetics, the Catechol Dioxygense Literature and Employing [VO(DBSQ)(DTBC)]$_2$ as the Catalyst Resting State. A proposed system for the active vanadium catechol dioxygenase mechanism is provided in Figure 4.13. This mechanism is of course consistent with our kinetic studies, but then also incorporates key features from the literature of the Fe-base catechol

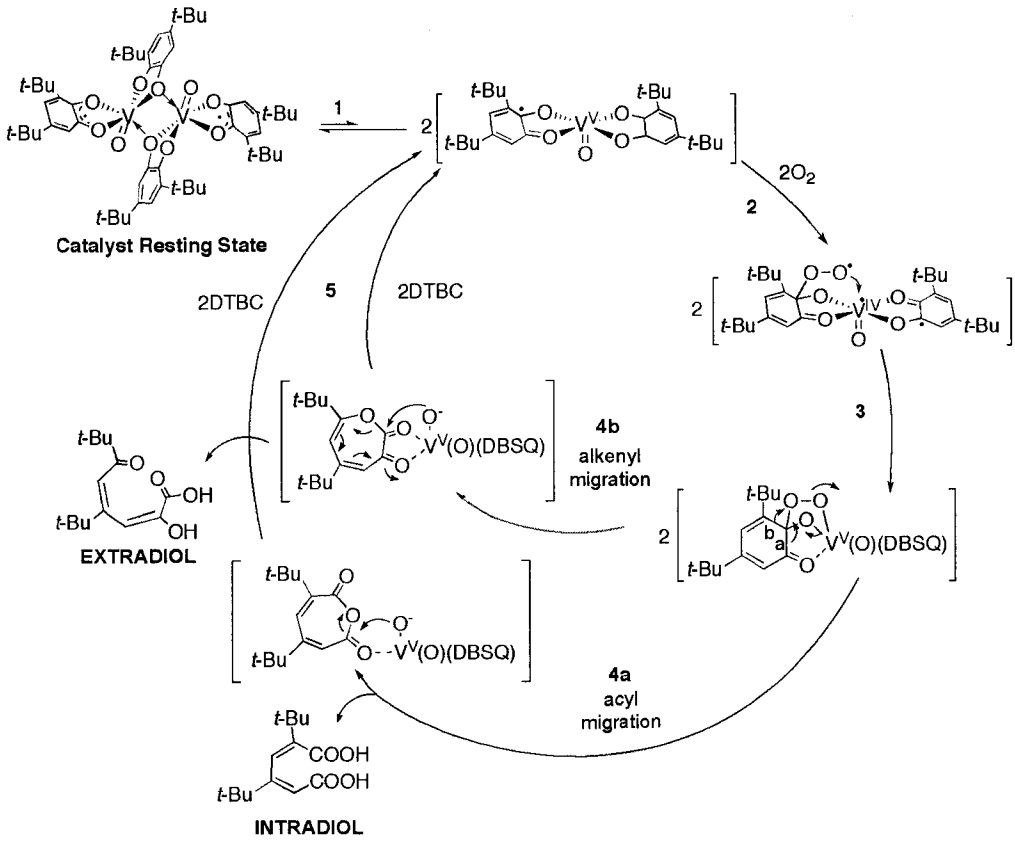

Figure 4.13 Proposed, minimal ("Ockham's razor") mechanism of vanadium-based DTBC dioxygenases based on the evidence provided and as well as literature evidence[27,28] for steps 3 and 4 above.[26]

dioxygenases, notably the substrate activation mechanism clarified by Que and co-workers,[27] as well as a common, branching intermediate for intradiol vs extradiol cleavage pathways as detailed by Bugg and co-workers.[28]

Based on our earlier finding and the kinetic studies herein, Pierpont's complex is identified as *the catalyst resting state.* In step 1 in Figure 4.13, the $[VO(DBSQ)(DTBC)]_2$ reversibly fragments in even weakly coordinating solvent to form 2 equivs of monomer. Five lines of evidence support this step: (1) the kinetic studies and MacKinetics curve-

fitting; (2) an experiment in which even a drop of DMSO added to $[VO(DBSQ)(DTBC)]_2$ in toluene changes the signature 9-line EPR spectrum to the asymmetric spectrum as shown in Figure S4.17 along with a dramatic color change from blue to violet; (3) Pierpont's demonstration of a facile dimer, monomer equilibrium for related Mo complexes;[29] (4) literature structural studies show that vanadium compounds with coordination numbers of 5 or 6 are the most common so that only the monomer can react quickly with O_2 (formally 7 coordinate compounds typically contain a cyclic peroxo component occupying two adjacent sites;[30] we thank Prof. Pierpont for this point); and (5) the mechanism in which intact $[VO(DBSQ)(DTBC)]_2$ persists inside the catalytic cycle with, for example, only one vanadium being active, Figure S4.13 of the Supporting Information (i.e., similar to enzymic half-site reactivity[31]), both cannot fit the observed kinetic data (vide supra) as well as seems sterically prohibitive with no clear chemical advantage that at least we have been able to discern. In step 2, O_2 binds to the semiquinone ligand[32] (or catecholate ligand[xv]) in [VO(DBSQ)(DTBC)]-monomer as a fast, but still rate-determining, step in the catalytic cycle, consistent with the kinetic results. A subsequent V-OO bond formation step is required in analogy to the postulated mechanisms of enzymatic dioxygenases and their models (and by chemistry in order to get the needed O-O bond cleavage step); hence, in step 3, an inner-sphere electron transfer from the redox "non-innocent"[33] DTBC ligand to V(V) to form V(IV) and bound semiquinone is postulated. Hence, the mechanism predicts that it is crucial to have *two* catecholate/semiquinone ligands on *one* vanadium, as once O_2 is bound, the second catecholate ligand is needed for the DTBC/V(V) $\rightarrow$ DBSQ/V(IV)$^{\bullet}$ step which in turn

[xv] Note that it is not known if O_2 reacts initially with semiquinone or the more nucleophilic catecholate, a point brought to our attention by Prof. Pierpont. Hence, the intermediate after step 2 in Figure 4.13 is written to accommodate either of these possibilities.

allows the V–O_2 bond formation step. The presence of a spectator terminal oxo ligand[26d] in the catalyst, with its competing π-bonding effects, in Figure 4.13 is noteworthy as is the observation that the two DTBC ligands present appear to have prevented a dioxo, $V(O)_2$ moiety from being present, a structural feature that in turn avoids a transient tri-oxo "$V(O)_3$" moiety that would have been a violation of Lipscomb's rule[34]—and, therefore, presumably of too high-energy to permit efficient catalysis.

Steps 3–4 are analogous to the Fe catechol dioxygenase mechanism,[35] a common intermediate branches into intradiol cleavage product or extradiol cleavage product depending on a migration of an acyl group (step 4a) or an alkenyl group (step 4b).[36] The $V(O)(DBSQ)^{2+}$ released in step 5 is written as DTBC-dependent, but fast consistent with the zero-order dependence seen on DTBC as well as the find that this step is fast based on the MacKinetics numerical integration kinetic model. The active VO(DBSQ)(DTBC) monomer catalyst returns to the dimeric, $[VO(DBSQ)(DTBC)]_2$ catalyst resting state about 10 times for every ca. 3 times it reacts with O_2 for another catalytic cycle.

Of course like all mechanisms, especially those brand new such as the one above, Figure 4.13 is offered—and should be viewed—as a specific hypothesis requiring further testing and attempts to refine or refute its overall features as well as it intimate steps. The basic features of Figure 4.13, such as the identification of $[VO(DBSQ)(DTBC)]_2$ as the catalyst resting state, its fragmentation to monomer to enter the catalytic cycle, and the reaction of that monomer with O_2, are expected to stand the test of time, however.

Effect of Added Tridentate Ligands to Catechol Oxidative Cleavage Activity. Based on the mechanism in Figure 4.13, a prediction is that added ligands are not likely to have beneficial effect, even if they are multidentate ligands that are useful in other

dioxygenase catalysts.[37] In fact, the *in-situ* addition of tridentate ligands such as 1,4,7-triazacyclononane (TACN), to a $[VO(DBSQ)(DTBC)]_2$ catalyzed DTBC oxygenation solution suppresses almost completely the dioxygenase reaction (the yield of intradiol product **2** decreased from ~40% to <0.2%), while the undesired autoxidation pathway increases (the yield of product **6** increased from ~18% to 41%).[xvi] This experiment both (i) confirms the importance of having two DTBC ligands in the active catalyst, and (ii) argues that the design of kinetically highly active but more selective catechol oxygenation catalysts based on vanadium will be challenging.

A Return to the Question of the Broader Generality of Autoxidation-Initiated Dioxygenases or Other Reactions. An important question is are there other examples of autoxidation-product initiated chemistry? Is this a more general concept? As noted in the Introduction, this concept is very likely much more widespread even if rarely detected, given that autoxidation and the resultant ROOH products are a primary way that organic compounds degrade in air.

One highly relevant case that may be autoxidation-initiated chemistry is that of saturated hydrocarbon oxidations with 2,6-dichloropyridine-*N*-oxide as the oxygen donor and beginning with $[Ru^{II}(TPFPP)(CO)]$ as the precatalyst (TPFPP is the 5,10,15,20-tetrapentafluorophenylporphyrinato ligand). This system shows induction periods and evidence exists that a Ru*(V)*-oxo species or a Ru*(IV)*-oxo porphyrin radical-cation is the reactive species.[38] In addition, the CH_2Cl_2 solvent plus O_2 have been described as "non-

[xvi] The use of another tridentate ligand, 1,4,7-trimethyl-1,4,7-triazacyclononane (Me_3-TACN), gives the same results: the addition of either a stoichiometric or an excess amount of Me_3-TACN (310 equivs.) vs the precatalyst $(n\text{-}Bu_4N)_7SiW_9V_3O_{40}$ catalyzed DTBC oxygenation to primarily the autoxidation product **6** in 27%–44% yield.

innocent"[38b] and would seem to be a prime candidate for an at least plausible autoxidation-product-induced reaction and catalyst formation step.

We found at least one clear example of autoxidation-product-enhanced *reduction* catalysis as well, notably the ethyl-benzene autoxidation product C_6H_5–CH(OOH)–CH_3 enhancing the rate of ethyl-benzene reduction by the tri-ruthenium cluster cation precatalyst,[39,40] $[Ru_3(\mu_2\text{-}H)_3(\eta^6\text{-}C_6H_6)(\eta^6\text{-}C_6Me_6)_2(\mu_3\text{-}O)]^+$. The details of the catalysis-triggering process is known in some detail in that case: this substitutionally inert complex gets oxidized by the C_6H_5–CH(OOH)–CH_3 hydroperoxide autoxidation product, and that resultant complex is more readily turned into the true $Ru(0)_n$ nanocluster ethyl-benzene reduction catalyst[41] under H_2—an example of autoxidation-product-enhanced reduction catalysis.

There are surely other examples of autoxidation-product-enhanced catalysis as well, although they are either buried in the literature and hence hard to find or simply unrecognized. Cyclopentadienyl ligand removal under O_2 and activation of hydrogenation catalysts probably qualifies as one example;[42] another is probably the better known phosphine oxidation to $O{=}PR_3$ in the presence of trace O_2, a process which opens a site of coordinative unsaturation, thereby turning on catalysis.[43] However, unless a ROOH autoxidation product is the actual oxidant for the PR_3, this case might not fall under the definition provided.[xi]

And, of course, there is the present, apparently best studied example of an autoxidation-product-initiated reaction: that of a record catalytic lifetime vanadium catechol dioxygenase initiated autocatalytically via the autoxidation product H_2O_2 to form, ultimately, Pierpont's $[VO(DBSQ)(DTBC)]_2$ catalyst resting state. That is, we

have discovered an example of the seemingly improbable situation of where *undesired autoxidation* turns on the *desired dioxygenase chemistry*, a novel "*autoxidation-initiated dioxygenase*". Since the series of radical-chain reactions known as autoxidation is the common, central pathway by which organic compounds such as fats, plastics, gasoline, lubricating oils, rubber, and so on degrade to hydroperoxides, ROOH, as the primary initial products (or H_2O_2 plus benzoquinones in the case of catechols),[44] it seems highly likely that autoxidation-product-initiated reactions are much more common than heretofore appreciated.

Conclusions

The main findings from this study can be summarized as follows:

(i) An example of the seemingly unlikely case of an autoxidation-product-initiated dioxygenase has been discovered. Autoxidation of the DTBC substrate to the corresponding benzoquinone, with co-production of H_2O_2, was shown to be key to the catalyst evolution process, the H_2O_2 being a key to the V-leaching, autocatalytic catalyst production and resultant, observed sigmoidal kinetic curves. Of interest here is that this result is very non-biomimetic; H_2O_2 inhibits at least some dioxygenase enzymes.[45]

(ii) The novel, more general concept of autoxidation-product induced catalysis is hypothesized to be more general, but little recognized. This hypothesis is supported by independent examples of both oxidative as well as reductive catalysis extracted from the literature.

(iii) Our previous finding[5] that Pierpont's important, structurally characterized complex $[VO(DBSQ)(DTBC)]_2$ is directly connected to the catalytic cycle and serves as a catalyst resting state was verified via kinetic studies.

(iv) Our studies confirm the conclusion in our earlier paper[5] that attempts to support and prepare non-leachable V-based dioxygenase catalysts will require new strategies especially if H_2O_2 and powerful σ- and π-donor ligands such as $[DTBC]^{2-}$ will be present or can be formed.

(v) A detailed mechanism was postulated, Figure 4.13, that is supported by the identity of the catalyst resting state, kinetics from that resting state, as well as a sizeable amount of relevant literature.[5,35] The mechanism in Figure 4.13—still a working hypothesis that should be viewed as such, as with all new mechanisms—is nevertheless a welcome addition to a literature in which mechanistic knowledge was previously non-existent for any man-made catalyst that is as highly catalytic and long lived as the present system (i.e., 30,000-100,000 TTOs). The mechanism in Figure 4.13 contains insights as well as sub-hypotheses that can and should be used to guide future research.

(vi) The mechanism in Figure 4.13 provides support for the broader generality of the mechanistic insights from the labs of Que,[27,35] Funabiki,[15a,c] Bugg,[28] and others that when into the construction of Figure 4.13 following the reaction between the [VO(DBSQ)(DTBC)] monomer and O_2. Restated, the way that the precedent in the literature from the seminal contributions of the above authors fits so naturally into Figure 4.13 provides support for the broader generality of the substrate-activation, C–OO–V formation, Criegee rearrangement, and other steps.[27,28,35]

(vii) Point (vi) then, in turn, supports the probably greater generality of important mechanistic insights from the literature[35] and in Figure 4.13 such as (a) a major difference between dioxygenase and monooxygenases is that the former avoid O–O bond-cleavage activation of O_2. That is, Fe(II) extradiol,[35] Fe(III) intradiol,[35] as well as the present V(V/IV) combined intra- and extra-diol dioxygnease avoid O-O bond cleavage until after a substrate C-O-O bond has been made.[35,46] Hence, "easier" dioxygenations use substrate prior coordination as a key to their catalysis; more difficult substrates (e.g., unactivated alkanes) require O_2 activation with 2 e^- and 2 H^+ to species such as Fe=O that can then do these harder activations. This in turn implies that it will be difficult to develop true dioxygenases for RH and other difficult substrates, a conclusion Sen has also reached.[47]

The above conclusions are, however, not meant to imply that additional work is not needed. Studies understanding the detailed catalyst evolution steps are especially needed[xvii] as are studies of other (i.e., non-3,5-DTBC) catechols. Further tests of the mechanism in Figure 4.13 are possible and thus need to be performed along with studies testing if Figure 4.13 extends in a general way to other systems such as molybdenum.[29] Indeed, it is likely that the area of man-made, highly active, long-lived dioxygenase catalysts supported by kinetic studies and understood mechanistically is just beginning.

Acknowledgement. We thank Professor Steven H. Strauss for letting us use his high precision gas pressure transducer and vacuum line. Professor Cortland G. Pierpont is also thanked for his multiple, valuable comments and insights into V-based catechol chemistry as well for reading a penultimate version of the manuscript. This research is supported by NSF fund 9531110.

[xvii] Included in the list of ill-understood observations is why impure DTBC has the induction-period-reducing effect that it has (Figure 4.3c) yet gives the same products (**2–6**) compared to recrystallized DTBC.

Supporting Information Available: O_2-uptake of DTBC plus the precatalyst (n-$Bu_4N)_7SiW_9V_3O_{40}$ with the addition of H_2O_2 plus 3,5-DBQuinone; O_2-uptake of DTBC plus the precatalyst (n-$Bu_4N)_7SiW_9V_3O_{40}$ with the addition of AIBN; O_2-uptake of DTBC plus the precatalyst (n-$Bu_4N)_7SiW_9V_3O_{40}$ with the addition of NaDBSQ; O_2-uptake of DTBC plus the precatalyst (n-$Bu_4N)_7SiW_9V_3O_{40}$ in water-saturated 1,2-$C_2H_4Cl_2$; O_2-uptake of DTBC plus the precatalyst (n-$Bu_4N)_7SiW_9V_3O_{40}$ in o-dichlorobenzene; negative ion ESI–MS spectrum of the product solution from an experiment probing the catalyst evolution stoichiometry; control experiments testing the effectiveness of transferring H_2O_2 with a stainless steel needle; stirring rate controls: the establishment of O_2 mass-transfer limitations; solvent vapor pressure correction example; two other representative O_2-uptake curves of kinetic runs of $[VO(DBSQ)(DTBC)]_2$ plus excess DTBC; plausible stoichiometries for conversion of $SiW_9V_3O_{40}^{7-}$ to the active catalyst, $[V^V(O)(DBSQ)(DTBC)]_2$ plus initial experimental tests of those stoichiometries; confirmed formation of $[VO(DBSQ)(DTBC)]_2$ from $V(DTBC)_3^-$ under catalytic conditions; presentation of the mechanism involving intact $[VO(DBSQ)(DTBC)]_2$; figures showing different mechanistic schemes give poor fits to the $[VO(DBSQ)(DTBC)]_2$ O_2-uptake Data in Figure 4.7 in the main text; calculated catalyst reaction order using the chemical models in Figure 4.11; the EPR of $[VO(DBSQ)(DTBC)]_2$ and the EPR of $[VO(DBSQ)(DTBC)]_2$ with addition of a drop of DMSO.

References

[1] Weiner, H.; Finke, R. G. *J. Am. Chem. Soc.* **1999**, *121*, 9831-9842.

[2] Hill, C. L.; Weinstock, I. A. *Nature* **1997**, *388*, 332-333.

[3] Watzky, M. A.; Finke, R. G. *J. Am. Chem. Soc.* **1997**, *119*, 10382-10400.

[4] Widegren, J. A.; Aiken, J. D., III; Özkar, S.; Finke, R. G. *Chem. Mater.* **2001**, *13*, 312-324.

[5] Yin, C.-X.; Finke, R. G. "Vanadium-Based, Record Catalytic Lifetime Catechol Dioxygenases: Evidence For a Common Catalyst," *J. Am. Chem. Soc.* **2005**, in press.

[6] Tyson, C. A.; Martell, A. E. *J. Phys. Chem.* **1970**, *74*, 2601-2610.

[7] (a) Bianchini, C.; Frediani, P.; Laschi, F.; Meli, A.; Vizza, F.; Zanello, P. *Inorg. Chem.* **1990**, *29*, 3402-3409. Bianchini and co-worker's studies show that H_2O_2 is the primary product when DTBC is oxidized to the benzoquinone, at least for Rh(III) and Ir(III) and under their mildly catalytic reaction conditions (ca. 30 total turnovers). (b) Barbaro, P.; Bianchini, C.; Mealli, C.; Meli, A. *J. Am. Chem. Soc.* **1991**, *113*, 3181-3183. (c) Barbaro, P.; Bianchini, C.; Frediani, P.; Meli, A.; Vizza, F. *Inorg. Chem.* **1992**, *31*, 1523-1529. (d) Barbaro, P.; Bianchini, C.; Linn, K.; Mealli, C.; Meli, A.; Vizza, F.; Laschi, F.; Zanello, P. *Inorg. Chim. Acta* **1992**, *198-200*, 31-56. For an earlier work by others see: Muto, S.; Tasaka, K.; Kamiya, Y. *Bull. Chem. Soc. Jpn.* **1977**, *50*, 2493-2494.

[8] Finke, R. G.; Rapko, B.; Saxton, R. J.; Domaille, P. J. *J. Am. Chem. Soc.* **1986**, *108*, 2947-2960.

[9] Hornstein, B. J.; Finke, R. G. *Inorg. Chem.* **2002**, *41*, 2720-2730.

[10] White, L. S.; Hellman, E. J.; Que, L., Jr. *J. Org. Chem.* **1982**, *47*, 3766-3769.

[11] Muto, S.; Bruice, T. C. *J. Am. Chem. Soc.* **1980**, *102*, 4472-4480.

[12] Yin, C.-X.; Finke, R. G. "Is It True Dioxygenase or Classic Autoxidation Catalysis? Re-Investigation of a Claimed Dioxygenase Catalyst Based On a Ru_2-Incorporated, Polyoxometalate Precatalyst," *Inorg. Chem.* **2005**, in press.

[13] Lyon, D. K.; Ph. D. Dissertation, University of Oregon, Eugene, OR, 1990, p 252; see pp 142–145.

[14] Lühring, P.; Schumpe, A. *J. Chem. Eng. Data* **1989**, *34*, 250-252.

[15] (a) Funabiki, T.; Mizoguchi, A.; Sugimoto, T.; Yoshida, S. *Chem. Lett.* **1983**, 917-920. (b) Nishida, Y.; Shimo, H.; Kida, S. *J. Chem. Soc., Chem. Commun.* **1984**, 1611-1612. (c) Funabiki, T.; Mizoguchi, A.; Sugimoto, T.; Tada, S.; Mitsuji, T.; Sakamoto, H.; Yoshida, S. *J. Am. Chem. Soc.* **1986**, *108*, 2921-2932. (d) An exceptional case is $RuCl_2(PPh_3)_3$ catalyzed DTBC oxygenation in which benzoquinone disappears in the early stages according to GLC analysis: Matsumoto, M.; Kuroda, K. *J. Am. Chem. Soc.* **1982**, *104*, 1433-1434.

[16] Weiner, H.; Hayashi, Y.; Finke, R. G. *Inorg. Chim. Acta* **1999**, *291*, 426-437.

[17] (a) Lide, D. R. *CRC Handbook of Chemistry and Physics, 85th Edition*; CRC Press, 2004-5. (b) McMillen, D. F.; Golden, D. M. *Ann. Rev. Phys. Chem.* **1982**, *33*, 493-532.

[18] See the use of H_2O_2 to solublize $Nb_6O_{19}^{8-}$ into monomeric Nb-peroxy species useful in subsequent syntheses: Finke, R. G.; Droege, M. W. *J. Am. Chem. Soc.* **1984**, *106*, 7274 and reference 11 therein.

[19] "Peroxy Compounds of the Transition Metals," Connor, J. A.; Ebsworth, E. A. V. *Adv. Inorg. Chem. Radiochem.* **1964**, *6*, 279.

[20] Butler, A.; Clague, M. J.; Meister, G. E. *Chem. Rev.* **1994**, *94*, 625

[21] Evidence for polyoxometalate degradation in H_2O_2: (a) Aubry, C.; Chottard, G.; Platzer, N.; Brégeault, J.-M.; Thouvenot, R.; Chauveau,F.; Huet, C.; Ledon, H. *Inorg. Chem.* **1991**, *30*, 4409. (b) Brégeault, J.-M.; Aubry, C.; Chottard, G.; Platzer, N.; Chauveau,F.; Huet, C.; Ledon, H. In *Dioxygen Activation and Homogeneous Catalytic Oxidation*; Simándi, L. I., Ed.; Elsevier Publishers: Amsterdam, 1991; pp 521-529.

[22] Lead references to Venturello's $\{PO_4[W(O)(O_2)_2]_4\}^{3-}$ epoxidation catalyst utilizing H_2O_2 and which can be formed *in situ* from phosphotungstates: (a) Venturello, C.; Alneri, E.; Ricci, M. *J. Org. Chem.* **1983**, *48*, 3831. (b) Venturello, C.; D'Aloisio, R.; Bart, J. C.J.; Ricci, M. *J. Mol. Catal.* **1985**, *32*, 107.

[23] Original work using the pseudoelementary step concept: (a) Field, R. J.; Noyes, R. M. *Acc. Chem. Res.* **1977**, *10*, 214-221. (b) Noyes, R. M.; Field, R. J. *Acc. Chem. Res.* **1977**, *10*, 273-280. (c) Noyes, R. M.; Furrow, S. D. *J. Am. Chem. Soc.* **1982**, *104*, 45-48.

[24] Hagen, C. M.; Vieille-Petit, L.; Laurenczy, G.; Süss-Fink, G.; Finke, R. G. *Organometallics,* **2005**, *24*, 1819-1831, see footnote 45 therein.

[25] Morris, A. M.; Yin, C.-X.; Finke, R. G. unpublished results and experiments in progress.

[26] The terminal V-O oxo is represented in Figure 4.13 as a V=O simply out of convenience; it certainly has some triple bond character based on Pierpont's structural studies. More specifically, the V–O bonds in $[VO(DBSQ)(DTBC)]_2$ (bond length

1.581(4) Å[26a]) looks like a triple bonds[26b,c] in comparison to the V=O bond in the $VO(catecholate)_2^{2-}$ ion length of 1.616(4) Å. However, competing p bonding from the good π donors catecholate ligands is also present and needs to be a part of any discussion of the best descriptions of the V-O bonds. Two of the V–O(catecholate) bond lengths in $[VO(DBSQ)(DTBC)]_2$ are quite short, 1.827(4) Å, in comparison to V–O(semiquinone) bond length of 1.975–1.987 Å, showing the variable interactions present between V and catecholate. or semiquinone oxygen atoms. (a) Cass, M. E.; Green, D. L.; Buchanan, R. M.; Pierpont, C. G. *J. Am. Chem. Soc.* 1983, *105*, 2680-2686. (b) We thank Professor C. G. Pierpont for a discussion and his insights on this point. (c) Nugent, W. A.; Mayer, J. M. *Metal-ligand Multiple Bonds*, John Wiley & Sons: New York, 1988; pp 33-36. (d) The classic Rappé-Goddard importance of a spectator oxo ligand also merits mention with respect to Figure 4.13: Rappé, A. K.; Goddard, W. A., III *J. Am. Chem. Soc.* **1982**, *104*, 3287-3294.

[27] Jang, H. G.; Cox, D. D.; Que, L., Jr. *J. Am. Chem. Soc.* **1991**, *113*, 9200-9204.

[28] (a) Winfield, C. J.; Al-Mahrizy, Z.; Gravestock, M.; Bugg, T. D. H. *Perkin 1* **2000**, 3277-3289. (b) Bugg, T. D. H.; Lin, G. *Chem. Commun.* **2001**, 941-952.

[29] (a) A Mo analog $[Mo^{VI}O(DTBC)_2]_2$ dissociates into monomer in coordinating solvent as demonstrated by NMR: Buchanan, R. M.; Pierpont, C. G. *Inorg. Chem.* **1979**, *18*, 1616-1620. (b) The tetramer (chiral square) $[Mo^{IV}(\mu\text{-}O)(3,6\text{-}DTBC)_2]_4$ also dissociates into monomer upon ligand addition: Liu, C.-M.; Nordlander, E.; Schmeh, D.; Shoemaker, R.; Pierpont, C. G. *Inorg. Chem.* **2004**, *43,* 2114-2124.

[30] (a) Nugent, W. A.; Mayer, J. M. *Metal-ligand Multiple Bonds*, John Wiley & Sons: New York, 1988; pp 159-162. (b) The Cambridge Structural Database (version 5.26 Nov 2004) via Conquest (version 1.7) software.

[31] Enzymic half-site reactivity is observed in proteins composed of n identical subunits but which react with a substrate or an inhibitor with only n/2 subunits saturated with that ligand. Binding of the ligand to one site typically induces a conformational change of the second binding site, thereby rendering the second site inactive. (a) Levitzki, A.; Stallcup, W. B.; Koshland, D. E., Jr. *Biochemistry* **1971**, *10*, 3371-3378. (b) Seydoux, F.; Malhotra, O. P.; Bernhard, S. A. *CRC Crit. Rev. Biochem.* **1974**, *2*, 227-257.

[32] The proposed C_2 (instead of C_1) site of attachment of O_2 to the 3,5-di-*tert*-butylsemiquinone ligand in $[VO(DBSQ)(DTBC)]_2$ shown in Scheme 3 is consistent with the major product being 3, 4,6-di-*tert*-butyl-2*H*-pyran-2-one, rather than its isomer, 3,5-di-*tert*-butyl-2*H*-pyran-2-one. We note, however, that both C_1 and C_2 binding of O_2 can give the intradiol product, **2**, a detail not included in Figure 4.13 only to keep if from being too cluttered. In the view of electronic effect, a comparable computed net *cationic* charges at C_1 (0.44) versus C_2 (0.42) have been reported for a Co(III)-(di-*tert*-butylcatecholato)$(MeC(CH_2PPh_2)_3)$.[32a] (a) Bencini, A.; Bill, E.; Mariotti, F.; Totti, F.; Scozzafava, A.; Vargas, A. *Inorg. Chem.* **2000**, *39*, 1418-1425. (**b**) Mechanisms with O_2

bound to the C_2 site of 3,5-DTBC are commonly proposed in the literature: Cox, D. D.; Que, L., Jr. *J. Am. Chem. Soc.* **1988**, *110*, 8085-8092. (c) Viswanathan, R.; Palaniandavar, M. *J. Chem. Soc., Dalton Trans.* **1995**, 1259-1266. (d) Funabiki, T.; Yamazaki, T. *J. Mol. Catal. A: Chem.* **1999**, *150*, 37-47. (e) Yamahara, R.; Ogo, S.; Watanabe, Y.; Funabiki, T.; Jitsukawa, K.; Masuda, H.; Einaga, H. *Inorg. Chim. Acta* **2000**, *300-302*, 587-596.

[33] (a) Jorgensen, C. K. *Absorption Spectra and Chemical Bonding in Complexes*, Pergamon Press: Oxford, 1962. (b) Collman, J. P.; Hegedus, L. S.; Norton, J. R.; Finke, R. G. *Principles and Applications of Organotransition Metal Chemistry*, University Science Books: Miller Valley, CA, 1987, pp 192-197.

[34] Pope, M. T. *Heteropoly and Isopoly Oxometalates,* Springer-Verlag: New York, 1983; pp 18-19.

[35] (a) Que, L., Jr.; Ho, R. Y. N. *Chem. Rev.* **1996**, *96*, 2607-2624. (b) Costas, M.; Mehn, M. P.; Jensen, M. P.; Que, L., Jr. *Chem. Rev.* **2004**, *104*, 939-986.

[36] The mechanism in Figure 4.13 contains a testable $^{18}O_2$ labeling prediction that will reveal whether or not O-scrambling occurs with the initial "spectator oxo" present in the catalyst, an experiment which can, then be compared to literature precedent.[36a,36b] This experiment is under investigation; we hope to be able to report it in due course. (a) White, L. S.; Nilsson, P. V.; Pignolet, L. H.; Que, L., Jr. *J. Am. Chem. Soc.* **1984**, *106*, 8312-8313. (b) Funabiki, T.; Mizoguchi, A.; Sugimoto, T.; Tada, S.; Mitsuji, T.; Sakamoto, H.; Yoshida, S. *J. Am. Chem. Soc.* **1986**, *108*, 2921-2932.

[37] (a) Dei, A.; Gatteschi, D.; Pardi, L. *Inorg. Chem.* **1993**, *32*, 1389-1395. (b) Jo, D.-H.; Que, L., Jr. *Angew. Chem., Int. Ed.* **2000**, *39*, 4284-4287. (c) Lin, G.; Reid, G.; Bugg, T. D. H. *J. Am. Chem. Soc.* **2001**, *123*, 5030-5039.

[38] (a) Groves, J. T.; Bonchio, M.; Carofiglio, T.; Shalyaev, K. *J. Am. Chem. Soc.* **1996**, *118*, 8961-8962. (b) Grover, J. T. "Mechanisms of Metalloporphyrin-Catalyzed Oxidations," ADHOC 2002 Conference, Activation of Dioxygen and Homogeneous Catalytic Oxidation, Emory University, Atlanta, GA, June 2-7, 2002. (c) Grove's aerobic olefin epoxidation dioxygenase: Groves, J. T.; Quinn, R. *J. Am. Chem. Soc.* **1985**, *107*, 5790-5792. This classic system has not been commercialized due, it is our understanding, to its low catalytic turnover frequencies (ca. 1 turnover/h), irreversible inactivation to Ru(III), product inhibition, and eventual oxidative inactivation of the porphyrin-based catalyst system. It is a remarkable system nevertheless.

[39] Schissler, D. O.; Stevenson, D. P. *J. Chem. Phys.* **1954**, *22*, 151-152, showing the easily autoxidized benzylic C–H bond has a BDE of 77 ± 3 kcal/mol.

[40] Süss-Fink, G.; Therrien, B.; Vieille-Petit, L.; Tschan, M.; Romakh, V. B.; Ward, T. R. In *Abstracts of Papers, 226th ACS National Meeting, New York*; American Chemical Society: Washington D. C., 2003, pp INOR-369.

[41] Hagen, C. M.; Vieille-Petit, L.; Laurenczy, G.; Süss-Fink, G.; Finke, R. G. *Organometallics*, **2005**, *24(B)*, 1819-1831.

[42] Hamlin, J. E.; Hirai, K.; Gibson, V. C.; Maitlis, P. M. *J. Mol. Catal.* **1982**, *15*, 337-347.

[43] (a) van Bekkum, E.; van Rantwijk, F.; van de Putte, T. *Tetrahedron Lett.* **1969**, 1. (b) Augustine, R. L.; van Peppen, J. F. *J. Chem. Soc., Chem. Commun.* **1970**, 571. (c) Strohmeier, W.; Hitzel, E. *J. Organomet. Chem.* **1975,** *91*, 373. (d) Strohmeier, W.; Hitzel, E. *J. Organomet. Chem.* **1975,** *102*, C37. (e) Strohmeier, W.; Lukacs, M. *J. Organomet. Chem.* **1977,** *129*, 331. (f) Strohmeier, W.; Lukacs, M. *J. Organomet. Chem.* **1977,** *133*, C49. (g) Strohmeier, W.; Weigelt, L. *J. Organomet. Chem.* **1977,** *133*, C43.

[44] Weiner, H.; Trovarelli, A.; Finke, R. G. *J. Mol. Catal. A: Chemical* **2001**, *191*, 217-252 and references therein to the extensive prior literature of autoxidation.

[45] Que, L., Jr. *Coord. Chem. Rev.* **1983**, *50*, 73-108.

[46] (a) Funabiki, T. In *Catalysis by Metal Complexes*; Funabiki, T., Ed.; Kluwer Academic Publishers: Dordrecht, The Netherlands, 1997; Vol. 19, pp 80-83. (b) A caveat there is that it is not clear whether the above discussions are applicable to arene *cis*-dihydroxylation reaction catalyzed by Rieske "dioxygenases" (e.g., naphthalene dioxygenase, toluene dioxygenase). However, these so-called "dioxygenases" would appear to not be true dioxygenases in that they require NAD(P)H as a cofactor, presumably making them mechanistically related at least somewhat to cytochrome P_{450}.

[47] Specifically, Sen concluded that: "While, from a practical standpoint, it is more desirable for both oxygen atoms of O_2 to be used for substrate oxidation, there appears to be no known catalytic system that operates as an artificial 'dioxygenase' under mild conditions toward 'difficult' substrates, such as those possessing unactivated primary C–H bonds". Lin, M.; Hogan, T.; Sen, A. *J. Am. Chem. Soc.* **1997**, *119*, 6048-6053.

Supporting Information For

Autoxidation-Product-Initiated Dioxygenases: Vanadium-Based, Record Catalytic Lifetime Catechol Dioxygenase Catalysis and Its Mechanism of Action

Cindy-Xing Yin, Yoh Sasaki and Richard G. Finke

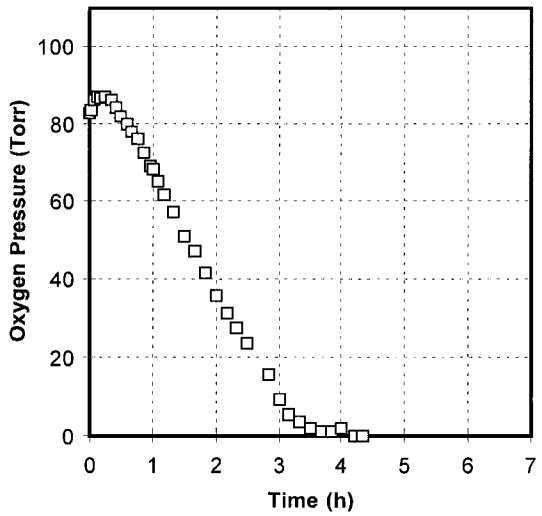

Figure S4.1 O_2-uptake of DTBC plus the precatalyst $(n\text{-}Bu_4N)_7SiW_9V_3O_{40}$ with the addition of H_2O_2 plus 3,5-DBQuinone. Conditions: 1.8 mmol 3,5-DTBC, 5.7 μmol precatalyst, 8.9 mL 1,2-$C_2H_4Cl_2$, 40 °C, and 0.8 atm O_2; note that the final pressure has been subtracted from the initial pressure so that the *net pressure change* is shown above. 3,5-DBQuinone (0.32 mmol) was added at t = 2 min, and 0.31 mmol H_2O_2 was added at t = 4 min. This experiment shows 3,5-DBQuinone plus H_2O_2 together have no increased effect on the induction period over adding H_2O_2 alone (Figure 4.4A in the main text).

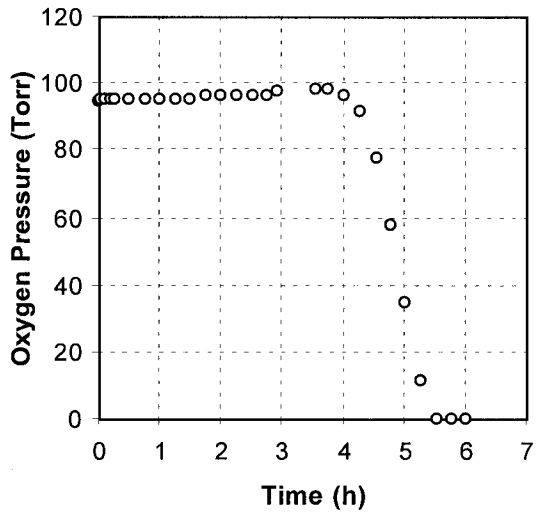

Figure S4.2 O_2-uptake of DTBC plus the precatalyst $(n\text{-}Bu_4N)_7SiW_9V_3O_{40}$ with the addition of AIBN. Conditions: 1.8 mmol 3,5-DTBC, 5.7 μmol precatalyst, 9.1 mL 1,2-$C_2H_4Cl_2$, 40 °C, and 0.8 atm O_2; note that the zeroed, net pressure change is shown above. AIBN (0.018 mmol, 0.054 mmol in a separate run with identical results due to a same decomposition rate of AIBN in dilute solutions[1]) was added at t = 2 min. This experiment shows that the radical initiator AIBN has no effect on the O_2-uptake kinetics.

[1] Sheppard, C. S.; Kamath, V. R. *Polym. Eng. Sci.* **1979**, *19*, 597-606.

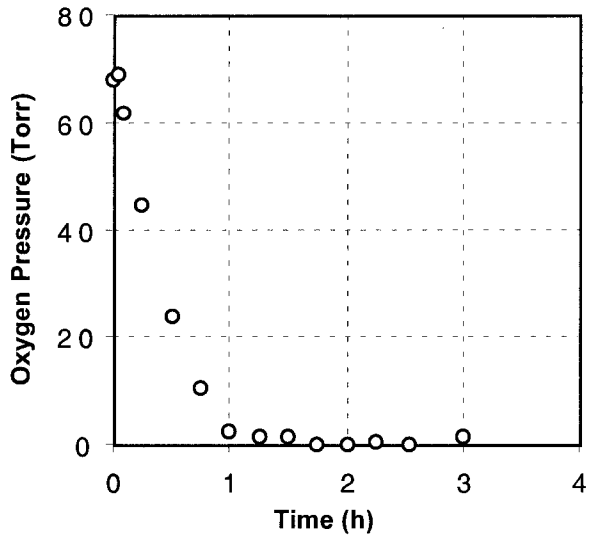

Figure S4.3 O_2-uptake of DTBC plus the precatalyst $(n\text{-}Bu_4N)_7SiW_9V_3O_{40}$ with the addition of NaDBSQ. Conditions: 1.8 mmol 3,5-DTBC, 5.7 μmol precatalyst, 9.2 mL 1,2-$C_2H_4Cl_2$, 40 °C, and 0.8 atm O_2; note that the zeroed, net pressure change is shown above. NaDBSQ (0.33 mmol) was added at t = 2 min. This kinetic experiment, together with the product analysis showing the autoxidation product, **6**, only (products 2-5 are < 0.5%), reveals that this is an autoxidation reaction, and not a DTBC dioxygenation reaction.

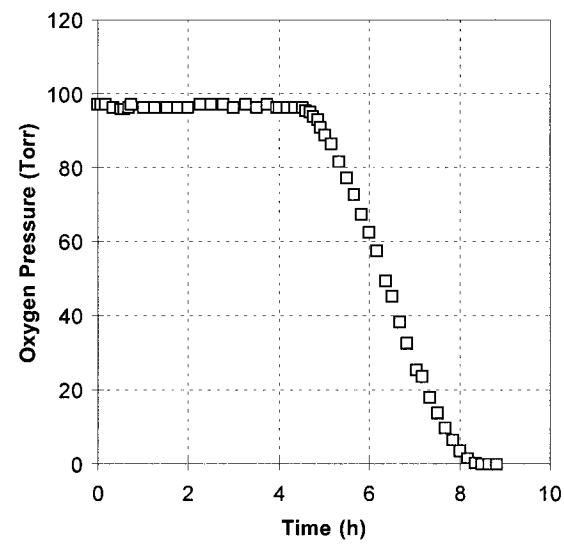

Figure S4.4 O_2-uptake of DTBC plus the precatalyst $(n\text{-}Bu_4N)_7SiW_9V_3O_{40}$ in water-saturated 1,2-$C_2H_4Cl_2$. Conditions: 1.8 mmol 3,5-DTBC, 5.7 μmol precatalyst, 8.3 mL 1,2-$C_2H_4Cl_2$, 40 °C, and 0.8 atm O_2; note that the net pressure change is shown above. Water-saturated 1,2-$C_2H_4Cl_2$ was prepared by shaking standard pre-dried 1,2-$C_2H_4Cl_2$ with an equal volume of water outside the drybox. This experiment confirms the result with water added at the start of reaction (Figure 4.4A in the main text in which 1.3 mmol water is added and a 4.8 h induction period), in that a longer induction period is observed in the present experiment (4.6 h compared to 3.5 h at standard conditions).

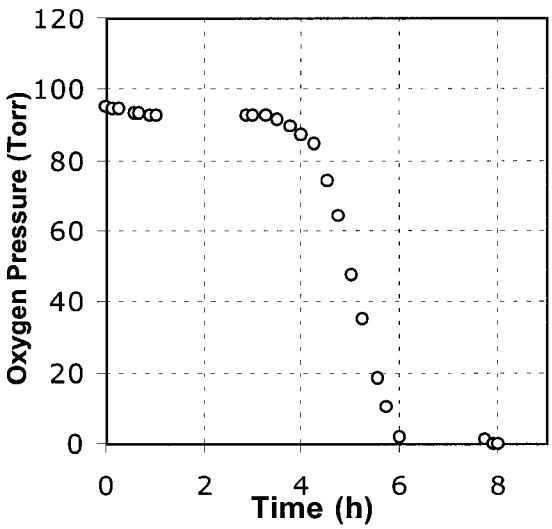

Figure S4.5 O_2-uptake of DTBC plus the precatalyst $(n\text{-}Bu_4N)_7SiW_9V_3O_{40}$ in *o*-dichlorobenzene. Conditions: 1.8 mmol 3,5-DTBC, 5.7 μmol precatalyst, 9.4 mL *o*-dichlorobenzene, 40 °C, and 0.8 atm O_2; note that the net pressure change is shown above. This experiment shows that using the more oxidation-resistant solvent, *o*-dichlorobenzene, gives the same O_2-uptake curve as when 1,2-$C_2H_4Cl_2$ is employed in the main text. This, in turn, eliminates the possibility of solvent-involvement in the dioxygenase reaction of DTBC.

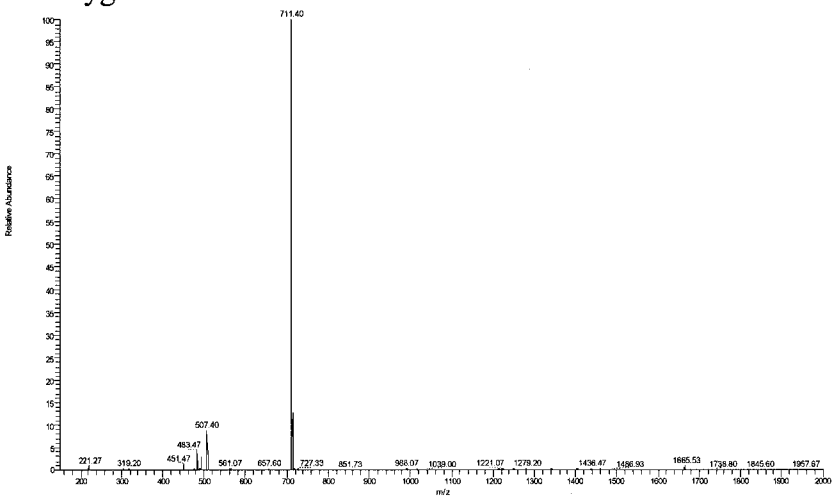

Figure S4.6 Negative ion ESI–MS spectrum of the product solution of 0.05 mmol $(n\text{-}Bu_4N)_7SiW_9V_3O_{40}$ and 0.3 mmol DTBC in 8 mL 1,2-$C_2H_4Cl_2$ under O_2. The m/z = 711.4 peak corresponds to $V(DTBC)_3^-$ and m/z = 507.4 peak corresponds to $VO(DTBC)_2^-$ as detailed elsewhere.[2] A similar spectrum was obtained with the reaction solution of 0.05 mmol $(n\text{-}Bu_4N)_7SiW_9V_3O_{40}$, 0.2 mmol DTBC and 0.05 mmol H_2O_2 in 8 mL 1,2-$C_2H_4Cl_2$ under O_2 which, again, exhibited the m/z = 711.4 peak assigned to $V(DTBC)_3^-$ and the m/z = 507.4 peak assigned to $VO(DTBC)_2^-$.

[2] Yin, C.-X.; Finke, R. G. "Vanadium-Based, Record Catalytic Lifetime Catechol Dioxygenases: Evidence For a Common Catalyst," *J. Am. Chem. Soc.* **2005**, in press.

Control Experiments:

A. Control Experiment Testing the Effectiveness of Transferring H_2O_2With A Stainless Steel Needle. In order to test if H_2O_2 decomposes to a significant extent when a stainless steel needle syringe is used to sample the solutions containing H_2O_2 and under our other conditions and timescale, a series of iodimetric titration control experiments were performed as detailed below.

Run	Weight of H_2O_2 (32 μL) Before Sampling (g)	Moles of H_2O_2 Before Sampling (mmol)	Titrated H_2O_2 After Sampling (mmol)	Percentage of H_2O_2 Detected (%)
1	0.0342	0.2966	0.2916	98.3
2	0.0342	0.2966	0.2900	97.8
3	0.0344	0.2984	0.2879	96.5
4	0.0317	0.2750	0.2588	94.1

The results show that an average of 96.7% of H_2O_2 was detected even when a stainless steel needle syringe was used to transfer the H_2O_2. Consequently, surface corrosion and exposed metal that could disproportionate H_2O_2 in the stainless steel needle syringes used have only a small, tolerable effect on the H_2O_2 titer.

B. Stirring Rate Controls—The Establishment of O_2 Mass-transfer Limitations.

Gas-to-solution mass-transfer-limitations (hereafter MTL) is a common phenomenon in reactions between dissolved reagents and dissolved gases.[3] It is always important to determine the gas-to-solution MTL of one's apparatus and stirring conditions before initiating experiments using gases.

[3] Aiken, J. D., III; Finke, R. G. *J. Am. Chem. Soc.* **1998**, *120*, 9545-9554

In our autoxidation kinetics, the induction period is not affected by possible MTL as no gas is consumed. However, the slope of the post induction period could be affected by MTL. To avoid measuring reaction rates in the MTL regime, lowering the precatalyst concentration, speeding up the stirring rate, or both are usually applied. Below is the rate vs precatalyst concentration curve used to detect MTL for two different stirring rates *using our O_2-uptake line equipped with a mercury manometer.*

The post-induction period reaction rates were measured from the oxygen-uptake curves generated using different concentrations of the precatalyst, $(n\text{-}Bu_4N)_7SiW_9V_3O_{40}$. Two different stirring rates were examined. **Stirring rate i**: 3/8'' × 3/16" egg-shaped magnetic stir bar in the reaction flask, 3/2" × 3/8" octagonal magnetic stir bar in the oil bath, magnetic stirring rate ca. 420 rpm. **Stirring rate ii:** 3/4" × 3/8" egg-shaped magnetic stir bar in the reaction flask, no stir bar in the oil bath, magnetic stir rate ca. 800 rpm. As expected, at the higher stirring rate using the same reaction flask, the chemical reaction rate limiting regime (i.e., the non-MTL regime) exists up to the higher concentration range of precatalyst of ca. 0.5–0.7 mM. In order to avoid measuring rates in the MTL regime with the mercury manometer O_2-uptake line, a precatalyst concentration ≤0.5 mM plus a ≥800 rpm stirring rate is necessary and was employed in the experiments described in the main text.

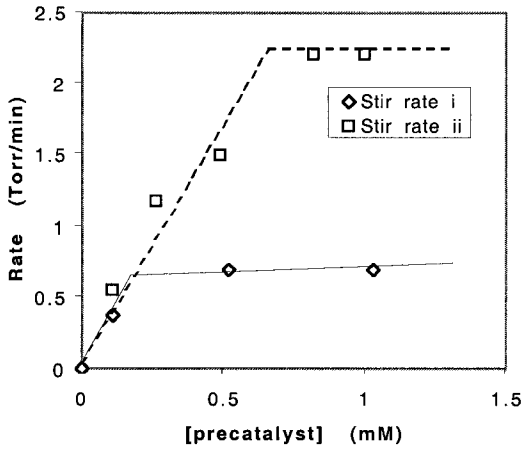

Figure S4.7 The rate vs precatalyst concentration plot showing complete mass-transfer-limitations above ca. 0.15 mM precatalyst concentration at the slower, 420 rpm stirring rate and above ca. 0.5 mM precatalyst concentration at the faster, 800 rpm stirring rate in the O_2-uptake line equipped with a Hg-manometer.

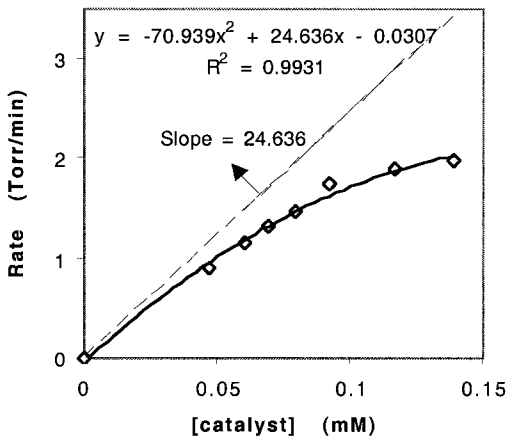

Figure S4.8 The rate vs catalyst ($[VO(DBSQ)(DTBC)]_2$ concentration plot showing the mass-transfer-limitations line (slope = 24.636 Torr/min·mM) for the O_2-uptake line monitored by an automatic O_2 pressure transducer. The line was obtained by a polynomial curve-fit to obtain the initial rate as the coefficient of the second term of the polynomial.[4] Stirring method: 5/8'' × 5/16" magnetic stir bar in a 22 mm × 175 mm culture tube sealed in the Fisher-Porter bottle, magnetic stirring rate ca. 1200 rpm (no stirrer in the oil bath). This plot shows that for this apparatus and at ≥1200 rpm stirring rate, there is ca. 28% of a MTL at 0.05 mM catalyst (the typical maximum employed in the kinetic experiments herein), and ca. 30% of a MTL at 0.10 mM catalyst concentration, the latter being the highest value used in a single kinetic experiment in the present work. The same MTL percentages through 0.05 mM to 0.10 mM ensure that

[4] Wilkins, R. G. *Kinetics and Mechanism of Reactions of Transition Metal Complexes,* 2nd ed.; VCH: New York, 1991; pp 3-4.

such MTL effects should be cancelled out as a systematic error in the kinetic analysis. The initial rate in Figure 4.7 in the main text is 0.86 Torr/min at 0.05 mM, below the 1.2 torr O_2/min mass-transfer limit (calculated as 24.636 Torr/min·mM × 0.05 mM).

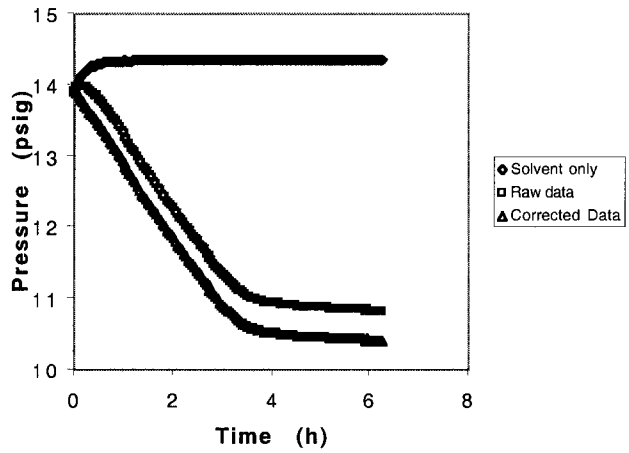

Figure S4.9 A solvent vapor pressure curve used to correct the raw data from O_2-uptake line monitored by the automatic pressure transducer plus an example showing a set of raw data and corrected O_2-uptake data. The solvent vapor pressure curve was obtained using 1,2-$C_2H_4Cl_2$ after equilibrating in a 40 °C oil bath for 25 min and followed by a standard cycle of 15 purges in our apparatus.

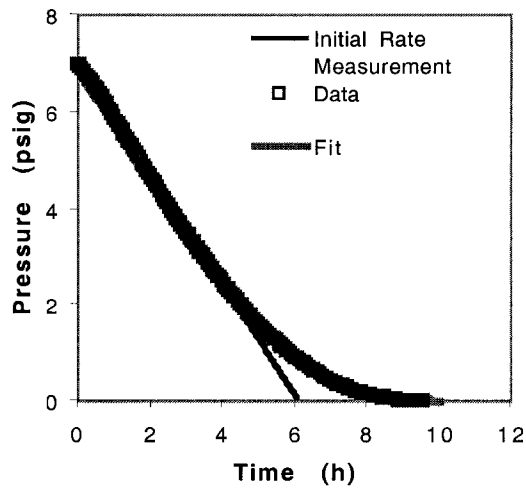

Figure S4.10 O_2-uptake curve of a representative kinetic run of DTBC plus $[VO(DBSQ)(DTBC)]_2$; note that the net pressure change is shown above. Reaction conditions: 3.58 mmol 3,5-DTBC, 0.4 μmol catalyst, 9 mL 1,2-$C_2H_4Cl_2$, 40 °C and 1.7 atm O_2. The initial rate was obtained by performing a linear regression on the the first 1.5 h of data; the fit was obtained by a numerical integration with the steps shown in Figure 4.11 in the main text ($k_3 = 700\ h^{-1}$, $k_4 = 2 \cdot 10^8\ M^{-1}h^{-1}$, $k_5 = 10^7\ M^{-1}h^{-1}$ and $k_6 = 4 \cdot 10^9\ M^{-3}h^{-1}$ as the best parameters from a grid search as detailed in the Experimental Section in the main text).

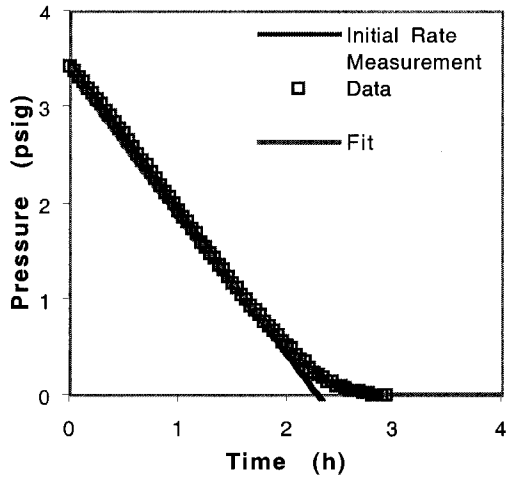

Figure S4.11 O_2-uptake curve of a representative kinetic run of DTBC plus $[VO(DBSQ)(DTBC)]_2$; note that the net pressure change is shown above. Reaction conditions: 1.8 mmol 3,5-DTBC, 0.6 μmol catalyst, 8 mL 1,2-$C_2H_4Cl_2$, 40 °C and 1.7 atm O_2. The initial rate was obtained by performing a linear regression on the data during the first 1 h; the fit data were obtained by a numerical integration with the steps shown in Figure 4.11 in the main text ($k_3 = 600\ h^{-1}$, $k_4 = 10^8\ M^{-1}h^{-1}$, $k_5 = 6 \cdot 10^7\ M^{-1}h^{-1}$ and $k_6 = 3 \cdot 10^9\ M^{-3}h^{-1}$ as the best parameters from a grid search as detailed in the Experimental Section in the main text).

Plausible Stoichiometries for Conversion of $SiW_9V_3O_{40}^{7-}$ to the Active Catalyst, $[V^V(O)(DBSQ)(DTBC)]_2$ Plus Initial Experimental Tests of Those Stoichiometries. It should be possible to write more specific stoichiometries for the conversion of A, $SiW_9V_3O_{40}^{7-}$ (the prototype polyoxometalate studied herein) to the catalyst, $[V^V(O)(DBSQ)(DTBC)]_2$, via the involvement of the autocatalytic product, B, H_2O_2 generated by the autoxidation of 3,5-DTBC to the benzoquinone, **6**. That, in turn, should provide predicted reactions that can be subjected to experimental verification or refutation. In what follows in Figure S4.12 we use the precedent of $V(O)O_2^+$ leaching from polyoxometalates by H_2O_2 as a key part of our scheme (e.g., the precedent of decavanadate plus hydrogen peroxide:[5,6] $V_{10}O_{28}^{6-} + H_2O_2 \rightarrow V(O)O_2^+$). Note that Figure

[5] "Peroxy Compounds of the Transition Metals," Connor, J. A.; Ebsworth, E. A. V. *Adv. Inorg. Chem. Radiochem.* **1964**, *6*, 279-381.
[6] Butler, A.; Clague, M. J.; Meister, G. E. *Chem. Rev.* **1994**, *94*, 625.

S4.12 is just a hypothesized set of reactions that requires much more study, although we present next the evidence we obtained in general support of this scheme.

$$\underline{\mathbf{A \rightarrow B}} \qquad (1)$$

$$DTBC + O_2 \rightarrow H_2O_2 + DBQuinone \qquad (1a)$$

$$SiW_9V_3O_{40}^{7-} + H_2O_2 \rightarrow V(O)O_2^+ + SiW_9V_2O_{39}^{10-} + 2H^+ \qquad (1b)$$

$$V(O)O_2^+ + 2DTBC + 0.25\,O_2 \rightarrow 1/2[VO(DBSQ)(DTBC)]_2 + H_2O_2 + H^+ + 0.5H_2O \qquad (1c)$$

Sum

$$\underset{\mathbf{A}}{\underline{SiW_9V_3O_{40}^{7-}}} + 3DTBC + 1.25O_2 \rightarrow \underset{\rightarrow\ \mathbf{B}}{\underline{H_2O_2}} + 1/2[VO(DBSQ)(DTBC)]_2 + 0.5H_2O + 3H^+ + SiW_9V_2O_{39}^{10-} + DBQuinone \qquad (1')$$

$$\underline{\mathbf{A + B \rightarrow 2B}} \qquad (2)$$

$$\underset{\mathbf{A}}{\underline{SiW_9V_3O_{40}^{7-}}} + \underset{\mathbf{B}}{\underline{H_2O_2}} + 1.25O_2 + 3DTBC \rightarrow \underset{\rightarrow\ \mathbf{2B}}{\underline{2H_2O_2}} + SiW_9V_2O_{39}^{10-} + 1/2[VO(DBSQ)(DTBC)]_2 + 3H^+ + 0.5H_2O + DBQuinone \qquad (2')$$

Figurer S4.12 Plausible, More Detailed Reactions For H_2O_2 Autoxidation-Product-Mediated Conversion of a V-Polyoxometalate to Pierpont's Dioxygenase Catalyst, $[V^V(O)(DBSQ)(DTBC)]_2$.

We performed an initial test of the predicted stoichiometry in equation (1') above via two experiments in which $SiW_9V_3O_{40}^{7-}$ was treated with 4 to 6 equivalents of DTBC and the O_2 uptake stoichiometry and reaction products were determined. Key differences in the experimental conditions of the *stoichiometry* experiments vs the *catalytic conditions* examined so far are: (1) a stoichiometric ratio of the precatalyst to DTBC had to be used in the stoichiometry experiments (ca. 0.05 mmol $SiW_9V_3O_{40}^{7-}$ vs 0.2–0.3 mmol DTBC) in order to produce sufficient material for analysis (vs a ratio of ca. 0.006 mmol precatalyst vs 1.8 mmol DTBC in the catalytic runs); and (2) DTBC was added to the

precatalyst in the stoichiometry experiments (whereas the reverse order of addition was employed in the catalytic runs).

In one experiment, $SiW_9V_3O_{40}^{7-}$ was treated with 4 equivalents of DTBC and 1 equivalent of H_2O_2. The measured O_2-uptake was 29 ± 3% relative to DTBC and GC showed 56 ± 6% conversion of DTBC to DBQuinone as the primary product. Significantly, ≤3% of the dioxygenase products **2-5** were formed, *indicating that the conditions of the stoichiometry experiments are producing different chemistry than the catalytic conditions.* The observed O_2 / DBQuinone is 0.52 (±0.08)/ 1 vs a predicted 1.25:1 from Figure S4.12. In a second experiment employing 6 equivalents of DTBC, the O_2-uptake was 37 ± 2% relative to DTBC for a ratio of O_2 / DBQuinone of 0.63 (±0.05)/ 1 (vs the predicted 1:1) and GC revealed a 59 ± 4% conversion of DTBC to DBQuinone with little (≤2%) dioxygenase products **2-5** being formed.

The product solutions from the above two experiments were examined by negative ion ESI–MS to determine which V-species were present. Two major peaks, assignable as before,[2] to $[VO(DTBC)_2]^-$ and $[V(DTBC)_3]^-$, were observed, Figure S4.6. Interestingly, Pierpont's catalyst resting state, $[VO(DBSQ)(DTBC)]_2$, was *not* detectable in the product solution by either ESI–MS or EPR and despite our ready detection of this catalyst resting state by these methods.[2] This is a key finding: we already have shown in our earlier work that $[V(DTBC)_3]^-$ yields diagnostic dioxygenase products **2-5** with a short induction period (~10 min) when treated with excess DTBC under catalytic conditions (see Figure 4 elsewhere[2]). It appears, then, that the catalytic conditions involving a large excess of DTBC to vanadium (i.e., and not the conditions for the

stoichiometry studies employed above) are required for the formation of $[VO(DBSQ)(DTBC)]_2$, *vide infra.*

Reflection on these initial studies testing the plausible reactions in Figure S4.12 reveals several insights: first, the lack of the *dioxygenase* products **2-5** in the above experiments (i.e., at levels ≤3%) means that the conditions chosen in future studies of Figure S4.12 should be the *catalytic conditions*; indeed, it is reassuring that Pierpont's catalyst resting state is *not* seen under conditions where the dioxygenase products **2-5**, that are the hallmark of its presence,[2] are also *not* seen. Second, the observed ca. 0.6:1 vs predicted 1.25:1 O_2 / DBQuinone stoichiometries makes it clear that a competing, parallel reaction of DTBC + H_2O_2 → DBQuinone + $2H_2O$ is occurring under the conditions of the stoichiometry experiment. If one corrects for this by subtracting out the amount of DBQuinone formed from the DTBC consumed, then one finds that ca. 2 equivalents of DTBC react with 1 equivalent of $SiW_9V_3O_{40}^{7-}$ plus 1 equivalent of H_2O_2 to produce detectable amounts of $V(DTBC)_3^-$ and $VO(DTBC)_2^-$. The detection of $VO(DTBC)_2^-$ by ESI-MS is consistent with this species being at least a plausible intermediate en route to $[VO(DBSQ)(DTBC)]_2$, although this specific conversion remains to be demonstrated.

Overall, then, the reactions hypothesized in Figure S4.12 and these initial tests (i) provide independent evidence that H_2O_2 assisted, V-leaching from polyoxoanions to form species such as $V(DTBC)_3^-$ and $VO(DTBC)_2^-$ can and does occur (as detected by ESI–MS and their respective m/z = 711 and 507), but (ii) show that *neither* the diagnostic dioxygenase products, **2-5**, nor the previously demonstrated[2] conversion of $V(DTBC)_3^-$ into active catalyst capable of forming **2-5**, occurs under non-catalytic conditions. Perhaps most importantly, (iii) the above experiments indicate that a detailed

understanding of the reactions underlying the kinetically observed pseudoelementary steps will require its own, separate studies and probably a full paper aimed at testing and refining Figure S4.12.

Confirmed formation of $[VO(DBSQ)(DTBC)]_2$ from $V(DTBC)_3^-$ under catalytic conditions using EPR. The experimental procedures are detailed in the previous paper.[2] The reaction conditions are as following: 1.8 mmol DTBC and 0.003 μmol $[Na(CH_3OH)_2]_2[V^V(DTBC)_3]_2 \cdot 4CH_3OH$ were allowed to react with O_2 at 40 °C in 8 mL toluene. The reaction solution was sampled for EPR experiments. The post-reaction solution gives the 9-line EPR spectrum ($g = 2.006$, $A_{51V} = 3.08$ G) that is the signature of Pierpont's $[VO(DBSQ)(DTBC)]_2$ catalyst resting state.[2] The organic products are: **2**, in 25 ± 1% yield, **3**, in 5 ± 1% yield, **4**, in 8 ± 1% yield and **6**, in 20 ± 1% (established by GC). These are somewhat different from the product yields in our standard solvent (1,2-$C_2H_4Cl_2$), as reported in Table 2 elsewhere,[2] due to the use of toluene as the solvent. This result appears to confirm the finding that the specific conditions of especially an excess of DTBC to vanadium are key to the formation of this catalytic resting state, conditions that remain to be explored in future experiments aimed at refining Figure S4.12.

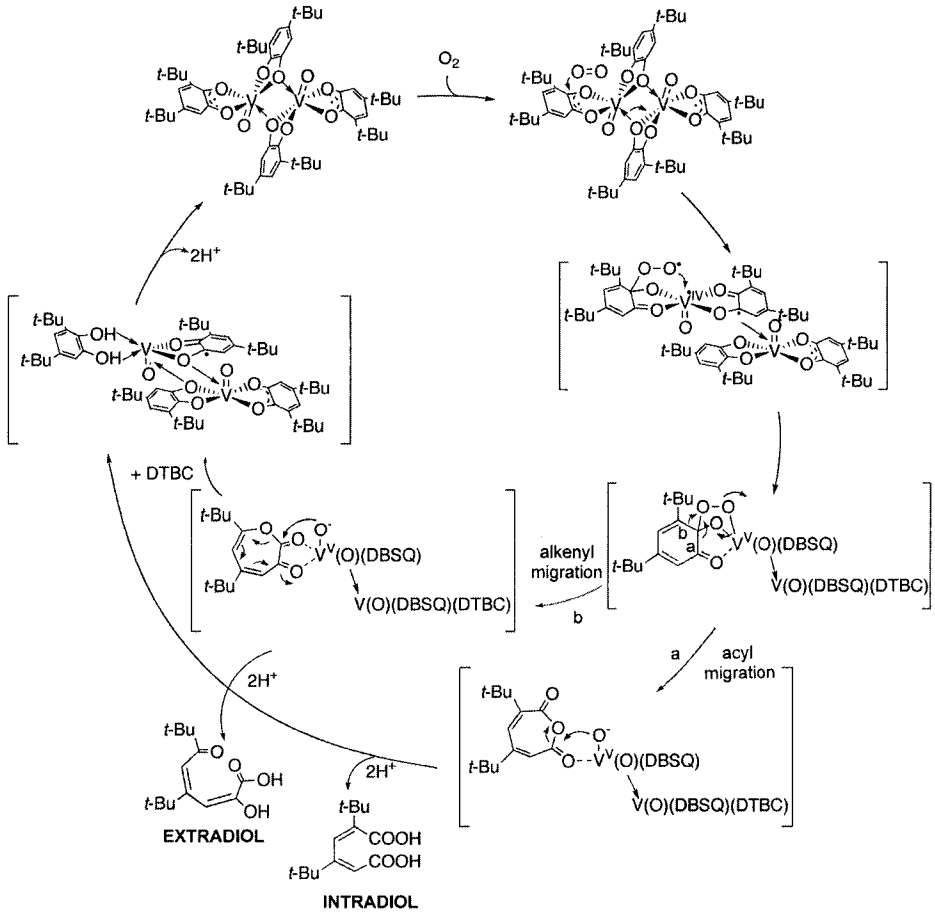

Figure S4.13 One other conceivable mechanism involving intact $[VO(DBSQ)(DTBC)]_2$ in the catalytic cycle. Brief discussion of this mechanism is provided in the main text. The kinetics rule out this mechanism as an exponential curve, and not the linear loss of O_2 pressure seen, is predicted for the conditions of the kinetic experiments and observed rate law of first order in $[VO(DBSQ)(DTBC)]_2$ and $[O_2]$.

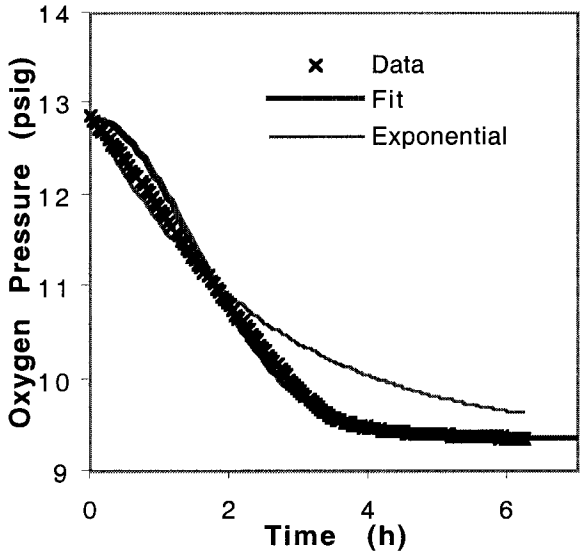

Figure S4.14 O_2-uptake curve of a representative kinetic run of DTBC plus $[VO(DBSQ)(DTBC)]_2$ and a poor curve-fit ala Figure 4.11 in the main text except that step (6) in Figure 4.11 was replaced with [VO(DBSQ)] + DTBC → [VO(DBSQ)(DTBC)] (the formation of monomer only). The data and fit above are also compared to a simple first-order kinetic curve ($pO_2(t) = pO_{2,t=0}\exp\{-k_{initial}(t)\}$). Reaction conditions: 1.8 mmol 3,5-DTBC, 0.4 μmol catalyst, 8 mL 1,2-$C_2H_4Cl_2$, 40 °C and 1.7 atm O_2.

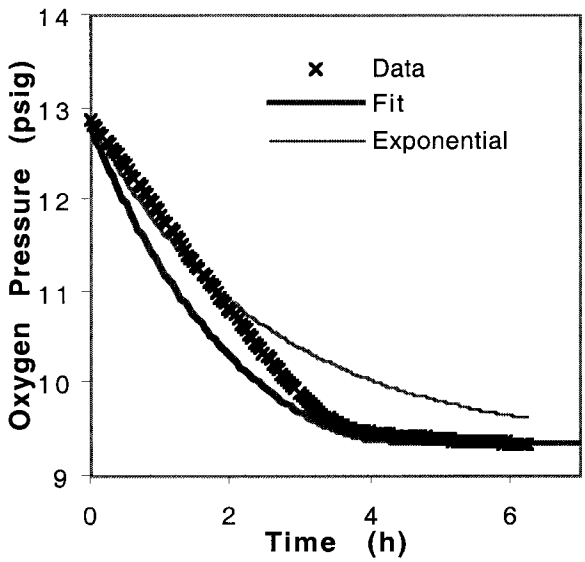

Figure S4.15 O_2-uptake curve of a representative kinetic run of DTBC plus $[VO(DBSQ)(DTBC)]_2$ and a poor curve-fit ala the mechanism in Figure S4.13. The data and fit above are also compared to a simple first-order kinetic curve ($pO_2(t) = pO_{2,t=0}\exp\{-k_{initial}(t)\}$). Reaction conditions: 1.8 mmol 3,5-DTBC, 0.4 μmol catalyst, 8 mL 1,2-$C_2H_4Cl_2$, 40 °C and 1.7 atm O_2.

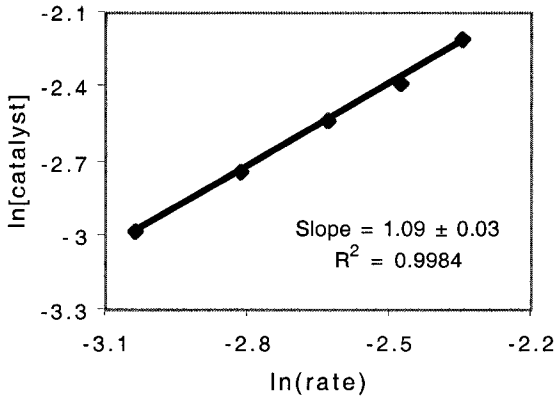

Figure S4.16 Calculated initial rate vs the catalyst concentration. The initial rates were measured from fitting data obtained by performing numerical integrations using the chemical equations and rate constants in Figure 4.11 in the main text.

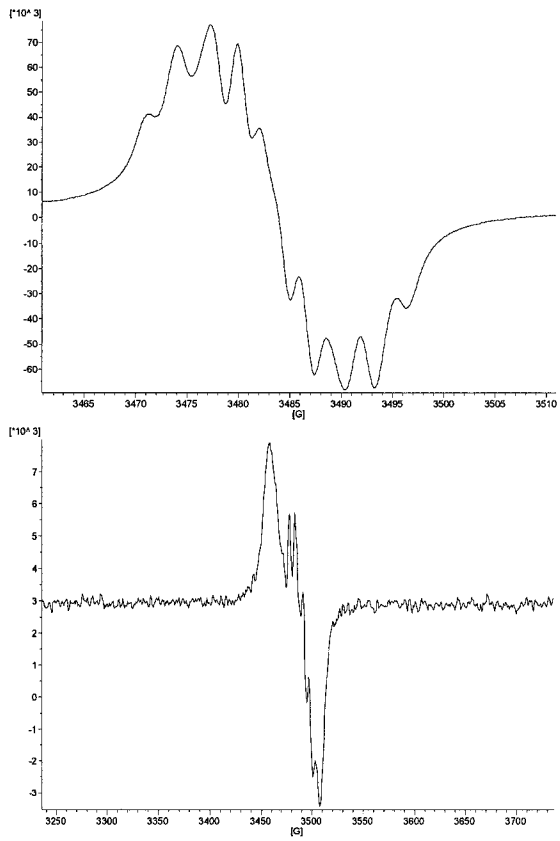

Figure S4.17 The 9-line characteristic EPR spectrum of $[VO(DBSQ)(DTBC)]_2$ (g = 2.006, A_{51V} = 3.01 G; scan width 50 G) and the EPR spectrum of the same solution with the addition of a drop of DMSO solvent (g = 2.02 for the broad peak and g = 2.002 for the other 5 peaks, A_{51V} = 6.35 G for the 5 sharp peaks; scan width 500 G). This experiment shows that the $[VO(DBSQ)(DTBC)]_2$ dimer structure is easily destroyed by the addition of O-substituted ligands, such as DMSO, presumably due to solvated monomer formation, V(O)(DBSQ)(DTBC)(DMSO).

CHAPTER V

IS IT TRUE DIOXYGENASE OR CLASSIC AUTOXIDATION CATALYSIS? RE-INVESTIGATION OF A CLAIMED DIOXYGENASE CATALYST BASED ON A RU_2-INCORPORATED, POLYOXOMETALATE PRECATALYST

This dissertation chapter contains the manuscript of a full paper accepted by *Inorganic Chemistry*, **2005**, in press. This study is a re-investigation of previously published work, from another lab. All the data obtained argues against the previous claim by others that the Ru_2-sandwich polyoxometalate precatalyst acts as an inorganic dioxygenase. The following studies show that the adamantane hydroxylation reaction occurs via a more general, free-radical-chain mechanism.

Is It True Dioxygenase or Classic Autoxidation Catalysis? Re-Investigation of a Claimed Dioxygenase Catalyst Based on a Ru_2-Incorporated, Polyoxometalate Precatalyst

Cindy-Xing Yin and Richard G. Finke

Abstract

A 1997 *Nature* paper (*Nature* **1997,** *388,* 353–5) and a 1998 *JACS* paper (*J. Am. Chem. Soc.* **1998,** *120,* 11969–76) reported that a novel Ru_2-incorporated sandwich-type polyoxometalate, $\{[WZnRu^{III}_2(OH)(H_2O)](ZnW_9O_{34})_2\}^{11-}$, is an all-inorganic dioxygenase catalyst for the hydroxylation of adamantane and the epoxidation of alkenes using molecular oxygen. Specifically, it was reported that the above Ru_2-containing polyoxometalate catalyzes the following reaction by a non-radical-chain, dioxygenase mechanism: $2RH + O_2 \rightarrow 2ROH$ (R = adamantane). A re-investigation of the above claim has been performed, resulting in the following findings: (1) iodometric analysis detects trace peroxides (0.5% relative to adamantane), the products of free-radical-chain autoxidation, at the end of the adamantane hydroxylation reaction; (2) a non-dioxygenase product, $H_2{}^{18}O$, is observed at the end of an adamantane hydroxylation reaction

performed using $^{18}O_2$; (3) kinetic studies reveal a fractional rate law consistent with a classic radical-chain reaction; (4) a non-dioxygenase ~1:1 adamantane products/O_2 stoichiometry is observed in our hands (instead of the claimed 2:1 adamantane/O_2 dioxygenase stoichiometry); (5) adamantane hydroxylation is initiated by the free radical initiator, AIBN (2,2'-azobisisobutyronitrile), or the organic hydroperoxide, *t*-BuOOH; (6) four radical scavengers completely inhibit the reaction; and (7) $\{[WZnRu^{III}_2(OH)(H_2O)](ZnW_9O_{34})_2\}^{11-}$ is found to be an effective catalyst for cyclohexene free-radical-chain autoxidation. The above results are consistent with and strongly supportive of a free-radical-chain mechanism, not the previously claimed dioxygenase pathway.

Introduction

Dioxygenases are defined as a class of enzymes capable of catalyzing the insertion of both oxygen atoms of oxygen into a substrate, Figure 5.1.[1,2,3] Dioxygenases are, therefore, unique and of central importance in oxygenation catalysis owing to their O_2 atom efficiency. No protons or electrons are needed for the reaction and, hence, no H_2O byproduct—representing wasted $2e^-/2H^+$ or H_2 in comparison to monooxygenases—is generated. Dioxygenases are, therefore, key systems for biomimetic studies aimed at more efficient and selective oxygenation catalysts.

The first Ru-based non-enzymatic dioxygenase catalyst was reported by Groves and co-workers, who found that dioxo(tetramesitylporphyrinato)ruthenium(VI), [Ru(TMP)$(O)_2$], catalyzes the aerobic epoxidation of olefins at ambient temperature.[4]

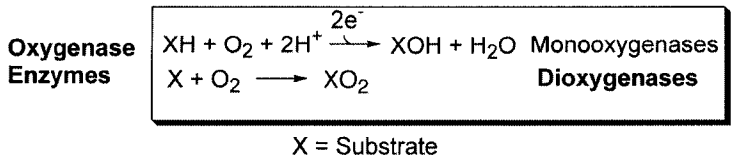

Figure 5.1 Monooxygenase- and dioxygenase-catalyzed oxygenation reactions

Our group has reported that vanadium-containing polyoxometalates serve as all-inorganic catechol dioxygenases with record catalytic total turnovers of over 100,000.[5] Subsequent mechanistic studies provide evidence for a novel autoxidation-product-initiated dioxygenase,[6] in which the autoxidation of catechol generates quinone and H_2O_2, followed by release of vanadium from the vanadium-containing polyoxometalate to give a common,[7] V-based catalyst.[6] Mizuno and co-workers have reported that [γ-$SiW_{10}\{Fe^{3+}(OH_2)\}_2O_{38}]^{6-}$ catalyzes the epoxidation of cyclooctene in, it is believed, a dioxygenase manner.[8] There are of course a few catalytic, and many more stoichiometric, Fe-based dioxygenase model systems[3,9,10,11] that are important toward understanding nature's Fe-based dioxygenase enzymes. These interesting Fe systems[3,9,10,11] are, however, not the focus of the present work.

In 1997, a *Nature* paper reported that the Ru_2-incorporated sandwich-type polyoxometalate, $\{[WZnRu^{III}_2(OH)(H_2O)](ZnW_9O_{34})_2\}^{11-}$, **1**, is an all-inorganic dioxygenase;[12] a full paper was published in *JACS* a year later.[13] Those papers are currently considered significant progress towards realizing an all-inorganic, and thus robust, dioxygenase catalyst.[14]

However, scrutiny of the data from the above two publications indicates that the evidence for the claimed dioxygenase is weak. First, organic-soluble Q_{11}-**1** (Q is

tricaprylmethylammonium from QCl added as a phase-transfer reagent) gives rise to a 10 hour induction period at 80 °C prior to the observation of any adamantane hydroxylation activity.[12] The observed induction period demands that the as-added Q_{11}-**1** is *not* the catalyst; instead **1** must be a *precatalyst.* Additionally, pre-incubation of the precatalyst Q_{11}-**1** with O_2 at 80 °C for 12 hours is necessary to initiate the alkene epoxidation.[12] Second, when we attempted to fit the published observed rate constant versus oxygen pressure curve using the published rate equation,[13] the attempt failed, Figure 5.2. This demands that either: (a) the proposed mechanism is wrong; (b) there are some errors in the kinetics vs pO_2 data; or (c) both (a) and (b). Third, in the proposed mechanism, ≥1 electron is needed to activate the precatalyst to a putative Ru(II) state, but our work does not support this claim (*vide infra*). Moreover, a well-known source of *reductant* under *oxidizing (O_2) conditions* is the initial autoxidation product ROOH, with the **ROO–H** bond serving as a *reductant* to strong enough oxidants in a classic Haber–Weiss fashion.[15,16,17,18,19,20.21] Fourth, the original work reported that radical scavengers had no effect on the catalytic activity,[12,13] but this is *negative evidence*; in addition, it is well known that conclusions based on such one-point radical-scavenger experiments are fraught with problems—the use of the wrong scavenger (typically with too-low a scavenging rate constant)[22] or too low a concentration of scavenger being two common problems leading to such negative, sometimes very misleading results. In fact, we find that we can inhibit the adamantane oxidation reaction readily with four inhibitors (*vide infra*), positive evidence suggestive of a free-radical-based, classic autoxidation reaction, not the claimed dioxygenase. Rather clearly, then, this heralded claim[12,13] of a novel dioxygenase catalyst merits a careful re-investigation.

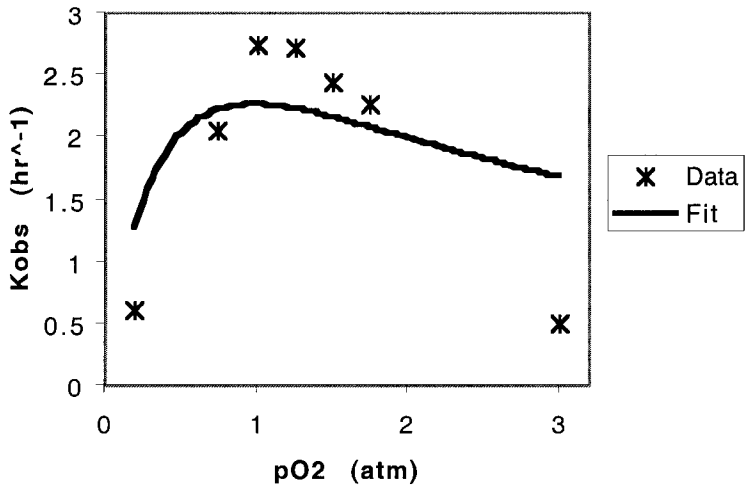

Figure 5.2 Kinetic data from Figure 4 of the prior work[13] plus our attempted fit using the published rate equation ($K_{obs} = K_1k_2[O_2]/(1 + K_1[O_2])^2$).[13] Both K_1 and k_2 were allowed to vary; the "best" fit is $K_1 = 1.0 \pm 0.5\ M^{-1}$ and $k_2 = 9 \pm 1\ M^{-1}h^{-1}$ [the (underestimated) error bars are from the fit, which is obviously poor ($R^2 = 0.55$)]. The curve-fit was accomplished with MacCurveFit ver 1.1.2. As a control we showed that an identical curve-fit, as well as identical K_1, k_2 and R^2 values, were obtained when we used Origin ver 7.0383 from OriginLab.

Herein we provide the following evidence inconsistent with the claimed dioxygenase, but fully consistent with and supportive of a classic, radical-chain autoxidation reaction: (i) the detection of trace hydroperoxide by iodometric analysis; (ii) the detection of $H_2{}^{18}O$, a non-dioxygenase product, when labeled $^{18}O_2$ is used; (iii) kinetics of the maximum rate post the induction period and in the reaction's steady-state, $d[product]/dt_{max} = k_{obs}[adamantane]^{3/2}[Q_{11}\text{-}\mathbf{1}]^{1/2}[O_2]^{\approx 1/2}$, kinetics diagnostic of a radical-chain reaction; (iv) a ~1:1 adamantane products/O_2 (not the claimed 2:1) stoichiometry as expected for a non-dioxygenase; (v) the ability to initiate the chain reaction with AIBN or ROOH (the latter serving, presumably, as a RO**O–H** reductant for Ru^{III} in Q_{11}-**1**); (vi) the ability to inhibit the reaction with 4 radical scavengers; and (vii) the ability of Q_{11}-**1** to

catalyze cyclohexene autoxidation efficiently along with its inability to perform catechol dioxygenase catalysis.

Experimental Section

Materials. All reaction solutions were prepared under oxygen- and moisture-free conditions in a Vacuum Atmosphere drybox (<5 ppm O_2, as continuously monitored by an oxygen sensor). 1,2-dichloroethane (Aldrich, HPLC grade), *o*-dichlorobenzene (Aldrich, HPLC grade) and DMSO (Aldrich, anhydrous grade) were dried with pre-activated 4 Å molecular sieves and stored in the drybox. Adamantane (Aldrich, 99+%) was dried under vacuum at room temperature overnight and stored in the drybox. 2,2'-azobisisobutyronitrile (AIBN) (Aldrich, 98%), 2-phenyl-*N*-*tert*-butylnitrone (Aldrich, 98%, PBN hereafter) and galvinoxyl (Aldrich) were stored in a freezer; 4-*tert*-butylcatechol (Aldrich, 97%) and 2,6-di-*tert*-butyl-4-methylphenol (Aldrich, 99+%, BHT) were used as received. *Tert*-butyl hydroperoxide in decane with molecular sieves (Aldrich, ~5.5 M as labeled) was stored in a refrigerator. $Na_2WO_4 \cdot 2H_2O$ (Aldrich, 99%), $ZnNO_3 \cdot 6H_2O$ (Fisher chemicals), $RuCl_3 \cdot 3H_2O$ (Aldrich, 99.98%), Aliquat® 336 (Aldrich; hereafter Q^+Cl^-) were used as received. Zinc powder (Aldrich, -100 mesh, 99.998%) was washed with dilute acid (2% HCl), water, ethyl alcohol and diethyl ether; and then dried under vacuum overnight before use. Isotopic $^{18}O_2$ gas (95.6%) was purchased from Cambridge Isotope Lab, Inc. Chemicals used in the iodometric titration are: NaI, $Na_2S_2O_3 \cdot 5H_2O$ and isopropyl alcohol (Fisher scientific); glacial acetic acid (Mallinckrodt), and KIO_3 (Mallinckrodt, analytical reagent). Deionized water was used for solution preparations. Cyclohexene (Aldrich, 99%) was distilled over sodium under

argon and stored in the drybox. Prior to use, it was passed through a neutral alumina column under nitrogen to remove traces of hydroperoxides. $[Bu_4N]_5Na_3[(1,5\text{-}COD)Ir{\cdot}P_2W_{15}Nb_3O_{62}]$ was made by our most recent method[23,24] (except that crystalline $[(1,5\text{-}COD)Ir(CH_3CN)_2]BF_4$ was employed in the synthesis[25]) and then stored in the drybox.

Instrumentation. Infrared spectra were obtained on a Nicolet 5DX spectrometer using KBr disks. The nuclear magnetic resonance spectra in D_2O or $CDCl_3$ (Cambridge Isotope Lab, Inc.) were obtained on a Varian Inova (JS-300) NMR spectrometer. A high precision (±0.02 psig at 14 psig or ±0.15%) oxygen pressure transducer was purchased from Omegadyne Inc., model number PX02C1-100G10T-OX. (**CAUTION:** standard pressure transducers need to be cleaned by the manufacturer before their use with oxygen, as any leftover oil from calibration or dirt inside the transducer is potentially flammable/explosive in the presence of O_2.) The automatic data collection was implemented by integration of the pressure transducer to an analog-to-digital converter; the data were collected electronically with LabView 6.1 software. A more detailed view of this apparatus is available elsewhere[26] (note that there it is used for H_2, not O_2 reactions). GC analyses were performed on a Hewlett-Packard 5890 Series II gas chromatograph equipped with a FID detector and a SPB-1 capillary column (30 m, 0.25 mm I. D.) with the following temperature program for adamantane hydroxylation products: initial temperature, 140 °C (initial time, 4 min); heating rate, 5 °C/min; final temperature, 180 °C (final time, 3 min); FID detector temperature, 250 °C; injector temperature, 250 °C. An injection volume of 1 μL was used. Product peaks were identified by comparison to authentic sample peaks; product amounts were quantitated by

external calibration using authentic samples. GC-MS analyses were carried on an Agilent 6890 series GC system with a SPB-1 capillary column and an Agilent 5973 Mass Selective Detector. The temperature program is the same as that used above in GC analyses. TGA-MS analyses were performed on a TGA 2950 Thermogravimetric Analyzer (TA Instruments, Inc.) coupled with a ThermoStar mass analyzer (Balzer Instrument). CHN elemental analyses were performed by Atlantic Microlab, Inc. (Norcross, Georgia). Cyclic voltammetric data were obtained using a standard three-electrode cell with an EG&G PAR model 173 potentiostat/galvanostat controlled by a model 175 Universal Programmer. The reference electrode was Hg/Hg_2Cl_2 in saturated NaCl (0.236 V vs SHE). The auxiliary electrode was a 0.5 cm^2 platinum flag, and the working electrode was a glassy carbon electrode. Prior to use, the working electrode was polished on a felt pad with a water slurry of 0.3 μm alumina polishing powder, followed by rinsing with distilled water and dichloromethane.

Preparation of Precatalyst $\{[WZnRu^{III}_2(OH)(H_2O)](ZnW_9O_{34})_2\}^{11-}$. The precursors $Na_{12}[WZn_3(H_2O)_2(ZnW_9O_{34})_2]\cdot 46\sim 48H_2O$ (pre-crystallization yield 71 g, 51%; lit. 90–95 g, 65–68%) and $[Ru^{II}(DMSO)_4]Cl_2$ (recrystallized yield ca. 4.0 g, 70–79%; lit. 72%) were both synthesized and recrystallized according to the literature.[27,28] The ^{1}H-NMR of recrystallized $[Ru^{II}(DMSO)_4]Cl_2$ was identical to a recent published preparation by Nomiya and coworkers.[29] ^{1}H NMR ($CDCl_3$): δ (major peaks) 2.63, 2.72, 3.30, 3.42, 3.48 and 3.51; literature ($CDCl_3$): δ (major peaks) 2.60, 2.72, 3.32, 3.43, 3.48, 3.50.[29] $K_{11}[WZnRu_2(ZnW_9O_{34})_2]\cdot 15H_2O$ was prepared and recrystallized twice from hot water according to the literature.[30] Yield 3.73 g, 16%; lit. 5.7 g, 24%. $K_{11}[WZnRu_2(ZnW_9O_{34})_2]\cdot 15H_2O$ was examined by ^{1}H-NMR in D_2O: δ 4.8 (solvent peak

only, no remaining DMSO). The UV-visible spectrum in water shows only one peak at 284 nm (ε = 24 000 $M^{-1}\cdot cm^{-1}$), different from the literature which reports two peaks at ~300 nm (ε = ~50 000 $M^{-1}\cdot cm^{-1}$) and 430 nm.[30] The 430 nm peak has been assigned as a O→Ru charge transfer band.[30] TGA in the 50–250 °C range on a sample predried in a vacuum oven (at ca. 1 Torr) overnight at 40 °C showed a 2–3% weight loss corresponding to 7–10 waters, that is $K_{11}[WZnRu(III)_2(OH)(H_2O)(ZnW_9O_{34})_2]\cdot 7\text{–}10H_2O$. The organic counterpart of this polyoxometalate salt $Q_{11}\{[WZnRu_2(OH)(H_2O)](ZnW_9O_{34})_2\}$, Q_{11}-**1**, was synthesized via the published method[30] with the following additional steps: after drying over $MgSO_4$, the organic phase was separated from $MgSO_4$ by a filtration on a glass frit. The filtrate was then dried under vacuum overnight at room temperature. The yield of the gum-like, red-orange compound was ca. 50–65%; no literature yield has been reported. IR data (as a drop on KBr, as done previously[13]): 723 (s), 766 (s), 871 (m), 921 (m) cm^{-1} (see the Supporting Information, Figure S5.1); literature[12,13]: 765 (s) [a broad peak with a full width at half maximum of ca. 80 cm^{-1} (720–800 cm^{-1}), two identifiable peaks within this range at ca. 730 and 750 cm^{-1}], 881 (m), 928 (m) cm^{-1}. The microanalysis data confirm the previous finding by another researcher in our labs (i.e., for an independent preparation)[5] that precatalyst **1** is impure. The composition is approximated by $Q_{11}\{[WZnRu_2(OH)(H_2O)](ZnW_9O_{34})_2\}\cdot nQCl$; the value of n was estimated from the CHN analysis (n = 2–4 for three different batches of Q_{11}-**1**). Herein the value of n ≈ 2–3 gives the "best" fit to the analysis; calculated (for the formulation shown above, and n = 2–3) [found; repeat found (i.e., repeat analysis)]: C, 39.51–40.88 [40.57, 40.68]; H, 7.16–7.41

[7.52, 7.38]; and N 1.84–1.91 [1.64, 1.55].[xviii] No elemental analysis was reported in the original paper[30] for comparison. Cyclic voltammogram of Q_{11}-**1** in 1,2-$C_2H_4Cl_2$ (with 0.1 M $TBAClO_4$, at a glassy carbon working electrode, vs SSCE at a sweep rate of 100 mV/s) shows two irreversible oxidation peaks at +0.94 V and +1.22 V, but no reduction peaks out to even –1.0 V (Figure S5.5 in the Supporting Information).

General Procedures for Oxygen-uptake Experiments. Adamantane hydroxylation was monitored either by the formation of 1-adamantanol (via periodic sampling and subsequent GC analysis) or by the oxygen pressure decrease (via the computer-interfaced oxygen pressure transducer, *vide supra*). The reaction flask is a pressurized Fischer–Porter bottle attached via Swagelock quick-connects and flexible stainless steel tubing to both an oxygen tank and to the pressure transducer (total volume 148 mL).[26] In the drybox, the adamantane substrate (typically 341–817 mg, 2.5–6.0 mmol) was weighed into a 22 mm × 175 mm Pyrex culture tube along with a 5/8 × 5/16" Teflon stir bar. The precatalyst (typically 25–60 mg, 2.5–6.0 μmol) was weighed into a 5 mL glass vial with a pre-weighed stainless steel spatula. Then the precatalyst was dissolved in 1,2-$C_2H_4Cl_2$ (unless stated otherwise) and quantitatively transferred into the culture tube with a disposable pipet. The culture tube was then placed inside the Fischer–Porter bottle, sealed, brought out of the drybox, placed in a temperature-controlled oil bath, and attached to the oxygen uptake apparatus via the quick-connects. Stirring was initiated and the solution was equilibrated in the oil bath (80 °C) under N_2 (from the drybox gas) for 40 min. The Fischer-Porter bottle was then purged 15 times

[xviii] The uncertainty in determining the exact value of n (±1) in Q_{11}-**1**·nQCl contributes to an error of ≤±4% in the estimation of the molecular weight of Q_{11}-**1** used throughout this work. However, this error will not change the major conclusions in this paper. This ≤±4% error is also smaller than the error (≥8% for n ≥ 2) in the prior work where no such molecular weight correction was considered.[12,13]

with ~14 psig of O_2 (or ~1.8 atm; the atmosphere pressure at the ca. 1 mile-high altitude of Fort Collins, Colorado is around 632 Torr, or 0.83 atm); 15 s/purge, equilibrate 1 min 15 s; 5 min total time elapsed before the pressure recordings were started. The reaction vessel was then pressurized to 14 ± 1 psig and t = 0 was set. During GC sampling, a 500 μL syringe with a 20 inch stainless-steel needle was used to sample 200–300 μL aliquots of the reaction solution under a positive oxygen flow. Following sampling, two additional purges with O_2 were performed. The sample solution was diluted with 1,2-$C_2H_4Cl_2$ (41 fold) and then analyzed by authentic-sample-calibrated GC.

Pressure Control Experiment at 1 atm O_2. This control was performed to ensure that reaction products did not change when the reaction was run at 1.0 vs 1.8 atm O_2. To start, 6.0 mmol of adamantane, 6.0 μmol of precatalyst Q_{11}-**1**, and 12.0 mL of 1,2-dichloroethane were measured into a 22 mm × 175 mm Pyrex culture tube along with a 5/8 × 5/16" Teflon stir bar. The culture tube was then placed inside the Fischer–Porter bottle, sealed and brought out of the drybox. The Fischer-Porter bottle was placed in a dry ice/ethanol bath (-72 °C). After the reaction solution was frozen, two pump and fill cycles were performed with 1 atm O_2. Next, the dry ice/ethanol bath was replaced by a temperature-controlled oil bath (80.0 ± 0.5 °C) and stirring was initiated; t = 0 was set when the oil bath reached 80.0 °C (ca. 25 min). At the end of the reaction (t = 24 h), the product yields were determined by calibrated GC to be 13 ± 1% of 1-adamantanol and 2.5 ± 0.1% of 2-adamantanone. These values are the same within experimental error as the yields (12 ± 1% of 1-adamantanol and 2.2 ± 0.4% of 2-adamantanone) under the Standard Conditions employed (6.0 mmol of adamantane, 6.0 μmol of Q_{11}-**1**, 12.0 mL of 1,2-dichloroethane, and 1.8 atm O_2).

Reaction-Scale Control Experiment. A control was performed to make sure the reaction scale has no effect on the yields or selectivity. A run at the conditions used in the previous studies[12,13] (0.25 mmol of adamantane, 0.25 μmol of precatalyst Q_{11}-**1**, and 0.5 mL of 1,2-dichloroethane) was performed in a ca. 15 mL pressure tube (Ace Glassware) with a 3/8 × 3/16" Teflon stir bar. The reaction mixture was frozen by a dry ice/acetone bath (-79 °C) and subjected to two pump and fill cycles using O_2. The pressure tube was filled with ca. 1 atm oxygen gas through an opening on the plunger valve sealing the pressure tube, the opening was then closed, the dry ice bath was replaced by a temperature-controlled oil bath (80.0 ± 0.5 °C), and stirring was initiated; t = 0 was set when the oil bath reached 80.0 °C (ca. 15 min). At the end of the reaction (24 h), the product yields were determined by calibrated GC to be 15 ± 1% of 1-adamantanol and 2.7 ± 0.1% of 2-adamantanone. These values are the same within experimental error as the yields (12 ± 1% of 1-adamantanol and 2.2 ± 0.4% of 2-adamantanone) under the Standard Conditions we employ of a 24-fold increase: 6.0 mmol of adamantane, 6.0 μmol of Q_{11}-**1**, 12.0 mL of 1,2-dichloroethane, and 1.8 atm O_2. Trace products were also identified.[xix]

Organic Peroxide Detection and Quantitation. A qualitative test of peroxide presence was performed by shaking a 10% KI/starch solution with the final reaction mixture obtained from a standard, scaled-up run (6.0 mmol of adamantane, 6.0 μmol of Q_{11}-**1**, 12.0 mL of 1,2-dichloroethane, and 1.8 atm O_2) after 24 hours of reaction time. The aqueous layer slowly turned violet. Quantitative analysis of organic peroxide was accomplished by the standard iodometric titration method[21,31] performed immediately following a standard run of adamantane hydroxylation. Specifically, 40 mL of isopropyl

alcohol and a Teflon stir bar were introduced into a 250 mL Erlenmeyer flask. The flask was equipped with a gas inlet tube and a reflux condenser; 2 mL of glacial acetic acid and a 2 mL aliquot of the reaction solution (24 h) from the scaled-up reaction were then added into the flask. The mixture was purged to remove oxygen by bubbling with argon gas for 15 min through either a stainless steel syringe or a soft Teflon syringe needle (the latter as a control to avoid possible ROOH decomposition by the steel syringe needle). The experiments using different syringes gave equivalent results; hence the stainless steel syringe needle did not induce ROOH decomposition on the timescale and at the temperature of our experiments. The solution was heated to reflux and 10 mL of a saturated solution of sodium iodide in isopropyl alcohol (prepared by refluxing 25 grams of sodium iodide in 100 mL of isopropyl alcohol) was added to the refluxing solution from the top of the condenser; the solution was then refluxed for 5 additional minutes. The mixture was removed from the heating plate and titrated immediately with aqueous 0.01 M standard sodium thiosulfate solution (standardized using a primary standard KIO_3 solution with H^+/KI through titration). A blank titration was performed for each peroxide titration using the same procedure as above, except that the sample solution was replaced by a 0.5 M adamantane solution in 1,2-$C_2H_4Cl_2$ (to mimic the reaction conditions). The results, which are described in the main text, are the average of four titrations of product solutions from two identical adamantane hydroxylation experiments. In addition, ca. 5.5 M of commerical *t*-BuOOH was titrated as a control experiment to check the titration method in our hands (observed 5.9 M in two repeat titrations, results in good agreement with the labeled value).

$H_2{}^{18}O$ Detection. The prior work claimed that "no $H_2{}^{18}O$ was observed" (see p. 354 elsewhere[12]) in the catalytic adamantane hydroxylation using $^{18}O_2$; however, no detection limit was given.[12] In our studies, a control was performed first using the cheaper (than $H_2{}^{18}O$) D_2O (m/z = 20) to mimic the $H_2{}^{18}O$ (m/z = 20) and to estimate our detection limit. In this control, D_2O (0.45 μL, 0.025 mmol, the same amount as the $H_2{}^{18}O$ generated from the reaction at 100 turnovers based on 0.25 μmol Q_{11}-**1**) was deliberately injected into 0.5 mL 1,2-dichloroethane and, then, this solution was added to ~100 mg pre-dried 4 Å molecular sieves (Mallinckrodt, Grade 514GT, predried at >250 °C under vacuum overnight, followed by cooling and then storage under vacuum before use in the air). The solution and mol sieves were swirled by hand for a ca. 1 minute period (controls, *vide infra*, showed that longer mixing times (1 hr vs 1 min) of the molecular sieves with sample solution did not give a stronger signal (at m/z = 20), that is, did not change the results). The solution was then removed by a disposable pipet. The molecular sieves were collected using a stainless steel spatula, placed into a glass vial, and then into an aluminum pan of a TGA apparatus (TGA 2950, TA Instruments) using a pair of stainless steel tweezers, all quickly as possible in the open air. Upon heating the molecular sieves at 10 °C/min or, separately, 50 °C/min up to 600 °C in the TGA apparatus, $D_2O^{\bullet+}$ (m/z = 20), $H_2O^{\bullet+}$ or $DO^{\bullet+}$ (m/z = 18), $HO^{\bullet+}$(m/z = 17), and the deuterium-exchange product H–$O^{\bullet+}$–D (m/z = 19) were detectable by the mass analyzer (resolution ≥±0.5 amu) directly coupled to the TGA instrument. These controls demonstrate that our detection limit of D_2O (as a surrogate for $H_2{}^{18}O$ in the real run,) is lower than ~0.025 mmol (<10% compared to the adamantane substrate) and assuming no major differences in the detectability of D_2O vs $H_2{}^{18}O$.

Next, we repeated the adamantane hydroxylation experiment using $^{18}O_2$. A run at the standard conditions (0.25 mmol of adamantane, 0.25 μmol of precatalyst Q_{11}-**1**, 0.5 mL of 1,2-dichloroethane) of the previous studies[12,13] was performed in a ca. 15 mL pressure tube (Ace Glassware) with a 3/8 × 3/16" Teflon stir bar. The reaction mixture was frozen by a dry ice/acetone bath (-79 °C) and subjected to two pump and fill cycle using $^{18}O_2$ (ca. 1 atm $^{18}O_2$ was introduced to the pressure tube through the opening on the plunger valve sealing the pressure tube). The opening was closed and the dry ice bath was replaced by a temperature-controlled oil bath (80.0 ± 0.5 °C); t = 0 was set when the oil bath reached 80.0 °C (ca. 15 min). The reaction was stopped after 24 h. The reaction solution (~0.5 mL) was mixed for ca. 1 minute with ~100 mg of Mallinckrodt, Grade 514GT 4 Å molecular sieves pre-dried at at >250 °C under vacuum overnight as detailed above. Next, the solution was removed using a disposable pipet. The mol sieves were transferred into a closed vial with a stainless steel spatula, then quickly placed in the aluminum TGA pan in the open air using a pair of stainless steel tweezers (ramp 50 °C/min to 600 °C during TGA-MS analysis). Ion currents corresponding to $H_2{}^{18}O$ (m/z = 20 and 19 for $H^{18}O^{\bullet+}$) and H_2O (m/z = 18 and 17 for $HO^{\bullet+}$) were detected.

A blank control was also performed in the exact same manner as above, except that no precatalyst, Q_{11}-1, was added. In that control, pre-activated mol sieves were mixed with 0.5 mL 0.5 M adamantane solution that had been stirred under $^{18}O_2$ at 80 °C for 24 h. The expected, unavoidable background $H_2{}^{16}O^{\bullet+}$ peaks (m/z = 18 and 17) were observed; signals at m/z = 20 (due, apparently, to m/z = 20 $Ar^{\bullet 2+}$ and/or *possibly* some $H_2{}^{18}O^{\bullet+}$ and $H^{18}O^{\bullet+}$ formed from $^{18}O_2$ in the EI detector) and m/z = 19 were also observed,

but their level is less than 1/3 that of the signals from the run with Q_{11}-**1**. The observed mass spectra are given in Figure 5.4.

In one TGA-MS control experiment, an opening on the TGA chamber was left unplugged during the heating (i.e., the molecular sieves were deliberately exposed to moist air). Higher signals of $H_2O^{\bullet+}$ (m/z = 18 and 17 for $HO^{\bullet+}$) were observed along with higher signals at m/z = 20 ($Ar^{\bullet 2+}$) and 19; we interpret the latter as unresolved m/z = 18 from the large $H_2{}^{16}O^{\bullet+}$ peak due to a mass analyzer resolution of only around 1–0.5 amu. Hence, it is crucial for controls to be performed, such as the one above to establish the background signal.

H_2O Yield. The amount of H_2O produced was estimated by TGA from the weight loss during heating up to 550 °C in two repeat experiments (e.g., from a 119 mg sample in one run produced from the 100 mg of original mol sieves), Figure S5.2 of the Supporting Information. A total weight loss of 19% (18% from a 122 mg sample in the repeat run) was observed, 15% of that loss being observed in a sharp weight drop by 100 °C with the other 4% being more slowly evolved up to 550 °C. Concomitant MS analysis (e.g., Figure 5.4) confirms that H_2O is being evolved throughout this temperature range up to 550 °C. The ratio of $H_2{}^{16}O$ to $H_2{}^{18}O$ was calculated from the integral area of the ion currents of $(H_2{}^{16}O^{\bullet+} + H^{16}O^{\bullet+})/(H_2{}^{18}O^{\bullet+} + H^{18}O^{\bullet+})$ up to 550 °C.

Detection of ^{18}O-Containing Organic Products. In the adamantane hydroxylation experiment using $^{18}O_2$ under the procedure described in the above section, the organic products after 24 h were tested for $^{18}O_2$ inclusion by GC-MS. The reaction solution was diluted with 1,2-$C_2H_4Cl_2$ (41 fold) and then analyzed by GC-MS. The major product, 1-adamantan-^{18}O-ol (m/z = 154 as the molecular ion peak), exhibited an

abundance of $^{18}O/(^{18}O + ^{16}O)$ of ca. 96% once a correction for the 95.6% abundance of the $^{18}O_2$ used was made, *vide infra*). The 2-adamantan-^{18}O-one (m/z = 152) contains 39% ^{18}O. The other trace products (yield ≤ 0.5%) are: adamantane-1,3-di-^{18}O-ol (m/z = 172) containing ^{18}O in 60% abundance (di-^{18}O-ol vs di-^{18}O,^{16}O-ol ratio of 1:4.4; no di-^{16}O-ol was detected) and 2-adamantan-^{18}O-ol (m/z = 154) containing ^{18}O in 55% abundance, all after correction for the 95.6% abundance of the $^{18}O_2$ used.

Attempted Preparation of 1-Adamantyl Peroxide. There is only one published preparation of 1-adamantyl peroxide, one with no experimental details.[32] Details of our three attempted preparations of this peroxide are provided in the Supporting Information.

Kinetic Experiments. Kinetic experiments were performed under the same conditions as the previous researchers performed their kinetic runs (2.5 mmol of adamantane, 2.5 μmol of precatalyst Q_{11}-**1,** 5.0 mL of 1,2-dichloroethane, 80 °C);[13] the only exception is the higher pressure 1.8 atm employed herein vs the 1 atm used in the prior work.[13] The start-up procedures are the same as stated in the "General Procedures for Oxygen-uptake Experiments". The kinetics of 1-adamantanol formation were followed by authentic-sample-calibrated GC. Steady-state/maximum rates, post the induction period, were measured as shown in Figure S5.3 of the Supporting Information. Kinetic derivations were done, therefore, under the steady-state assumption as detailed in the Supporting Information.

Kinetic Results Fitting By Mackinetics. Mackinetics (a free software designed by Walter S. Leipold III, P.E. for chemical reaction kinetics modeling; product information is at http://members.dca.net/leipold/mk/advert.html) was used to curve-fit the kinetic results in Figure 5.8. To start, a set of chemical equations together with

experimental data were written into Mackinetics (the exact reactions used in Mackinetics are listed in the Supporting Information). Next, a grid search was performed to fit the kinetic parameters to one or more sets of experimental data. Specifically, the kinetic parameter search was performed first in a broad range of the parameters (10^{-9}–10^{9}) by the grid search command in Mackinetics. Then, the grid search was narrowed down to a bit more than half the previous range (e.g., if the first search gave $k_1 = 0.01$ and $k_2 = 0.1$ as the best fit in the range of 10^{-9}–10^{9}, then the second search was performed in the range of 10^{-7}–10^{3} for k_1 and 10^{-6}–10^{4} for k_2); the center of the new range was always set to equal the result from last grid search as in the above examples. The search was deemed finished once a grid search was performed in a range no larger than two orders of magnitude. The data for curve-fits shown (in Figure 5.8) are those obtained by performing a final integration, using the best set of kinetic parameters, and then co-plotting that data with the observed, experimental data.

Determination of the Reaction Stoichiometry. Two different methods were applied in the stoichiometry studies: a two-point method to mimic that used in the original work,[13] and a more precise and more reliable multi-point, real-time method employing a ±0.15% high-precision pressure transducer. The reaction conditions employed for the two-point method were: 1.5 mmol adamantane, 1.5 μmol Q_{11}-**1**, 3 mL 1,2-dichloroethane, and 80 °C in the first two runs (6 fold higher than the scale used in the previous studies[13]); reaction conditions in a third, repeat run were (24 fold higher than before[13]): 6.0 mmol adamantane, 6.0 μmol Q_{11}-**1**, 12 mL 1,2-dichloroethane, and 80 °C. The specific details of the two-point method mimicking the literature[13] are: after introducing 1 atm of O_2 into the reaction flask at room temperature, the pressure was

recorded (by a mercury manometer or, in the third run, the oxygen pressure transducer was used) and then the reaction flask was sealed and heated up in an 80 °C oil bath (t = 0 was set when the oil bath reached 80.0 °C; this took ca. 10–30 min). After 24 hours, the reaction flask was removed from the oil bath and cooled to ambient temperature over 30 min. Then, the second pressure point was recorded by reopening the valve connected to the manometer (or, in the third run, the O_2 pressure transducer).

The multi-point, real-time method allows collection of data by the oxygen pressure transducer connected to the reaction flask as described back in the Instrumentation Section. The reaction conditions for the real-time method employed a 24-fold increase in the absolute amounts, *vide supra*: 6.0 mmol adamantane, 6.0 μmol Q_{11}-**1**, 12 mL 1,2-dichloroethane, and 80 °C in the first run; then 6.0 mmol adamantane, 6.0 μmol Q_{11}-**1**, 6 mL 1,2-dichloroethane, and 80 °C in the remaining four runs (a 24-fold increase in reagents and a 12-fold increase in the amount of solvent). The other procedures employed are the same as described in the section titled "General Procedures for Oxygen-uptake Experiments". Data points were taken every 10 min. The results are shown in Table 5.1 and Figure 5.7. The ΔpO_2 data collected in Table 5.1 were obtained by first correcting the initial part of the data for the vapor pressure due to the solvent (i.e., the rise in the pressure due to the solvent's vapor pressure as is apparent for the one run shown in Figure 5.7). The solvent vapor pressure was measured in an independent experiment in which solvent only was present. The resulting $\Delta P(O_2) = P(O_2, \text{initial}) - P(O_2, \text{final})$ proved to be the same within experimental error as the ΔpO_2 determined from the uncorrected data as shown for the one run in Figure 5.7.

Initiation and Inhibition Experiments. Initiation and inhibition experiments were performed with a slight variation of the "General Procedures for Oxygen-uptake Experiments". The initiation experiments employing the addition of H_2O_2 (0.2 mmol, 20 μL, 30% w.t. H_2O_2) or H_2O (0.9 mmol, ~17 μL, as a control in a separate run) were started as normal experiments except, after 12 purges of oxygen, the initiator was added into the reaction flask via a 1 mL airtight syringe and the reaction flask was then purged 3 more times with O_2. The other initiation and inhibition experiments were all started with the additives pre-mixed with the reaction mixture in the drybox (0.2 mmol AIBN, ~0.2 mmol *t*-BuOOH, 6 μmol Zn, 0.2 mmol PBN, 0.2 mmol galvinoxyl, 0.21 mmol 4-*tert*-butylcatechol or 0.2 mmol BHT in nine separate runs). The formation of 1-adamantanol was followed by GC.

Cyclohexene Autoxidation Experiments. This control was performed to see if Q_{11}-**1** is a good autoxidation catalyst for readily autoxidized substrates, such as cyclohexene, and in comparison to known autoxidation precatalysts such as the $[Bu_4N]_5Na_3[(1,5\text{-COD})Ir{\bullet}P_2W_{15}Nb_3O_{62}]$ complex.[21] First, ~9 μmol precatalyst ($[Bu_4N]_5Na_3[(1,5\text{-COD})Ir{\bullet}P_2W_{15}Nb_3O_{62}]$ or Q_{11}-**1** in two independent runs) were weighed out in the drybox into a 50 mL round-bottom reaction flask equipped with an egg-shaped 3/4 × 3/8" Teflon stirring bar. Next, 6 mL pre-dried HPLC grade 1,2-dichloroethane and 1 mL distilled cyclohexene (chromatographed through an 8 cm × 1 cm neutral alumina column in the drybox prior to use to remove trace peroxides) were transferred into the flask and then the flask was sealed with a Teflon stopcock and taken out of the drybox. The flask was connected to an oxygen-uptake line through an O-ring joint, and the reaction solution was frozen in a dry ice-ethanol bath (-72 °C) for 10 min and two pump

and fill cycles with ~1 atm O_2 were performed. Next, the dry ice bath was replaced with a temperature-controlled oil bath, the flask was brought up to 40 ± 0.4 °C, and t = 0 was set. The reaction was stopped after 24 h, and the product solution was diluted with 1,2-$C_2H_4Cl_2$ (41 fold) for GC analysis (SPB-1 capillary column): temperature program, initial temperature, 50 °C (initial time, 4 min); heating rate, 10 °C/min; final temperature, 160 °C (final time, 5 min); injector temperature, 250 °C; detector temperature, 250 °C. The results are presented in Table 5.3; GC traces are shown as Figure S5.6 in the Supporting Information.

Attempted Catechol Oxygenation Reactions. This experiment was performed to see if Q_{11}-**1** could serve as a precatalyst for known catechol dioxygenase reactions.[5,9] To start, ~400 mg 3,5-di-*tert*-butylcatechol that had been recrystallized three times (from pentane under Ar, m.p. = 99–100 °C) was weighed out in the drybox into a 50 mL round-bottom reaction flask equipped with a septum, side-arm and an egg-shaped 3/4 × 3/8" Teflon stirring bar. (NB: it is important to recrystallize the 3,5-di-*tert*-butylcatechol ≥3 times to remove impurities like 3,5-di-*tert*-butylsemiquinone.)[5,6] Approximately 8 mL pre-dried HPLC grade 1,2-dichloroethane were transferred into the flask using a 10-mL glass syringe, the flask was sealed with a Teflon stopcock, and then taken out of the drybox. The flask was connected to the oxygen-uptake line through its O-ring joint, and the reaction solution was frozen in a dry ice/ethanol bath (-72 °C) for 10 min after which two pump and fill cycles with ~1 atm O_2 were performed. Next, the dry ice bath was replaced with a temperature-controlled oil bath, the flask was brought up to 40 ± 0.4 °C, and allowed to equilibrate with stirring for 25 min during which a solution of precatalyst, Q_{11}-**1** was prepared as follows. In the drybox, 47.2 mg of Q_{11}-**1** (ca. 7.3 μmol) was

weighed into a glass vial and dissolved in ca. 0.2 mL 1,2-dichloroethane. The catalyst solution was drawn into a gastight syringe and brought out of the drybox with its needle protected from air in a septum-capped-vial. The catalyst was then injected through the sidearm of the 40 °C reaction flask and t = 0 was set. The pressure reading from the manometer was used to follow the reaction. The reaction was stopped at 133 h, and the product solution was diluted (21 fold) with 1,2-$C_2H_4Cl_2$ prior to GC analysis. The final product is the autoxidation product 3,5-di-*tert*-butylbenzoquinone (17%); no dioxygenase cleavage products[5] were detected despite our ability to routinely detect ≤1% of those products.[7]

Results and Discussion

A Choice of Standard Reaction Conditions. The standard conditions in the previous work[12,13] are: 0.25 mmol of adamantane, 0.25 μmol of precatalyst, **1**, 0.5 mL of 1,2-dichloroethane, 1 atm of oxygen, and 80 °C. In the previous *kinetic* studies, the above amounts of reagents were scaled up 10-fold (except O_2).[13] We have employed these exact same conditions and concentrations, including the 10-fold scale-up for kinetic studies, except that we have scaled up the product studies by 24-fold *in the absolute amounts of reagents used* (i.e., while keeping the absolute concentrations the same) in order to achieve better precision in especially the O_2-uptake studies. Additionally, the slightly higher O_2 pressure we applied (1.8 atm of O_2 vs 1 atm in the prior work[12,13]) was found to exhibit little effect on the reaction kinetics (which are ca. half order in O_2, see Figure 5.6C, *vide infra*) and no detectable effect on the product yields as demonstrated in the following control experiment: the yields at 1 atm O_2 (of 13 ± 1% of 1-adamantanol

and 2.5 ± 0.1% of 2-adamantanone) are the same within experimental error as the yields at 1.8 atm O_2 (where 12 ± 1% of 1-adamantanol and 2.2 ± 0.4% of 2-adamantanone are formed).

Moreover, under our (scaled-up) standard conditions (namely 6.0 mmol of adamantane, 6.0 μmol of precatalyst, 12.0 mL of 1,2-dichloroethane, 1.8 atm of oxygen, and 80 °C), the yield of the main product,[xix] 1-adamantanol, 12 ± 1% after 24 h, is identical within experimental error to that reported in the prior work, 12.3% at 24 h.[13] The minor product, 2-adamantanone was detected at a yield of 2.2 ± 0.4%, Figure 5.3, compared to none in the prior work. Mass balance in our studies averaged 95 ± 5% with a range of 92–99% (mass balance was not reported in the previous work[12,13]).

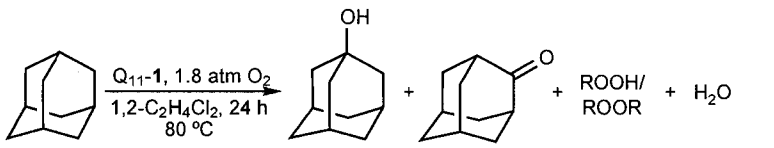

	1-adamantanol	2-adamantanone	organic peroxide (s)	(by TGA-MS)
Previous work	12.3%	-	-	-
Current study	12 ± 1%	2.2 ± 0.4%	0.5%	~8%

Figure 5.3 Adamantane hydroxylation under standard conditions. Product yields (the average of five runs) were determined by authentic-sample-calibrated GC.

Peroxide Detection and Quantitation. Since adamantyl hydroperoxide (Adm-OOH) should be the primary, at least initial product generated from a free-radical-chain autoxidation reaction, and since the peroxide Adm-OO-Adm is expected as part of

[xix] Other trace products detected are: ~0.2–0.3% adamantane-1,3-diol (m/z = 168) and ~0.4–0.5% 2-adamantanol (m/z = 152). The upper limit of these trace products is ~0.5%, estimated by the Effective Carbon Numbers (Grob, R. L.; Ed. *Modern Practice of Gas Chromatography*; 3rd ed.; John Wiley & Sons, Inc.: New York, 1995, pp 279-280). The order of GC elution of these products on a low-polarity column (SPB-1 in this study) is: adamantane, 1-adamantanol, adamantane-1,3-diol, 2-adamantanone, and then 2-adamantanol.

termination of a Adm-OO• radical chain, we performed experiments to see if these ROOH / ROOR could be detected in the reaction products. Iodometric titration of a freshly reacted solution (24 hours reaction time) revealed a small, but non-zero, amount (0.5%, relative to the substrate) of organic peroxide products ROOH and/or ROOR. Note that the conversion is relatively low, and it is known in the literature that ROOR products are typically under-detected in autoxidation reactions,[33,34] so that we regard the 0.5% peroxide as *a lower limit* on the amount of peroxides actually present. Three attempts were made to prepare authentic 1-adamantyl hydroperoxide following the ambiguous procedures available in the literature,[32] but all failed. Nevertheless, detection of any peroxide is inconsistent with published claim of solely a dioxygenase[12,13] and demands at least *some* contribution from an autoxidation route. Furthermore, in the Kinetic Studies section presented next, we will show that the rate law provides compelling support for an autoxidation pathway.

$^{18}O_2$ Labeling Studies and $H_2{}^{18}O$ Detection. The prior work claimed that "no $H_2{}^{18}O$ was observed" when the reaction was run under $^{18}O_2$ (see p. 354 elsewhere[12]), but failed to give a $H_2{}^{18}O$ detection limit.[12] On the other hand, the autoxidation mechanism predicts that $H_2{}^{18}O$ will be formed if $^{18}O_2$ is used. Hence, whether or not H_2O is formed is a clear test to distinguish between the claimed dioxygenase pathway vs a well-precedented, classic autoxidation mechanism.

First, control experiments were performed to confirm our ability to detect trace amounts of $H_2{}^{18}O$ (D_2O was used instead here as a m/z = 20 surrogate for the m/z = 20 $H_2{}^{18}O^{\bullet+}$ formed from the more expensive $^{18}O_2$). Our detection limit is ≤0.025 mmol (≤10% yield); details are available in the Experimental Section.

Next, an adamantane hydroxylation reaction, Figure 5.3, was performed at the smaller scale of 0.25 mmol adamantane, 0.25 μmol Q_{11}-**1**, 0.5 mL 1,2-$C_2H_4Cl_2$ and with 1 atm $^{18}O_2$ (i.e., 1/24 of our normal scale, to reduce the amount of $^{18}O_2$ required). After 24 h (ca. 150 turnovers), pre-activated 4 Å molecular sieves were added to the reaction solution. The reaction solution was removed by a pipet. Next, the molecular sieves were collected and then subjected to TGA-MS analysis. Besides the unavoidable $H_2{}^{16}O^{\bullet+}$ background peaks (m/z = 18, plus a fragment peak due to $HO^{\bullet+}$ at m/z = 17), the results reveal the presence of $H_2{}^{18}O^{\bullet+}$ (m/z = 20 with its fragment peak of $H^{18}O^{\bullet+}$ at m/z = 19). In a control, 0.5 mL adamantane solution was stirred under $^{18}O_2$ for 24 h at 80 °C and subsequently treated as above with pre-activated 4 Å molecular sieves. A lower level of signals at m/z = 20 or 19 was observed which was less than one third that with the precatalyst, **1**, Figure 5.4. The background peaks are due, apparently, mostly to m/z = 20 $Ar^{\bullet 2+}$ and the limited ability of the 0.5–1.0 amu resolution mass analyzer to deal with the background of $Ar^{\bullet 2+}$ or $H_2{}^{16}O^{\bullet+}$. These results, alone, argue strongly against the prior dioxygenase mechanism as the *sole* pathway as previously claimed, as that pathway does not produce H_2O.

The GC-MS of the organic products and their ^{18}O content was also examined. GC-MS of the reaction solution after 24 h shows a 96% abundance of ^{18}O in the main product: 1-adamantan-^{18}O-ol. Interestingly, the 2-adamantan-^{18}O-one contains only 39% ^{18}O, while the trace products (yield ≤ 0.5%) also incorporate less than 100% ^{18}O: adamantane-1,3-di-^{18}O-ol contains ^{18}O in 60% abundance (the di-^{18}O-ol / di-^{18}O,^{16}O-ol ratio is 1/4.4; no di-^{16}O-ol was detected), and 2-adamantanol contains ^{18}O in only 55% abundance. Reflection on these data yield the following insights: (i) a dioxygenase

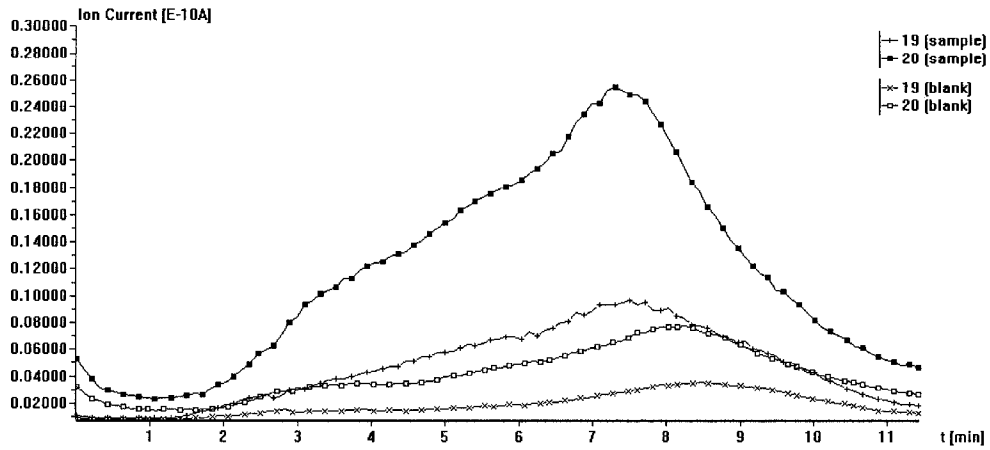

Figure 5.4 TGA-MS results of the molecular sieves added to, then harvested from, the adamantane hydroxylation reaction solution under $^{18}O_2$ plus precatalyst Q_{11}-**1**. A blank consisting of the molecular sieves mixed with adamantane solution stirred under $^{18}O_2$ without Q_{11}-**1** is shown for comparison. The ion currents at 20 (m/z, $H_2{}^{18}O^{\bullet+}$) and 19 (m/z, $H^{18}O^{\bullet+}$) were followed by a mass analyzer (resolution $\geq\pm$ 0.5 amu) coupled to the TGA instrument. Note the high signal at the start of the heating (the left-most part of the graph); this rise is due to the contamination of residual Ar gas (doubly charged $Ar^{\bullet 2+}$, m/z = 20) present in the TGA instrument chamber at the start of the analysis.

mechanism can not account for these results; instead, an intermediate such as $R^{18}O^{18}OH$ which can exchange ^{18}O with ^{16}O in the polyoxometalate *seems* to be required; and (ii) the ^{16}O observed in the ketone product (2-adamantanone) could also be due to an ^{18}O exchange with $H_2{}^{16}O$ in the solvent via a gem-diol intermediate.[35,36] We did confirm that the ^{16}O content of the $\{[WZnRu^{III}{}_2(OH)(H_2O)](ZnW_9O_{34})_2\}^{11-}$ polyoxometalate, **1** (17.5 μmol for 70 ^{16}O atoms in 0.25 μmol of **1**) is sufficient to account for the observed total ^{16}O incorporation (5.7 μmol) into all the products. That is not to say that this previously undetected, putative O-exchange pathway is anything approaching well understood, however.

Kinetic Studies. A series of kinetic experiments were performed to determine the reaction orders of adamantane, oxygen and precatalyst, **1**. The formation of the main product, 1-adamantanol, was followed by GC (as was done in the prior kinetic studies[13]),

which necessitated the use of the post-induction period, *steady-state, maximum rate* of the reaction[37] (i.e., and since the initial rate of 1-adamantanol production is zero during the induction period[xx]). The steady-state rate law we observed is listed below; it is *a fractional-order rate law, one diagnostic of a free-radical-chain reaction, Figure 5.5, in the reaction's steady-state.*

$$\left\{\frac{d[1\text{-adamantanol}]}{dt}\right\}_{\text{max, steady-state}} = k_{obs}[\text{adamantane}]^{3/2}[Q_{11} - 1]^{1/2}[O_2]^{\approx 1/2}$$

Initiation

(1) $\text{Adm}-\text{H} + \text{Ru}_2^{\text{III}} + \text{O}_2 \xrightarrow{k_1} \text{Ru}_2^{\text{III/IV}}\text{OOH} + \underset{\substack{\text{(mostly 1-adm•;}\\ \text{but some 2-adm•)}}}{\text{Adm•}}$

Propagation

(2) $\text{Adm•} + \text{O}_2 \xrightarrow[\text{fast}]{k_2} \text{AdmOO•}$

(3) $\text{AdmOO•} + \text{Adm}-\text{H} \xrightarrow{k_3} \underset{\text{(primary autoxidation product)}}{\text{AdmOOH}} + \text{Adm•}$

Concurrent Ru_2 - Catalyzed AdmOOH - Based Reaction

(4) $\text{AdmOOH} + \text{Ru}_2^{\text{III/IV}} \xrightarrow{k_4} \text{AdmOO•} + \text{H}^+ + \text{Ru}_2^{\text{III}}$

(5) $\text{AdmOOH} + \text{Ru}_2^{\text{III}} \xrightarrow{k_5} \text{AdmO•} + \text{OH}^- + \text{Ru}_2^{\text{III/IV}}$

(6) $\text{OH}^- + \text{H}^+ \xrightarrow[\text{fast}]{k_6} \text{H}_2\text{O}$

(7) $\text{AdmO•} + \text{AdmOOH} \xrightarrow{k_7} \text{AdmOH} + \text{AdmOO•}$

(8) $\text{AdmO•} + \text{Adm}-\text{H} \xrightarrow{k_8} \text{AdmOH} + \text{Adm•}$

(9) $2\text{AdmOO•} \xrightarrow{k_9} 2\text{AdmO•} + \text{O}_2$

Termination

(10a) $2\text{AdmOO•} \xrightarrow{k_{10}} \text{AdmOOAdm} + \text{O}_2$

(10b) $2\text{AdmOO•} \xrightarrow{k'_{10}} \underset{\text{(possible when one AdmOO• is 2-AdmOO•)}}{\text{1-AdmOH} + \text{2-Adm=O}} + \text{O}_2$

Figure 5.5 Proposed, minimalistic, radical-chain-initiated adamantane hydroperoxylation plus concurrent Ru_2-catalyzed, ROOH-based adamantane reaction consistent with the observed stoichiometry and rate law (Adm ≡ adamantane; AdmOH ≡

[xx] Under our conditions, the induction period of adamantane hydroxylation reaction is less than 1 hour, much shorter than the 10 hour in the prior work.[12,13] The difference is expected for a radical-chain autoxidation reaction: different grades of solvent, adventitious ROOH, other initiators or inhibitors are well known to change the observed length of such induction period.[21]

1-adamantanol; Adm=O ≡ 2-adamantanone; AdmOOH ≡ 1-adamantyl peroxide; Ru_2^{III} ≡ **1** (precatalyst); $Ru_2^{III/IV}$ ≡ oxidized **1**)

The logarithmic plot of the substrate dependence is shown in Figure 5.6A. The logarithmic plot of the precatalyst dependence is shown in Figure 5.6B, and the somewhat scattered plot of the rate vs $p[O_2]^{1/2}$ is given in Figure 5.6C. A typical kineticcurve (from which the maximum rate at steady-state was determined) is shown in the Supporting Information, Figure S5.3. We also performed a control showing that the $ClCH_2CH_2Cl$ solvent does *not* appear to be involved in the autoxidation reaction.[38,39,40,xxi]

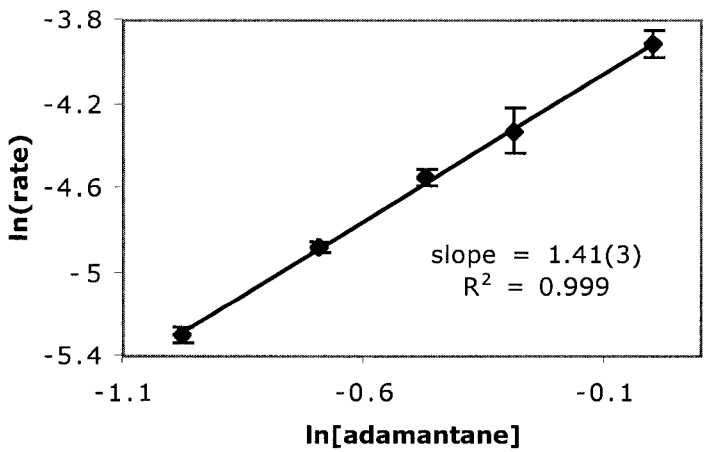

Figure 5.6A Logarithmic plot of the post-induction period, steady-state, maximum rate $[(d[1\text{-adamantanol}]/dt)_{max}]$ vs the substrate concentration. Reaction conditions: 1.9–5.0 mmol adamantane, 2.5 μmol precatalyst, Q_{11}-**1**, 5 mL of 1,2-$C_2H_4Cl_2$ and 1.8 atm of oxygen. The reaction order in the substrate is 1.5 within ±0.1 (i.e., within ±7%).

[xxi] We wondered if the $ClCH_2CH_2Cl$ solvent could serve as a H radical source in the autoxidation, since the C–H BDE of $ClCH_2CH_2Cl$ is ca. 101 kcal/mol[38] (as estimated from the data listed in Table 9-66 elsewhere[39]) vs that of adamantane of 99 kcal/mol.[40] Hence, we performed a control experiment using *o*-dichlorobenzene (C–H BDE ca. 111 kcal/mol[39]) instead of 1,2-dichloroethane as the solvent. Identical product yields and reaction rates rule out the possibility that 1,2-dichloroethane is a major player in the radical reactions, despite the relative concentration of the two, 13 M of $ClCH_2CH_2Cl$ vs 0.5 M of adamantane, a factor of 26:1.

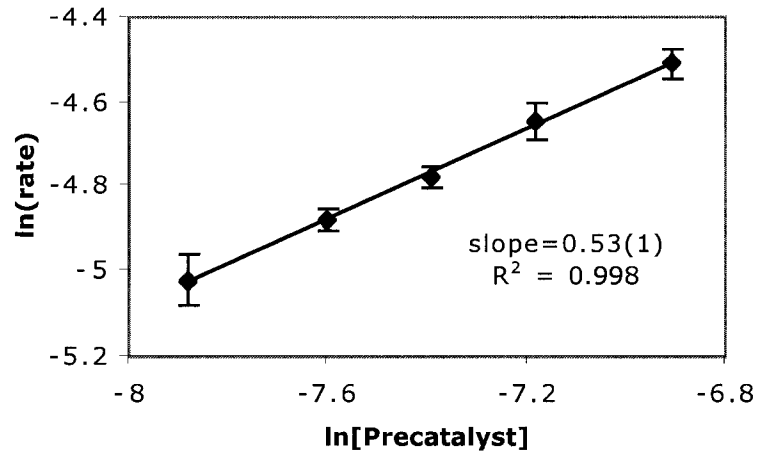

Figure 5.6B Logarithmic plot of the post-induction period, steady-state, maximum rate $[(d[1\text{-adamantanol}]/dt)_{max}]$ vs the precatalyst concentration. Reaction conditions: 2.5 mmol adamantane, 1.9–5.0 μmol precatalyst, Q_{11}-**1**, 5 mL of 1,2-$C_2H_4Cl_2$ and 1.8 atm of oxygen. The order with respect to the polyoxometalate, $Q_{11}\{[WZnRu^{III}_2(OH)(H_2O)](ZnW_9O_{34})_2\}$, is 0.5 within ±0.03 (i.e., within ±6%).

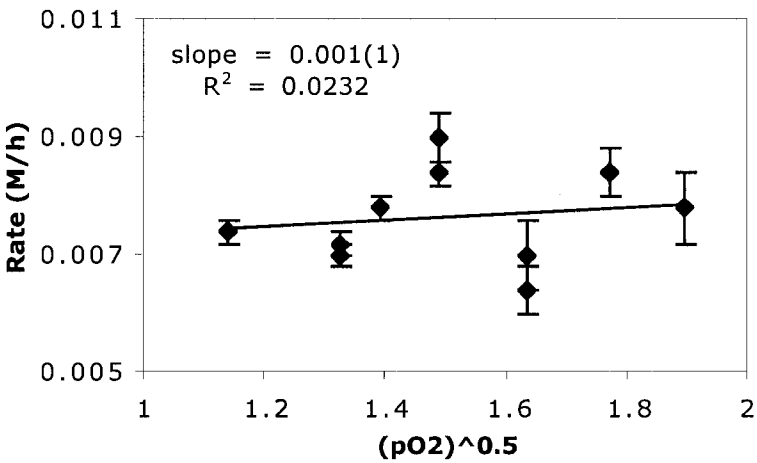

Figure 5.6C Plot of the post-induction period, steady-state, maximum rate $[(d[1\text{-adamantanol}]/dt)_{max}]$ vs the square root of the oxygen pressure, $pO_2^{1/2}$. Reaction conditions: 2.5 mmol adamantane, 2.5 μmol precatalyst, Q_{11}-**1**, 5 mL of 1,2-$C_2H_4Cl_2$ and 1–3.6 atm of oxygen. The reaction order is ca. 0.5 within the observed experimental error; note that the small range of the y or rate axis makes the data appear noisier than they really are (±≤14% error bars, similar to the error in Figure 5.6A and 5.6B, ±≤13%). A zero-order plot of the oxygen pressure, pO_2, is provided in the Supporting Information, but does not yield a better fit to the data. (The direct "Ru_2^{III} (**1**) + RH → $Ru_2^{II/III}$ + R• + H^+" implied by a zero-order pO_2 was further ruled out on the basis of electrochemical

data and thermodynamic grounds; see Figure S5.4 and Figure S5.5 provided in the Supporting Information.)

The rate law derived for the radical-chain in Figure 5.5 mechanism using the steady-state approximation (see the derivation in the Supporting Information) gives: d[product]/dt = k_{obs}[adamantane]$^{3/2}$[precatalyst]$^{1/2}$[O_2]$^{1/2}$. Such *fractional rate laws are typically highly diagnostic of radical-chain mechanisms*,[18,20] since they are virtually impossible to rationalize by other, precedented mechanisms. *In short, the radical-chain mechanism in Figure 5.5 is consistent with, and overall strongly supported by,*[xxii] *the observed kinetics.*[41,xxiii]

Our observed [O_2]$^{\approx 1/2}$ oxygen dependence, [precatalyst]$^{1/2}$ and [adamantane]$^{3/2}$ observations are obviously quite different from [O_2]$^{\sim 1 \rightarrow 0}$, second-order [precatalyst]^2, and zero-order substrate, [adamantane]^0, kinetics reported in the previous work.[13] It is not exactly clear how the prior workers obtained the rate law they reported; at times during our studies it seemed as if we were studying a different system. But our identical precatalyst synthesis, properties (save the λ = 430 peak), and product yields, would seem to ensure the systems are, in fact, the same. Also, the following comments seem relevant

---

[xxii] The R^2 value (0.023) of our $pO_2^{\approx 1/2}$ fit in Figure 5.6C is poor. It is, then, the [adamantane]$^{3/2}$ and [precatalyst]$^{1/2}$ dependences, Figure 5.6A and 5.6B, more than the $pO_2^{\approx 1/2}$ fit that offer the main kinetic support for the radical-chain mechanism.

[xxiii] Note that we did consider in detail the alternative, O_2-free, direct initiation step of Adm–H + $Ru_2^{III} \rightarrow$ Adm• + $Ru_2^{II/III}$, since it is consistent with a [pO_2]^0 treatment of our kinetic data, Figure S5.4 of the Supporting Information and since it has some general precedent[37]—albeit for ~+1.8 V (vs NHE) oxidants such as Co^{3+}/Co^{2+}. The lower—but still, overall, high!—oxidation potential of adamantane (E_{ox} = 2.72 V vs SCE) compared to a non-cyclic alkane (2,3-dimethylbutane, E_{ox} = 3.45 V vs SCE)[41] is at least somewhat consistent with this alternative step. In order to test this alternative route thermodynamically, cyclic voltammetry of the Q_{11}-**1** (i.e., Ru_2^{III} in Figure 5.5) in dichloroethane was performed: the absence of any well-defined Ru^{III}/Ru^{II} peak, Figure S5.5 in the Supporting Information, argues against this alternative initiation step. (NB: the $Ru_2^{III} + e^- \rightarrow Ru_2^{II/III}$ reduction potential of *+0.13 V in H_2O* vs SCE claimed in the prior work[30] is at best not obvious from the unlabeled cyclic voltammogram provided, one which shows no obviously chemical reversible peaks and one in which it is not even possible to tell where the CV scan was initiated.) Finally, and as the literature notes,[37] autoxidation's initiation step is the least understood of the elementary reactions in autoxidation despite more than 60 years of research in autoxidation.[37]

to the previously reported kinetics: (a) the earlier work used post-induction period rates derived from obviously non-linear, bi-phasic kinetic data (see the plots in Figure 2 elsewhere[13]); (b) we have shown in Figure 5.2 that the prior authors' own O_2-dependence data rule out their proposed dioxygenase mechanism; and (c) in the final analysis, our kinetic results are repeatable and, we believe, reliable. Of course, only the prior authors can repeat and support, or refute and retract, their prior 2:1 O_2-uptake, H_2O non-formation and kinetic work, something we physically can not do.

There is, of course, *extensive* precedent for the autoxidation of hydrocarbons by oxygen in the presence of metal catalysts dating back to the 1950s (see the references summarized elsewhere[21]). Labinger's recent excellent work on isobutane autoxidation, and the references cited therein, provide specific, excellent precedent for the mechanism in Figure 5.5 past the initiation step.[34] Interestingly, in both that case and in Figure 5.5, the facile consumption of the initial ROOH product is a key, precedented,[34] feature of the system. Labinger's work also makes clear that fairly high selectivity reactions are possible from even such multistep autoxidation schemes.[34] In short, the observed products, kinetics and the extant literature provide strong support for the proposed, classic autoxidation mechanism, Figure 5.5, as do the additional experiments which follow.

O_2-uptake Stoichiometry Studies. We performed several trials at different scales (6-fold or 24-fold) either by two-point pressure readings of a manometer (i.e., a reproduction of the literature method[13]) or by higher precision, more reliable, multi-point, real-time pressure readings through the use of a high-precision oxygen pressure

transducer (±0.02 psig at 14 psig, i.e., ±0.15%).[xxiv] The average stoichiometric ratio of adamantane products:oxygen we observe, Table 5.1, is 1.0(±0.3):1 (the ±0.3 error bar refers to 3s). Our observed 1:1 stoichiometry is completely at odds with the previously claimed 2:1 dioxygenase stoichiometry.[13]

A representative oxygen-uptake curve obtained via the O_2 pressure transducer is shown in Figure 5.7. This specific experiment, repeated *four times*, yields a stoichiometry of ~1.0 eqv. of adamantane per O_2. The 24 fold smaller scale (i.e., and 24 fold lower O_2-consumed volume available for measurement) is one problem with the

Table 5.1 The O_2-uptake stoichiometry for the adamantane hydroxylation reaction run on different scales.[a]

	O_2 Consumed (mmol)	1-adamantanol Yield (mmol)	2-adamanta-none Yield (mmol)	Ratio of ΣProducts:O_2
Two-point Method	[b]0.4 ± 0.1	0.31 ± 0.02	0.08 ± 0.01	**1.0 ± 0.3**
	[b]0.5 ± 0.1	0.40 ± 0.02	0.08 ± 0.01	**1.0 ± 0.2**
	0.96 ± 0.06	0.73 ± 0.02	0.14 ± 0.01	**0.9 ± 0.1**
Multi-point, real-time Method	0.8 ± 0.1	0.77 ± 0.06	0.14 ± 0.01	**1.1 ± 0.1**
	1.2 ± 0.1	1.09 ± 0.03	0.21 ± 0.07	**1.1 ± 0.1**
	1.4 ± 0.1	1.17 ± 0.04	0.22 ± 0.01	**1.0 ± 0.1**
	1.5 ± 0.1	1.12 ± 0.06	0.21 ± 0.01	**0.9 ± 0.1**
	[c]1.1 ± 0.2	0.82 ± 0.02	0.27 ± 0.01	**1.0 ± 0.2**

[a]Reaction conditions are scaled up proportionally (6 times or 24 times) from the conditions used in the literature[12,13] to increase the precision of our results: 0.25 mmol substrate, 0.25 μmol precatalyst, 80 °C, reaction time 24 h; the solvent volume (1,2-dichloroethane) is scaled up by factors of 6, 12 or 24 in the various experiments.
[b]Reaction time 72 h.
[c]This run was performed in *o*-dichlorobenzene rather than the normal solvent (1,2-dichloroethane).

[xxiv] The sensitivity of manometer vs pressure transducer is actually about the same (±0.13% vs ±0.15%, respectively), but the pressure transducer is capable of handling pressure readings in a broader range (0–100 psig compared to the <1 psig range of the manometer). Hence, with the pressure transducer we were able to scale up the reaction, thereby allowing real-time pressure readings over a ca. 12 psig range, ca. 12 fold better than our manometer allows.

prior studies.[13,xxv] The lack of a detailed experimental section (e.g., one noting the precision of the pressure readings in the prior O_2-uptake experiments) is another problem with the previous work.[13] Obviously, any two-point O_2-uptake experiment is another potential problem in light of the full, complex curve in Figure 5.7.

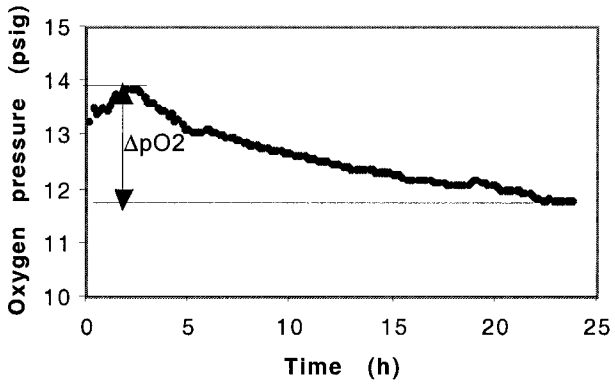

Figure 5.7 Full oxygen pressure versus time curve recorded by an oxygen pressure transducer. The pressure rise for the first 2 h is due to solvent pressure equilibration following the introduction of O_2 into the reaction flask via a cycle of 15 purges, a procedure which initially cools the system some and unavoidably sweeps solvent vapor out of the system, thereby initially lowing the pressure recorded at t = 0.

A detailed comparison of the observed stoichiometry vs that predicted by the mechanism in Figure 5.5, and as a function of time (i.e., of the chain-length), is possible only via a numerical integration computer model of Figure 5.5 analogous to what Labinger has so nicely done for isobutane autoxidation, a system fairly close to that in Figure 5.5 except for different initiation steps.[34] Although we are continuing to work on a version of Figure 5.5 complete with the needed rate constants, so far it appears that an insufficient number of the required rate constants are known in the literature to allow any

[xxv] Given the scale used for the stoichiometry study in the previous work,[13] the uncertainty in pressure readings might be sizeable in comparison to the actual pressure loss. The amount of oxygen consumed is estimated to be 0.025 mmol (0.25 mmol adamantane, assuming 20% conversion at 48 h and a 2:1 ratio). With an assumed 100 mL total volume, only a 5 (±0.1) mmHg pressure change would have been observed at room temperature, so that a reading error of ±1 mmHg would introduce an error of ±20%.

more detailed, meaningful computer model (i.e., more detailed than the minimum numerical integration model already in the Supporting Information). However, the main point for the present work is that the experimentally observed stoichiometry is *not* the previously claimed, 2:1 value at least in our hands. Instead, it is closer to ~1:1(±0.3), findings consistent with the autoxidation pathway in Figure 5.5.

Effects of Radical Initiators and Hydroperoxides. We also studied the effects of several additives introduced at the start of the reaction: the radical initiator AIBN (2,2'-azobisisobutyronitrile), *tert*-butyl hydroperoxide (TBHP), H_2O_2, and, following the earlier report,[12] zinc powder. In the case of AIBN, TBHP or H_2O_2, 0.2 mmol were added, which is ca. 33 equivalent versus the amount of the precatalyst Q_{11}-**1**. The amount of Zn powder added was chosen to reproduce the literature[12] (ca. 5 equivalent Zn vs the amount of Q_{11}-**1**). Two identical runs for the first two additives were performed and the repeatability proved good, Figure 5.8.

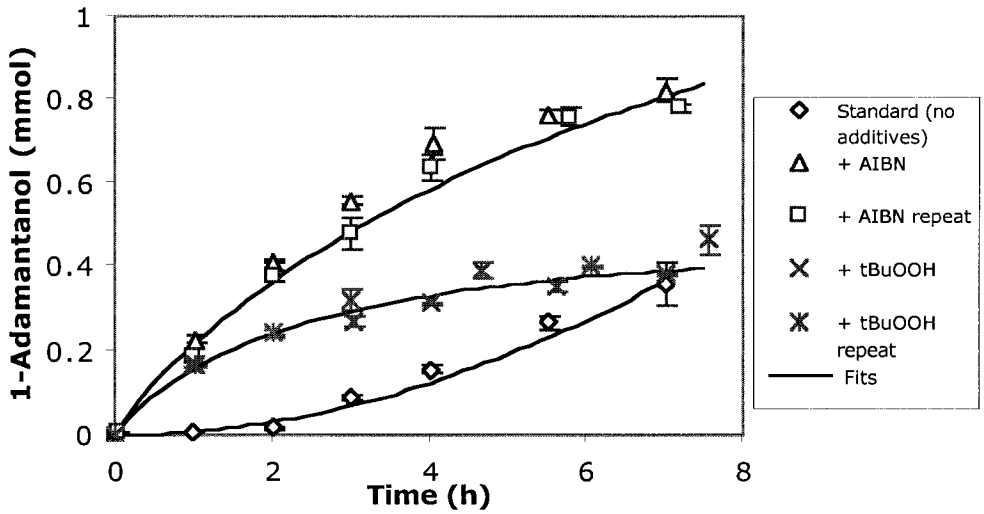

Figure 5.8 The effects of adding the radical initiator (AIBN) (0.2 mmol) or anhydrous TBHP (ca. 0.2 mmol) at the start of the adamantane hydroxylation reaction. The kinetic model used in Mackinetics for the fit under standard conditions is basically the k_1–k_3 and k_{10} steps of the radical-chain mechanism in Figure 5.5; see the Supporting Information for further details.

The radical initiators AIBN and TBHP *eliminate the induction period,* and the initial rates of product formation increase ca. 20 fold from ~0.01 mmol/h to ~0.2 mmol/h with AIBN and ~0.17 mmol/h with added TBHP. The major product yield with TBHP is essentially the same as the Standard Conditions yield (13 ± 1% 1-adamantanol), while the run with AIBN increases the 1-adamantanol yield to 19 ± 1% after 24 h. The selectivities (the 3°/2° ratio, ratio of 1-adamantanol to 2-adamantanone times a statistical factor of 3 to correct for the number of available 3°/2° C–H bonds) with or without the radical initiator are same within experimental error: 16(±3):1 vs 14(±1):1, providing evidence that the deliberately initiated and normal reactions are one and the same, namely autoxidation.

Mackinetics was used to fit the kinetic curves following the formation of 1-adamantanol. The elementary steps entered into the program are the appropriate steps from the autoxidation mechanism in Figure 5.5 as detailed in the Supporting Information. A grid search was performed on the independent rate constants to generate the best-fit rate via numerical integration; the resulting rate constants are given in Table 5.2. The good fits provide additional kinetic evidence in support of the mechanism in Figure 5.5.

Neither H_2O_2 (30% in H_2O) nor Zn (-100 mesh, 99.998%, prewashed with dilute HCl to activate the surface and dried under vacuum at RT) has a measurable effect on the induction period or the resultant kinetic curve, Figure 5.9. The product yields after 24 hours with 33 equivalents (vs precatalyst Q_{11}-**1**) of added 30% H_2O_2 (in H_2O) are the same as the normal yields within experimental error. A control of adding H_2O only (the same amount as added in the 30% H_2O_2 experiment) shows that the addition of H_2O alone leads to a longer induction period (~2.5 hours vs ~1 hour for the addition of 30% H_2O_2 in

Table 5.2 The estimated rate constants obtained from fitting the radical-chain mechanism in Figure 5.5 to the kinetic data in Figure 5.8.[a]

	$k_{initiation}$ or k_1 ($M^{-1}\cdot h^{-1}$)	$k_{H\text{-}abstraction}$ or k_3[b] ($M^{-1}\cdot h^{-1}$)	$k_{termination}$ or ($k_{10} + k_{10}'$) ($M^{-1}\cdot h^{-1}$)	$k_{propagation}$ ($M^{-1}\cdot h^{-1}$)[c]	
				Experimental	Related literature[42]
Standard Conditions	~0.0015	~3.5	~1	-	-
Standard Conditions +AIBN	~10 (in h^{-1})	~1	~2	k_3' ~80 at 80 °C[d]	0.288 at 30 °C
Standard Conditions + *t*-BuOOH	~20 (in h^{-1})	~0.1	~1.5	k_2'' ~100 at 80 °C[e]	0.0162 at 30 °C

[a]The rate constants refer to 80 °C. The observed rate constants from a three or four parameter fit are not expected to be accurate to better than $10^{\pm 1}$.
[b]AdmOO• + Adm–H → AdmOOH + Adm•; the absolute rate constant for reaction of cumene toward its own peroxy radical is 10.8 $M^{-1}\cdot h^{-1}$ (or 0.18 $M^{-1}\cdot s^{-1}$) at 30 °C.[37]
[c]$k_{propagation}$ equals the k_3' or k_2'' for the reactions defined in footnotes *d* and *e* below (and discussed more in the Supporting Information), rate constants which should not be confused with the k_2 and k_3 of Figure 5.5.
[d](CN)Me_2COO• + Adm–H → (CN)Me_2COOH + Adm•
[e]*t*-BuOO• + Adm–H → *t*-BuOOH + Adm•

H_2O). Therefore, pure hydrogen peroxide would be expected to eliminate the induction period in the absence of the masking, inhibiting effect of added H_2O. The product yields for the run with added Zn are reduced to 7 ± 1% 1-adamantanol compared with our standard yield of 12 ± 1%, zinc apparently serving as an (inefficient) radical inhibitor. Although we do not see a large reduction of the induction period (from 10 h to ~1 hour) as seen in the previous work,[12] our result with added Zn is actually similar in that *a 1 hour induction period results in both cases.* Restated, it appears that added Zn serves primarily to remove inhibitors present in the prior reaction conditions.[12] This shows just how misleading the interpretation of such "additive" experiments can be in the absence of reliable kinetic studies supporting a reliable mechanism from which to interpret such inhibitor (i.e., such single-point kinetic) experiments.

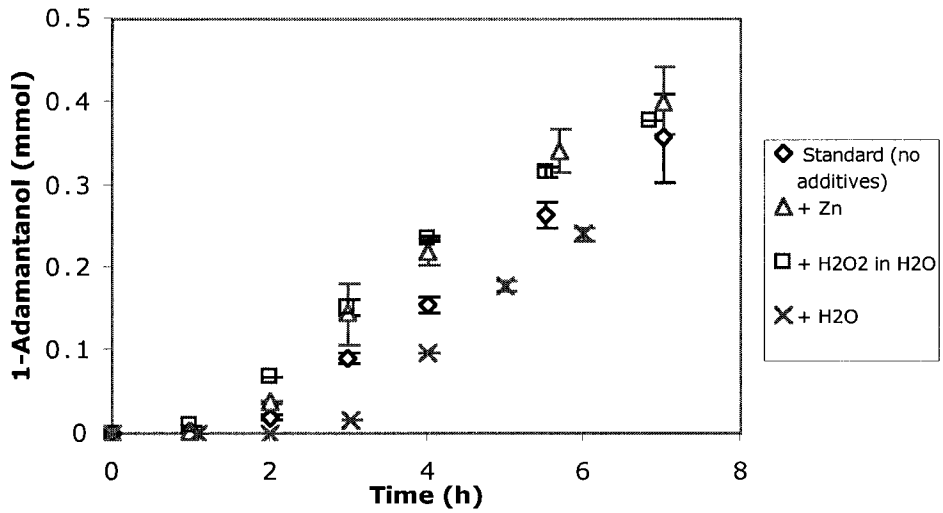

Figure 5.9 The lack of any significant effects upon adding Zn (0.028 mmol) or 30% H_2O_2 (0.2 mmol) in H_2O and the inhibition effect upon adding H_2O at the start of the adamantane hydroxylation reaction.

In summary, organic hydroperoxide (ROOH), organic hydroperoxide radicals (ROO•, derived from AIBN plus O_2), or hydrogen peroxide (HOOH) have a significant effect on the reaction as expected for the presence of free radicals in the adamantane hydroxylation reaction. The higher stability of the 3° radical over the 2° radical also explains the selectivity observed for 1-adamantanol over 2-adamantanol/2-adamantanone.

Effects of Radical Inhibitors. Four radical scavengers, 4-*tert*-butylcatechol, 2,6-di-*tert*-butyl-4-methylphenol (BHT or butylated hydroxyltoluene), galvinoxyl or 2-phenyl-*N*-*tert*-butylnitrone (PBN hereafter) were added at the start of the reaction (0.2 mmol vs 6 mmol substrate) in four independent experiments.

All four runs gave *zero%* 1-adamantanol after 24 hours (detection limit 0.001–0.01 mmol, or 0.02–0.2%). These inhibition results further support the free

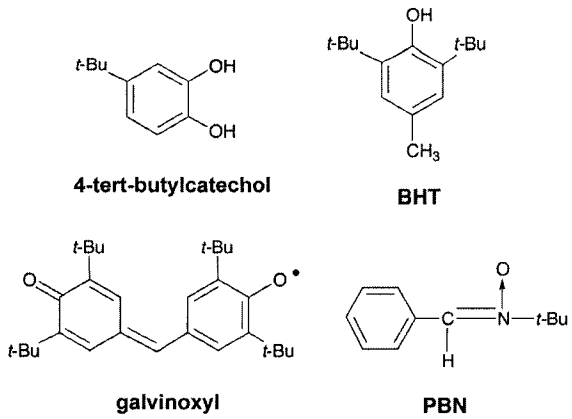

Figure 5.10 Radical inhibitors used in the present studies. Two of the inhibitors, 4-*tert*-butylcatechol and BHT, are the identical scavengers used in the prior work.[12,13]

radical-initiated mechanism of adamantane hydroxylation with Q_{11}-**1**. Note that we have used the same two radical scavengers (*tert*-butylcatechol and BHT) used in the previous studies, but which were claimed to have no effect.[12,13,xxvi] Moreover, positive inhibition results were obtained in our hands even with a 30-fold lower inhibitor concentration than that employed in the prior work.[12,13]

Our ability to inhibit or initiate (*vide supra*) the reaction with known, free-radical inhibitors or initiators provides disproof of the claim in the prior work that "...the induction period is related to the activation of the ruthenium polyoxometalate with molecular oxygen".[12] Instead, the induction period is fully accounted for by classic, free-radical autoxidation chemistry.

[xxvi] There are at least two possibilities for lack of positive results in the prior work: (i) the radical inhibitors used previously degraded; and/or (ii) the inhibitors were not concentrated enough to inhibit the radical reaction. There is literature precedent of BHT giving negative inhibition results due to the use of too low a concentration.[22] However, at a 30-fold lower inhibitor concentration than the previous studies, we found that (16 mM) *tert*-butylcatechol, BHT, galvinoxyl or PBN completely inhibited adamantane hydroxylation, while *tert*-butylcatechol, BHT or BHA (used previously at 500 mM) showed no effect in the previous work.[12,13] Hence, the inhibitor concentration is not the reason for the literature report of non-inhibition. It is quite possible that the inhibitors the authors used had degraded, but no details on the source or purity of the inhibitors used are available. Unfortunately, these scavenging results, along with the reported 2:1 adamantane:O_2 stoichiometry, the reported rate law, and the claimed non-reactivity of cyclohexene—which is easily autoxidized as expected in our experiments—are aspects of the prior work that proved unrepeatable in our hands while following the previously published experimental details.

Cyclohexene Autoxidation and Catechol Dioxygenase Control Experiments.

Our previous study of the polyoxometalate-supported transition metal precatalyst, [(1,5-COD)Ir•$P_2W_{15}Nb_3O_{62}$]$^{8-}$, showed it initiates autoxidation with O_2 leading to ~70 products, 27 of which were identified.[21] That paper also points out the ca. 70 products in the GC trace is a simple, but powerful, method to detect autoxidation catalysis. Hence, we tested Q_{11}-**1** for its ability to catalyze cyclohexene autoxidation in comparison to a control with [(1,5-COD)Ir•$P_2W_{15}Nb_3O_{62}$]$^{8-}$. The prediction is, of course, that it will.

GC traces of both precatalyst's oxidation mixtures show similar product profiles, Figure S5.6 of the Supporting Information. Table 5.3 shows the yields of the three major products of the two runs (not including cyclohexen-1-yl hydroperoxide). The results in Table 5.3 demonstrate that Q_{11}-**1** is an efficient precatalyst for the facile autoxidation of cyclohexene.

Table 5.3 The autoxidation of cyclohexene in 1,2-dichloroethane at 38 °C and 1 atm O_2.[a]

Precatalyst	Yield (%) (Selectivity[b])		
	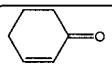	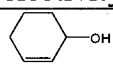	
Q_{11}{[$WZnRu_2(OH)(H_2O)$]($ZnW_9O_{34})_2$}	19 ± 1 (11 ± 1)	9.4 ± 0.5 (5.2 ± 0.4)	1.8 ± 0.1 (1)
$[Bu_4N]_5Na_3$[(1,5-COD)Ir•$P_2W_{15}Nb_3O_{62}$][c]	6.6 ± 0.4 (7 ± 1)	3.3 ± 0.2 (3.3 ± 0.4)	1.0 ± 0.1 (1)

[a]Reaction conditions: cyclohexene 1.0 mL, 1,2-dichloroethane 6.0 mL, precatalyst 8.6–8.8 μmol, 38 °C, 1 atm O_2, reaction time 48 hours.
[b]Selectivity was calculated as the ratio of the product to cyclohexene oxide.
[c]This precatalyst is not totally soluble in the 1,2-dichloroethane solvent, but we did not wish to introduce an additional variable by changing the solvent.

Precatalyst Q_{11}-**1** was also tested in the catechol dioxygenase reaction[5,9] of 3,5-di-*tert*-butylcatechol (3,5-DTBC hereafter) oxygenation. As expected, precatalyst, **1**,

$\{[WZnRu^{III}_2(OH)(H_2O)](ZnW_9O_{34})_2\}^{11-}$ is *inactive* over 133 h for the 3,5-DTBC dioxygenase reaction, a result consistent with the same result[5] by another researcher from our group using an earlier, separate batch of **1**. The *inability* to catalyze the catechol dioxygenase catalysis, plus the *ability* to catalyze cyclohexene autoxidation, further refutes the claim that inorganic precatalyst Q_{11}-**1** acts as an inorganic dioxygenase.

Some Additional Control Experiments. We performed the following additional experiments in part in response to issues raised by Professor Neumann to whom we provided a preprint of this paper; details are reported in the Supporting Materials. We thank Prof. Neumann for raising the issues which follow. A control experiment testing the possible effects of excess Q^+Cl^- in the precatalyst **1** as an initiator to the autoxidation, as well as the catalytic ability of Q^+Cl^- without precatalyst **1**, showed that there is no discernable effect within experimental error of changing the amount of Q^+Cl^- present. In addition, changing the solvent pretreatment to exactly that used in the prior work had no effect. Our attempt to repeat the prior report of *trans*-cyclooctene epoxidation failed, the *cis*-oxide being the primary product in our hands. The results of these additional controls offer no evidence for a dioxygenase pathway but, rather, are consistent with the autoxidation pathway in Figure 5.5. We also requested a sample of $Q_{11}\{[WZnRu_2(OH)(H_2O)](ZnW_9O_{34})_2\}$ from Prof. Neumann (i.e., a sample made in his labs) for a control experiment to see how it behaves in our hands but, unfortunately, never received a response to that specific request.

Critical Re-analysis of the Other Data Previously Claimed in Support of a Dioxygenase Mechanism. For the sake of completeness, it is important to analyze the other prior data previously interpreted in terms of a dioxygenase pathway[12,13] to be sure

that the mechanism in Figure 5.5 can explain *all* of the available data. This is done in the Supporting Information for the interested reader. The end result is that the autoxidation mechanism in Figure 5.5 is consistent with all of the available data.

Conclusions

We have re-investigated the interesting, *albeit impure as reported*,[5] sandwich-type polyoxometalate precatalyst, $Q_{11}\{[WZnRu_2(OH)(H_2O)](ZnW_9O_{34})_2\}$, for its adamantane[43,44,45,46,47,48,49,50,51,xxvii] hydroxylation reaction. Trace amounts of peroxide could be detected at the end of the reactions. $H_2{}^{18}O$ is shown to be formed from $^{18}O_2$, refuting the prior negative evidence, presented without stated detection limits, that no $H_2{}^{18}O$ was observed.[12] Kinetic studies yield a fractional rate law which is readily and quantitatively—if not only—explained by a radical-chain reaction. The stoichiometry of adamantane products/O_2 determined by two different methods is a net ~1:1 autoxidation stoichiometry in our hands instead of the previously reported 2:1 dioxygenase stoichiometry. The radical initiator AIBN and the organic hydroperoxide *t*-BuOOH eliminate the induction period completely, increasing the initial rate about 20 fold. Four radical scavengers completely inhibited the adamantane hydroxylation reaction, including two inhibitors previously reported to have no effect but which completely inhibit the reaction in our hands at 1/30 the prior, reported concentrations. A further analysis and critique of the previous work[12,13] has also been included as part of the Supporting Information.

[xxvii] A question we considered is whether or not adamantane is a substrate unusually susceptible for autoxidation from this work and prior work.[43,44,45,46,47,48,49,50,51] Its 99 kcal/mol C–H BDE[40] argues "no". However, our opinion is that adamantane should not be used as the *only* substrate for any type of oxidation catalysis. Substrates such as cyclohexene or propene are much tougher tests of any claim of dioxygenase catalysis.

The clear conclusion of this work is that the polyoxometalate precatalyst $Q_{11}\{[WZnRu_2(OH)(H_2O)](ZnW_9O_{34})_2\}$ prepared as previously described is a classic autoxidation catalyst, at least in our hands. There is no compelling evidence for, and now strong evidence against, the prior claim of a novel *dioxygenase* catalyst for adamantane hydroxylation based on the precatalyst $Q_{11}\{[WZnRu_2(OH)(H_2O)](ZnW_9O_{34})_2\}$. Significant parts of the prior work (the adamantane products/O_2 stoichiometry; the rate law; the results with radical inhibitors; the claimed non-reactivity of cyclohexene[xxviii] despite its weak and thus reactive allylic C-H bond) have not proved repeatable from the sometimes inadequate experimental details provided, again at least in our hands. A main component of the present work is that we have emphasized Platt's scientific method involving the *disproof* of alternative hypotheses.[52,xxix] The significance of Platt's method is impossible to overemphasize: "for exploring the unknown, there is no faster method".[52]

[xxviii] The previous work reported that cyclohexene (with its 87 kcal/mol allylic C-H BDE) gave "no products" (see p. 11974 elsewere[13]; no detection limits were provided) even though adamantane with its stronger, 99 kcal/mol C-H BDE does react. We find it hard to accept this observation as supporting a dioxygenase as previously proposed since: (i) the evidence is negative; and (ii) the result is unprecedented and counter-intuitive, that is, to our knowledge there is no known oxidant of any type that will preferentially activate adamantane's 99 kcal/mol C-H bonds but leave untouched the weaker, 87 kcal/mol allylic C-H bond of cyclohexene. Of course there is also (iii) our finding that cyclohexene is in fact readily autoxidized under the same conditions which autoxidize adamantane.

[xxix] A lingering, alternative hypothesis that is difficult to disprove completely is the "magic ingredient or impurity" hypothesis: that is, that there is some ingredient or impurity present in one study and one lab, only, which is a key to the claimed dioxygenase chemistry (i.e, and despite our attempt to reproduce the previously published work as closely as possible). *If* correct and *if* such a putative magic ingredient were identified, then that would of course be a profound finding—a "magic bullet" that would be a key to turning on (or off) dioxygenase vs autoxidation catalysis for at least $Q_{11}\{[WZnRu_2(OH)(H_2O)](ZnW_9O_{34})_2\}$. *However*, the one reasonable and logical possibility here that we can see, namely an adventitious radical-chain initiator in our studies, can be ruled out by our observed kinetics. Those kinetics implicate a reasonably reproducible initiation step that depends on the polyoxometalate precatalyst complex plus dioxygen and adamantane. In short, the magic ingredient hypothesis has no support at present as well as the following evidence squarely against it: (i) the reaction's reproducibility in our hands; (ii) our kinetics and the implied initiation step; (iii) the fact that our $Q_{11}\{[WZnRu_2(OH)(H_2O)](ZnW_9O_{34})_2\}$ precatalyst is made by the published prescription and has the spectroscopic signatures indicated in the prior work (save the $\lambda = 430$ nm band); and (iv) the *identical* 12% yield of the main product, 1-adamantol. *The latter is a powerful piece of evidence, as it places the restriction on the dioxygenase mechanism that it must coincidentally provide the same yield of the product as the now documented autoxidation mechanism!* Accordingly, the burden of support of the "magic ingredient" hypothesis is left to its proponents.

Moreover, Platt's method with its emphasis on disproof helps shield us as fallible, human researchers against the well-established but still flourishing, insidious problem in science of "experimenter expectancy,"[53] that is, of our seeing what we wish to see in our results (i.e., rationalizing our results in terms of our initial hypothesis or beliefs and/or attempting the impossibility of "proving" something rather than focusing on disproof). In the present case, our attempted disproof focused on the key hypothesis in oxidation catalysis, one apparent in Ingold's recent work[22] and one stated concisely in the conclusion section of Limburg's 2003 review: "Radicals are far more frequently involved in oxygenation reactions than originally assumed, in fact, they appear almost omnipresent".[54] We could not disprove the radical catalysis hypothesis in the present case; instead, our results strongly support it. Certainly any future claim of new dioxygenase catalysis must thoroughly test for and attempt to disprove rigorously the *omnipresent autoxidation catalysis hypothesis*: the well-established existence of classic, often facile, free-radical-chain autoxidation.

Note Added In Proof. Nomiya and co-workers have independently checked the preparation of $K_{11}[WZnRu_2(OH)(H_2O)(ZnW_9O_{34})_2]$, K_{11}-**1**, reported by Neumann and co-workers;[30] they find a yellow-brown material results that is sometimes a mixture of crystals.[29,55] They also find that the UV-visible absorption spectrum of K_{11}-**1** does not exhibit the reported 430 nm peak,[55] analogous to the findings reported herein. Nomiya and co-workers also find no reversible $Ru^{III/II}$ or $Ru^{IV/III}$ redox peaks at positive potentials,[55] results again consistent with our findings for Q_{11}-**1**. Overall, Nomiya reports[29,55] that they find it very difficult to reproduce the reported preparation[30] of K_{11}-**1**

as a primary product when *cis*-$[RuCl_2(DMSO)_4]$ is used as the ruthenium source, even though they followed the original synthesis "as close as possible".[29]

Acknowledgement. We thank Jeremy J. Nelson in Professor C. Michael Elliott's Group at Colorado State University for performing the electrochemistry experiments on **1** reported in the Supporting Information. Each of the following persons read the paper and provided comments that led to revisions that strengthened the paper: the Associate Editor of *Inorganic Chemistry* who handled the paper and an anonymous referee who shared his or her expertise with radical autoxidation chemistry, its mechanisms and possible stoichiometries. This work was supported by NSF grant 0314678.

Supporting Information Available: 22 pages consisting of: IR spectrum of $Q_{11}\{[WZnRu_2(OH)(H_2O)](ZnW_9O_{34})_2\}$; a TGA curve from the mol sieves / $H_2{}^{18}O$ experiment; a typical kinetic curve following the formation of 1-adamantanol showing how the maximum, steady-state rate measurements were made; plot of the maximum rate vs pO_2; cyclic voltammgram of $Q_{11}\{[WZnRu_2(OH)(H_2O)](ZnW_9O_{34})_2\}$; rate law derivation for the proposed mechanism in Figure 5.5 of the main text at the steady-state; rate law derivation for the mechanism with the alternative initiation step not involving O_2 (and leading to a zero-order pO_2 dependence) at the steady-state; kinetic models used in Mackinetics to fit the observed kinetic curves in Figure 5.8; attempted synthesis of 1-adamantyl peroxide; GC traces of cyclohexene autoxidation catalyzed by Q_{11}-1 and $[Bu_4N]_5Na_3[(1,5\text{-COD})Ir{\bullet}P_2W_{15}Nb_3O_{62}]$; control experiments testing the effect of excess Q^+Cl^- in the precatalyst **1**; control experiment testing the catalytic ability of Q^+Cl^- without precatalyst 1; control experiment testing for any effects of solvent pretreatment; control experiment testing for the reported *trans*-cyclooctene epoxidation reaction; discussions of

the other putative evidence in the prior work;[12,13] tabulated literature overview of adamantane oxidation by ruthenium complexes and different oxidants (O_2, hydroperoxides, etc.)

References

[1] Hayaishi, O.; Katagiri, M.; Rothberg, S. *J. Am. Chem. Soc.* **1955**, *77*, 5450-5451.

[2] Nozaki, M. *Top. Curr. Chem.* **1979**, *78*, 145-186.

[3] Funabiki, T.; Editor *Oxygenases and Model Systems [In: Catal. Met. Complexes, 1997; 19]*; Kluwer Academic Publishers: Dordrecht, The Netherlands, 1997.

[4] Groves, J. T.; Quinn, R. *J. Am. Chem. Soc.* **1985**, *107*, 5790-5792.

[5] Weiner, H.; Finke, R. G. *J. Am. Chem. Soc.* **1999**, *121*, 9831-9842.

[6] Yin, C.-X.; Sasaki, Y.; Finke, R. G. "Autoxidation-Product-Initiated Dioxygenases: Vanadium-Based, Record Catalytic Lifetime Catechol Dioxygenase Catalysis and Its Mechanism of Action," manuscript in preparation..

[7] Yin, C.-X.; Finke, R. G. "Vanadium-Based, Record Catalytic Lifetime Catechol Dioxygenases: Evidence For a Common Catalyst," *J. Am. Chem. Soc.* **2005**, in press.

[8] Nishiyama, Y.; Nakagawa, Y.; Mizuno, N. *Angew. Chem., Int. Ed. Engl.* **2001**, *40*, 3639-3641.

[9] Que, L., Jr.; Ho, R. Y. N. *Chem. Rev.* **1996**, *96*, 2607-2624.

[10] Krüger, H.-J. In *Biomimetic Oxidations Catalyzed by Transition Metal Complexes*; Meunier, B., Ed.; Imperial College Press: London, 2000, pp 363-413.

[11] Yamahara, R.; Ogo, S.; Masuda, H.; Watanabe, Y. *J. Inorg. Biochem.* **2002**, *88*, 284-294 and references therein.

[12] Neumann, R.; Dahan, M. *Nature* **1997**, *388*, 353-355.

[13] Neumann, R.; Dahan, M. *J. Am. Chem. Soc.* **1998**, *120*, 11969-11976.

[14] Hill, C. L.; Weinstock, I. A. *Nature* **1997**, *388*, 332-333.

[15] Haber, F.; Weiss, J. *Naturwissenschaften* **1932**, *20*, 948-950.

[16] Haber, F.; Weiss, J. *Proc. R. Soc. London* **1934**, *A147*, 332-351.

[17] Kharasch, M. S.; Fono, A.; Nudenberg, W.; Bischof, B. *J. Org. Chem.* **1952**, *17*, 207-220.

[18] Huyser, E. S. *Free Radical Chain Reactions*; John Wiley & Sons: New York, 1970.

[19] Kochi, J. K.; Editor *Free Radicals, Vol. 2*; John Wiley & Sons: New York, 1973.

[20] Fossey, J.; Lefort, D.; Sorba, J. *Free Radicals in Organic Chemistry*; John Wiley & Sons Ltd: New York, 1995.

[21] Weiner, H.; Trovarelli, A.; Finke, R. G. *J. Mol. Catal.* **2003**, *191*, 217-252.

[22] Ingold, K. U.; MacFaul, P. A. In *Biomimetic Oxidations Catalyzed by Transition Metal Complexes*; Meunier, B., Ed.; Imperial College Press: London, 2000, pp 45-89.

[23] Weiner, H.; Aiken, J. D., III; Finke, R. G. *Inorg. Chem.* **1996**, *35*, 7905-7913.

[24] Hornstein, B. J.; Finke, R. G. *Inorg. Chem.* **2002**, *41*, 2720-2730.

[25] Day, V. W.; Klemperer, W. G.; Main, D. J. *Inorg. Chem.* **1990**, *29*, 2345-2355.

[26] Lin, Y.; Finke, R. G. *Inorg. Chem.* **1994**, *33*, 4891-4910.

[27] Tourné, C. M.; Tourné, G. F.; Zonnevijlle, F. *J. Chem. Soc., Dalton Trans.: Inorg. Chem. (1972-1999)* **1991**, 143-155.

[28] Evans, I. P.; Spencer, A.; Wilkinson, G. *J. Chem. Soc., Dalton Trans.: Inorg. Chem. (1972-1999)* **1973**, 204-209.

[29] Nomiya, K.; Torii, H.; Nomura, K.; Sato, Y. *J. Chem. Soc., Dalton Trans.* **2001**, 1506-1512.

[30] Neumann, R.; Khenkin, A. M. *Inorg. Chem.* **1995**, *34*, 5753-5760.

[31] Wagner, C. D.; Smith, R. H.; Peters, E. D. *Anal. Chem.* **1947**, *19*, 976-979.

[32] Son, V. V.; Ivashchenko, S. P.; Son, T. V. *Zh. Obshch. Khim.* **1990**, *60*, 710-712.

[33] van Sickle, D. E.; Mayo, F. R.; Arluck, R. M.; *J. Am. Chem. Soc.* **1965**, *87*, 4824-4832.

[34] Labinger, J. A. *Catal. Lett.* **1994**, *26*, 95-99.

[35] Samuel, D.; Silver, B. L. In *Advan. Phys. Org. Chem.*; Gold, V., Ed.; Academic Press: London and New York, 1965; Vol. 3, pp 123-186.

[36] Cohn, M.; Urey, H. C. *J. Am. Chem. Soc.* **1938**, *60*, 679-687.

[37] Howard, J. A. In *Free Radicals*; Kochi, J. K., Ed.; John Wiley & Sons: New York, 1973; Vol. 2, pp 3-62.

[38] McMillen, D. F.; Golden, D. M. *Ann. Rev. Phys. Chem.* **1982**, *33*, 493-532.

[39] Lide, D. R. *CRC Handbook of Chemistry and Physics, 85th Edition*; CRC Press, 2004-5.

[40] Kruppa, G. H.; Beauchamp, J. L. *J. Am. Chem. Soc.* **1986**, *108*, 2162-2169.

[41] Bravo, A.; Bjorsvik, H.-R.; Fontana, F.; Minisci, F.; Serri, A. *J. Org. Chem.* **1996**, *61*, 9409-9416.

[42] Hendry, D. G.; Mill, T.; Piszkiewicz, L.; Howard, J. A.; Eigenmann, H. K. *J. Phys. Chem. Ref. Data* **1974**, *3*, 937-978.

[43] Smith, G. W.; Williams, H. D. *J. Org. Chem.* **1961**, *26*, 2207-2212.

[44] Muto, T.; Urano, C.; Hayashi, T.; Miura, T.; Kimura, M. *Chem. Pharm. Bull.* **1983**, *31*, 1166-1171.

[45] Bressan, M.; Morvillo, A.; Romanello, G. *J. Mol. Catal.* **1992**, *77*, 283-288.

[46] Ishii, Y.; Nakayama, K.; Takeno, M.; Sakaguchi, S.; Iwahama, T.; Nishiyama, Y. *J. Org. Chem.* **1995**, *60*, 3934-3935.

[47] Ishii, Y.; Sakaguchi, S. *Catalysis Surveys from Japan* **1999**, *3*, 27-35.

[48] Che, C.-M.; Cheng, K.-W.; Chan, M. C. W.; Lau, T.-C.; Mak, C.-K. *J. Org. Chem.* **2000**, *65*, 7996-8000.

[49] Kojima, T.; Matsuo, H.; Matsuda, Y. *Inorg. Chim. Acta* **2000**, *300-302*, 661-667.

[50] Wong, W.-K.; Chen, X.-P.; Guo, J.-P.; Chi, Y.-G.; Pan, W.-X.; Wong, W.-Y. *J. Chem. Soc., Dalton Trans.* **2002**, 1139-1146.

[51] Wong, W.-K.; Chen, X.-P.; Chik, T.-W.; Wong, W.-Y.; Guo, J.-P.; Lee, F.-W. *Eur. J. Inorg. Chem.* **2003**, 3539-3546.

[52] Platt, J. R. *Science* **1964**, *146*, 347-353.

[53] Broad, W.; Wade, N.; Betrayers of the Truth, Simon and Schuster, New York, 1982; see Chapter 6, p. 107 on "Self-Deception and Gullibility".

[54] Limburg, C. *Angew. Chem. Int. Eng. Ed.* **2003**, *42*, 5932-5954; the indicated quote is from p. 5950.

[55] Nomiya, K.; Torii, H.; Nomura, K.; Sato, Y. unpublished results (cited with permission).

Supporting Information For

Is It True Dioxygenase or Classic Autoxidation Catalysis? Re-investigation of a Claimed Dioxygenase Catalyst Based on a Ru_2-Incorporated, Polyoxometalate Precatalyst

Cindy-Xing Yin and Richard G. Finke

IR Spectrum of $Q_{11}\{[WZnRu^{III}_2(OH)(H_2O)](ZnW_9O_{34})_2\}$

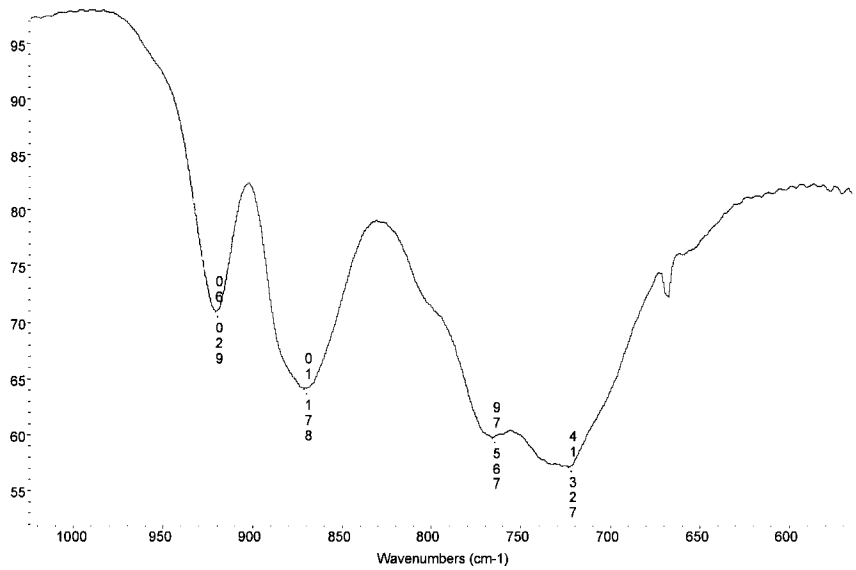

Figure S5.1 IR spectrum of $Q_{11}\{[WZnRu^{III}_2(OH)(H_2O)](ZnW_9O_{34})_2\}$ used in our studies, IR being one of the simplest and quickest ways to identify (fingerprint) polyoxometalates. The observed peaks at 723 (s), 766 (s), 871(m) and 921 (m) cm^{-1} match with the literature values of 765 (s) [a broad peak with a full width at half maximum of ca. 80 cm^{-1} (720–800 cm^{-1}), two identifiable peaks within this range at ca. 730 and 750 cm^{-1}], 881 (m), and 928 (m) cm^{-1}.[1,2]

TGA Curve of the Molecular Sieves Harvested from the $H_2{}^{18}O$ Detection Experiment

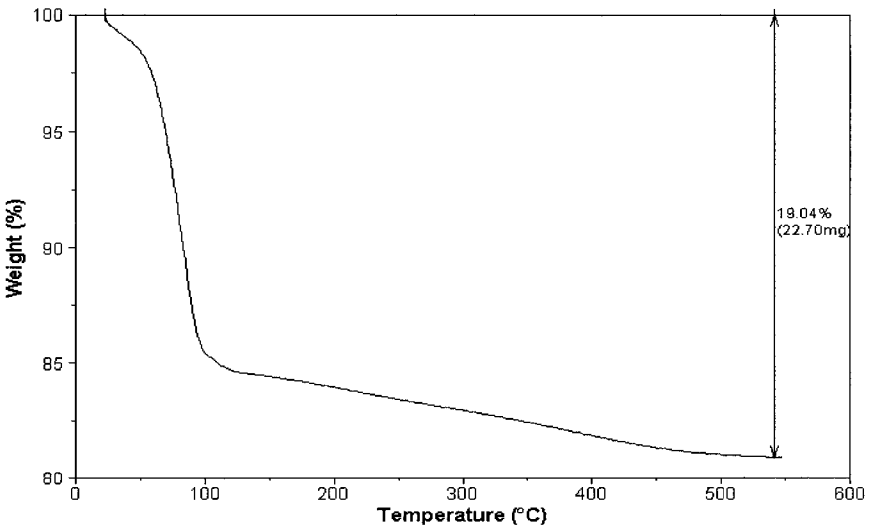

Figure S5.2 TGA weight loss vs temperature curve of the molecular sieves mixed and then harvested from the reaction of adamantane with Q_{11}-**1** under $^{18}O_2$.

---

[1] Neumann, R.; Dahan, M. *Nature* **1997**, *388*, 353-355.
[2] Neumann, R.; Dahan, M. *J. Am. Chem. Soc.* **1998**, *120*, 11969-11976.

A Typical Kinetic Curve Following the Formation of 1-Adamantanol Showing How the Maximum, Steady-State Rate Measurements Were Made

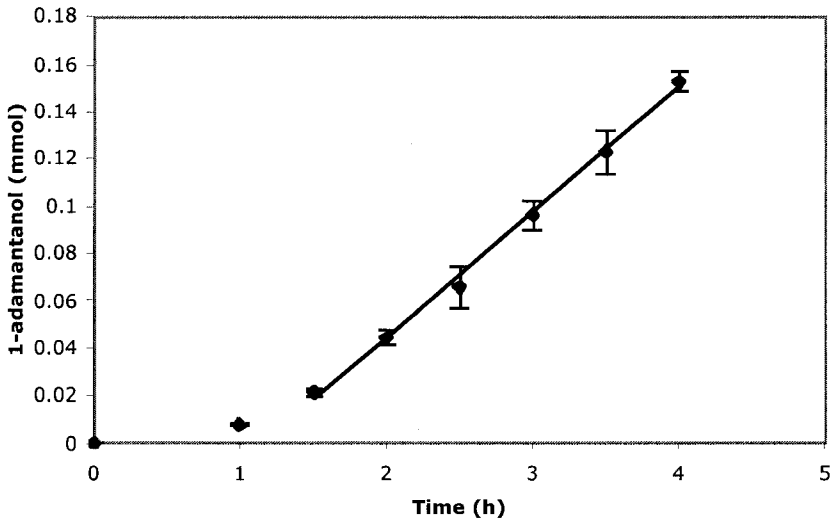

Figure S5.3 A typical kinetic curve following the formation of 1-adamantanol vs time by authentic-sample-calibrated GC. The maximum/steady-state rate, $(d[1\text{-adamantanol}]/dt)_{max}$, was determined from the linear part of the post-induction period as shown, by a linear regression on the indicated data points.

Plot of the Maximum Rate vs pO_2 Showing the Fit to the Data By a Zero-Order pO_2 Dependence

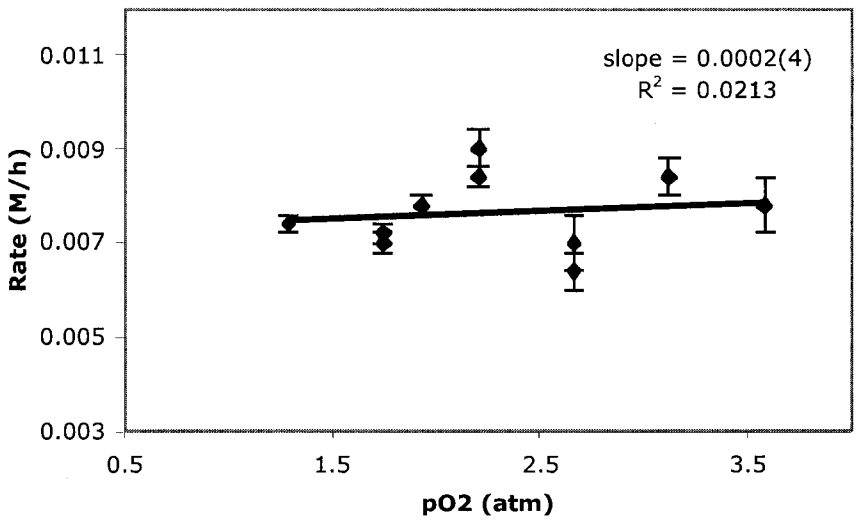

Figure S5.4 Plot of the post-induction period, maximum, steady-state rate $[(d[1\text{-adamantanol}]/dt)_{max}]$ vs pO_2. Reaction conditions: 2.5 mmol adamantane, 2.5 μmol precatalyst, Q_{11}-**1**, 5 mL of $1,2\text{-}C_2H_4Cl_2$ and 1–3.6 atm of oxygen. This plot is provided primarily for a comparison to the half-order plot shown in Figure 5.6C in the main text.

Cyclic Voltammogram of $Q_{11}\{[WZnRu_2(OH)(H_2O)](ZnW_9O_{34})_2\}$

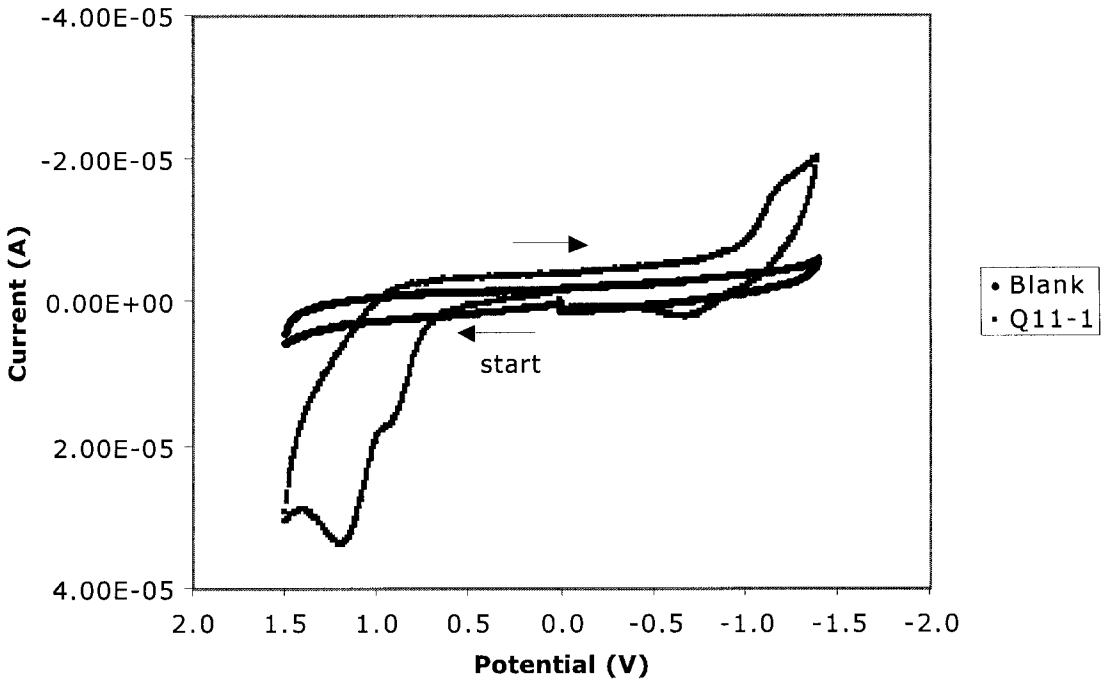

Figure S5.5 Cyclic voltammogram of $Q_{11}\{[WZnRu_2(OH)(H_2O)](ZnW_9O_{34})_2\}$, **1**, in 1,2-$C_2H_4Cl_2$ with 0.1 M $TBAClO_4$, on a glassy carbon electrode, vs SSCE, and with a scanning rate of 100 mV/s. The two irreversible oxidation peaks are at +0.94 V and +1.22 V. Notably, there clearly is no obvious reduction peak for **1**, anywhere near the ≥1 V positive potential that might begin to argue for a Ru_2^{III} (**1**) + Adm–H → $Ru_2^{II/III}$ + Adm• + H^+ initiation step (adamantane $E_{1/2}$ = 2.72 V vs SCE[3]), a step which would give a zero-order dependence on the pO_2 (Figure S5.3; see also the kinetic derivation which follows in two pages for the zero-order pO_2 case).

[3] Bravo, A.; Bjorsvik, H.-R.; Fontana, F.; Minisci, F.; Serri, A. *J. Org. Chem.* **1996**, *61*, 9409-9416.

Rate Law Derivation for the Minimalistic Mechanism in Figure 5.5 of the Main Text at the Steady-State

Initiation

(1) $\mathrm{Adm-H} + \mathrm{Ru_2^{III}} + \mathrm{O_2} \xrightarrow{k_1} \mathrm{Ru_2^{III/IV}OOH} + \underset{\text{(mostly 1-adm•; but some 2-adm•)}}{\mathrm{Adm•}}$

Propagation

(2) $\mathrm{Adm•} + \mathrm{O_2} \xrightarrow[\text{fast}]{k_2} \mathrm{AdmOO•}$

(3) $\mathrm{AdmOO•} + \mathrm{Adm-H} \xrightarrow{k_3} \underset{\text{(primary autoxidation product)}}{\mathrm{AdmOOH}} + \mathrm{Adm•}$

Concurrent Ru_2 - Catalyzed AdmOOH - Based Reaction

(4) $\mathrm{AdmOOH} + \mathrm{Ru_2^{III/IV}} \xrightarrow{k_4} \mathrm{AdmOO•} + \mathrm{H^+} + \mathrm{Ru_2^{III}}$

(5) $\mathrm{AdmOOH} + \mathrm{Ru_2^{III}} \xrightarrow{k_5} \mathrm{AdmO•} + \mathrm{OH^-} + \mathrm{Ru_2^{III/IV}}$

(6) $\mathrm{OH^-} + \mathrm{H^+} \xrightarrow[\text{fast}]{k_6} \mathrm{H_2O}$

(7) $\mathrm{AdmO•} + \mathrm{AdmOOH} \xrightarrow{k_7} \mathrm{AdmOH} + \mathrm{AdmOO•}$

(8) $\mathrm{AdmO•} + \mathrm{Adm-H} \xrightarrow{k_8} \mathrm{AdmOH} + \mathrm{Adm•}$

(9) $\mathrm{2AdmOO•} \xrightarrow{k_9} \mathrm{2AdmO•} + \mathrm{O_2}$

Termination

(10a) $\mathrm{2AdmOO•} \xrightarrow{k_{10}} \mathrm{AdmOOAdm} + \mathrm{O_2}$

(10b) $\mathrm{2AdmOO•} \xrightarrow{k'_{10}} \underset{\text{(possible when one AdmOO• is 2-AdmOO•)}}{\mathrm{1\text{-}AdmOH + 2\text{-}Adm{=}O}} + \mathrm{O_2}$

(Adm ≡ adamantane; AdmOH ≡ 1-adamantanol; Adm=O ≡ 2-adamantanone; AdmOOH ≡ 1-adamantyl peroxide; Ru_2^{III} ≡ **1** (precatalyst); $Ru_2^{III/IV}$ ≡ oxidized **1**)

By the rate of initiation = the rate of termination (i.e., from the steady-state assumption[4]):

$$k_1[\mathrm{Ru_2^{III}}][\mathrm{Adm-H}][\mathrm{O_2}] = 2(k_{10} + k'_{10})[\mathrm{AdmOO•}]^2$$

$$\therefore [\mathrm{AdmOO•}] = \left(\frac{k_1}{2(k_{10} + k'_{10})}\right)^{1/2} [\mathrm{Adm-H}]^{1/2}[\mathrm{Ru_2^{III}}]^{1/2}[\mathrm{O_2}]^{1/2}$$

If one makes the assumption that the AdmOO• is the main radical which reacts with Adm–H (i.e., that k_7[AdmOOH] >> k_8[Adm–H]), that is if the loss of Adm–H occurs primarily via the k_3 step, then one can rationalize from the *observed* kinetics as follows:

---

[4] Huyser, E. S. *Free Radical Chain Reactions*; John Wiley & Sons: New York, 1970.

$$-\frac{d[Adm-H]}{dt} = k_3[Adm-H][AdmOO\bullet]$$

$$= k_3\left(\frac{k_1}{2(k_{10}+k_{10}')}\right)^{1/2}[Adm-H]^{3/2}[Ru_2^{III}]^{1/2}[O_2]^{1/2}$$

Rate Law Derivation for the Mechanism with the Alternative Initiation Step Not Involving O_2 (and Leading to a Zero-Order pO_2 Dependence) at the Steady-State

Initiation

(1) $Adm-H + Ru_2^{III} \xrightarrow{k_1} Ru_2^{II/III} + \underset{\text{(mostly 1-adm•; but some 2-adm•)}}{Adm\bullet} + H^+$ (This first step is the main difference in this alternative mechanims)

Propagation

(2) $Adm\bullet + O_2 \xrightarrow[\text{fast}]{k_2} AdmOO\bullet$

(3) $AdmOO\bullet + Adm-H \xrightarrow{k_3} \underset{\text{(primary autoxidation product)}}{AdmOOH} + Adm\bullet$

Concurrent Ru_2 - Catalyzed AdmOOH - Based Reaction

(4) $AdmOOH + Ru_2^{II/III} \xrightarrow{k_4} AdmO\bullet + OH^- + Ru_2^{III}$

(5) $AdmOOH + Ru_2^{III} \xrightarrow{k_5} AdmOO\bullet + H^+ + Ru_2^{II/III}$

(6) $OH^- + H^+ \xrightarrow[\text{fast}]{k_6} H_2O$

(7) $AdmO\bullet + AdmOOH \xrightarrow{k_7} AdmOH + AdmOO\bullet$

(8) $AdmO\bullet + Adm-H \xrightarrow{k_8} AdmOH + Adm\bullet$

(9) $2AdmOO\bullet \xrightarrow{k_9} 2\,AdmO\bullet + O_2$

Termination

(10a) $2AdmOO\bullet \xrightarrow{k_{10}} AdmOOAdm + O_2$

(10b) $2AdmOO\bullet \xrightarrow[\text{(possible when one AdmOO• is 2-AdmOO•)}]{k_{10}'} 1\text{-}AdmOH + 2\text{-}Adm=O + O_2$

(Adm ≡ adamantane; AdmOH ≡ 1-adamantanol; Adm=O ≡ 2-adamantanone; AdmOOH ≡ 1-adamantyl peroxide; Ru_2^{III} ≡ **1** (precatalyst); $Ru_2^{II/III}$ ≡ reduced **1**)

The same derivation method yields:

$$-\frac{d[Adm-H]}{dt} = \frac{d[product]}{dt} = k_3\left(\frac{k_1}{2(k_{10}+k_{10}')}\right)^{1/2}[Adm-H]^{3/2}[Ru_2^{III}]^{1/2}$$

Kinetic Models Used in Mackinetics to Fit the Observed Kinetic Curves in Figure 5.8

Fitting kinetic curves using chemical elementary steps is useful in supporting or refuting a proposed mechanism. In the main text (Figure 5.8), we used the freeware, Mackinetics, to fit the kinetic curves for the generation of the major product, 1-adamantanol. A grid search for the best-fit rate constants was performed as detailed in the Experimental Section of the main text. Below the models used in Mackinetics are provided (illustrated by chemical equations on the right-hand side). The notation on the left-hand side below is what is actually entered into Mackinetics (i.e., in that program's notation).

The first two steps in all three models set up an "oxygen reservoir" to mimic the oxygen concentration in the solution using the calculation method first used by D. K. Lyon[5] and using literature O_2 solubility data (Henry's constant of 15340 Pa m^3/mol at 293.2 K).[6]

Standard Conditions

We simplified the mechanism in Figure 5.5 of the main text into the four steps listed below for the purposes of the curve-fitting. The implied assumption is, as in the kinetic derivations, that the follow-up reactions converting adamantyl peroxide (AdmOOH below) into 1-adamantanol are fast compared to the formation of AdmOOH from adamantane.

reset

---

[5] Lyon, D. K.; Ph. D. Dissertation, University of Oregon, Eugene, OR, 1990, p 252; see pp 142–145.
[6] Lühring, P.; Schumpe, A. *J. Chem. Eng. Data* **1989**, *34*, 250-252.

reactions

dioxygengas -> dioxygen, kf1=1E9
dioxygen -> dioxygengas, kr1=7E10

adm -> admdot, k1=0.0015
admdot + dioxygen -> admOOdot, k2=1E10
admOOdot + adm -> product + admdot, k3=3.5
admOOdot + admOOdot -> dead, k4=1

$$Adm-H + Ru_2^{III} \xrightarrow{k_1} Adm\bullet + H^+ + Ru_2^{II/III}$$
$$Adm\bullet + O_2 \xrightarrow{k_2,\ fast\ (10^{10})} AdmOO\bullet$$
$$AdmOO\bullet + Adm-H \xrightarrow{k_3} Adm\bullet + AdmOOH \xrightarrow{fast} AdmOH$$
$$2AdmOO\bullet \xrightarrow{k_4} Termination\ products$$

end
...
...
...
#Only first 7 hours' data were fitted.

Standard Conditions Plus the Addition of AIBN

reset
reactions

dioxygengas -> dioxygen, kf1=1E9
dioxygen -> dioxygengas, kr1=7E10

initiator -> initdot + initdot, k1'=10
initdot + dioxygen -> initOOdot, k2'=1E10
adm + initOOdot -> admdot + initOOH, k3'=80
initOOH + admdot -> product + initOdot, k4'=1E9
admdot + dioxygen -> admOOdot, k2=1E10
admOOdot + adm -> product + admdot, k5'=1
admOOdot + admOOdot -> dead, k6'=2

$$AIBN \xrightarrow{k_1'} 2(CN)(CH_3)_2C\bullet + N_2$$
$$(CN)(CH_3)_2C\bullet + O_2 \xrightarrow{k_2',\ fast\ (10^{10})} (CN)(CH_3)_2COO\bullet$$
$$Adm-H + (CN)(CH_3)_2COO\bullet \xrightarrow{k_3'} Adm\bullet + (CN)(CH_3)_2COOH$$
$$Adm\bullet + (CN)(CH_3)_2COOH \xrightarrow{k_4'} (CN)(CH_3)_2CO\bullet + AdmOH$$
$$Adm\bullet + O_2 \xrightarrow{k_2,\ fast\ (10^{10})} AdmOO\bullet$$
$$AdmOO\bullet + Adm-H \xrightarrow{k_5'} Adm\bullet + AdmOOH \xrightarrow{fast} AdmOH$$
$$2AdmOO\bullet \xrightarrow{k_6'} Termination\ products$$

end
...
...
...

Standard Conditions Plus the Addition of TBHP (tBuOOH)

reset
reactions
dioxygengas -> dioxygen, kf1=1E9
dioxygen -> dioxygengas, kr1=7E10

tBuOOH -> tBuOOdot + Hdot, k1''=20
tBuOOdot + adm -> tBuOOH + admdot, k2''=100
admdot + tBuOOH -> product + tBuOdot, k3''=8E8
admdot + dioxygen -> admOOdot, k2=1E10
admOOdot + adm -> product + admdot, k4''=0.1
admOOdot + admOOdot -> dead, k5''=1.5

$$(CH_3)_3COOH \xrightarrow{Ru_2^{III},\ k_1''} (CH_3)_3COO\bullet + H^+$$
$$Adm-H + (CH_3)_3COO\bullet \xrightarrow{k_2''} Adm\bullet + (CH_3)_3COOH$$
$$Adm\bullet + (CH_3)_3COOH \xrightarrow{k_3''} AdmOH + (CH_3)_3CO\bullet$$
$$Adm\bullet + O_2 \xrightarrow{k_2,\ fast\ (10^{10})} AdmOO\bullet$$
$$AdmOO\bullet + Adm-H \xrightarrow{k_4''} Adm\bullet + AdmOOH \xrightarrow{fast} Adm$$
$$2AdmOO\bullet \xrightarrow{k_5''} Termination\ products$$

end
...
...

We note that the above mechanisms (based on the radical-chain autoxidation pathway in Figure 5.5 of the main text) have multiple, unconstrained variables (rate constants) that can be used to accomplish the "best" fits. Hence, the (good) fits shown in Figure 5.8 in the main text are considered *only* supporting evidence for the radical-chain mechanism in Figure 5.5 of the main text—but still fully consistent with, and supportive of, the (non-dioxygenase), radical-chaim mechanism used in the fit.

Attempted Synthesis of 1-Adamantyl Peroxide

The precursor 1,3-dehydroadamantane (DHA) was prepared according to the literature:[7] 1,3-dibromoadamantane was refluxed with Na-K alloy in diethyl ether under argon; yield, 33% (including ~26% adamantane impurity by ^{1}H-NMR); literature, 77% (including ~10% adamantane impurity).[7] ^{1}H-NMR (in C_6D_6 of the crude material): δ 2.73(s), 2.05(t), 1.64(s), 1.14(d), 1.91(d) with peaks at 1.72(s) and 1.83(s) attributed to adamantane; literature δ (after isolation) 2.73(s), 2.05(t), 1.66(m), 1.15(d), 1.91(d). The impure 1,3-DHA (0.09 g, 0.7 mmol) was dispersed into 10 mL diethyl ether in a 50 mL round-bottomed flask in the drybox, and the flask was then sealed and brought out of the drybox. Next, 0.32 mL 30 w.t.% H_2O_2 was added under air into the DHA solution. The solution was then refluxed at ca. 35 °C for 5 hours. Workup was involved the addition of 5 mL water followed by condensing the mixture under vacuum. Then, 5 mL 0.02 M NaOH were added in order to precipitate 1-adamantyl peroxide. The resultant white powder gives broad multiple peaks around δ 1.3–2.3 in $CDCl_3$ for ^{1}H-NMR analysis instead of the four single peaks (δ 1.48, 1.68, 2.01, 8.54 in $CDCl_3$) claimed in the

[7] Pincock, R. E.; Schmidt, J.; Scott, W. B.; Torupka, E. J. *Can. J. Chem.* **1972**, *50*, 3958-3964.

literature.[8] In two separate, repeat trials, the H_2O_2 was transferred under Ar (2nd trial) or by vacuum transfer into the frozen DHA solution (3rd trial); the DHA and H_2O_2 mixture was then filled with Ar and refluxed at ca. 35 °C (5 h) under Ar (to suppress the oxygenation reaction of DHA). ^{1}H-NMR was used to monitor the reaction in the 3rd trial, products at the end of the reflux give ^{1}H NMR ($CDCl_3$) signals of δ 0.002 (s), 1.68 (s), 2.32 (s), 9.04 (s). After storing the refluxed solution in the drybox overnight, the ^{1}H NMR ($CDCl_3$) signals shifted to δ 0.08 (m), 1.58–1.66 (m), 1.73 (d), 1.76 (t), 1.82 (d), 2.15 (s), 2.20 (s), 3.74 (s). Obviously, 1-adamantyl hydroperoxide is unstable, decomposing even under N_2 at room temperature.

[8] Son, V. V.; Ivashchenko, S. P.; Son, T. V. *Zh. Obshch. Khim.* **1990**, *60*, 710-712.

GC Traces of Cyclohexene Autoxidation Catalyzed By Q_{11}-1 And $[Bu_4N]_5Na_3[(1,5\text{-}COD)Ir{\bullet}P_2W_{15}Nb_3O_{62}]$

$[Bu_4N]_5Na_3[(1,5\text{-}COD)Ir{\bullet}P_2W_{15}Nb_3O_{62}]$

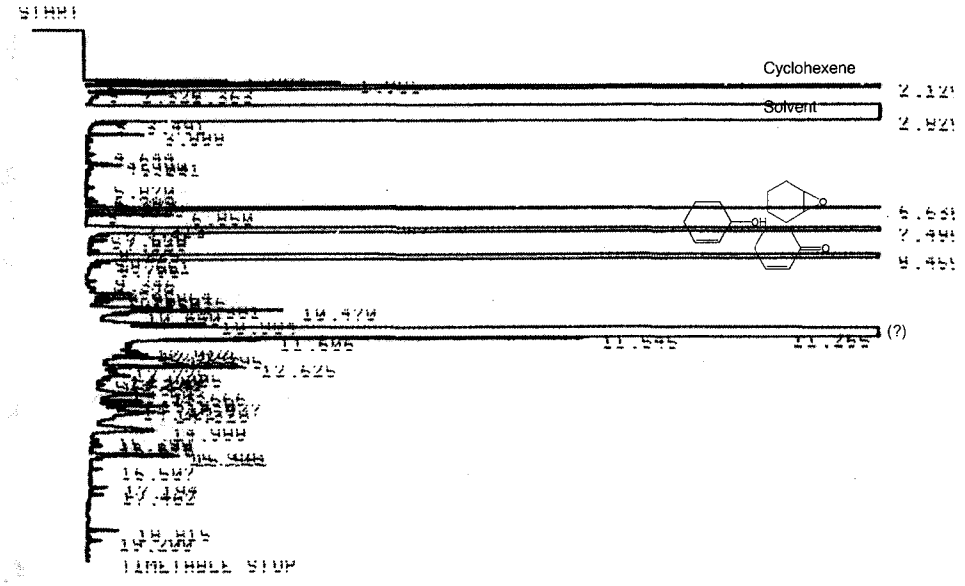

Q_{11}-1

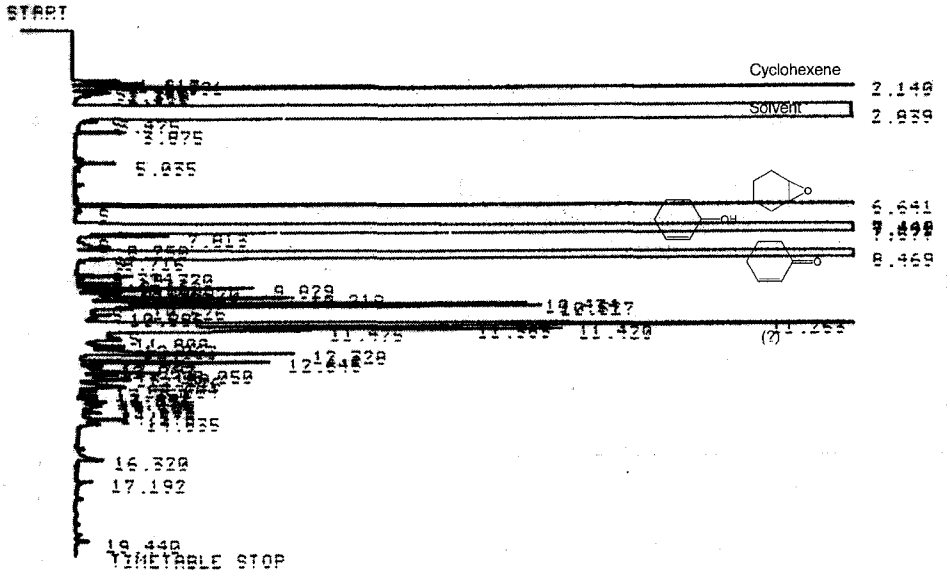

Figure S5.6 The GC traces of cyclohexene autoxidation catalyzed by $[Bu_4N]_5Na_3[(1,5\text{-}COD)Ir{\bullet}P_2W_{15}Nb_3O_{62}]$ and Q_{11}-**1**. Give the literature precedent that such GC traces (and the products they detect) are as compelling a single piece of evidence as exists for cyclohexene autoxidation,[9] the GC traces for Q_{11}-**1** (and its similarity to that for $[Bu_4N]_5Na_3[(1,5\text{-}COD)Ir{\bullet}P_2W_{15}Nb_3O_{62}]$) provide unequivocal evidence that Q_{11}-**1** is a good cyclohexene autoxidation catalyst.

[9] Weiner, H.; Trovarelli, A.; Finke, R. G. *J. Mol. Catal.* **2003**, *191*, 217-252.

Control Experiments Testing the Effect of Excess Q^+Cl^- in the Precatalyst 1

We had two samples of **1** with apparent different amounts of excess Q^+Cl^-, as estimated by the CHN analysis, to use in these control experiments. The first sample of **1** contained 2–3 equivalents excess QCl per Q_{11}-**1** (CHN results are available in the main text); this sample of Q_{11}-**1** exhibits a maximum reaction rate of d[1-adamantanol]/dt = 0.0072 (±0.0002) mM/h. The second sample contained 9–10 equivalents of QCl (this sample was prepared by a previous researcher in our lab; its CHN results are available elsewhere[10]). The second sample gave a maximum reaction rate of d[1-adamantanol]/dt = 0.0068 (±0.0004) mmol/h. *These results show that a varying amount of excess QCl does not change the kinetic performance of Q_{11}-**1**·nQCl (n = 2–10) in the adamantane hydroxylation reaction.*

An attempt was made to extract the excess QCl out of the Q_{11}-**1**·nQCl precatalyst (n = 9–10) with *n*-pentane. However, CHN analysis on the resultant product showed that the sample (washed with pentane 5 times, then dried under vacuum) still contains the same amount of 9–10 equiv excess QCl.

Control Experiment Testing the Catalytic Ability of QCl without Precatalyst 1

This control was set up as a standard reaction: 2.5 mmol adamantane, 0.053 mmol QCl (ca. 21 equiv. of Q_{11}-**1**), 5.0 mL 1,2-$C_2H_4Cl_2$, 80 °C, and 1.8 atm O_2. After 24 h the diluted reaction solution was analyzed by GC. The yield of 1-adamantanol is 1.5 ± 0.1%, and that of 2-adamantanone is 0.31 ± 0.02%. The 3°/2° ratio is 15, the same as the ratio observed using Q_{11}-**1** (16 (±3):1). The same selectivity shows that the adamantane

[10] Weiner, H.; Finke, R. G. *J. Am. Chem. Soc.* **1999**, *121*, 9831-9842.

hydroxylation reaction with only QCl present is also a free-radical autoxidation, albeit one slow on the time scale of the reaction catalyzed by Q_{11}-**1**.

Control Experiment Testing for Any Effects of Solvent Pretreatment

The 1,2-$C_2H_4Cl_2$ solvent used in the previous studies was treated by H_2SO_4, $SnCl_2$, then distilled under ambient condition prior to use.[2] Hence, we did the following control experiment to test whether or not this treatment of the solvent could lead to a different kinetic performance than we saw using pre-dried HPLC grade 1,2-$C_2H_4Cl_2$ (Aldrich).

First, 20 mL ACS grade 1,2-$C_2H_4Cl_2$ solvent was shaken with 20 mL 9 M H_2SO_4. The organic layer was then treated with ca. 20 mL of a 0.1 M $SnCl_2$ (Aldrich, 99.995+%) solution. The resultant 1,2-$C_2H_4Cl_2$ was distilled under air, degassed with Ar, and then transferred into the drybox for use.

The maximum rate for a standard run with the solvent pre-treated as above is d[1-adamantanol]/dt = 0.0076 (±0.002) mM/h, same within experimental error as the standard rate, 0.0072 (±0.002) mM/h. And, the induction period is the same as before (≤ 0.5 h). Hence, there is no discernable difference based on the solvent or its pretreatment.

Control Experiment Testing for the Reported *Trans*-Cyclooctene Epoxidation Reaction. *Trans*-cyclooctene was reported to produce cyclooctene oxide at a *trans*:*cis* ratio of 20:1 and 12.5% yield in the prior work.[2] Although this *epoxidation* reaction has no direct bearing on the adamantane *hydroxylation* reaction, we attempted to repeat this experiment as follows. First, *trans*-cyclooctene was prepared as in the literature.[11] GC of the substrate prior to reaction showed decomposition had already begun (the cyclooctene peak area decreased with time along with the appearance of a peak for the cyclooctene

[11] Shea, K. J.; Kim, J.-S. *J. Am. Chem. Soc.* **1992**, *114*, 3044-3051.

oxide due to simply having the metastable *trans*-cyclooctene in air (O_2) as hinted at in the literature[11]). NMR of the substrate is consistent with the GC result: δ 5.51, 2.35, 1.3–1.9, 0.89 (literature for the *trans*-cyclooctene,[11] δ 5.50, 2.36, 2.02–1.88, 1.82, 1.42, 0.79) together with peaks assigned to *cis*-cyclooctene oxide δ 2.90, 2.17, 1.52, 1.31.

The epoxidation reaction conditions were chosen to match as close as possible the previously reported conditions: ca. 0.24 mmol of *trans*-cyclooctene, 0.24 μmol of Q_{11}-**1**, 0.5 mL 1,2-$C_2H_4Cl_2$, 80 °C, and 0.87 atm O_2. After 24 h, the reaction solution was diluted and analyzed by GC. A single peak ascribed to ca. 10 ± 1% cyclooctene oxide was detected (literature 12.5%)[2]. The reaction solution was then evaporated under vacuum and then dissolved in $CDCl_3$ for ^{1}H-NMR analysis. The observed hydrogens of the oxirane ring were attributed to *cis*-cyclooctene oxide (δ 2.9); no *trans*-cyclooctene oxide oxirane ring hydrogens could be observed (δ 2.72).[11] We view our inability to repeat the prior report of *trans*:*cis* oxide product in a 20:1 ratio[2] as *inconclusive*, however, due to the instability of the *trans*-cyclooctene starting material. Due to that instability, *trans*-cyclooctene is *not* a substrate that we recommend be used in attempts to provide definitive evidence for or against dioxygenase catalysis.

Discussions of the Other Putative Evidence in the Prior Work[1,2]

1. Hydroxylation occurred exclusively at the tertiary carbon as compared to free-radical oxidation reactions, for which the rate ratio of hydroxylation at the tertiary vs secondary carbon is only 3:1.

The observed selectivity was used as evidence by the authors against a free-radical mechanism.[1,2] In fact, the 2-adamantyl (secondary) radical is less stable than 1-adamantyl

(tertiary) radical,[12] so that the higher selectivity for tertiary vs secondary C–H bonds is readily explained by a free-radical mechanism. Similarly, chromic acid was reported to oxidize adamantane via a caged radical pair producing 71% 1-adamantanol and 9% 2-adamanantone[13] (much higher selectivity than the ratio of 3:1 seen before[14,15]). Hence, high selectivity does not unambiguously demand a non-radical mechanism (for a summary of adamantane hydroxylation reactions catalyzed by ruthenium catalysts see Table S5.1 in the Supporting Information). The selectivity argument in the prior work is flawed/was misused in our opinion.

2. Easily auto-oxidized substrates like cumene are less active than adamantane.

Without knowledge of a) the exact oxidant (in this case, C–H bond activating ROO• and the less selective RO•); b) the rate law for that process; and c) controls with ROO• and RO• radicals, any comparison of cumene with adamantane is ambiguous in our opinion.

3. The kinetic isotope effect of 5.7 ± 0.2 for in 1,3-adamantane-d_2 hydroxylation.

The observed kinetic isotope effect shows that hydrogen abstraction step is a rate-determining step. This is, however, consistent with the radical-chain mechanism in Figure 5.5 in the main text.

4. Isolation and identification of a ruthenium oxo or peroxo species by IR and its use in alkene epoxidation.

The observation of a putative ruthenium oxo or peroxo species after Q_{11}-1 was treated with O_2 was claimed on the basis of the IR of a KBr pellet. However, the assignment is not definitive due to the low resolution of the IR spectra. Even if correct, the connection

---

[12] Tabushi, I.; Aoyama, Y.; Kojo, S.; Hamuro, J.; Yoshida, Z. *J. Am. Chem. Soc.* **1972**, *94*, 1177-1183.
[13] Bingham, R. C.; Schleyer, P. v. R. *J. Org. Chem.* **1971**, *36*, 1198-1201.
[14] Smith, G. W.; Williams, H. D. *J. Org. Chem.* **1961**, *26*, 2207-2212.
[15] Kojima, T.; Matsuo, H.; Matsuda, Y. *Inorg. Chim. Acta* **2000**, *300-302*, 661-667.

of that isolated, stable species to the typically transient, unstable true catalysts is unclear until and unless a connection, of the observed IR data to the kinetics of catalysis, can be made.

5. Epoxidation of Trans-cyclooctene to give a 20:1 Trans:Cis Ratio of Products.

First, this *epoxidation* reaction has no logical bearing on the mechanism of the *adamantane C-H bond hydroxylation* reaction. In addition, at least we were unable to repeat this reported result (*vide supra*).

In short, these last five pieces of putative evidence in the original work do not provide compelling evidence for a non-radical-chain, dioxygenase mechanism as previously claimed.[1,2]

Table S5.1 Literature overview of adamantane oxidation by ruthenium complexes and different oxidants (O_2, hydroperoxide, etc.)

	System	Selectivity[a]	KIE[b]	Inhibited?	Evidence/Comments
1	$RuCl_3 + NaIO_4$ Carlsen, P. H. J. *Syn. Commun.* **1987,** *17(1),* 19-23.	75:ND[d]	-	-	An early report of ruthenium catalyzed oxidation of alkanes in CCl_4-CH_3CN-water. **Carbonium ions** accounted for the observed product. Site selectivity is poor.
2	*cis*-$[RuCl_2(Me_2SO)_4]$, *cis*-$[RuCl_2(phen)_2]$, *trans*-$[RuCl_2(dpp)_2]$ or $[RuCl(dpp)_2]PF_6 + HClO_4$ dpp ≡ 1,3-bis(diphenylphosphino)propane Bressan, M. et al. *J. Chem. Soc., Chem. Commun.* **1989,** 421-2.	(30–35):1	-	-	A **Ru^{IV}=O** species was suggested to abstract hydrogen radical from RH via a **free-radical path** forming [Ru^{III}-OH·····R•] then giving out ROH as the product. [Ru^{II}] was re-oxidized to Ru^{IV}=O fulfilling the catalytic cycle.
3	*trans*-$[Ru^{VI}(L)(O)_2]^{2+}$ (stoich[c]) L≡ Che, C.-M. et al. *JACS* **1989,** *111,* 9048-56. 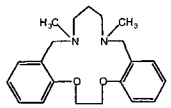	> 75:1	-	-	X-ray crystal structure solved for *trans*-$[Ru^{IV}(L)(O)(H_2O)][ClO_4]_2 \cdot 2H_2O$, different IR resonance observed for Ru=O and RuO_2. Kinetics show rate = k[Ru(VI)][organic substrate]. ***Trans*-oxo Ru complex** was considered as the reactive intermediate.
4	Ru^{III}-EDTA + O_2 Ru^{V}=O(EDTA) (stoich[c]) Ru^{III}-EDTA-ascorbate + O_2 Khan, M. M. T. *Studies in Surf. Sci. and Catal.* **1991,** *66,* 31-45.	60:1 60:1 2.25:1	12 10.5 ~3	- - -	**Active catalyst [Ru^{V}=O(EDTA)]$^-$** characterized by elemental analysis, UV-vis, IR and cyclic voltammetry. A radical cage mechanism was proposed for the first two systems and an ionic mechanism for the last system shown left.
5	*trans*-$[Ru^{VI}(dmbipy)_2O_2][ClO4]_2$ (stoich[c]) dmbipy ≡ 5,5-di-Me-2,2-bipyridine Che, C.-M. et al. *J. Chem. Soc., Dalton Trans.* **1991,** 379-84.	61:ND	14 ± 2	-	*Trans*-oxo Ru(VI) complex characterized by elemental analysis, UV-vis and cyclic voltammetry (high redox potential, $E°(Ru^{VI-IV})$ = 1.0 V). A H-atom abstraction pathway was proposed based on KIE. **A metal oxo intermediate** was suggested.
6	$[Ru^{V}L(O)]^{2+}$ (stoich[c]) HL ≡ Che, C.-M. et al. *J. Chem. Soc., Dalton Trans.* **1991,** 1259-63. 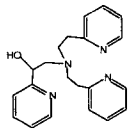	60:ND	5.3	-	The title compound was reported to be more reactive than any previous Ru=O complexes. Cyclohexane is oxidized at room temperature. The exact pathway of **Ru^{V}=O** reacting with RH is not clear.

7	$[Ru^{II}(terpy)(dcbipy)(H_2O)]^{2+}$ + TBHP $[Ru^{IV}(terpy)(dcbipy)O]^{2+}$ (stoich[c]) terpy ≡ 2,2':6',2''-terpyrdine dcbipy ≡ 6,6'-di-chloro-2,2'-bipyridine TBHP ≡ *tert*-butyl hydroperoxide hereafter Che, C.-M. et al. *J. Chem. Soc., Dalton Trans.* **1991,** 1901-7.	9.5:1 28:ND	- -	- -	A **Ru^{IV}=O** species was proposed to pre-associate with **alkenes** (alkanes, in particular cyclohexane, was not active) prior to their oxidation to form epoxides or other products. Possibility of Ru^{IV}=O as an intermediate was ruled out in the catalytic reaction by Ru^{II} and TBHP, but no mechanistic study was performed on the stoichiometric system.
8	$RuO_2 \cdot 2H_2O + NaIO_4$ Bakke, J. M. et al. *Acta Chem. Scand.* **1991,** *45,* 418-23.	116:1	5.3 for tricyclo[5,2,1,0]decane	-	The reaction was proposed to proceed by **hydride abstraction and carbocation formation**. The free radical mechanism was argued against by the high selectivity of adamantane oxidation and the absence of chlorinated product in CCl_4/H_2O.
9	$RuCl_3 \cdot nH_2O + RCO_2H + R'CHO + O_2$ Murahashi, S.-I. et al. *JACS* **1992,** *114,* 7913-4.	30:1	5.5	-	Ru (or Fe) catalysts in presence of aldehydes and acids were highly active in alkane oxidation with O_2. An **oxometal** was assumed to form from the metal plus peracid (acetic acid + aldehyde + O_2). An industrial strategy for cyclohexanone synthesis was proposed based on the high activity.
10	$RuTMP(O)_2$ + *N*-oxide RuTPP(CO) + HBr + *N*-oxide RuTMP(CO) + HBr + *N*-oxide $RuTDCPP(O)_2$ + HBr + *N*-oxide $RuTMP(O)_2$ + HCl/Br + *N*-oxide Hirobe, M. et al. *JACS* **1992,** *114,* 10660-2.	> 24:1 66:trace 96:1 46:1 (95-204):1[e]	- - - - -	- - - - -	Catalytic ability of Ru porphyrins enhanced by the addition of HCl or HBr. A significant amount of adamantane-1,3-diol was produced (ca. 1/4–1/3 of product). No mechanistic studies were reported. *N*-oxide ≡ 2,6-di-Cl-py *N*-oxide; TPP ≡ tetraphenylporphyrinato; TMP ≡ tetramesitylporphyrinato; TDCPP ≡ tetrakis(2,6-dichlorophenyl)porphyrinato.
11	*cis*-$[RuCl_2(DMSO)_4]$ + LiClO *trans*-$[RuCl_2(DPP)_2]$ + LiClO $[RuCl(DPP)_2]PF_6$ + LiClO DPP ≡ 1,3-bis(diphenylphosphino)propane Morvillo, A. et al. *J. Mol. Catal.* **1992,** *71,* 149-55.	35:1 30:1 30:1	- - 5.6	- - -	KIE indicate that C–H bond breaking in the transition state. The precatalyst is not forming ruthenium oxides by ^{31}P-NMR. **An oxo- or dioxo-ruthenium complex** is proposed as a possible, dominant species.

12	$K[Ru^{III}(saloph)Cl_2] + O_2$ saloph ≡ 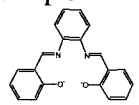 Khan, M. M. T. et al. *J. Mol. Catal.* **1992,** *75,* L49-51.	4.5:1	-	-	A **high valent Ru(V) oxo complex** was proposed to transfer its oxygen atom to the substrate.
13	*cis*-$[Ru(H_2O)_2(dmso)_4](BF_4)_2$ + NaClO $K_6[Ru(H_2O)(PW_{11}O_{39}]$ + NaClO *cis*-$[Ru(H_2O)_2(dmso)_4](BF_4)_2$ + TBHP $K_6[Ru(H_2O)(PW_{11}O_{39}]$ + TBHP Bressan, M. et al. *J. Mol. Catal.* **1992,** *77,* 283-8.	39:1 39:1 9:1 12:1	2.5-4 for all	- - - -	Hypochlorite oxygenations proceed via **oxo-metal species** while TBHP oxygenations are dominated by a **free-radical mechanism**. These are based on the adamantane selectivity and different products (epoxidation or allylic attack) using 1-octanene. Sigmoidal curves were observed for cyclohexane oxidation activity and oxygen consumption.
14	*cis*-$[Ru^{VI}LO_2]^{2+}$ L ≡ 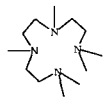 Che, C.-M. et al. *J. Chem. Soc., Dalton Trans.* **1992,** 2109-16.	34:ND	-	-	X-ray crystal structure of the title compound was solved after several steps of refinement. *Cis*-$[Ru^{VI}LO_2]^{2+}$ was not stable in acetonitrile solvent, it is slowly reduced to *cis*-$[Ru^{V}LO_2]^{+}$ and finally to *cis*-$[Ru^{II}L(MeCN)_2]^{2+}$. *Cis*-$[Ru^{VI}LO_2]^{2+}$ was studied by cyclic voltammetry. No mechanistic studies were performed.
15	$[Ru(R^1COCR^2COR^3)_3] + CF_3COOH + O_2$ $R^1 = R^3 = Me$, $R^2 = H$ Ingrosso, G. et al. *Gazz. Chim. Acta.* **1993,** *123,* 179-80.	9:1	-	Yes	A Ru-based non-porphyrin active site assists the selective monooxygenation of nonactivated C–H bonds by dioxygen. CF_3COOH is crucial in the oxidation. No mechanistic results were provided.
16	$RuCl_2(PPh_3)_3$ + TBHP Murahashi, S.-I. et al. *Tetrahedron Lett.* **1993,** *34,* 1299-302.	10.2:1	8.4	-	A **Ru(IV)=O** abstracts hydrogen from the substrate forming a caged {Ru(III)-OH R•} species; two pathways yield either ROH or ROO-*t*-Bu products.
17	$[Ru^{II-III}Cl_{1-2}(LL)_2]^+ + KHSO_5$ $[Ru^{II-III}Cl_{1-2}(LL)_2]^+ + PhIO$ Bressan, M. et al. *Inorg. Chim. Acta.* **1993,** *211,* 217-20.	(12–14):1 (30–54):1	1 3-5 (hexane)	-	Based on different selectivity and KIE results, the first system was proposed to oxidize via a **per oxo-metal species** and the second via typical **oxo-metal derivatives**. LL ≡ DPP (1,3-bis(diphenylphosphino)propane) or DPE (1,2-bis(diphenylphosphino)ethane)

18	*cis*-$[Ru(dmp)_2(H_2O)_2](PF_6)_2 + H_2O_2$ dmp ≡ 2,9-di-Me-1,10-phenanthroline Drago, R. S. et al. *JACS* **1994,** *116,* 2424-9.	7:1	4.0	Yes	A **radical mechanism during induction period to generate a high valent Ru=O species** was proposed. Free-radical chain involvement could not be excluded. Induction period for the epoxidation reaction could be removed by the addition of H_2O_2 (generating Ru=O).
19	5%Ru/C + CH_3CO_3H Murahashi, S.-I. et al. *Tetrahedron Lett.* **1994,** *35,* 7953-6.	16:1	4.8	-	Cytochrome P-450 type mechanism with $Ru^n \rightarrow$ **Ru^{n+2}=O** was proposed. An alternative mechanism with a cationic intermediate **$Ru^nOH{\cdot}R^+$** was discussed also.
20	$BaRuO_3(OH)_2$ + TFA + bpy Lau, T.-C. et al. *J. Chem. Soc., Dalton Trans.* **1995,** 943-4.	97:1	4.0 and 7.7[g]	-	A **dioxoruthenium(VI)** species, $[Ru^{VI}(bpy)O_2(CF_3CO_2)_2]$ was considered to be the active intermediate. The system is capable of oxidizing ethane and propane with good yields.
21	$RuTMP(O)_2$ + HCl/Br + *N*-oxide (system same as Reference **#10**) Hirobe, M. et al. *Heterocycles* **1995,** *40,* 867-903.	(95-204):1[e]	-	-	The addition of acid (HCl or HBr) enhanced the catalytic activity of the ruthenium porphyrin complex in the oxidation of alkanes and aliphatic alcohols. $Ru(TMP)(O)_2$ plus *N*-oxide showed higher activity than $Ru(TMP)(O)_2$ by itself. The active intermediate was formulated as **$[Ru^{VI}(por)(X)(O)]^+$** (X ≡ Cl or Br). Total turnovers of up to 120,000 are reported in the oxidation of adamantane.
22	$[Ru(H_2O)_2(bipy)_2]^{2+}$ + TBHP (stoich[c]) $[RuO_2(bipy)\{IO_3(OH)_3\}] + IO_4^-$ (stoich[c]) Griffith, W. P. et al. *J. Chem. Soc., Dalton Trans.* **1995,** 3537-42.	ND:13 ND:45	- -	- -	Epoxidations of alkenes and oxidation of alkanes and alcohols are catalyzed by a series of $Ru(L)O_x$ complexes (L ≡ bipy and phen) and other bimetallic complexes. No mechanistic information was provided.
23	$[Ru^{II}(TPFPP)(CO)]$ + 2,6-di-Cl-py *N*-oxide TPFPP ≡ tetrapentafluorophenylporphyrinato Groves, J. T. et al. *JACS* **1996,** *118,* 8961-2.	76:ND	3.05 for adamantane	-	**Ru(III)-OD(X)(por)$^+$** was proposed to be the catalyst (without induction period). OD refers to $pyCl_2NO$ as oxygen donor, X ≡ OD or other ligands. Adamantane-1,3-diol was obtained as ca. 1/10 of the main product, 1-adamantanol.
24	$[Ru^{III}Cl_2(TPA)]^+$ + *m*-chloroperbenzoic acid TPA ≡ tris(2-pyridylmethyl)amine Kojima, T. *Chem. Lett.* **1996,** 121-2.	23:1	-	-	Title complex was synthesized and characterized by X-ray crystallography. When used together with TBHP, there is no oxidation activity toward adamantane. A **high-valent Ru=O species** was suggested as the active intermediate.

25	$[Ru^{II}(TPFPP)(CO)]$ + 2,6-di-Cl-py *N*-oxide TPFPP ≡ tetrapentafluorophenylporphyrinato Groves, J. T. et al. *Studies in Surf. Sci. and Catal.* **1997,** *110,* 865-72..	>210:1	4.8 for adamantane	-	This is a further mechanistic study of the system in Ref #23. A short induction period (< 1h) was observed. $[Ru^{VI}(TPFPP)(O)_2]$ was ruled out as the active intermediate by turnover rates. **OxoRu(V) and Ru(III) species** are proposed to be the key intermediates in the "rapid oxygenation" catalytic cycle.
26	$\{[WZnRu^{III}_2(OH)(H_2O)](ZnW_9O_{34})_2\}^{11-} + O_2$ Neumann R. et al. *JACS* **1998,** *120,* 11969-76.	12.3: ND	5.7 for adamantane	No	Kinetic and spectroscopic evidence are reported. An induction period was observed for adamantane hydroxylation. A **non-radical high valent Ru=O** was suggested as the active intermediate in a dioxygenase type mechanism.
27	Ru^{III}-EDTA + ascorbic acid + O_2 Shukla, R. S. *Studies in Surf. Sci. and Catal.* **1998,** *113,* 897-905.	3.8:1	3.48	-	Kinetics studies gave: rate = $k[Ru^{III}\text{-EDTA}][\text{ascorbic acid}][O_2][\text{saturated substrate}]^{<1}[H^+]^{-1}$. An **ionic mechanistic route** was discussed, a tertiary complex of ascorbic acid-Ru^{III}L-OO^- abstract hydride from substrate then transfer O to substrate.
28	$[RuCl(L)(tpy)]Cl_n$ + MCPBA $[RuCl(L)(tpm)]Cl_n$ + MCPBA L ≡ bpy, dmpa or dmgly Yamaguchi, M. et al. *Inorg. Chem. Commun.* **1998,** *1,* 299-301.	(3-40):1 (9-28):1	- -	- -	Effective hydroxylation of adamantane was observed with the coproduct of 1-chloroadamantane (yield 5–9%). No induction period was observed. No mechanistic studies were performed. tpy ≡ 2,2',2''-terpyridine; tpm ≡ tris(pyrazolyl)methane; dmpa ≡ *N,N*-dimethylpicolylamine; dmgly ≡ *N,N*-dimethylglycinate.
29	$5\%Ru/C + CH_3CO_3H$ $RuCl_3 \cdot nH_2O + CH_3CO_3H$ $Ru^{II}Cl_2(PPh_3)_3$ + TBHP Murahashi, S.-I. et al. *J. Org. Chem.* **2000,** *65,* 9186-93.	19:1 30:1 -	6.8[f] 9.2[f]	- - No	**High valent Ru=O species** are suggested for the mechanisms of both $Ru^{II}L_n$ with TBHP and Ru^nL_m with CH_3CO_3H on the basis of kinetic studies, isotope effects and product analyses.
30	$[Ru^{II}(TPA)Cl]_2$ or $[Ru^{II}Cl(5\text{-}Me_3TPA)]_2$ + TBHP or cumeneHP Kojima, T. et al. *Inorg. Chim. Acta.* **2000,** *300-2,* 661-7.	(2.0-3.1):1	6	Yes	X-ray crystal structure was solved for $[Ru^{II}Cl(5\text{-}Me_3TPA)]_2(PF_6)_2$. **Free radical chain (Haber-Weiss) mechanism** was proposed for the reactions, although without ruling out the involvement Ru=O species.

31	*cis*-[Ru^{VI}(6,6'-Cl_2bpy)$_2O_2$](ClO_4)$_2$ (stoich[c]) *cis*-[Ru^{II}(6,6'Cl_2bpy)$_2$(OH_2)$_2$](CF_3SO_3)$_2$ +TBHP Che, C.-M. et al. *J. Org. Chem.* **2000,** *65,* 7996-8000.	75:ND 7:1	6.5 4.8	- Yes	The first system behaved **differently from Gif system** in competitive oxidation and KIE; while the second system was believed to catalyze via **a free-radical mechanism.**
32	$RuCl_3 \cdot nH_2O$ + CH_3CO_3H Murahashi, S.-I. et al. *Chem. Commun.* **2001,** 65-66.	30:1	2.9	-	The lower KIE was explained due to a more reactive species using TFA (trifluoroacetate) as solvent than using ethyl acetate. **L_nRu^V=O** was suggested as the active species.
33	[Ru($R_{1\text{-}3}$-TPA)] + PhIO $R_{1\text{-}3}$ vary from ^{t}BuCONH, ^{t}BuCH_2NH and H. Jitsukawa, K. et al. *Tetrahedron Lett.* **2001,** *42,* 3467-9.	(3.5–12.1):1	-	-	Different activities toward the hydroxylation of alkanes and the epoxidation of olefins were observed for different $R_{1\text{-}3}$-TPA ligand. Electron withdrawing groups enhance the epoxidation while electron donating groups enhance the hydroxylation.
34	*trans*-$RuCl_2(PPh_3)(\kappa^3\text{-L})$ + TBHP L≡ Wong, W.-K. et al. *J. Chem. Soc., Dalton Trans.* **2002,** 1139-46.	70:1	-	Yes	Four of six *trans*-$RuCl_2(PPh_3)(L^{1\text{-}6})$ complexes were solved for X-ray crystal structures. The title compound was found to be the most active precatalyst (with an induction period). **Free radical species** were suggested to be involved in the mechanism.
35	[(n-$C_4H_9)_4N]_4H[SiW_{11}Ru^{III}(H_2O)O_{39}]\cdot 2H_2O + O_2$ Mizuno, N. et al. *New J. Chem.* **2002,** *26,* 972-4.	(11–15):1[e]	-	-	Heterogeneous ruthenium silicotungstate (title compound) was synthesized. It is able to catalyze alkanes and alcohols with oxygen efficiently. Adamantane-1,3-diol was formed together with monosubstituted products (ca. 1/3 of 1-adamantanol). No mechanistic studies were performed.
36	[RuCl(N4PY)]Cl + MCPBA(+ *N*-oxide) [Ru(N2PY2O)(Me_2SO)] + MCPBA(+ *N*-oxide) N4PY ≡ N2PY2O ≡ MCPBA ≡ *m*-chloroperbenzoic acid Yamaguchi, M. et al. *Chem. Lett.* **2002,** 434-5.	≥ 30:1 ≥ 61:1	- -	- -	Adamantane was oxidized by the two title ruthenium complexes with the addition of MCPBA (plus 2,6-dichloropyridine *N*-oxide in some runs). The other product observed are 1-chloroadamantane (yield 0–9%) and adamantane-1,3-diol (0–12%). A **Ru(III) intermediate** was suggested to form by the interaction of MCPBA and the catalyst, the Ru(III) then react with *N*-oxide giving an **oxoruthenium species**. A free-radical mechanism was not discussed.

37	*cis*-[RuCl(CH_3CN)(κ^4-L)][BF_4] + TBHP L ≡ 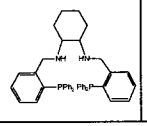 Wong, W.-K. et al. *Eur. J. Inorg. Chem.* **2003,** 3539-46.	5:1	-	Yes (for *cyclo*-C_6H_{10})	The title compound was the best catalyst (highest TOF and highest *ee*) in a group of four compounds with resolved X-ray structures. Oxidation of various organic compounds with TBHP and title catalyst involves a **free radical mechanism** (by product study and inhibition results).

[a]Selectivity is the adamantane product ratio of 3°/2°, calculated by 3×[1-adamantanol]/([2-adamantanol]+[2-adamantanone]).
[b]KIE refers to the k_H/k_D ratio for the oxidation of C_6H_{12} and C_6D_{12} unless otherwise noted.
[c]Stoichiometric amount added instead of catalytic amount in the oxidation of adamantane, yield based on Ru=O oxidant.
[d]Not detected (2-adamantanol or 2-adamantanone).
[e]1,3-adamantane-di-ol is not included in the selectivity calculation.
[f]The KIE was determined at low conversions (<2%).
[g]The two KIE numbers are for the oxidation of cyclohexanol and cyclohexanone, repectively.

CHAPTER IV

SUMMARY

This dissertation focuses on kinetic and catalytic studies of dioxygenase systems. Vanadium catechol dioxygenase catalysts are highly reactive systems compared to other catechol dioxygenases. The similar selectivity of ten out of eleven reported vanadium catechol dioxygenase systems hints there is a common catalyst and if one involves Ockham's Razor. Initial attempts to identify a common catalyst by isolating and then purifying the reaction mixture were not successful; however, spectroscopic and spectrophotometric results proved quite telling. The identity of the common catalyst was identified in its resting state as the Pierpont's complex, $[VO(DBSQ)(DTBC)]_2$.

Kinetic studies of polyoxometalate precatalysts evolving into the common catalyst have shown that selective oxidation is initiated and autocatalytically turned on by facile autoxidation of the substrate. The generality of autoxidation-product-initiated chemical reactions is hypothesized to be little recognized and probably more general—an important finding of this dissertation.

The re-investigation of a Ru_2-sandwich polyoxometalate for adamantane hydroxylation reaction demonstrates the prevalence of free-radical-chain autoxidation catalysis. In an earlier, literature study, product identification appears to have been incomplete due to too low detection limits of the instruments employed (complicated, perhaps, by a low conversion percentage). One point inhibition experiments done by others may have also been misleading due to either a low concentration of the inhibitor, use of an inhibitor with a low inhibition rate constant, or degradation of the inhibitor. The most useful tests for determining a free-radical-chain mechanism are (ranked by their importance in this case): determining the kinetic rate law, initiation / inhibition tests, product selectivity studies, establishing the reaction stoichiometry, and other control experiments (e.g., cyclohexene autoxidation, etc.).

In summary, spectroscopic and mechanistic studies of vanadium catechol dioxygenases identified the true catalyst therein and indicate that the desired dioxygenase catalysis is actually initiated by autoxidation to produce H_2O_2. Product and mechanistic studies of a Ru_2-incorporated polyoxometalate revealed that the adamantane hydroxylation reaction is catalyzed via a free-radical-chain mechanism instead of the previously claimed dioxygenase pathway.

APPENDIX A

GENERAL STATEMENT ON "JOURNALS-FORMAT" THESES

(Written by Professor Richard G. Finke)

The Graduate School at Colorado State University allows, and the Finke Group in particular encourages, so-called journals-format theses. Journals-format theses, such as the present one, consist of a student written and lightly edited literature background section, chapters corresponding (in the limiting, ideal case) to final-form papers either accepted or at least submitted for publication, a summary or conclusions chapter, and short bridge or transition sections between the chapters as needed to make the thesis cohesive and understandable to the reader. The "bridge" sections and summary are crucial so that the thesis fulfills the requirement that the thesis be an entity (an official requirement of most Graduate Schools). All chapters (manuscripts) in a journals-format thesis must of course be written initially by the student, with subsequent (ideally light) editing by the Professor, the student's committee, and even the student's colleagues where appropriate and productive.

The advantages for doing a journals-format thesis are several-fold and compelling. Specifically, some of the major advantages are: the level of science (i.e. of refereed, accepted publications) is at the highest level; the student and Professor must interact closely and vigorously (i.e. to bring both the science and the writing to their highest level), hence the student is getting the best education possible and is being at least exposed to (if not held to) the highest standards; the needed clean-up or control experiments that invariably come up have all been identified and completed before the

student leaves; there are no further time demands once the student has left the University (since all the publications are at least submitted; it is terribly inefficient to try to complete either writing or often specialized experiments once the student has left); and the American tax payers, who ultimately pay the bill for the research, are getting their money's worth since all the research is published and thus widely disseminated in the highest form, as refereed science. Professorial experience teaches that a student who has achieved a journals-format thesis has indeed received a better education and has learned critical thinking and clear writing skills that will serve them well for a lifetime.

Experience also teaches, however, that much more than light editing is often needed in at least some student theses; it follows, then, that considerable professorial writing and editing might be needed for at least the initial chapters of most journals-format thesis. Indeed, a journals-format thesis is not recommended (and may not even be possible) for less strong students. Hence, the issue arises of exactly how much of the science and the writing, in the final (or submittable) chapters, is due to the student vs. the Professor and whether or not this level of contribution constitutes that acceptable of a new Ph.D. and independent investigator.

To deal with this issue, several recommendations are made; the recommendations below have been discussed with the committee signing Cindy-Xing Yin's dissertation. (Ms. Yin's dissertation is the twelfth such thesis from the Finke Group following Dr. C. Garr's, Dr. Y. Lin's, Dr. M. Pohl's, Dr. J. Sirovatka,'s, Dr. J. Aiken's, Dr. R. Suto's, Dr. J. Widegren's and Dr. K. Doll's dissertations, and Ms. K. Weddle's, Mr. W. White's and Mr. C. Hagen's Masters theses.)

Recommendations

The recommendations are:

(i) That the present pages be enclosed in the thesis until such a time as it is no longer needed (i.e., when the policies and procedures for journals-format theses become routine);

(ii) That for each chapter it is detailed, and to the satisfaction of the committee and the advisor, who made what contributions, both of intellectual substance and writing. [Substantial contributions of other students or Professors should of course also be acknowledged. In the case of disagreements, the various drafts (i.e. as their electronic files) can be examined by the committee (in light of a knowledge of who wrote which draft) to easily determine who contributed what. In possible borderline or controversial cases it may even be advisable to keep all (electronic) drafts of the papers as a record];

(iii) That it be specifically stated whether or not all the experimental work is the Ph.D. candidate's [as is usually the case, although the increasing (desirable) collaboration among scientists worldwide makes this a non-trivial point].

(iv) Furthermore, it is recommended that allowances be made for the expectation that a greater degree of involvement of the professorial advisor is likely in a journals-format thesis than in a traditional thesis. [That this is reasonable follows from the fact that some Professors write 100% of all their papers; this, unfortunately, robs the student of the valuable experience of participating in the science and the end product as practiced at the highest levels. (It also creates an unmanageable writing burden for Professors involved in all but the narrowest of research areas or for Professors involved in more than one competitive research area];

(v) Notwithstanding (iv), there needs to be ideally no more than ca. 40% Professorial writing contribution in a given *early* chapter in the thesis, and there should be a clear evolution in the thesis of a decreasing professorial involvement to, say, a 10-20% direct contribution in the last chapter or two.

(vi) As a further aid towards separating out the candidate's and the professorial (and other) contributions, it is recommended that the Introductory (usually literature background) chapters(s) and at least the final chapter be lightly edited only, so that authentic examples of the student's contributions are documented in an unambiguous form.